Université de Montréal

Thermosensitive Chitosan-based Hydrogels for Extrusion-based Bioprinting and Injectable Scaffold for Articular Tissue Engineering

Par

Maedeh Rahimnejad

Institut de Génie Biomédical, Département de Pharmacologie et Physiologie,

Faculté de Médecine

Thèse présentée en vue de l'obtention du grade de Philosophiæ Doctor (Ph.D.)

en Génie Biomédical

Février 2022

Université de Montréal

Institut de Génie Biomédical, Département de Pharmacologie et Physiologie, Faculté de Médecine

---

Thermosensitive Chitosan-based Hydrogels for Extrusion-based Bioprinting and Injectable Scaffold for Articular Tissue Engineering

Présenté par

Maedeh Rahimnejad

A été évalué(e) par un jury composé des personnes suivantes

Prof. François Yu
Président-rapporteur

Prof. Sophie Lerouge
Director

Prof. Nicole R Demarquette
Codirector

Prof. Christos Boutopoulos
Représentant de la doyenne

Prof. Houman Savoji
Membre du jury

Prof. Luc Mongeau
Examinateur externe

Résumé

La bio-impression est une forme avancée de fabrication additive qui permet de créer des structures 3D vivantes (contenant des cellules) et de créer des modèles 3D de tissus ou, à plus long terme, des tissus implantables pour remplacer les tissus ou organes malades ou endommagés. La bio-impression connaît une croissance rapide mais doit faire face à plusieurs défis. L'un d'entre eux consiste à trouver des matériaux extrudables contenant des cellules (appelée bioencres) qui combinent toutes les propriétés requises. Les hydrogels de chitosan thermosensibles qui forment des solutions à température ambiante mais gélifient rapidement à la température du corps sont d'intéressants candidats comme bioencre mais à ce jour il n'y a pas encore eu de résultats convaincants démontrant leur potentiel. De plus, les méthodes rhéologiques permettant de prédire leur imprimabilité font toujours défaut. L'objectif général de ce doctorat était d'étudier et optimiser les hydrogels thermosensibles à base de chitosan fabriqué avec un mélange de deux bases faibles, (bêta-glycérophosphate et hydrogénocarbonate de sodium) pour la bio-impression par extrusion, notamment pour l'ingénierie des tissus articulaires.

Nous avons tout d'abord développé une approche rhéologique pour évaluer leur potentiel en tant que bioencres. Les cinétiques de gélification à température ambiante et du corps ont été caractérisées. Puis les essais de viscosité et de récupération ont été adaptés pour prendre en compte l'absence de stabilité des gels. La fidélité de forme et les propriétés mécaniques des structures imprimées ont également été caractérisées en fonction du taux de cisaillement appliqué et les résultats corrélés avec les données rhéologiques.

Nous avons démontré qu'il était possible d'imprimer une structure avec une fidélité et une maniabilité adéquate; cependant, une concentration élevée de chitosan (3%p/v) est nécessaire, ce qui entraîne un taux de mortalité élevé des cellules, tandis que réduire la concentration à 2%p/v entraîne une très mauvaise fidélité de la forme. Nous avons surmonté ces limites en utilisant une approche basée sur la bio-impression FRESH (Freeform reversible embedding of suspended hydrogel). Un bain de support chaud a été conçu afin de soutenir les structures bioprintées et d'améliorer la thermoréticulation du chitosan pendant l'impression. Cette approche augmente drastiquement la fidélité et les propriétés mécaniques des structures imprimées avec une concentration de chitosane (2% p/v) adaptée à l'encapsulation de cellules.

Enfin, nous avons étudié l'impact du chargement de particules de bioverre osteoconducteurs dans ces hydrogels thermosensibles, en vue de leur utilisation pour la fabrication de tissus osseux minéralisés. Les propriétés mécaniques et la cytocompatibilité in vitro étant affectées de manière négative par l'ajout de bioglass, notre stratégie a consisté à concentrer le bioverre sous forme de microbilles, puis incorporer ces microbilles dans l'hydrogel à base de chitosan chargé de cellules. Cette nouvelle stratégie a permis d'améliorer considérablement les propriétés mécaniques et la viabilité des cellules. Cet hydrogel bioactif hybride n'est pas utilisable comme bioencre, mais il est injectable et pourrait être utilisé comme matrice injectable pour la régénération de défauts osseux. Cependant, il reste encore beaucoup d'optimisation à faire pour la bio-impression de tissus de gradient complexes.

Mots-clés : Rhéologie, bioimpression 3D, bioencre, biomatériau injectable, hydrogel de chitosan thermosensible, tissu articulaire, bioverre.

Abstract

Bioprinting is an advanced method that enables to engineer living 3D structures mimicking the tissue complexity found in-vivo. It allows to create 3D tissues to study drugs/biological mechanisms, also, in longer-term, implantable tissue to replace diseased/damaged body tissues/organs. Bioprinting is growing rapidly but faces several challenges. One of them is to find ideal bioinks which combine all the required properties. Hydrogels are generally used since cells require an aqueous environment. But it is very challenging to stack hydrogels into a 3D structure because hydrogels are weak by nature and cannot support the structure without collapsing. Among the potential candidates are thermosensitive chitosan hydrogels which form solutions at room temperature but rapidly gel at body temperature. However, their potential in bioprinting has not been yet studied. Moreover, comprehensive rheological methods to predict their printability are still missing. The general objective of this Ph.D. was to study and optimize the thermosensitive chitosan-based hydrogels for extrusion-based bioprinting and injectable scaffold for articular tissue engineering.

The first objective was to develop a rheological approach to study printability of these time- and temperature-dependent hydrogels and assess their potential as bioinks. Chitosan-based physical hydrogels prepared by combining chitosan acidic solution with weak bases like beta-glycerophosphate and sodium-hydrogen-carbonate were studied. Gelation kinetics, shear-thinning viscosity as a function of shear rate corresponding to that applied during printing, and recovery tests were performed. The resolution and mechanical properties were characterized as a function of applied shear rate and results were correlated with rheological data. This work allowed us to determine the best chitosan hydrogel formulation for 3Dprinting and compare it with conventionally used bioink, alginate/gelatin. This methodology can also be useful for other temperature- and time-dependent materials.

We demonstrated that printing structures with adequate fidelity and handability using chitosan-based hydrogels was feasible; however, a high concentration (3%w/v) was required, leading to high mortality rate of encapsulated cells. Decreasing chitosan concentration resulted in poor shape fidelity. The second objective was therefore to develop a method using Freeform reversible embedding of suspended hydrogel (FRESH) bioprinting to overcome these limitations. A warm support bath was designed to support chitosan-based bioprinted structures and enhance chitosan thermo-crosslinking during printing. This approach

drastically increases the fidelity and mechanical properties of structures printed with low concentration chitosan (2%w/v) suitable for cell encapsulation.

Lastly, we studied the impact of loading bioglass particles into such thermosensitive hydrogels for potential bone-mineralized tissue repair, which could promote bone ingrowth through osteoconductivity. The mechanical properties and in-vitro cytocompatibility are affected adversely by bioglass addition. A new strategy was implemented to encapsulate bioglass within chitosan-based microbeads, then incorporate these microbeads in the cell-laden chitosan-based hydrogel. This strategy improved mechanical properties and cell viability. This hybrid hydrogel could be used to form an injectable cell-loaded scaffold. The bioactive microbeads were freezable, increasing their potential for clinical applications.

We demonstrated the potential of the thermosensitive chitosan-based hydrogels for bioprinting, especially with the FRESH approach. This opens interesting avenues toward tissue engineering. However, much works still remain to be done before bioprinting complex gradient tissues.

Keywords: Rheology, Bioprinting, Bioink, Injectable biomaterial, Thermosensitive chitosan hydrogel, Articular tissue, Bioglass.

Table of Contents

RÉSUMÉ I

ABSTRACT III

LIST OF TABLES XI

LIST OF SUPPLEMENTAL TABLES XII

LIST OF FIGURES XIII

LIST OF SUPPLEMENTAL FIGURES XIX

LIST OF ABBREVIATIONS XXI

LIST OF PUBLICATIONS XXIII

REMERCIEMENTS XXVIII

CHAPTER 1 – INTRODUCTION 1

CHAPTER 2 - LITERATURE REVIEW (STATE OF ART) 3

2.1 Approaches for tissue engineering and repair of articular tissue 3

2.2 3D bioprinting 4

2.3 Bioprinting Technologies 5

2.3.1 Drop-on-demand bioprinting 6
2.3.2 Stereolithography 6
2.3.3 Extrusion-based bioprinting 7
2.3.4 Combination of droplet-based and extrusion-based modalities 8

2.4 Freeform reversible embedding of suspended hydrogel (FRESH) bioprinting method 9

2.5 Bioinks and Biomaterial inks 11
2.5.1 Definitions and main design criteria 11
2.5.2 Hydrogels 13
2.5.3 Injectable biomaterials and main bioinks 13

2.6 Chitosan hydrogels 20

2.7 Thermosensitive chitosan-based hydrogels 21
2.7.1 CH-BGP hydrogels 21
2.7.2 New chitosan thermosensitive hydrogels 23
2.7.3 Chitosan bioinks and injectable hydrogels for mineralized tissues bioprinting 24

2.8 Printability (resolution, fidelity, mechanical properties, cytocompatibility) 25

2.9 Rheological concepts 27
2.9.1 Theory 27
2.9.2 Summary of useful rheological tests for printability 35

2.10 Rheology of FRESH support bath 37

CHAPTER 3 - HYPOTHESES AND OBJECTIVES 40
3.1.1 Hypothesis and objective 1 40
3.1.2 Hypothesis and objective 2 40
3.1.3 Hypothesis and objective 3 41

CHAPTER 4 - A RHEOLOGICAL APPROACH TO ASSESS THE PRINTABILITY OF THERMOSENSITIVE CHITOSAN-BASED BIOMATERIAL INKS 42

4.1 Abstract 42

4.2 Introduction 43

4.3 Materials and methodology 45

4.3.1 Materials 45

4.4 Preparation of chitosan thermosensitive hydrogels 46

4.4.1 Preparation of pre-hydrogel solutions for rheological characterization 46

4.4.2 Preparation of alginate/gelatin hydrogel (control group) 47

4.4.3 Rheological tests 47

4.4.4 Printing procedure 48

4.4.5 Printing resolution, hydrogel uniformity and structural integrity 49

4.4.6 Post-printed mechanical properties 50

4.4.7 Statistical analyses 50

4.5 Results 50

4.5.1 Time sweep at 22 and 37°C 50

4.5.2 Shear thinning behavior 53

4.5.3 Shear recovery 54

4.5.4 3D printing of pre-hydrogel solutions 57

4.5.5 Post printed mechanical strength 60

4.6 Discussion 62

4.7 Conclusion 66

4.8 Supplemental Information 68

4.9 Summary of paper 1 and introduction of objective 2 72

CHAPTER–5 - FRESH BIOPRINTING OF BIODEGRADABLE CHITOSAN THERMOSENSITIVE HYDROGELS 73

5.1 Abstract 73

5.2 Introduction 75

5.3 Materials and Methods 77

5.3.1 Materials 77

5.3.2 Chitosan and chitosan-gelatin bioinks preparation 77

5.3.3 FRESH bath preparation 78

5.3.4 Rheological characterization 78

5.3.5 Printing procedure 79

5.3.6 Resolution and shape fidelity 79

5.3.7 Mechanical properties characterization 80

5.3.8 Bioprinting of stem cell loaded hydrogels 80

5.3.9 Statistical analyses 81

5.4 Results and Discussion 82

5.4.1 FRESH bath optimization and characterization 82

5.4.2 Rheological behavior of chitosan-based hydrogel bioinks 83

5.4.3 Optimization of printing parameters 85

5.4.4 Printed structures on glass and within the FRESH bath 87

5.4.5 Post-printed mechanical properties 88

5.4.6 Cell viability 90

5.5 Conclusion 92

5.6 Supporting Information 94

5.7 Summary of paper 2 and introduction to the next objective 99

CHAPTER 6 - INJECTABLE CELL-LADEN HYBRID BIOACTIVE SCAFFOLD CONTAINING BIOACTIVE GLASS MICROSPHERES 100

6.1 Abstract 100

6.2 Introduction 101

6.3 Materials and Methods 104

6.3.1 Materials 104

6.3.2 Preparation of chitosan thermosensitive macrogel with and without Bioglass 105
6.3.3 Characterization of chitosan-BG hydrogels 106
6.3.4 Fabrication and characterization of microbeads for hybrid hydrogels 106
6.3.5 Statistical analyses 108

6.4 Results 108
6.4.1 Effect of BG addition on CH hydrogels 108
6.4.2 BG-rich microbeads size and morphology 111
6.4.3 Mechanical properties of hybrid hydrogels 112
6.4.4 Bioactivity: 113
6.4.5 Cytocompatibility (Cell viability and Rate of ion release) 117
6.4.6 Injectability 119
6.4.7 Freezing and long-term storage 120

6.5 Discussion 120

6.6 Conclusion 123

6.7 Supporting Information 125

CHAPTER 7 – GENERAL DISCUSSION AND CONCLUSION 128

7.1 Rheological approach to predict printability 128

7.2 Potential of Chitosan thermogel as bioinks 130

7.3 Chitosan bioink in FRESH bioprinting 131

7.4 Advantages of chitosan thermosensitive hydrogels as bioinks 132

7.5 Chitosan thermogel as embedding hydrogels 136

7.6 Potential of injectable/printable chitosan thermogel for mineralized tissue engineering 137

7.7 Conclusion 141

7.8 Originality 141

7.9 Impact and Contribution.....142

REFERENCES.....143

List of Tables

Table 1. Summary of synthetic based biomaterials mostly used in 3D bioprinting: properties and applications. 14

Table 2. Summary of natural based biomaterials mostly used in 3D bioprinting: properties, and applications. 17

Table 3. Useful rheological tests to study the printability of thermosensitive hydrogels. 36

Table 4. Most commonly used biomaterials as a FRESH bioprinting support bath 38

Table 5. Concentration of chitosan and gelling agents of the various tested hydrogels (CH: Chitosan, BGP: Beta-glycerophosphate, SHC: Sodium hydrogen carbonate, PB: Phosphate buffer at pH=8). 47

Table 6. Printing parameters used on the 3D Discovery bioprinter: needle size, n-1 slope according to viscosity vs shear rate graph and corresponding shear rate as a function of needle size according to equation 1. Constant parameters were: Flow rate = 1.25 µL/s (mm3/s); feed rate = 6 mm/s; layer thickness = 0.3 mm. 49

Table 7. Concentration of chitosan and gelling agents in the studied hydrogels (CH: Chitosan, BGP: Beta-glycerophosphate, SHC: Sodium hydrogen carbonate, PB: Phosphate buffer). BG was added to reach final concentration of 1-6% w/v for macrogels. 105

Table 8. Main FTIR vibrational bands associated with 0% and 4%BG microbeads over 7 days soaking at SBF. 115

Table 9. EDX analysis: elemental composition (relative atomic concentration) of chitosan microbeads containing 0, 2 and 4% BG, over 7 days soaking in SBF (NA: Not available; ND: Not detectable). 117

Table 10. Printability window in Pluronic FRESH bath. 135

List of Supplemental Tables

Table S 1. Main shear recovery data from chitosan (mean, SD and SD%), as a function of shear rate (10, 100, 500 nd 1000 s-1). 70

Table S 2. Main shear recovery data from alginate-gelatin (mean, SD and SD%), as a function of shear rate (10, 100, 500 nd 1000 s-1). Recovery test were performed after 1 and 10 min rest (mimicking the time in the printing cartridge). 71

List of Figures

Figure 1. Two main approaches of tissue engineering including: A) cell seeding on surface of the scaffold; and B) cell encapsulation within the 3D scaffold (prepared using www.biorender.com). 3

Figure 2. Schematic image of the difference of 3D printing and bioprinting; Reprinted from [16]; An open-access article distributed under the terms of the Creative Commons Attribution License (CC BY). 5

Figure 3. Schematic image of various 3D bioprinting technologies mainly include drop-on-demand bioprinting (inkjet, laser-assisted), extrusion and stereolithography; Reprinted from [19]; An open-access article distributed under the terms of the Creative Commons Attribution License (CC BY)..... 5

Figure 4. Image of 3D Discovery® of RegenHU bioprinted used in this project. 8

Figure 5. Multi-print heads bioprinting at a same time, one as a support structure and the other as a bioink filling the support structure (prepared using www.biorender.com). 9

Figure 6. A) FRESH bioprinting of low viscous bioink within a gelatin microparticles support bath, B-C) FRESH bioprinted heart, and D) The bioprinted heart after support bath removal; Reprinted from [55]; An open-access article distributed under the terms of the Creative Commons Attribution License (CC BY). 10

Figure 7. Bioprinting of bioink in a self-healing support bath, the support bath behaves as a rigid body at low stresses but flow as a viscous fluid at high stress when the extruder nozzle is moving; Reprinted from [60]; An open-access article distributed under the terms of the Creative Commons Attribution-Noncomercial License (CC BY). 11

Figure 8. Chemical structure of chitosan, deacetylated form of chitin (Image Reprinted from https://en.wikipedia.org/wiki/Chitosan). 21

Figure 9. A) Chitosan gelation with beta-glycerophosphate with temperature increase to 37°C (Reprinted from [189]; An open-access article distributed under the terms of the Creative Commons Attribution License (CC BY)); B) Thermogelation with temperature increase of CH-BGP hydrogel (Reprint and Copyright (2021) with permission from Elsevier Inc. [187]). 22

Figure 10. Thermogelation mechanism of the chitosan-based hydrogels prepared in Lerouge lab (prepared using www.biorender.com). 24

Figure 11. Quantitative study of filaments uniformity during extrusion; Reprint and Copyright (2021) with permission from IOP Publishing [213]..... 26

Figure 12. A) filament width, and thickness using a single layer assessment (Reprint and Copyright (2021) with permission from Elsevier Inc. [215]); B) improved printability resulting from different extruded bioinks (Reprinted from [220]; An open-access article distributed under the terms of the Creative Commons Attribution License (CC BY)). 27

Figure 13. Schematic image showing linear viscoelastic region for both gel-like and solid structure using vertical dotted lines (Image Reprinted from https://wiki.anton-paar.com/ca-en/amplitude-sweeps/)..... 29

Figure 14. Schematic flow behavior (viscosity) curves of Newtonian, and non-Newtonian (shear thinning, shear thickening materials) (Image Reprinted from https://knowledge.ulprospector.com/9796/pc-better-performance-through-rheology/). 30

Figure 15. The relation of applied shear stress and cell viability (Reprinted from [233]; An open-access article distributed under the terms of the Creative Commons Attribution License (CC BY)). 31

Figure 16. Schematic typical rheological behavior of fluids with Herschel-Bulkley, Bingham model, plot of shear stress vs shear rate (prepared using www.biorender.com)..... 32

Figure 17. Common rheological tests for bioinks. (a) Shear rate sweep, (b) stress ramp, (c) oscillatory stress ramp (amplitude sweep), (d) frequency sweep of different biomaterials: solid-like gels (gray) and viscoelastic liquids (black), (e) rotational recovery (varying shear rate), (f) oscillatory recovery (varying oscillatory strain) (Reprinted from [238]; An open-access article distributed under the terms of the Creative Commons Attribution License (CC BY))..... 33

Figure 18. Rheometric evaluation of bioinks, with time- and temperature-dependent sol–gel transition. G" > G', viscous behavior; G" = G', gel point; G' > G", elastic solid behavior (Reprint and Copyright (2021) with permission from Elsevier Inc. [240])..... 34

Figure 19. Schematic of the applied shear rates and temperature as a function of time during recovery tests. 48

Figure 20. Gelation kinetics of A and B chitosan-based hydrogels: a) Evolution of the storage (G') and loss (G'') moduli of hydrogels as a function of time at 22°C (mean +/-SD; n≥3). b) Evolution of the storage (G') and loss (G'') moduli as a function of time at 37°C. c) G' value after 10 min at 22°C and 1h at 37°C, respectively (mean +/-SD; n≥3); (** p<0.01, *** p<0.001, **** p<0.0001). Gels were made with SHC+BGP as gelling agents, while B gels were prepared with SHC+PB, as described in Table 5. 51

Figure 21. Shear thinning behavior of: a) viscosity of A3 formulations at various shear rates (0.01, 0.1, 1, 10 and 100 s-1) as a function of time at 22°C; b) Viscosity as a function of shear rate for both A2 and A3 formulations after 10 min at 22°C (mean; n≥3). The slope between 10 and 100 s-1 was used to evaluate the shear stress during printing using Equation 3. 53

Figure 22. Shear viscosity recovery under 4 different applied shear rates (10, 100, 500, 1000 s-1). The graphs present the complete cycle, namely at-rest state (shear at 0.001 s-1, generally for 10 min), printing step (shear rate at one of the 4 different tested shear rates for 1 min), post printed rest state at 22°C and post-printed rest at 37°C (shear back at 0.001 s-1): a) A2, b) Pre-gelled A2 (shear after gelation for 20 min at 37C); c) A3, d) A3 with 20min at rest instead of 10 min. The change of the shear rate is indicated with the vertical lines; Temperature 37°C is highlighted, otherwise 22°C) (mean +/-SD; n≥3)..... 56

Figure 23. Shear recovery tests of Alginate/gelatin hydrogels after 1- or 10-min rest times (mimicking time in the cartridge before printing. Four different shear rates (10, 100, 500, 1000 s-1) were applied (mean; n=6). 57

Figure 24. a) Descriptive results and images of filaments printed with a 22 G needle (0.41 mm inner diameter) with feed rates changing from 7 to 11 mm/s, for a) A2, b) A3 chitosan hydrogels and c) Alginate/gelatin filaments as comparison (mean +/-SD; n≥3).; d) 3D CAD honeycomb design model; e) picture of 10- and 20-layers printed structures made with A3 hydrogel. 59

Figure 25. Behavior under unconfined compression of chitosan-based hydrogel and Alginate/Gelatin: a) secant Young modulus of A3 printed with high (507 s-1)/medium (230 s-1) shear rate and alginate/gelatin

bioinks; pictures of the 5-layer honeycomb structures tested are also shown; b) stress-strain curve in unconfined compression (mean ± SD; n≥3). 61

Figure 26. Rheological properties of Pluronic support bath A) Temperature ramps (10-45 °C) of Pluronic 19% (w/v) +1% (w/v) NaCl (dotted line=37°C); B) Recovery tests: Storage modulus of Pluronic 19% + 1% NaCl (black curve) during various cycles of strain at 37 °C (2 min rest at 1% strain, 1 min under shear at 100% strain, red curve) (mean; n≥3). 82

Figure 27. Rheological properties of chitosan hydrogels ; A) Evolution of the storage (G') and loss (G'') moduli of hydrogels as a function of time and following the sudden increase of the temperature from 22 to 37 °C (the dotted black line represents the temperature as a function of time).; CH2: chitosan 2% w/v hydrogel; CH3 : chitosan 3% w/v hydrogel; CH-Gel: chitosan 2% w/v gelatin hydrogel); B) Yield stress of each formulation (strain controlled, 0.01-500%) (mean +/-SD; n≥3); C) viscosity as a function of shear rate after 10 min at 22 °C (mean; n≥3); D) Recovery test, showing the evolution of the storage modulus during a complete cycle, namely at-rest state at 22 °C (1% strain for 10 min), printing step at 22 °C (100% strain for 1 min), post printed rest state at 37 °C (1% strain for 5 min) (n≥3)(the red zone shows increase of temperature from 22 °C to 37 °C). 84

Figure 28. Illustration of how the FRESH method greatly reduces the diameter of printed filaments. Images of filaments printed with a 25G needle (0.26 mm inner diameter) with feed rates changing from 3 to 11 mm/s: A-C: on glass and D-F: within the support bath (mean +/-SD; n≥3; flow rate=0.5 mm3/s; G) Spreading ratio of the printed filaments at optimized printing condition (flow rate of 0.5 mm3/min and feed rate of 9 mm/s)(mean ± SD; n≥3; **** p<0.0001); H) Width of printed filaments (mean ± SD; n≥3). 86

Figure 29. The FRESH method strongly enhances the resolution and feasibility of creating 3D structures with chitosan hydrogels. Pictures of gridded structures after 24 h gelation at 37 °C; A-C) printed on warm glass substrate (10-layers); D-F) printed in the Pluronic support bath (10-layers); G) Illustration of handability of CH2 10-layer printed structure; H) CAD design of the gridded structure (scale 1 cm); I) Thickness of 20-layers printed structures after 24 h gelation at 37 °C, in comparison to the theoretical height (control ★) (mean ± SD; n≥3; * p<0.5, ** p<0.01, *** p<0.001, **** p<0.0001); J) Pictures of gridded, and cylindrical CH2 structures printed in the Pluronic support bath (20-layers). 87

Figure 30. Mechanical properties of 20-layer structures printed on glass and within the FRESH bath: A) stress-strain curve in unconfined compression; B) secant Young's Modulus at 30% deformation (CH2: 2% w/v chitosan, CH3: 3% w/v chitosan; CH-Gel: 2% w/v chitosan-2% w/v gelatin) (mean ± SD; n≥3; * p<0.05, ** p<0.01, **** p<0.0001). 89

Figure 31. Viability of encapsulated MSCs loaded in CH2 and CH-Gel hydrogels, printed within the support bath A) Live-dead images (Live cells appear in green, dead cells in red); B) percentage of live cells (mean ±SD; n>4). Controls correspond to hydrogel solutions simply injected in a well before and after the bioprinting process (*p<0.05, **p<0.01, ****p<0.0001 compared to the control before bioprinting; ($ p<0.05; $$$ p<0.001, compared to CH-Gel sample) (CH2: chitosan 2% w/v; CH-Gel: chitosan 2% w/v – gelatin 2% w/v) (Live/dead assays). 91

Figure 33. Schematic illustration of two main approaches studied: 1) Homogenous BG-chitosan hydrogel: and 2) Hybrid BG-chitosan hydrogel. 104

Figure 34. (A) Time sweep at 22ºC followed by 37ºC for CH/PB-SHC-BG hydrogels, when prepared 5 days after mixing BG and gelling agents (mean +/-SD; N≥3, n≥6); (B) Unconfined compression tests: secant modulus at 30% deformation; (blue zone, and red zone are for PB0.01 SHC0.075, and BGP0.1 hydrogels with 0, 1, 3 and 6% BG (mean +/-SD; N=2, n≥3); **** p<0.0001). 110

Figure 35. Beads morphology and size distribution: A-C) Light microscope images of PB-SHC microbeads containing 0, 2 and 4% (w/v) BG, respectively (Bar corresponds to 1 cm) (0%BG stained with Eosine, 2% and 4%BG stained with Toluidine blue); D) average circularity of microbeads (1=perfectly circular microbeads); E) Size distribution; and (F) mean diameter of chitosan microbeads with and without BG, quantified by the CellProfiler image analysis software (mean, N=3, n>1000), (** p<0.01, *** p<0.001, **** p<0.0001). 111

Figure 36. Unconfined compressive properties of hybrid hydrogels (Hyb), in comparison to hydrogels with similar concentration of BG but homogenously dispersed: secant modulus at 30% deformation (mean +/-SD; N=2, n=6) (** p<0.01, **** p<0.0001, ns=not significant) All hydrogels were prepared using PB0.01SHC0.075 gelling agent. For hybrid gels, since both the volumic bead content (20 or 50%) and the BG content in the beads vary, the global concentration of BG is indicated first in their name..... 112

Figure 37. FTIR spectra of chitosan microbeads with and without BG after 7 days soaking in SFB (black lines correspond to BG-loaded microbeads and the grey line corresponds to the 0%BG)..... 114

Figure 38. SEM images and EDX spectra of microbeads with and without BG after 0, 1, or 7 days soaking in simulated body fluid (SBF). A-C): SEM of 4% w/v BG at day 0, 1 and 7; D-F): corresponding EDX analysis; G, H, I, J): SEM and EDX of 0%BG control after 0 and 7 days in SFB..... 116

Figure 39. Viability of L929 fibroblasts encapsulated in chitosan hydrogels with either BG homogenous distribution or with BG microbeads. A) Osmolality of extracts; B) Metabolic activity (Alamar blue) and C) Viability (Live/dead) of encapsulated cells after 7 days (positive control=0%BG) (mean +/-SD; N=3, n≥6); (**** p<0.0001).; D) High cell mortality is already observed at day 1 in homogenous BG-rich hydrogels. 118

Figure 40. Light microscopy images of microbeads containing BG before and after injection through long 18G needle: A) dispersed in SBF; B) dispersed in the chitosan-based hydrogel. 119

Figure 41. Light microscope image of 2% BG microbeads before and after freezing at -20°C for 14 days. 120

Figure 42. Illustration of printed perfusable network embedded within thermosensitive chitosan hydrogels and effect of time on the network's resolution and continuity. 137

List of Supplemental Figures

Figure S 1. (a) phahermosouion of B3 in the syringe before printing; (b) printed filaments with B2 formulation (partially gel and partially water). 68

Figure S 2. Shear thinning behavior of B2, B3, and alginate/gelatin at 22°C (mean; n≥3). 68

Figure S 3. Shear recovery under 4 different applied shear rates (10, 100, 500, 1000 s-1) for pre-gelled A3 (samples previously subjected to 20 min gelation at 37C). Change of the shear rate is indicated by the vertical line; part of the test done at 37°C is highlighted in red, white zone is 22ºC) (mean +/-SD ; n≥3).69

Figure S 4. Mean diameter and images of filaments printed with a 25G needle (0.26 mm inner diameter) with feed rates changing from 3 to 11 mm/s: A-C: on glass with flow rate of 0.5, 1, 1.5 mm^3/s and D-F: within the support bath with flow rate of 0.5 mm^3/s for three formulations: 2% chitosan (CH), B) 2%chitosan-2% (w/v) gelatin (CH-Gel), and C) 3% chitosan-based hydrogel (mean +/-SD; n≥3)..... 94

Figure S 5. Rheological properties of Pluronic support bath A-B) Effects of added NaCl on temperature ramps (10-45 °C) of Pluronic 17% and 19% (w/v) (dotted line=37°C); C-D) Time sweep of Pluronic bath at 37 °C; (mean; n≥3). 95

Figure S 6. Rheological properties of Pluronic + 1% NaCl FRESH support bath A) Amplitude sweep, with controlled-shear deformation (0.01%-100%) of Pluronic19% + 1% NaCl at 37 °C; (mean; n≥3); B) Herschel Bulkley model of the Pluronic + 1% NaCl FRESH support bath (the straight line crossing the Y axis shows the yield stress). 95

Figure S 7. FRESH-bioprinted structures do not swell once immersed in saline, in contrast to those printed on glass: A) weight of the printed structure (expressed in % of weight of the equivalent volume of extruded filament), immediately after printing, after 1 h and 24 h soaking in PBS; B) images of the corresponding structures. 96

Figure S 8. FTIR analysis show absence of Pluronic in FRESH-printed CH structures. Some trace of Pluronic could however be present in CH-Gel hydrogels due to gelatin-Pluronic interactions (peaks attributed to the Pluronic are showed by dotted red lines). 97

Figure S 9. Live-dead assay of L292 fibroblast cells encapsulated in 3% (w/v) chitosan-based hydrogel after 24 h (live cells were stained with Calcein (green) and dead cells were stained with EthD-1 (red)). 97

Figure S 10. SEM images of CH2%, CH-GEL and CH3% hydrogels. 98

Figure S 11. Effect of BG concentration on the pH of the GA solutions and gelation kinetics of the corresponding chitosan hydrogels; A-B: pH variation of the BG-gelling agent solution over time at room temperature. C-F: Time sweep at 22ºC followed by 37ºC for CH/GA-BG hydrogels, when prepared immediately after mixing BG and gelling agents (C & D) or 5 days after mixing BG to gelling agent (E & F) (mean +/-SD; N≥3, n≥6). 125

Figure S 12. Evolution of the pH of hydrogels when made of GA+BG prepared immediately or 5 days before mixing with CH (In all cases the pH of the GA solution was adjusted to 8 prior to CH mixing). 126

Figure S 13. The pH of GA-BG solutions after pH adjustment at 8-8.5. 126

Figure S 14. Complex viscosity of 0%, 2% and 4%BG contained hydrogels at 37C 127

Figure S 15. SEM images of hydrogels with and without BG after 7 days soaking at SBF: A) 0%BG; B) 2%BG. 127

List of Abbreviations

BGP: Beta-glycerophosphate

BG: Bioglass

Ca: Calcium

CAD: Computer-aided design

CH: Chitosan

CNC: Cellulose nanocrystals

CO_2: Carbon dioxide

DDA: Degree of deacetylated groups

DA: Diacrylate

ECM: Extracellular matrix

FRESH: Freeform reversible embedding of suspended hydrogel

GAGs: Glycosaminoglycans

G': Storage modulus

G": Loss modulus

G*: Complex modulus

HA: Hyaluronic acid

HCL: Hydrogen chloride

LVR: Linear viscoelastic region

MA: Methacrylate

MMP: Matrix metalloproteinase

NH_3^+: Ammonium cation

NaCl: Sodium chloride

PEGDMA: Polyethylene glycol dimethacrylate

PEO-PPO-PEO: Poly(ethylene glycol), poly(propylene glycol), and poly(ethylene glycol)

PCL: Polycaprolactone

PEG: Polyethylene glycol

PB: Phosphate buffer

RGD: Arginine-glycine-aspartic acid

SLA: Stereolithography

SHC: Sodium hydrogen carbonate

3D: Three-dimensional

UV: Ultraviolet

XRD: X-ray powder diffraction

List of Publications

Journal Publications

Published:

- **Maedeh Rahimnejad**, Thierry Labonté-Dupuis, Nicole R. Demarquette, Sophie Lerouge "A Rheological Approach to Assess the Printability of Thermosensitive Chitosan-based Biomaterial Inks", Biomedical Materials Journal, Volume 16, Number 1, 26 Aug 2020, DOI: 10.1088/1748-605X/abb2d8.

- **Maedeh Rahimnejad**, Atma Adoungotchodo, Nicole R. Demarquette, and Sophie Lerouge "FRESH bioprinting of biodegradable chitosan thermosensitive hydrogels", Bioprinting Journal, Volume 27, 25 Apr 2022, DOI: 10.1016/j.bprint.2022.e00209.

Submitted and Under review:

- **Maedeh Rahimnejad**, Cindy Charbonneau, Zinan Hu, Sophie Lerouge "Injectable Cell-laden Hybrid Bioactive Chitosan-based Hydrogel Containing Bioactive Glass Microspheres", Submitted to Journal of ACS Biomaterials Science and Engineering.

Writing:

- Brenden Moeun, **Maedeh Rahimnejad** *(First co author)*, Sophie Lerouge, Joseph Matt Kinsella, Corinne Hoesli "Engineering Matrices for Sacrificial Embedded Writing via Controlled Gelation".

Conferences

- **Maedeh Rahimnejad**, Atma Adoungotchodo, David Joly Nicole Demarquette, Sophie Lerouge "FRESH Bioprinting Drastically Enhances the Printability of Chitosan Thermosensitive Hydrogels", Annual meeting of Canadian Biomaterials Society (CBS). Banff Center for the Arts and Creativity, Banff, Alberta, May 25-27, 2022, Presentation.

- Brenden N. Moeun, **Maedeh Rahimnejad**, Jacqueline Kort-Mascort, Salvador Flores-Torres, Marco Gasparrini, Steven Paraskevas, Joseph Matt Kinsella, Richard L. Leask, Sophie Lerouge, Corinne A. Hoesli "Designing embedded 3D printing matrices from prominent tissue engineering materials via controlled gelation", International Union of Pure and Applied Chemistry (IUPAC/CCCE). Virtual conference, August, 2021, Presentation.

- **Maedeh Rahimnejad**, Tommy Malaret, Cindy Charbonneau, Sophie Lerouge "Injectable cell-laden bioactive microsphere-based chitosan hydrogel for treatment of non-loading irregular bone defect", Annual meeting of Canadian Biomaterials Society (CBS). Virtual conference hosted by University of Waterloo, May 13-15, 2021, Presentation.

- **Maedeh Rahimnejad**, Thierry Labonté-Dupuis, Nicole R. Demarquette, Sophie Lerouge "Rheological Studies of Time- and Temperature Dependent Biomaterial Inks for Extrusion-based Bioprinting", 18th International Congress on Rheology (ICR) at Brazil, December 14-17, 2020, Presentation.

- **Maedeh Rahimnejad**, Thierry Labonté-Dupuis, Tommy Maralet, Nicole R. Demarquette, Sophie Lerouge "Thermosensitive Chitosan-Gelatin Bioink for Extrusion Based Bioprinting", ThéCell Conference at Montreal, December 1, 2020, Presentation.

- **Maedeh Rahimnejad**, Zinan He, Cindy Charbonneau, Sophie Lerouge "Injectable In Situ Cell-laden Thermogel for Bone-Mineralized Tissue Engineering", ThéCell Conference at Montreal, December 1, 2020, Poster.

- **Maedeh Rahimnejad**, Thierry Labonté-Dupuis, Zinan He, Cindy Charbonneau, Sophie Lerouge "Composite Chitosan-based Bioinks for Osteochondral Tissue Fabrication", 11th World Biomaterials Congress (WBC) at Glasgow, Scotland, December 11-15, 2020, Poster.

- **Maedeh Rahimnejad**, Thierry Labonté-Dupuis, Nicole R. Demarquette, Sophie Lerouge "Methods to Assess the Printability of Thermosensitive Hydrogels for Extrusion-based Bioprinting", Annual Meeting of The Canadian Biomaterials Society (CBS) at Quebec City, May 21-24, 2019, Poster.
- **Maedeh Rahimnejad**, Christine Andrea, Cindy Charbonneau, Nicole R. Demarquette, Sophie Lerouge "Preliminary Study towards a Bioactive Injectable Hydrogel for Bone Tissue Engineering and Bioprinting", Annual Meeting of the Canadian Biomaterials Society (CBS) at Quebec City, May 21-24, 2019, Poster.
- **Maedeh Rahimnejad**, Christine Andrea, Cindy Charbonneau, Sophie Lerouge "Study of Bioactive Chitosan-based Hydrogel for Mineralized Tissue 3D Bioprinting", 39e Journée de la Recherche du POES et de la Division d'Orthopédie de l'UdM at Montreal, April 11, 2019, Presentation.
- **Maedeh Rahimnejad**, Thierry Labonté-Dupuis, Nicole R. Demarquette, Sophie Lerouge "Printability of Chitosan Hydrogels for Extrusion-based Bioprinting: a Rheological Study", ThéCell Conference at Montreal, November 21, 2018, Poster.

Dedication

To my soulmate, Kamal!

My precious gold, my priceless jewel

Remerciements

This long journey of my life was not feasible without the enormous support and assistance from my supervisors, colleagues, and family members.

Foremost, I would like to express my sincere gratitude to my mentor, Dr. Sophie Lerouge, for her continuous and kind support during my Ph.D. research and writing of this thesis. Thank you, Sophie, for your advices, motivation, patience, enthusiasm, immense knowledge and more importantly, believing in me. Your daily follow-ups and your encouraging responses with “Congratulations”, “You are brilliant student”, and “You are like Lucky luck” had a broad impact, from pressure to motivation, on the way to fulfill this Ph.D.! Anyone worked with you know that hearing these words from you means a lot. Without your guidance and feedback this Ph.D. would not have been achievable.

I also acknowledge the valuable advices provided by my co-director, Dr. Nicole R Demarquette. Your kind words, and support always inspire me to complete this Ph.D. and motivate me to stand strong in my dream career. The completion of this thesis could not have been possible without your expertise.

My sincere gratitude goes to all my colleagues in LBeV team who have created a friendly and warm atmosphere. I did not only pursued research in the lab, but also lived a joyful life there. Thank you all for the days we worked together and for all the fun we had during virtual gatherings, and insanity time!

All the members of Dr. Corinne Hoesli and Dr. Joseph Matt Kinsella Teams at McGill University and, in particular Dr. Cindy Charbonneau at National Research Council Canada (NRC), deserve special thanks for all the support and knowledge they gave me. I appreciate your valuable insights and comments on my work.

Thanks to all my dear friends for always motivating me, cheering me up in tough situations and giving me a hope when I could not believe that I came this far.

I am also thankful to the financial support I received from FRQNT in the form of doctoral research scholarship program.

Last but not the least, this thesis is dedicated to my beloved extraordinary husband and soulmate, Kamal for all his love, strength and unconditional support, and I am very fortunate to have you. At the end of the day, he listened to the challenges of my research life, and sympathy with all my concerns. I do know how much

you self-devote for me to pursue my dreams, and I do acknowledge it. He always backed me up and ensured me that there is an end to a Ph.D. when it was impossible for me to see it. I am there now, my love!!

Finally, I would like to thank my family for all their love and inspiration. To my parents, maman Tarlan and baba Amrah, thank you for being my champions and for your unrestricted support. You taught me that achieving my goals is the only thing that will bring me the real happiness. To reach my goals, you backed me up to step in the challenging route of loving each other remotely, from two different lands. I hope that I make you proud!

Chapter 1 – Introduction

Three-dimensional (3D) bioprinting is an advanced tissue engineering method using an additive manufacturing process where the printed material contains live cells and is called a bioink. 3D bioprinting offers great potential for the engineering of living tissues with complex personalized geometries that would be long and difficult to achieve with conventional fabrication methods [1].

One of the potential tissue with complex structure is articular cartilage and its interface with bone (osteochondral tissue) [2, 3]. Cartilage tissue lacks self-healing properties when degeneration occurs by damages or diseases. The currently available treatments are limited, and articular cartilage tissue regeneration is still a challenging issue. In this regard, 3D bioprinting is particularly appealing to reproduce such complex gradient tissues.

Bioprinting has already allowed remarkable achievements such as feasibility of manufacturing heterogenous cell-laden scaffold with various geometries. However, it also faces several challenges. One of them is to find bioinks that fill the numerous design criteria for these applications, such as injectability, rapid cohesion with good mechanical properties, biodegradability and most importantly compatibility with cell encapsulations. These numerous specifications are presented in more detail in section 2.5.

Hydrogels are versatile and promising biomaterials to be used as bioinks, because of their unique properties similar to natural ECMs, including high water content suitable for cell survival, biodegradability, macroporosity, and biocompatibility [4]. But it is very challenging to stack a hydrogel into a 3D construct because hydrogels are weak by nature and cannot support the 3D structure without collapsing. Among the potential candidates are thermosensitive chitosan hydrogels which form a solution with physiological pH at room temperature and rapidly gel at body temperature, without any crosslinker. Chitosan is also biocompatible and biodegradable, which makes them attractive candidates in tissue engineering applications. However, these hydrogels have not shown satisfactory results for bioprinting. The general objective of this Ph.D. project was to study and optimize the potential of thermosensitive chitosan-based hydrogels for extrusion-based bioprinting and injectable scaffold for articular tissue engineering. In **Chapter 2**, we will present the main concepts and the literature review required to this project. The bioprinting technologies and bioinks will be presented, with particular focus in extrusion-based bioprinting. In addition, we will present the basics of rheology and its importance to predict the printability of bioinks.

Various type of bioinks will be discussed including synthetic and natural hydrogels. In particular, we will show potential of thermosensitive chitosan-based hydrogels to be used as a bioink. The specific objectives will also be presented at the **Chapter 3**.

The first objective of this Ph.D. was to propose a rheological approach to study the printability of time- and temperature-dependant hydrogels and to specifically assess the potential of the chitosan-based thermosensitive hydrogels as bioinks. This work, presented in **Chapter 4**, has been published in Biomedical Materials journal.

Secondly, we studied and optimized FRESH bioprinting of chitosan thermosensitive hydrogels to overcome the limitations of these hydrogels in conventional extrusion-based bioprinting. This work is presented in **Chapter 5** which has been accepted for publication in Bioprinting journal.

Lastly, to further improve the material for mineral tissues, we created injectable osteoconductive thermosensitive chitosan-based hydrogels compatible with cell encapsulation, by the addition of sintered bioglass (BG). This work is shown in **Chapter 6** which is submitted to journal of Biomedical Research Part A.

Chapter 7 will present the general discussion, limitations and possible recommendations followed by a conclusion.

Chapter 2 - Literature review (state of art)

2.1 Approaches for tissue engineering and repair of articular tissue

Tissue engineering is an interdisciplinary field using a combination of cells, biology, engineering, and materials science to create 3D functional tissue. Restoring, maintaining, or improving diseased or damaged tissues or complete organs is the primary goal of tissue engineering. Two main approaches are used in tissue engineering, one made of structures containing cells (Figure 1 B) and in the other one, cells are spreading on the scaffold after fabrication (Figure 1 A).

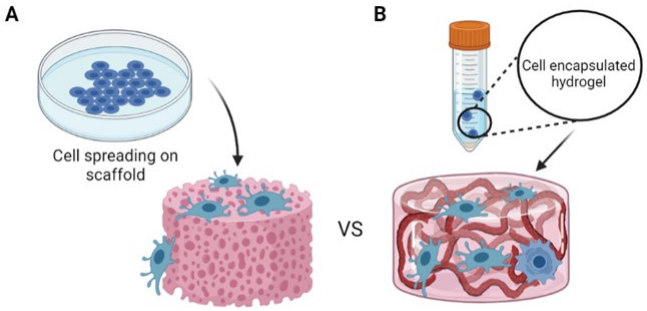

Figure 1. Two main approaches of tissue engineering including: A) cell seeding on surface of the scaffold; and B) cell encapsulation within the 3D scaffold (prepared using www.biorender.com).

As explained in the introduction, articular gradient tissue is one of the examples of complex tissue to engineer. Several conventional methods in tissue engineering have been used for the articular gradient tissue fabrication. The most commonly used strategies are electrospinning, freeze-casting [5, 6], freeze-drying [7, 8], thermally induced phase separation [9], sintering graded particles [10], vacuum infiltration [10], using microsphere, and 3D printing. But they all have some limitations. The emergence of 3D bioprinting addresses most of the issues in gradient complex tissue engineering which will be explained in the following section.

2.2 3D bioprinting

3D bioprinting is a novel and appealing method to create complex cell-laden 3D constructs. 3D printing is a procedure of building 3D scaffold consisting of an ink by using a computer-aided design (CAD). The main difference is that 3D bioprinting incorporates a bioink containing living cells, and/or bioactive agents e.g., growth factors to produce tissue-like structure as shown in Figure 2. To create scaffolds containing cells for biomedical applications, 3D bioprinting has remarkable advantages over conventional scaffold fabrication methods, and even over the 3D printing technique. In those cases, the scaffold is fabricated before cells are seeded on (Figure 1). This leads to non-uniform cell distribution (some will remain outside, and some may trap inside), prevents controlled heterogeneous cell distribution, and lead to poor cell retention and viability. Limitations of conventional methods are also low porosity, uncontrollable porosity, limited dimension, limited range of materials (few materials can be adopted for a specific fabrication method), difficulty to control the structural regularity and weak mechanical properties. The other issue in studies is that they only considered one or two aspects of the gradient structure like pores size or cell differentiation. They also lack the micro and nano-structural resemblance to native gradient tissues. Gradient scaffolds must demonstrate long-term (over 6 month) stability and functionality which is still challenging [11]. In contrast 3D bioprinting allows: 1) controlled cell seeding and distribution within the macroporous scaffold, 2) controllable porosity, 3) formation of heterogeneous cell-laden structures. It permits to create scaffolds with better controlled architecture, both on the micro and macro scale, and with personalized geometry [12]. Thus, 3D bioprinting will simplify gradient cell-laden scaffold fabrication such as osteochondral (interface between articular cartilage and bone) tissue engineering [13-15].

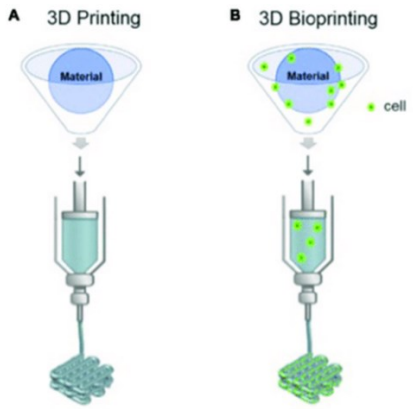

Figure 2. Schematic image of the difference of 3D printing and bioprinting; Reprinted from [16]; An open-access article distributed under the terms of the Creative Commons Attribution License (CC BY).

The primary aims of 3D bioprinting are to build a complete replacement for diseased and damaged tissues or whole organs in patients, as well as rapidly build small sized human-like tissue models or organoids (a small piece of tissue) for highly efficient diagnostics, pathological models, and drug discovery. A completely functioning bioprinted organ has not yet been achieved. Small-scale organoids, on the other hand, are now being used for a variety of purposes, including drug delivery [17, 18].

Nowadays, various 3D bioprinting machines have been designed and commercialized, which provide different printing modalities. 3D bioprinting modalities can be divided into several classes, including drop-on-demand bioprinting (inkjet bioprinting and laser-assisted bioprinting), extrusion-based bioprinting, and stereolithography, as shown in Figure 3.

2.3 Bioprinting Technologies

Several 3D bioprinting methods have been developed to manufacture highly functioning 3D tissues as shown in Figure 3, each with a distinct resolution and dimensions. Here main bioprinting techniques are reviewed. To be mentioned that this Ph.D. focuses on the extrusion-based bioprinting, therefore it is explained more comprehensively than other bioprinting techniques.

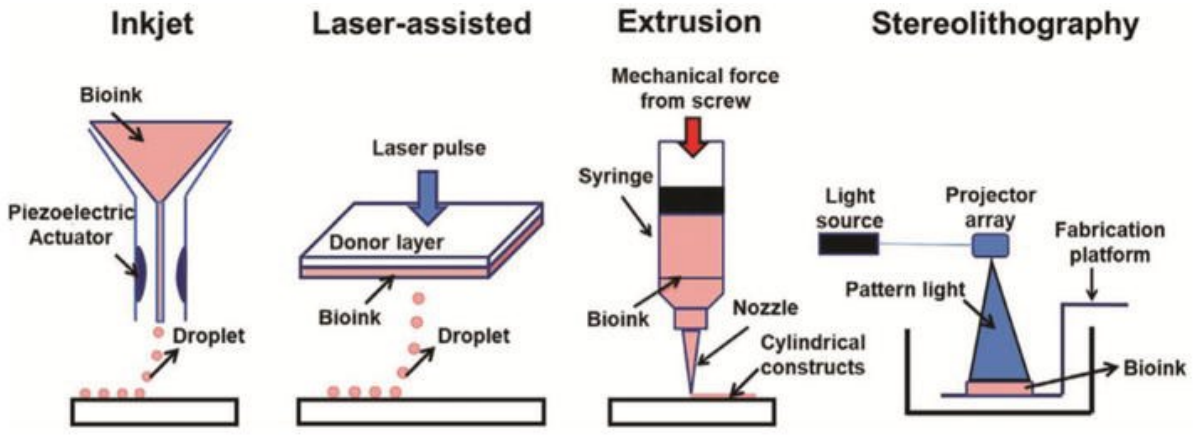

Figure 3. Schematic image of various 3D bioprinting technologies mainly include drop-on-demand bioprinting (inkjet, laser-assisted), extrusion and stereolithography; Reprinted from [19]; An open-access article distributed under the terms of the Creative Commons Attribution License (CC BY).

2.3.1 Drop-on-demand bioprinting

Drop-on-demand bioprinting ejects drops of a bioink precisely and with high speed from the printhead to form a 3D scaffold. Drop-on-demand bioprinting is classified into two main categories namely inkjet-based bioprinting and laser-assisted bioprinting. Herein, we explain them shortly.

- **Inkjet-based bioprinting**

Inkjet-based bioprinting technology consists in ejecting cell-loaded drops using thermal or piezoelectric actuators [20]. The approach highly relies on the bioink properties rather than printing machine parameters e.g., speed, pressure, nozzle tip, and substrate distance. As a result of this dependency, it is necessary for bioink to present low viscosity or fluid enough to allow the formation of droplets and deposition through the cartridge but also support itself mechanically after printing (deposition) [21]. The advantage of this modality is a micrometer resolution (10–100 μm) which is better than extrusion-based systems [22, 23]. The bioprinting procedure does not induce any remarkable damage to cells and has around 90% cell viability [24, 25]. In spite of several advantages, there still some limitations such as the limited number of bioinks (low viscosity bioinks only), weak mechanical strength of bioprinted structures, and limitations on the constructs size [26]. Drop dispensing of hydrogels without clogging and high resolution of deposited drops are still challenging [20].

- **Laser-assisted bioprinting**

In laser-assisted bioprinting, a nanosecond laser pulse is used to propel the bioink toward a receptive substrate by the rapid thermal expansion of the metallic layer [27]. Laser beam does not interact directly with bioinks. This improves the reproducibility with controlled propelled quantity. A nozzleless bioprinting prevents applying mechanical stress to the encapsulated cells, resulting in high cell survival (>95%). The system can also provide excellent resolution (>20 μm) [27, 28]. Not necessarily low viscosity bioink is required [29-33]. But the control of printing parameters in this method is challenging [34]. Moreover high resolution and intensity laser diodes are costly [35].

2.3.2 Stereolithography

Stereolithography (SLA) is a nozzle free process that uses photosensitive or photocurable inks to create 3D constructs through light mediated chemical reactions [36]. In this method, polymer deposition is followed

by exposition to ultraviolet (UV) light with the spectrum of 300–400 nm after curing of first layer, the printing is repeated to build multi layered scaffold. SLA technology provides advantages of precise control, determined geometry and high resolution of about 1.2-200 μm. It also has some drawbacks including photoinitiators used to cure photopolymers. The photoinitiators induce radical polymerization via hydrogen abstraction, photocleavage, and cationic photopolymerization where cationic photoinitiators are not utilized for tissue engineering because of the toxic by-products generation [37]. Some commercialized SLA based bioprinting technology are BioBots and FABION bioprinters.

2.3.3 Extrusion-based bioprinting

The extrusion-based bioprinting is a controlled bioink deposition using an automatic robotic system applying pressure for bioink extrusion to form cylindrical filaments. The speed of printing and deposition is low in comparison to other biofabrication techniques (1-10 μm s^{-1} to 700 mm s^{-1} in extrusion-based bioprinting vs 100,000 droplets s^{-1} in inkjet printing) [22], which can be a problem for cell viability when building large structures [38]. Moreover, this method has limited resolution (>100-200 μm). Hence, cells precise patterning is difficult [39]. However, extrusion-based bioprinting has also big advantages. Bioprinting high cell density is one of them [40]. Moreover, the range of acceptable viscosity is very large (30 mPa.s–6×10^7 mPa.s) [22]. Therefore, a broad range of biomaterials can be utilized, including melt polymers e.g., polycaprolactone (PCL) [41], cell aggregates [42, 43] and cell pellet [44], cell-laden hydrogels [45] and hydrogels combined with decellularized matrix components [46]. Nowadays, most commercialized bioprinting systems use extrusion-based bioprinting e.g., NovoGen MMX bioprinter, Fab@ Home, 3D Discovery® of RegenHU (the bioprinting system used in this Ph.D., that is shown in Figure 4), Biofactory, 3D Bioplotter of EnvisionTEC, BioBots, Bioassembly Bot, Cellink and BioScaffolder. Systems mostly are pneumatic microextrusion-based, except NovoGen MMX bioprinter and Fab@ Home printing system which are piston microextrusion [47] and RX1TM Bioprinter (Aspect Biosystems) using microfluidic print heads. For all these reasons, we will concentrate on extrusion-based bioprinting in this PhD.

Figure 4. Image of 3D Discovery® of RegenHU bioprinted used in this project.

Rheological properties are key properties of bioinks used for extrusion-based bioprinting. Indeed, the shear stress applied on cells on the nozzle tip wall may reduce cell viability (generally around 40-80% cell viability). Therefore, bioink should possess shear thinning properties, which will be explained in detail in section 2.5.1. Moreover, the bioink rheological properties strongly influence bioprinting quality and resolution. Therefore, rheological concepts and methods will be further detailed later (section 2.9) [40, 48].

2.3.4 Combination of droplet-based and extrusion-based modalities

Modern 3D bioprinters often combine different types of technologies in a single device. Thus some companies offer inkjet-based, extrusion-based bioprinting and even electrospinning facilities in one machine, or propose multi-functional and multi-print heads printing devices [49, 50] as shown in Figure 5. For instance, the 3D Discovery® (RegenHu) or GESIM combine extrusion-based and inkjet print head which can be used on a same construct. More generally, there is a rapidly growing number of commercialized and home-made bioprinters, all with their particular features and strength or weaknesses. The cost also largely varies from simple cost-effective extrusion-based systems, such as Cellink or Bioplot,

to complex platforms combining up to 4-6 print heads with different modalities such as 3D Discovery® (RegenHU), Bioplotter (EnvisionTEC) or Bioscaffolder (GESIM).

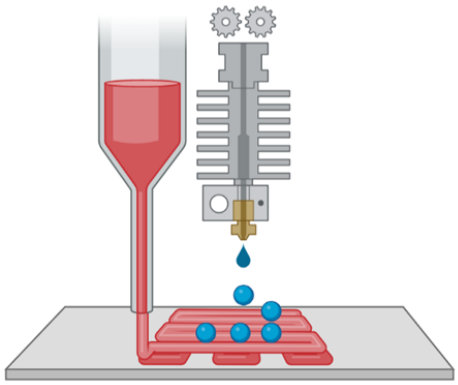

Figure 5. Multi-print heads bioprinting at a same time, one as a support structure and the other as a bioink filling the support structure (prepared using www.biorender.com).

2.4 Freeform reversible embedding of suspended hydrogel (FRESH) bioprinting method

Printing of soft, low viscosity biomaterials with slow polymerization or gelation in air often results in poor shape fidelity and resolution. To address this problem, the freeform reversible embedding of suspended hydrogels (FRESH) approach has emerged, which allows extruding biomaterials solution within a support bath [51, 52] (Figure 6). Feinberg AW team introduced the FRESH bioprinting approach in 2015 [53]. The support bath assists the biomaterials' rapid crosslinking or gelation in situ and holds them in place until the crosslinking completes without diffusing away. When a bioink is printed in air, gelation or solidification must occur very fast to prevent the printed filaments spreading or collapsing. Using FRESH bioprinting, there is a larger time window for gelation e.g., thermogelation, and bioink evaporation is avoided. It is a temporary thermo-reversible support that can be washed away after printing. Remarkable achievements obtained with this approach are e.g., a 5cm-long collagen-based human heart or a multiscale (100 µm to mm) perfusable vascular network [54].

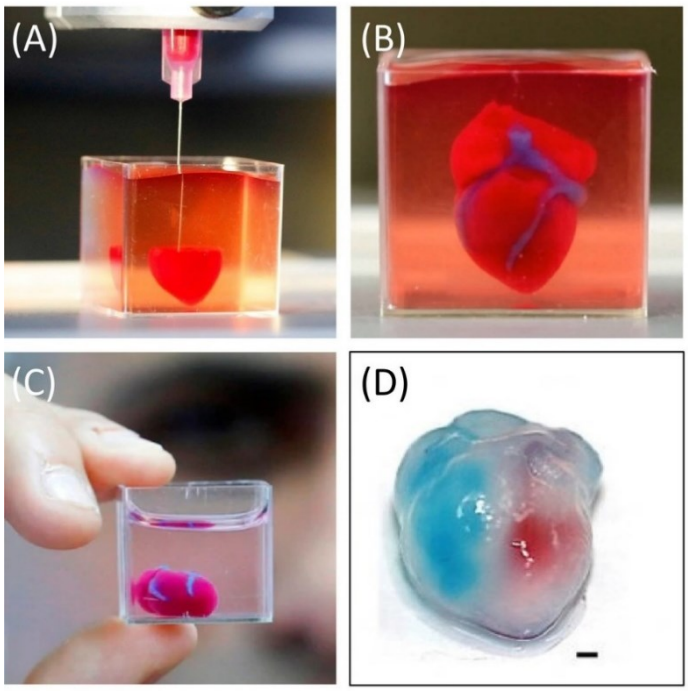

Figure 6. A) FRESH bioprinting of low viscous bioink within a gelatin microparticles support bath, B-C) FRESH bioprinted heart, and D) The bioprinted heart after support bath removal; Reprinted from [55]; An open-access article distributed under the terms of the Creative Commons Attribution License (CC BY).

In addition to cytocompatibility, the support bath must present specific rheological properties. First, the support bath should behave as a rigid body at low stresses whereas it must flow as a fluid at high stress [56]. The rheological properties of these materials are generally described by the Herschel−Bulkley model [57, 58], which will be discussed in detail in section 2.10. The literature has reported that the yield stress of the FRESH support bath should be equal to or higher than 100 Pa [58, 59]. Second, once the biomaterial is in place, the support bath should stop flowing and recover. Ideally, recovery should be quick enough to guarantee that the moving nozzle does not leave behind crevasses or air pockets [59] (Figure 7). Then, it has also been shown that the stiffness of the support bath, its storage modulus G', is of paramount importance to the process to provide adequate support for a low viscosity ink and yet allow its penetration. For more explanation about rheological requirement of FRESH bath, refer to the section 2.10.

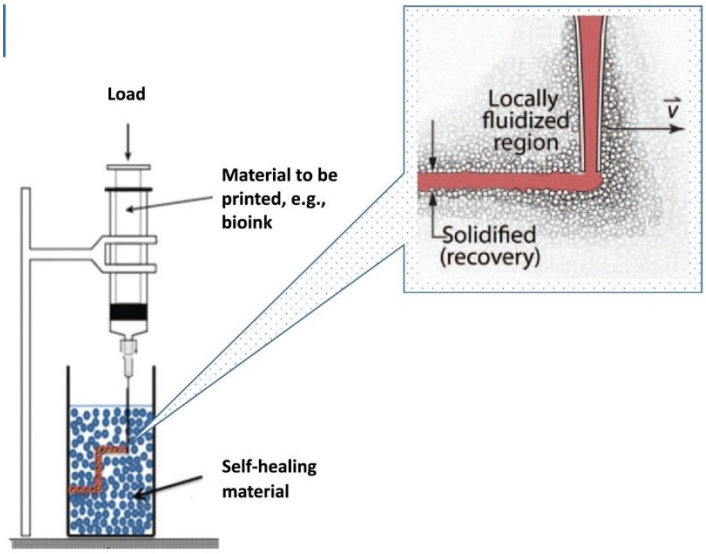

Figure 7. Bioprinting of bioink in a self-healing support bath, the support bath behaves as a rigid body at low stresses but flow as a viscous fluid at high stress when the extruder nozzle is moving; Reprinted from [60]; An open-access article distributed under the terms of the Creative Commons Attribution-Noncomercial License (CC BY).

2.5 Bioinks and Biomaterial inks

The biomaterials that are used in bioprinting systems to regenerate tissue-like structures, are categorized into two main classes namely biomaterial inks and bioinks. Herein, we will define them and explain their differences as follows.

2.5.1 Definitions and main design criteria

Bioinks generally refer to biomaterials that be considered as a cell-delivery precursor during bioprinting to create cell-laden scaffold [61]. It must have the ability to encapsulate cells and protect them during applied stress during bioprinting. In contrast, we will talk about biomaterial inks for the case where the cells are added after printing the scaffold or by another mean (for example drop by drop cell deposition of cells on an extruded biomaterial scaffold) [61, 62] e.g., PCL was printed as biomaterial ink and then filled with cell encapsulated alginate hydrogel [63, 64].

Main requirements of an ideal bioink are:

1) Bioinks must be homogeneous enough, thus show good and continuous printability without clogging and physically support the 3D printed model.

2) Bioinks must show proper rheological properties including shear thinning viscosity during printing and ability of recovery after shear removal. The required rheological properties for bioinks will be explained more in section 2.9.

3) To ensure good cell survival, the cells must be easy to homogeneously mix in the bioink solution, should not stay for long at non physiological temperatures, and should not be subjected to high shear stresses during printing. Then, once gelled, the bioink needs to present all properties required for cell survival and growth.

4) Bioinks must present biocompatibility and biodegradability without toxic by-products. Cells should survive, grow, and secrete ECM to replace the biodegradable matrix. Based on the composition of the bioink, concentration, cell culture media and temperature, the biodegradation rate of a 3D printed structure may be determined. The cell-laden structures must be able to maintain their structural integrity for a certain period of time, depending on their application [65]. For this reason, bioinks should provide cells a 3D structural support until they can produce their own ECM proteins on their own [20].

5) Bioink must provide adequate structural resolution, and shape fidelity after printing. More information will be explained in section 2.8.

6) They should provide adequate mechanical and structural support after printing.

7) They must show appropriate porosity and hydration degree for nutrition diffusion and waste removal. Porous networks containing cell-binding domains are the norm for cell survival. Using biomaterial with low porosity might inhibit cells from spreading and migrating [66].

8) In addition, bioinks must present easily manipulability and producibility by the bioprinter technique [22].

The utmost challenge is taking all these aspects into account.

Based on these requirements, hydrogels appear as interesting candidates for bioinks.

2.5.2 Hydrogels

Hydrogels are 3D networks of hydrophilic polymers that maintain large amount of water. Hydrogel can be either physical and/or chemical, depending on the bonds that form the polymeric network. Ionic interactions, high-molecular-chain entanglements, hydrophobic interactions, and hydrogen bonds all contribute to the creation of a physical hydrogel [67, 68]. In order to increase the hydrogel's mechanical strength and stability, chemical crosslinking e.g., covalent crosslinking can be employed. However, chemical crosslinking may lead to cell mortality due to chemical reagents, crosslinkers, or UV used for photopolymerization, which are toxic to the encapsulated cells [22].

Hydrogels responds to most of the design criteria described above. Their high hydration degree makes hydrogels a cell-friendly matrix, permeable 3D structure to recapitulate native ECM microenvironments. They also show tunable physical properties, biocompatibility, and biodegradability. However**, they generally present very poor mechanical properties, leading to poor resolution due to spreading of extruded filaments under the following layers.** Moreover, to be injectable, hydrogels must be either shear thinning or gel in situ. In situ gelling systems are in sol forms before entering in the body but change to hydrogel forms under a stimulus such as the change of temperature or pH at the site of injection [69]. Their gelation takes place without the use of potentially toxic crosslinking agent. One very interesting example of in situ hydrogels is thermosensitive chitosan-based hydrogels which will be discussed in detail in section 2.7.

The next section will present hydrogels previously proposed as bioink materials.

2.5.3 Injectable biomaterials and main bioinks

Injectable hydrogels generally are classified into two main categories including synthetic- and natural-based hydrogels. There are detailed in the following sections.

Synthetic-based hydrogels

Synthetic polymers are produced artificially by humans in a laboratory that are derived from petroleum-based raw materials. Biomaterials based on synthetic polymers present good reproducibility and better control on their biochemical features, mechanical properties, and printability, due to ease of tuning their chemical structure and molecular composition.

Table 1 summarizes the more commonly used synthetic hydrogels, their advantages, and limitations as well as their potential applications in extrusion-based bioprinting.

Table 1. Summary of synthetic based biomaterials mostly used in 3D bioprinting: properties and applications.

Polymer	Advantages	Drawbacks	Application	Bioprinting system	Ref.
Polyethylene glycol (PEG)	*Hydrophilic *Biocompatible *Non-immunogenic *Tunable mechanical properties *Able to be modified through various functional groups	*Low viscous to be used purely in 3D bioprinting *Inert biomaterial *Weak structures, requiring chemical modifications	Bone, Cartilage	Extrusion-based bioprinting [70], Droplet-based bioprinting [71, 72], Laser-assisted bioprinting [73]	[70, 74-81]
Polyethylene glycol dimethacrylate (PEGDMA)	*Photolable *High mechanical properties *Controllable mechanical strength by chemistry variation	*Photo initiator demand *Less cellular friendly	Cartilage, Bone	Droplet-based bioprinting [71, 72], Laser-assisted bioprinting [73]	[71-73, 82-84]
Modified_Pluronic e.g., methacrylation	*Thermosensitive *High resolution of post-printed structure	*Low mechanical strength *Fast degradation *Toxicity & poor cell viability	Drug delivery, Skin, Burn wound treatment, Cartilage	Extrusion-based bioprinting [85]	[85-90]

Polyethylene glycol (PEG), a polyether-based polymer is the most commonly used synthetic-based hydrogel in bioprinting. PEG is very hydrophilic, biocompatible, and non-immunogenic. It has tunable mechanical properties that facilitate the procedure of bioprinting and post bioprinted shape stability. Indeed, various functional groups such as acrylate, azide, thiol, carboxyl and amine can conjugate to both hydroxyl groups of PEG in order to tailor its structure and crosslink PEG backbone. It requires the modifications to be used

in bioprinting [71]. The functionalized PEG with diacrylate (DA) and methacrylate (MA) functional groups provides hydrogels with photolability properties [83, 84, 91]. PEG mechanical strength also can be tuned by chemistry variation [83]. Thus, polyethylene glycol dimethacrylate (PEGDMA) has higher mechanical properties (e.g., Young modulus, tensile strength) compared to pure PEG and natural polymers, which make it a great polymer for bioprinting, but requires exposition to UV light. Click chemistry is one of the cell-friendly modification methods, in which e.g., the thiol–ene click chemistry could be supported to produce PEG hydrogel. High cell viability was reported, though UV exposure was required [81, 92]. Another disadvantage of PEG-based hydrogels is that PEG is an inert biomaterial that does not have any domain for cell adhesion [93], and thus it requires to be blended with other proadhesive biopolymers. Moreover, it is not biodegradable.

Another most frequently studied synthetic hydrogel is Pluronic. Pluronic is a copolymer composed of poly(ethylene glycol), poly(propylene glycol), and poly(ethylene glycol) (PEO-PPO-PEO) sequences.[85]. The PPO sequence intramolecular incorporation provides temperature sensitivity property [88]. F-127 polymer is the most common type of Pluronic that is a triblock copolymer consisting of a central hydrophobic block of PPO flanked by two hydrophilic blocks of PEO. F-127 has high potential to be used in extrusion-based bioprinting technology because of its viscosity and shear thinning behaviour above 20°C; however, pure Pluronic become liquid easily by temperature decrease and is not stable enough for 3D scaffold, thus particular conditions and bioprinting systems are required including UV crosslinking and chemical modifications e.g., methacrylation [85]. Pluronic has been considered as sacrificial biomaterials including support materials [94] for vascular structure creation. Pluronic-based hydrogels demonstrated poor cell viability and support due to the inability of Pluronic bioink in safeguarding cells from bioprinting stress. For example, more than 90% bone marrow stromal cells death on the 3rd day was observed in bioprinted Pluronic hydrogels [95]. To overcome this limitation, encapsulation of bioactive compounds into hydrogels has been used [86, 96].

According to the Table 1, synthetic-based polymers lack bioactivity and are less cell friendly than natural polymers, limiting their applications as bioinks.

Natural-based hydrogels

Natural-based polymers are materials that widely occur in nature or are extracted from plants or animals. Naturally derived polymers are often used to form hydrogel bioinks, since they generally show excellent

biocompatibility for cells growth and proliferation, low toxicity, and good bioactivity. Moreover, they are generally biodegradable. Natural polymers have also some limitations such as batch to batch variability and uncontrolled degradations.

Table 2 presents the most common natural hydrogels used as bioinks in bioprinting, with their main advantages and drawbacks. The most commonly-used is alginate. Alginate has the interesting property to be quickly (almost instantaneously) physically gelled by divalent cations like as Ca^{2+} at ambient temperature, and maintains the initially biofabricated structure's shape [97]. Biocompatibility, minimal toxicity, and low cost are other advantages of this physical hydrogel. It however has strong limitations in bioprinting. Alginate hydrogels that are physically crosslinked have a short lifespan and can lose their initial mechanical strength in the physiological condition within a relatively short period of time, due to calcium (Ca) ion replacement by other ions. This necessitates additional crosslinking mechanisms to further stiffen the network structures [98]. Moreover, alginate chains are not biodegradable. In addition, alginate has a limited capacity to adhere to and interact with mammalian cells, thus the inclusion of cell adhesion peptide motifs is often performed to improve cell functions [98]. One other option to optimize the alginate bioink, is to mix alginate with other biomaterials, such as chitosan, gelatin, collagen or ECM compounds [99].

Table 2. Summary of natural based biomaterials mostly used in 3D bioprinting: properties, and applications.

Polymers	Advantages	Drawbacks	Application	Bioprinting system	Ref.
Alginate & derivatives	*Rapid physical crosslinking using divalent cations in room temperature *Controllable viscosity *Low toxicity *Good biocompatibility *Good support growth of chondrocytes & osteocytes	*Physically cross-linked alginate shows short term stability *Low mechanical strength *Low cell adhesion *Non-degradable in physiological condition *Variability & reproductivity	Cartilage, Bone, Retina, Skin, Liver, Cell encapsulation & delivery	Extrusion-based bioprinting [100, 101], Droplet-based bioprinting [102-108], Laser-assisted bioprinting [109-111]	[64, 98, 101, 112-116]
Hyaluronic acid & derivatives	*Good biocompatibility *Controllable biodegradation *Excellent response to chondrocytes	*Chondrocytes inflammation involvement *Low mechanical properties *Slow gelation *Low stability in physiological condition	Cartilage, Skin	Extrusion-based bioprinting [117-119], Laser-assisted bioprinting [120]	[80, 121-124]
Gellan gum & derivatives	*Thermally reversible hydrogel *Good biocompatibility *Inexpensive *Good processability	*High gelation temperature *Low Young modulus of physically cross-linked gellan gum *Loss stability & mechanical strength in vivo *Long term biodegradation	Bone, Cartilage, Brain like tissue	Droplet-based bioprinting [125], Extrusion-based bioprinting [126]	[45, 125, 127]
Collagen & derivatives	*Thermosensitive hydrogel *Immunoisolation effect on the encapsulated cells *Cellular adhesion	*Low mechanical properties *Low viscosity of pure collagen * immunogenicity & risk of virus and prions transmission	Cartilage, Skin, Bone	Droplet-based bioprinting [128-130], Extrusion-based bioprinting [131], Laser-assisted bioprinting [132]	[129-135]
Chitosan & derivatives	*Good biocompatibility *Good biodegradability *Hemostasis *Wound healing acceleration *Antimicrobial *Similarity to glycosaminoglycans	*Not soluble in water under physiological condition *Low cell adhesion *Low mechanical properties	Cartilage, Skin, Bone	Extrusion-based bioprinting [136-141]	[136-139, 142-145]

Gelatin & derivatives	*Promote cell adhesion & remodeling *Gelation in low temperatures *Biocompatible *Biodegradable *Non-immunogenic	*Lack of stability in 37 ºC for physically cross-linked gelatin *Toxicity for chemically cross-linked gelatin *Low stress shielding	Bone, Cartilage, Liver, Cardiac tissue	Extrusion-based bioprinting [97], Laser-assisted bioprinting [146, 147], Droplet-based bioprinting [148, 149]	[150-156]
Agarose & derivatives	*Thermally reversible physical hydrogels at 17-40 °C *Biocompatible *Good stress shielding	*Inert biomaterial *Highly viscous hydrogel	Cartilage, Bone, Nerve graft	Extrusion-based bioprinting [82], Laser-assisted bioprinting [157], Droplet-based bioprinting [158]	[44, 82, 157, 158]
Dextran & derivatives	*Bio & cytocompatible *Enzymatically degradable *Able to be modified through variety of methods	*Inert biomaterial	Skin, Cartilage, Cancer tissue model	Droplet-based bioprinting [159], Extrusion-based bioprinting [160]	[159-161]
Matrigel & derivatives	*Promote cell growth and differentiation *Promote faster vascularization *Good cell viability *Have bioactive compounds	*Expensive *Immunogenic *Non-reversible thermosensitive polymer	Bone, Cardiac tissue, Skin, Bladder, Kidney, Drug discovery platforms/Microfluidic	Extrusion-based bioprinting [162-164], Laser-assisted bioprinting [165]	[95, 162-165]

Other commonly used natural polymers are hyaluronic acid, collagen, gelatin etc. Hyaluronic acid (HA) is a main component of ECM. HA-based hydrogels are one of the most appealing biomaterials because HA is the most abundant polysaccharide in the human body and is biocompatible [166]. However, its interest in bioprinting is limited due to its poor mechanical properties which results in poor shape fidelity [167]. It also undergoes fast hydrolysis at physiological environment because of its hydrophilicity.

Collagen is the most plentiful structural protein of the ECM containing arginine-glycine-aspartic acid (RGD) domains which provide cell binding support [88]. Collagen has the potential to safeguard encapsulated cells during bioprinting over 85% of cell viability [84]. However, pure collagen bioink printing is challenging due to its low viscosity, resulting in poor shape fidelity (spreading on surface and thick width filaments which is much larger than needle inner diameter). Physical crosslinking of collagen can increase shape fidelity. Physically crosslinked collagen hydrogel; however, presents low mechanical properties, rapid degradation and shrinkage in the presence of cells, leading to the loss of the bioprinted structure. Another limitation of collagen is its possible immunogenicity and risk of transmission of virus and prions

responsible for neural degenerative diseases such as Creuzfeld Jacob [168, 169]. In this regard, gelatin is recommended.

Gelatin is a hydrolysis product from collagen. It contains a number of RGD sequences promoting cell adhesion, and facilitating cell remodeling [170]. Although gelatin bioink is a cell friendly and supportive, its stress shielding properties to safeguard cells from bioprinting stress are low [86]. In addition, gelatin is rarely 3D bioprinted as native pure hydrogel because of poor mechanical properties, poor resolution and shape fidelity, because it liquifies at body temperature.

Gellan gum, a water-soluble anionic polysaccharide is another natural polymer which is produced by bacteria. Its interest in bioprinting comes from its thermally reversible gelation processes similar to gelatin. However, three key issues may limit their clinical applications: 1) the gelation temperature is higher than 42 °C, which may impact adversely the cell viability during the gelation process [125]. 2) the physically crosslinked gellan gum hydrogels showed Young's modulus of <5 kPa, which is much lower than the native cartilage tissues (≥60 kPa) [125]. 3) Gellan gum hydrogels loss their stability and initial mechanical properties in vivo due to exchange of divalent cations with monovalent ions presenting in physiological solutions [125].

Agarose is a polysaccharide, isolated from red algae and seaweed. It lacks native ligands which allow cell-material interactions. Therefore, cells could not spread within the pure agarose scaffold due to no cell adhesion and retaining to a round shape, but they showed good cell viability [82].

Dextran is also used frequently in bioprinting. Dextran is non-toxic, highly water soluble, with Newtonian fluidic behaviour. However, dextran is an inert biomaterial often used to prevent protein adsorption and coagulation [171].

Other natural bioink used in extrusion-based bioprinting is Matrigel. Matrigel is a gelatin like protein mixture produced by mouse Engelbreth-Holm-Swarm sarcoma cells. Matrigel degrade in lower rate in physiological condition. It has showed high cell viability thanks to its bioactive compounds. However, it is an expensive bioink [172]. The major limitation of matrigel is its obtained source which is murine sarcoma cells, hence, it cannot be used for in vivo implantation due to immunological response [173].

Although most natural hydrogels explained above suffer from non-biodegradability and poor mechanical properties. Chitosan (CH) has been also proposed by several teams as an injectable cell-laden hydrogel,

especially for cartilage tissue engineering due to its good biocompatibility, biodegradability, as well as antimicrobial properties [67, 174-176]. Moreover, this polysaccharide shows similarity to the main component of the cartilage chemical structure, GAGs and promote the survival and growth of chondrocytes for up to 3 weeks [177-179]. The chitosan positive charges interact electrostatically with ECM molecules negative charges like glycosaminoglycans, which consequently links with growth factors and cytokines in order to balance the cellular fate procedures [67]. But chitosan has a poor cellular adhesiveness for adhesion, proliferation, and the development of the ECM [180]. Several modifications can be proposed to tune the mechanical properties, water solubility, gelation properties, cellular activity, and particular biological behavior for articular tissue defects repair [181-183]. It can form bioinks in combination to other materials to form polyelectrolytic complex [184]. More interestingly, as will be discussed in further details later, it is also able to create strong thermosensitive hydrogels, which form solution with physiological pH at room temperature and gel at body temperature.

2.6 Chitosan hydrogels

Chitosan is a polysaccharide composed of randomly distributed N-acetyl-glucosamine and N-glucosamine units, produced by the deacetylation of chitin, which is found in shrimp and crab shells. It is considered as chitosan when the number of deacetylated (N-glucosamine) units are higher than 50% (Figure 8). In addition to its molecular weight, the percentage of deacetylated groups (DDA) is an important parameter. Among other things, the DDA can be changed to tune its biodegradation rate. Chitosan is not expensive since it derived from chitin, the second most abundant natural biopolymer.

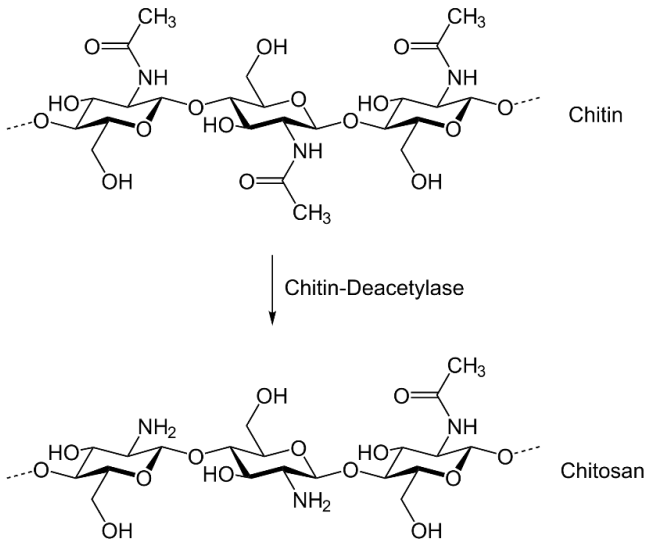

Figure 8. Chemical structure of chitosan, deacetylated form of chitin (Image Reprinted from https://en.wikipedia.org/wiki/Chitosan).

However, chitosan has a pK_a around 6.5 and is therefore not soluble in water under physiological conditions [185] which would be required for cells. It can be dissolved in acidic conditions and form hydrogels when mixed with a basis such as NaOH. But cell addition is then difficult. In early 2000, Chenite proposed a way to form neutral chitosan solutions that present thermosensitive properties and gel at body temperature, by mixing it with weak basis such as beta-glycerophosphate (BGP) [186, 187]. These unique properties make these materials very interesting candidates as cell-loaded injectable scaffolds and potential candidates for bioprinting, despite some limitations. The thermosensitive chitosan-based hydrogels will be explained comprehensively in the following section.

2.7 Thermosensitive chitosan-based hydrogels

2.7.1 CH-BGP hydrogels

As explained before, chitosan is a semi-crystalline biopolymer with no solubility in water. Solubility in acidic solutions can occur because of free amino groups protonation. Briefly, chitosan is dissolved in acidic solvent such as hydrogen chloride (HCl) because of its cationic chemical structure which is protonated in pH lower than its pk_a ~ 6.5, produce repulsion between polymer chains, thus can solubilize. Chenite el al. proposed to mix chitosan acidic solution with a weak base such as BGP with similar pk_a to chitosan (pk_a

=6.34), to form thermosensitive hydrogels (Figure 9) [186]. BGP screens the protonated amino groups, enabling to form a solution of neutral pH while preventing precipitation. When temperature increases, protons from CH to glycerol phosphate are transferred by heat, which lowers the repulsive interactions between amino groups and enables CH chains to connect through hydrophobic interaction and hydrogen bonding [188]. They can therefore form gel at body temperature and higher as presented in Figure 9B.

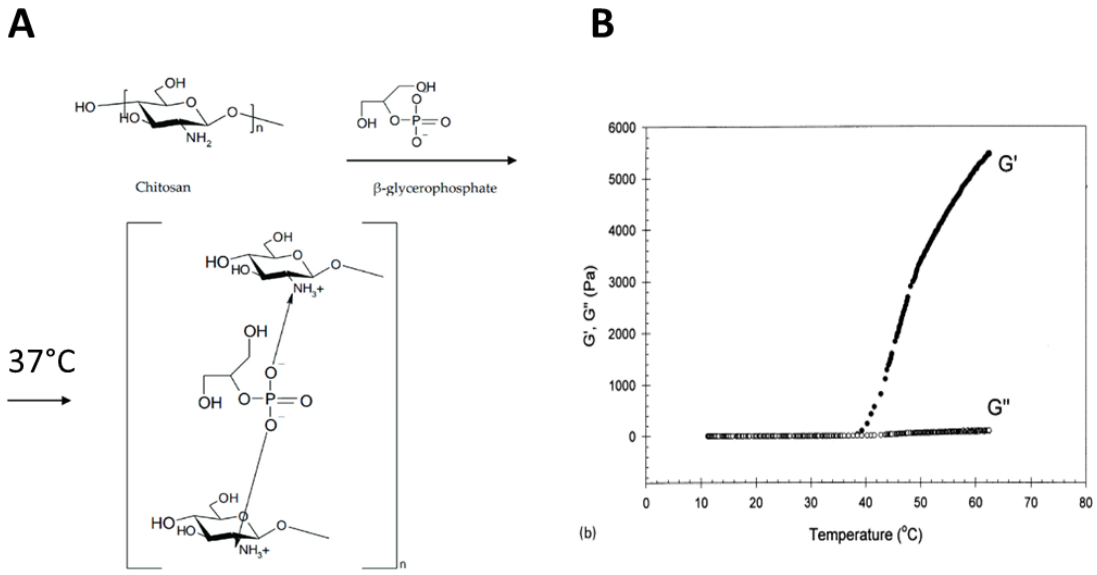

Figure 9. A) Chitosan gelation with beta-glycerophosphate with temperature increase to 37°C (Reprinted from [189]; An open-access article distributed under the terms of the Creative Commons Attribution License (CC BY)); B) Thermogelation with temperature increase of CH-BGP hydrogel (Reprint and Copyright (2021) with permission from Elsevier Inc. [187]).

CH-BGP gels have been employed in a variety of applications, including as drug and cell-loading hydrogels [190, 191]. However, their poor mechanical characteristics and slow rate of gelation make them undesirable for many applications. The gelation process may be sped by increasing the BGP concentration, however this drastically reduces the hydrogel's cytocompatibility and does not enhance its mechanical strength [192, 193]. This strongly limits their potential as a cell-laden hydrogel.

A few studies have been performed to evaluate the potential of CH-BGP hydrogels as bioink [141, 194]. CH-BGP bioinks with low viscosity provide excellent cell viability, but the slow gelation and the poor

mechanical properties after printing and even after gelation resulting in very poor shape fidelity and post-printed mechanical properties [141, 170]. To solve the problem, methylcellulose and cellulose nanocrystals (CNC) were added to the gel, leading to better resolution but the mechanical properties were only slightly increased (storage modulus increasing from 100 to 250 Pa) [140]. **Thus, despite their evident advantage, there is still no adequate thermosensitive chitosan hydrogel bioink. Further studies are needed to assess their bioprintability and optimize them for extrusion-based bioprinting.**

2.7.2 New chitosan thermosensitive hydrogels

To address above-mentioned issues, Lerouge lab`s proposed to use a new mixture of gelling agents such as sodium hydrogen carbonate (SHC) with phosphate buffer (PB) or beta-glycerophosphate (BGP) with same pK_a as chitosan at room temperature [188]. Their mixture with chitosan solution can neutralize the pH, and increasing mechanical properties of chitosan hydrogel through physical crosslinking at 37°C [67, 195] (Figure 10). For example, the pk_a of sodium hydrogen carbonate (SHC) is 6.33 independent of temperature [196], at room temperature, chitosan's ammonium cation (NH_3^+) is screened by SHC. Chitosan's pk_a decreases as the temperature rises, causing SHC to react with NH_3^+ and release carbon dioxide (CO_2) (Equation 1). A strong 3D network is formed by a more complete neutralization of chitosan chains due to the small size of SHC molecule and stronger interactions due to its decomposition into CO_2. While this physical gelation mainly takes place at a temperature close to body temperature because of the chitosan pk_a change, it initiates at room temperature with some ionic crosslinking [197].

$$ChitosanNH_3^+ + HCO^- \rightarrow chitosanNH_2 + H_2O + CO_2 \nearrow \quad \text{Equation 1}$$

The CH-SHC enhance the mechanical properties of the hydrogels, while ensuring physiological osmolality and rapid gelation at 37 °C [67, 68]. These gels show excellent cell survival and growth and were presented as very promising candidates for injectable cell-loaded scaffolds for cell therapy and tissue engineering [68].

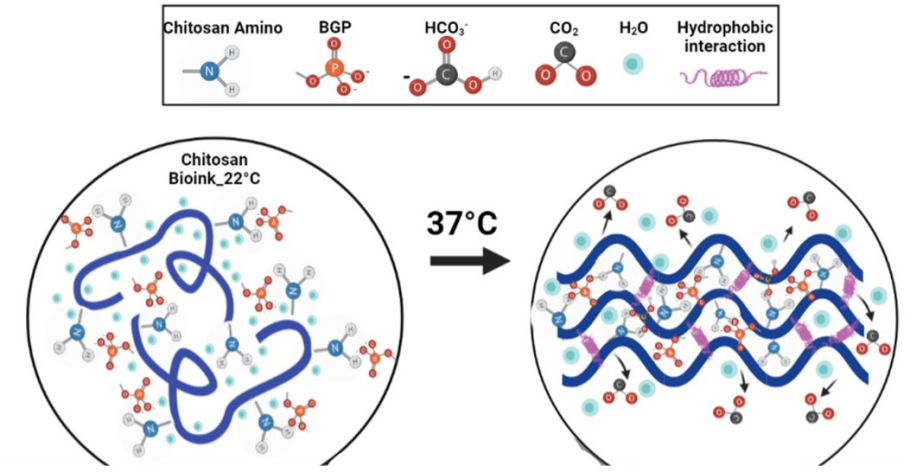

Figure 10. Thermogelation mechanism of the chitosan-based hydrogels prepared in Lerouge lab (prepared using www.biorender.com).

2.7.3 Chitosan bioinks and injectable hydrogels for mineralized tissues bioprinting

As mentioned in the introduction, bioprinting cartilage requires to bioprint its interface with bone tissues to ensure fixation. It is also explained that chitosan is a particularly appealing biomaterial for cartilage tissue engineering. Chitosan hydrogels lack inherent osteoconductivity and osteointegration with surrounding bone tissue, but it is possible to add bioceramics e.g., hydroxyapatite or bioactive glass, to enhance osteoblasts growth and promote bone formation [198-200].

Bioactive glass

Among the inorganic ceramics, bioactive glass (BG) is one that has received extensive attention, because of particularly its ability to bond with living tissues [201]. Hench et al. termed certain silicate-based glass compositions as “bioactive” for their ability to bond chemically to rat bone. Hench made a degradable glass in the Na_2O-CaO-SiO_2-P_2O_5 system. The composition of first FDA-approved in 1985 contains a silicate network 45 wt% SiO_2, incorporated with 24.5 wt% CaO, 24.5 wt% Na_2O, and 6.0 wt% P_2O_5, that was later termed 45S5 Bioglass. This bioglass bonded so strongly to the bone that it could not be removed without breaking the bone [202, 203]. It showed faster proliferation of osteoblasts and bone formation than hydroxyapatite particles. Moreover, higher bioactivity was reported due to ion release and rich silica layer

formation in comparison with hydroxyapatite. Growth factors and cell proliferation may be stimulated by BG degradation products. The gene expression of osteoblast can also be activated by these molecules [204].

CH-BGP-BG

In CH-BGP hydrogels, extracellular-related kinase phosphorylation promotes mineral deposition and osteogenic activity [205]. However, the osteoconductivity and osteointegration properties can be solved by combination of bioactive glass. Osteoconductive biomaterials allow bone growth on the scaffold's surface and down into pores and channels [206]. They assist in the adhesion and multiplication of osteoblast cells; leading to in vitro development of mineralized bone matrix in chitosan-based biomaterials [207, 208]. CH-BGP hydrogel mechanical characteristics were enhanced by adding 2% BG from storage modulus (G') of 6.56 ± 0.12 Pa to 9.11 ± 0.15 Pa at 37 °C, corresponding to a 39% increase in stiffness [209, 210]. However, mechanical properties are still far from ideal. An in-situ injectable thermosensitive chitosan-collagen-BGP hydrogel in combination with BG (0-2%w/v) was reported for bone tissue engineering with promoted bioactivity [210]. Later, by combining chitosan-gelatin-BGP with nano-BG, a thermosensitive hydrogel with enhanced elastic modulus and improved viscoelastic properties was developed [209]. The hydrogel promoted proliferation of osteoblasts and angiogenesis gene expressions, resulting in bone regeneration after in vivo injection [211]. However, low BG concentration is used since higher BG concentration affects the mechanical property adversely, meaning no proper gelation is taken place. Consequently, it negatively impacts the cell survival. This limits engineering of bioactive cell-laden structure, requiring further studies and new approaches. Therefore, **an osteoconductive bioink with adequate mechanical properties is still missing.**

2.8 Printability (resolution, fidelity, mechanical properties, cytocompatibility)

Among the design criteria of a bioink, an important one is printability. Printability is defined as the ability of a bioink to form a reproducible 3D scaffold without any clogging during the injection, resulting in printing an accurate, fine and high-quality pattern [20, 212]. Design parameters (such as filament width, orientation and layer thickness), bioink rheological behaviour, and printing procedure are three main classes that influence printability [212].

One way to assess printability is by looking at the shape and uniformity of the extruded filaments as shown in Figure 11. Using non-uniform bioinks results in deviated extrusion lines from the desired structure or

even curling up and adhering to the dispensing nozzle that decreases the resolution. Thus, only small and simple structures can be printed, rather than complex and large scaffolds.

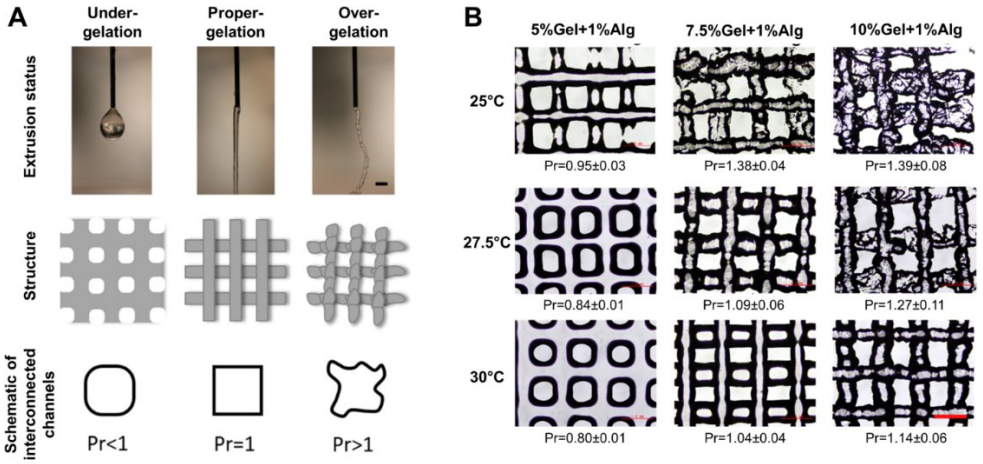

Figure 11. Quantitative study of filaments uniformity during extrusion; Reprint and Copyright (2021) with permission from IOP Publishing [213].

When discussing bioink printability, the term "shape fidelity" is the key one. Shape fidelity is the capacity of a bioink to keep its shape after it has been printed and covered with new layers. Bioinks with poor shape fidelity result in spreaded filaments with very limited thickness or height. As additional layers are added, geometries may collapse as a result of their own weight [75]. The shape fidelity of bioink has been measured using the printed filament itself (width, height or thickness using a single layer (Figure 12). A narrower filament width (and hence less spreading) was shown to be the most significant element in these analyses. Printability was evaluated based on which bioink formed the thinnest filaments [184, 214-216]. Other features commonly used to assess shape fidelity include circularity of pores in printed structures. Low pore circularity shows higher printability, as the pores are similar to the computer-aided design (CAD) shape [213].

In addition to bioinks properties, width and thickness of the printed filaments directly correlate to the printing parameters including pressure [214, 217], flow rate [218], feed rate [218], nozzle height [218, 219], and nozzle diameter [214]. Similar to shape fidelity, the width and height can also define the resolution, in a way that refers to the thinnest printed filaments. Shape fidelity and resolution affect the printed scaffold's mechanical properties and performance.

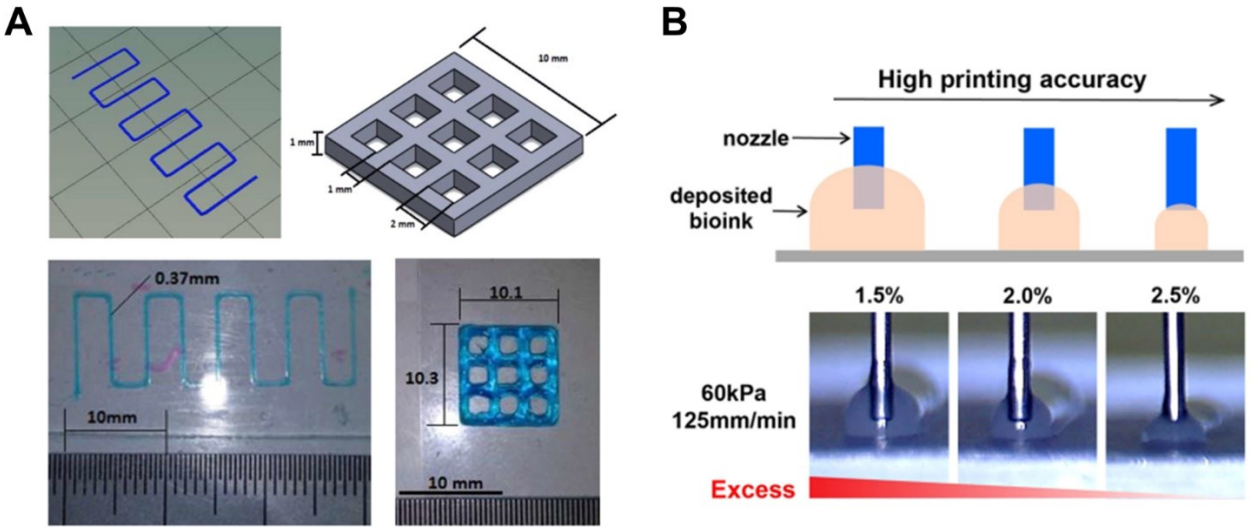

Figure 12. A) filament width, and thickness using a single layer assessment (Reprint and Copyright (2021) with permission from Elsevier Inc. [215]); B) improved printability resulting from different extruded bioinks (Reprinted from [220]; An open-access article distributed under the terms of the Creative Commons Attribution License (CC BY)).

Cell viability is also related to printability. Indeed, cell viability in a hydrogel is affected by the bioink's concentration and type, temperature, and time of culturing, but also by the printing process itself [221]. The use of very viscous hydrogels is common to achieve structures with excellent shape fidelity. But extruding them may require the use of high applied shear stress, which may harm cells encapsulated in the hydrogels. The relationship between cell viability and shear stress will be discussed more later, but it highlights the importance of shear thinning properties of the bioink. More generally, for extrusion-based bioprinting, the rheological parameters of a bioink candidate are critical [222]. The next section presents the important rheological concepts related to bioprinting.

2.9 Rheological concepts

2.9.1 Theory

Rheology is the study of the flow and deformation of a material under the influence of an external force. Rheometry is the measuring technology used to determine rheological properties. The rheological properties of a bioink will not only control their printability, but also the survival of the cells encapsulated within them.

Indeed, as stated before, the bioink should reduce as much as possible the effect of shear stresses on encapsulated cells during extrusion through the nozzle. Blaeser et al. pointed out that the shear stress applied during the extrusion procedure should be taken into consideration for improving printing resolution and cell viability [223]. The rheological properties, the size of the nozzle and the applied stress used for bioprinting of the hydrogels [223] are the main factors determining the shear stress exerted on the cell-laden hydrogels.

It is also possible to employ rheometry to characterize the mechanical behaviour of viscoelastic materials such as hydrogel bioinks and to investigate how temperature or exposure to a crosslinking agent affects the gelation of the bioink. In the case of chitosan thermosensitive hydrogels, for instance, the gelation kinetics at room temperature and 37°C could be studied using time sweep [67, 68, 195]. Although all the previous investigations have shown most common rheological studies of a candidate bioink to control and predict the printability, **the rheological characterization of time- and temperature-dependent hydrogels such as thermosensitive chitosan-based hydrogels are still not clear**, leading us to the first objective of this Ph.D. Here, the important and basic rheological parameters that may have remarkable effect on the bioink's printability are summarized here.

Bioinks present viscoelastic behaviour (displaying both solid-like and fluid-like characteristics), which can be characterized by rheometry using oscillatory testing, where the complex modulus (G*) can be decomposed in a storage and loss modulus. The storage modulus (G') is representative of solid-like behavior and shows that how much energy is required in order to distort it. In contrast, fluid-like behavior is represented by loss modulus (G") measuring energy lost during stress or strain sweep. It is important when measuring the viscoelastic characteristics, that the measurements are made in the material's linear viscoelastic region (LVR), where stress and strain are proportional. In the LVR, applied stresses are insufficient to cause damage of the structure. When applied stresses exceed the yield stress, non-linearities appear and material breaks. LVR is illustrated by dotted line in Figure 13.

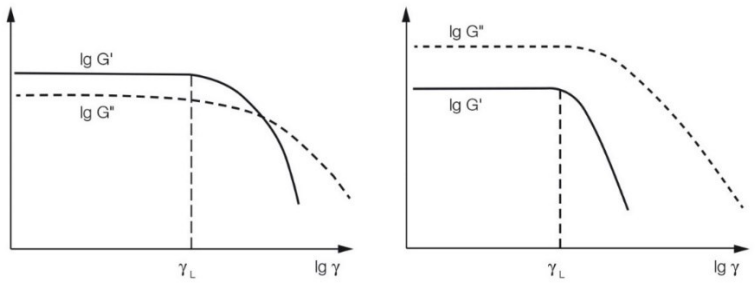

Figure 13. Schematic image showing linear viscoelastic region for both gel-like and solid structure using vertical dotted lines (Image Reprinted from https://wiki.anton-paar.com/ca-en/amplitude-sweeps/).

Both oscillatory and rotational modalities are used to study rheological behavior of the biomaterials. Here, we will present the basic rheological concepts.

Viscosity

Viscosity is the resistance of a fluid to flow under an applied stress. It relates the shear rate to the shear stress (Equation 2).

$$\eta = {}^{\tau}/_{\dot{\gamma}} \qquad \text{Equation 2}$$

Where the τ is shear stress (Pa) and $\dot{\gamma}$ is shear rate (s^{-1}). Biomaterial's flow behavior can be categorized as either Newtonian or non-Newtonian. Newtonian biomaterials present linear relationships between shear rate and shear stress (Figure 14), the viscosity being independent of the shear rate. Non-Newtonian materials show either shear thinning i.e. their viscosity is decreasing with the shear rate, or more rarely shear thickening behavior, i.e. the viscosity enhances with the shear rate [224] (Figure 14). It is generally recognized that good bioinks should present a reduction in viscosity during flow (shear-thinning behaviour) [225, 226] to therefore reduce the shear stress during printing. More shear thinning behavior results in less applied stress to the encapsulated cells.

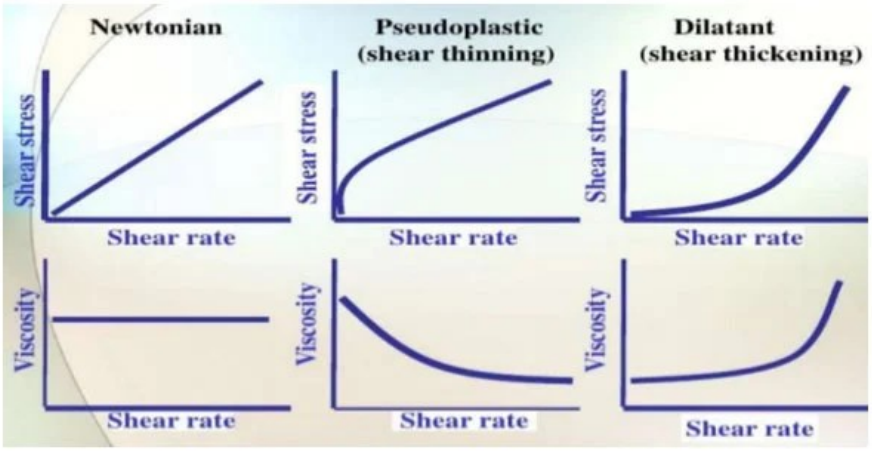

Figure 14. Schematic flow behavior (viscosity) curves of Newtonian, and non-Newtonian (shear thinning, shear thickening materials) (Image Reprinted from https://knowledge.ulprospector.com/9796/pc-better-performance-through-rheology/).

It is the composition and bonds between the macromolecular chains of hydrogels that define its viscosity. To keep a 3D printed construct in its intended form, the hydrogel must present sufficient viscosity in static condition. However, hydrogels with high concentrations have been shown to inhibit cell growth [227, 228]. Thus, to retain the geometry of a 3D printed construct, it is essential to utilise a hydrogel with low concentrations but high viscosity [229].

Shear stress

The hydrogel is subjected to shear stress throughout the extrusion process. The shear stress imposed on the bioink and embedded cells is determined by printing factors including printing pressure, nozzle diameter, and bioink viscosity [230, 231], which relates the shear rate to the shear stress.

Shear stress plays a crucial role in cell performance [232]. The more force needed to print a bioink, the more shear stress the encapsulated cells within the bioink will experience and the more cell death and damage will be caused during bioprinting [213, 218]. Several studies have demonstrated the relationship between the viability of cells and the applied shear stress, as seen in Figure 15 [231, 233].

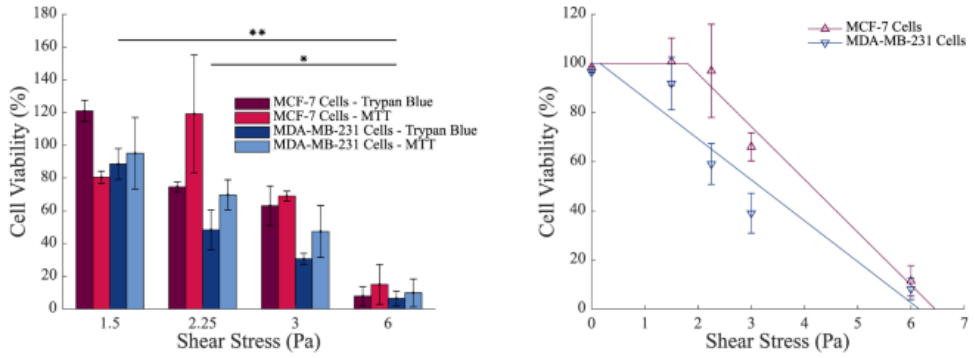

Figure 15. The relation of applied shear stress and cell viability (Reprinted from [233]; An open-access article distributed under the terms of the Creative Commons Attribution License (CC BY)).

To evaluate the shear stress encountered, it is important to know (1) the shear rate during extrusion, and (2) the viscosity of the material at this shear rate. Non-Newtonian bioinks passing through a needle during extrusion are exposed to a shear rate ($\dot{\gamma}_\omega$) described by Equation 3 [234]:

$$\dot{\gamma}_\omega = \frac{4Q}{\pi R^3}\frac{3n+1}{4n} \qquad \text{Equation 3}$$

where Q ($mm^3\ s^{-1}$) is the flow rate; R (mm) is the inner radius of the needle; and (n−1) is the slope of the log-log graph of viscosity versus shear rate rate, n is also known as the power low index. Then, using Equation 2, shear stress can be calculated.

When the rheological characteristics of hydrogels are time dependent, however, rheological evaluation might be complicated. It is not suitable to use a simple shear rate sweep (viscosity as a function of changing shear rate) [234]. Because the viscosity varies with time in these circumstances, the tests must be adjusted accordingly. Whilst most groups use temperature sweep and time sweep to study the gelation kinetics at room and body temperature, **there has been to date lack of appropriate rheological methods to characterize and optimize time- and temperature-dependent bioink's printability.**

Yield stress

Another critical parameter for bioprinting is the yield stress. In rheology, yield stress defines as a critical stress below which a biomaterial behaves like solid, and above which it starts to flow and show liquid-like

behavior [235]. This feature is important to avoid uncontrolled extrusion of inks and bioinks from the needle under simple gravity. A minimum value is thus required. A high yield stress may however impact cell viability adversely [236].

Determining a yield stress as an actual material constant may be challenging due to the measuring method and condition used. Consequently, there is no universal approach to assess yield stress and there exist a number of methods. Continuous shear stress or shear rate sweep, from low to high stress or rate, is perhaps the most widely used technique for assessing yield stress.

Herschel-Bulkley models are often used to calculate the yield stress from the stress/rate curves [59]. Bioinks generally follow the Herschel−Bulkley model, describing Non-Newtonian materials, where the shear stress (τ) relates to the shear rate ($\dot{\gamma}$) as follows:

$$\tau = \tau_0 + K\dot{\gamma}^n \qquad \text{Equation 4}$$

where τ_0 is the yield stress, below that the biomaterial behaves as a solid, K is the consistency index and representative of viscosity, and n is the flow behavior index. For n<1 the material is shear-thinning, whereas for n>1 it is shear-thickening. If n=1, the model equates to the Bingham plastic fluid (Figure 16).

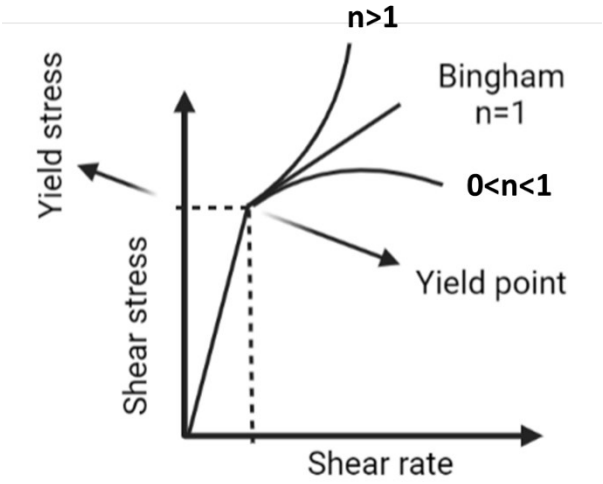

Figure 16. Schematic typical rheological behavior of fluids with Herschel-Bulkley, Bingham model, plot of shear stress vs shear rate (prepared using www.biorender.com).

In addition to bioinks, FRESH support baths also must show yield stress [237] which can be studied using Herschel–Bulkley model (detail information is presented in section 2.10).

Figure 17(a-c) presents other methods to evaluate the yield point. The stress curve is often manually extrapolated to zero shear rate in order to study a yield stress. A double logarithmic plot of viscosity against stress may be used to measure the yield stress in a shear stress or rate ramp (Figure 17 b). Another approach to determining yield behaviour is to use the oscillation stress/strain sweep test. Graphing the storage modulus (G') versus oscillation stress in a double logarithmic fashion shows the yield point when G' crosses G'' value (Figure 17 c).

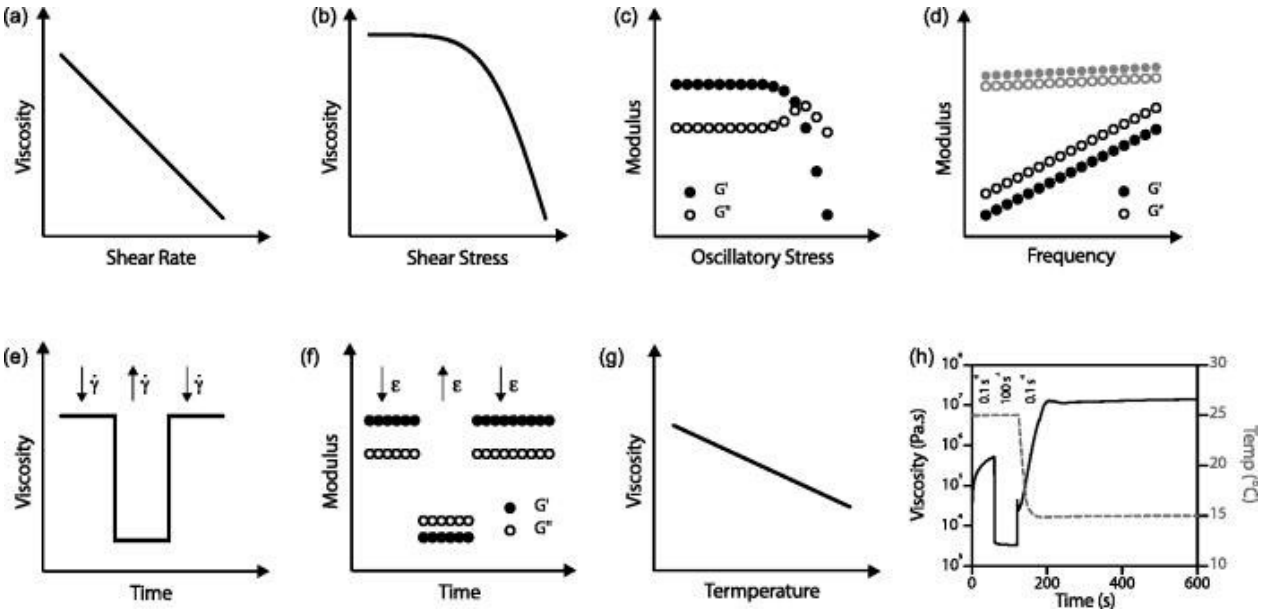

Figure 17. Common rheological tests for bioinks. (a) Shear rate sweep, (b) stress ramp, (c) oscillatory stress ramp (amplitude sweep), (d) frequency sweep of different biomaterials: solid-like gels (gray) and viscoelastic liquids (black), (e) rotational recovery (varying shear rate), (f) oscillatory recovery (varying oscillatory strain) (Reprinted from [238]; An open-access article distributed under the terms of the Creative Commons Attribution License (CC BY)).

Recovery

The extruded bioink filament should be strong enough to maintain its shape after bioprinting. Therefore, following the extrusion process, the bioink' network which is shear thinned must be able to self-heal and

recover to its primary phase (solid or gel-like state) [229]. The viscosity should recover fast after the shear stress is removed. Two main methods used to evaluate the recovering ability of a candidate bioink after shear removal are described in Figure 17 e & f. One consists in studying storage and loss modulus during and after shear removal using an oscillatory test (Figure 17 f). The other is evaluating shear viscosity during and after removal of applied stress or shear rate using a rotational test as shown in Figure 17 e. These tests appear particularly interesting for the study of bioinks since it also allows us to monitor shear thinning behavior of the hydrogel during applied shear stress.

Gelation kinetics

As mentioned above, the use of temperature-dependant hydrogels such as chitosan thermosensitive hydrogel raise special difficulties when assessing the printability of bioink since their properties will evolve with time. Moreover, hydrogel gelation plays an important role in post-printing mechanical stability. It is therefore very important to evaluate the gelation kinetics of the gel at various temperatures used during the printing process. Oscillatory test is usually used to study gelation kinetics, gelation time and temperature by following storage (G') and loss modulus (G"). When G'>G", the hydrogel shows gel-like behaviour and the G'=G" point is considered as gelation point or sol-gel transition point as shown in Figure 18 [239].

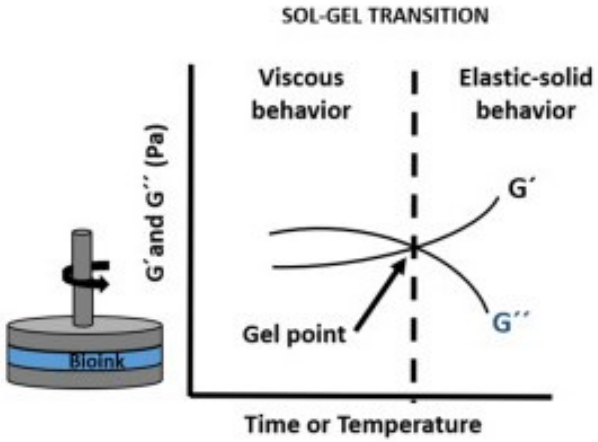

Figure 18. Rheometric evaluation of bioinks, with time- and temperature-dependent sol–gel transition. G" > G', viscous behavior; G" = G', gel point; G' > G", elastic solid behavior (Reprint and Copyright (2021) with permission from Elsevier Inc. [240]).

2.9.2 Summary of useful rheological tests for printability

The most useful rheological tests used to study printability of biomaterials were schematically shown in Figure 17 and discussed above. We can deduce that, in the case of a thermosensitive hydrogel, the following tests are required:

1) LVR must be determined using the stress sweep or/and frequency sweep tests to make sure that tests are done in the LVR region.

2) Time sweep and temperature sweep are the primarily rheological test to study thermosensitive hydrogels e.g., chitosan-based hydrogels to determine the sol-gel transition and gelation behaviour over time and by varying temperature.

3) Then, to evaluate viscosity and shear thinning behavior, shear rate sweep test can be applied, but adapted to get into account the time dependence of the viscosity at a given temperature.

4) To obtain the yield point and study flow behaviour under applied shear, the stress sweep test can be used through either oscillatory mode or rotational. Oscillatory mode gives information about storage and loss moduli, while with rotational mode, viscosity can be studied.

5) Finally, recovery test in oscillatory or rotational mode should be applied to evaluate the bioink potential of self-healing or recovery after shear removal, mimicking pre-printing, under shear and post-printing conditions. The use of those tests in different studies in the literature is summarized in the Table 3.

Table 3. Useful rheological tests to study the printability of thermosensitive hydrogels.

Test name	Rheological mode	Detail info.	Ref.
Time sweep	Oscillatory	*Study elastic moduli or complex viscosity over time e.g., gelation behavior over time, gelation time, etc. *Frequently used to study thermosensitive biomaterials Figure 17. h	[67]
Temperature sweep	Both rotational and oscillatory	*Used for thermosensitive bioinks e.g., chitosan, gelatin or Pluronic *Measuring viscosity or elastic moduli Figure 17. g	[238]
Shear rate sweep	Rotational	*Study non-Newtonian behavior *Calculate the viscosity *Study the flow properties of the bioink during extrusion Figure 17. a & b	[238]
Stress ramp/sweep	Both oscillatory and rotational	*Determine the yield stress of a non-Newtonian fluid *Stress or strain-controlled *Study viscosity or storage and loss modulus changes *Determine LVR Can be used to determine both the yield point, and the flow point at the critical stress Figure 17. b & c	[241]
Frequency sweep	Oscillatory	*Measuring storage and loss modulus *Determine if the bioink is viscoelastic liquid or gel Figure 17. d	[242]
Recovery	Both rotational and oscillatory	*The first step: at a low shear rate (or low oscillatory strain), the second step: at a high shear rate, and the third step: the primary shear rate. *Measuring viscosity or shear moduli *Bioinks should show recovery of 80%-90% of the original viscosity or storage moduli Figure 17. e & f	[238]

2.10 Rheology of FRESH support bath

As mentioned in section 2.4, the FRESH bioprinting method has been proposed for low viscosity hydrogels to provide both resolution and cell viability. The FRESH support bath requires some important rheological properties as mentioned before, including shear thinning during needle movement [243] and yield stress. Briefly, FRESH support bath must fit Bingham fluid or Herschel−Bulkley model. The most common support bath, made of gelatin microparticles (slurry) was found to fit the Bingham model: it presents a yield point or initial stress to flow, but then the flow behavior is linear [244] (Figure 16). Hydrogels usually rather fit Herschel−Bulkley model, which is a complementary model of Bingham: after it starts to flow, it shows non-linear shear thinning behaviour as shown in Figure 16 [245]. More information will be given in the paper in Chapter 4.

Yield stress of the bath can be controlled through molecular weight of material forming the bath, concentration, viscosity and storage modulus. It was shown that increasing yield stress led to smaller and finer regularly circular printed filaments [246]. However, at very stiff support bath with high concentration e.g., 8% (w/v) nanoclay-based bath, in which the bath yield stress was higher than the bioink, the rectangular shape and compression were observed on side of the printed filaments [247].

After needle passing and stress removal, the support bath must be self-healable/self-recoverable. It must recover quickly to its primary viscosity or shear moduli and demonstrate gel-like behavior. This property helps to entrap and support the deposited bioink prior to its gelation or crosslinking. The extent of fluidization of the support bath affects the resolution and shape fidelity of the printed bioink [248]. Therefore, maintaining high resolution and shape fidelity when using FRESH bioprinting technique is challenging and require comprehensive optimization.

The most common support bath consists of small gelatin microparticles slurry [249]. However, this material is not suitable for bioink that gel at 37°C since the gelatin slurry liquefies at this temperature. Several other materials have been proposed as FRESH support bath as summarized in Table 4.

Table 4. Most commonly used biomaterials as a FRESH bioprinting support bath

Materials	Rheological properties	How gel/solidify	How get removed after printing	Detail info.
Gelatin microparticles	Thermosensitive material Provide fast gel retention during nozzle movement within the bath. Act like a Bingham plastic [53]	Low temperature (<25°C)	Liquify by increasing the temperature 37°C [249]	Liquid at body temperature Not suitable for thermo crosslinking Not suitable for gelatin contained bioinks
Carbopol microgels (commercial polymer with polyacrylic acid chains)	Anionic Require basic solvents Printed outcome exhibits poor surface quality [250].	Dissolve in NaOH	Wash with PBS Monovalent cationic buffer solution causes the Carbopol microgels to shrink and lose their bulk plastic behavior.	Not recommended for cationic hydrogels [251]
Nanoclay e.g., Laponite	Like slurry Has plenty side OH groups Positive core groups Thermal stability ultraviolet transparency [252, 253]	Dissolve in water in vigorous stirring	Wash with NaCl	Not suit for cationic hydrogels because possible positive charges dissolve the bath Amine groups can cause the formation of small flocculated particles, often described as "seeds" [254]
Pluronic F127 (Pure & in combination with salts)	Poor mechanical strength at low concentrations (e.g., 7-12% w/v) Dissolve in aqueous solutions [255-259].	Gel at temperature range of 25°C–40°C (tunable by concentration variation)	Decreasing temperature to 22°C or lower	Gel at 37°C and liquify at 22°C Tunable gelation temperature Tunable storage modulus by concentration variation Recovery even at high concentrations e.g. 23%

Composition of Pluronic and additives	Addressing abovementioned issues of pure Pluronic (with low concentration) Laponite, is used as rheology modifier [255],increasing bath stiffness while decreasing gelation temperature.	Gel at temperature range of 25°C–40°C (tunable by concentration variation)	Decreasing temperature to 22°C or lower	It is gel at 37°C and liquify at 22°C Tunable gelation temperature Tunable storage modulus by concentration variation and additive addition

Chapter 3 - Hypotheses and Objectives

In the literature review presented in the previous chapter, we have shown that bioprinting has much potential in tissue engineering, including articular tissue engineering, but there is still a lack of biodegradable bioink that address all the design criteria.

Chitosan-based thermosensitive hydrogels have been shown to be very interesting hydrogels for cell therapy and regenerative medicine, especially when they are formed with a mixture of SHC and BGP or PB as gelling agents [67, 68]. They are injectable, gel in situ, have physiological pH and osmolality, and support the survival of loaded cells. However, their potential for bioprinting has not been assessed yet. **The general objective of this Ph.D. thesis is to study and optimize the potential of thermosensitive chitosan-based hydrogels for extrusion-based bioprinting and injectable scaffold for articular tissue engineering.**

3.1.1 Hypothesis and objective 1

The main and first hypothesis of this project was that thermosensitive chitosan-based hydrogels are interesting candidates for bioprinting. The first step of the project, therefore, consisted in studying their potential for extrusion-based bioprinting. It is a challenge since their rheological properties evolve with time and temperature. For this reason, a new rheological approach was proposed that considers time and temperature.

The general aims of the first paper were to propose a rheological approach to study the printability of time- and temperature-dependant hydrogels and to specifically assess the potential of the chitosan-based thermosensitive hydrogels as bioinks. More specifically, the rheological properties of chitosan hydrogels were studied as a function of their composition, chitosan concentration, and the type and concentration of gelling agents. Post-printed resolution, integrity, and mechanical properties were also characterized. This work has been published in Journal of Biomedical Materials; DOI: 10.1088/1748-605X/abb2d8.

3.1.2 Hypothesis and objective 2

We have shown in objective 1 that the thermosensitive chitosan hydrogel can print a structure with adequate fidelity and handability. However, a high concentration of chitosan (3%w/v) was required, leading to a high mortality rate of encapsulated cells due to the high viscosity of the solution in which cells are mixed and

the low porosity of the final hydrogel. Decreasing the viscosity resulted in a poor shape fidelity of structures formed with more than 5 layers due to the low mechanical properties of the printed filaments. Furthermore, maintaining the substrate and environment uniformly at 37°C is quite challenging and can lead to evaporation.

Therefore, the **second hypothesis** of this project was that using the FRESH technique with a warm bath could increase the fidelity of the printed structures while keeping chitosan at a low concentration compatible with cell encapsulation. Indeed, printing in a warm bath brings mechanical support to the bioprinted structures and enhances chitosan thermogelation or thermo-crosslinking during printing. **Objective 2 was therefore to study and optimize FRESH bioprinting of chitosan thermosensitive hydrogels.**

More specifically, we first designed an adequate support bath, mainly based on its rheological properties. Pluronic was chosen and further optimized by the addition of salts e.g., sodium chloride (NaCl). Then, we studied the printability of chitosan hydrogel, alone and in combination with gelatin when printed within the warm support bath, as well as shape fidelity, mechanical properties, and cell viability. This work has been accepted for publication in Bioprinting journal; DOI: 10.1016/j.bprint.2022.e00209.

3.1.3 Hypothesis and objective 3

To engineer or repair tissues that are mineralized or contain gradient or mineralization (as it is the case for articular tissue), the injectable or printable material needs to be osteoconductive. This is not the case with chitosan hydrogels but can be achieved by adding bioactive materials such as hydroxyapatite or bioglass. **The third objective of this work was therefore to create bioactive osteoconductive thermosensitive chitosan-based hydrogels compatible with cell encapsulation, by the addition of sintered bioglass (BG)**.

We **hypothesized** that concentrating bioglass in small microbeads instead of their homogenous distribution in the gel could improve mechanical properties due to less interference with the gelation mechanism resulting from a slowdown rate of ions release. By reducing the rate of ion release, such a composite hydrogel could also improve the survival and growth of encapsulated cells.

This work led to development of hybrid hydrogel containing BG microbeads that might form a promising injectable cell-laden bioactive biomaterial for treatment of bone defects at non-loading sites. This work is submitted to journal of Journal of Biomedical Materials Research Part A.

Chapter 4 - A Rheological Approach to Assess the Printability of Thermosensitive Chitosan-based Biomaterial Inks

This paper has been published in the "Journal of Biomedical Materials, Volume 16, Number 1; DOI: https://doi.org/10.1088/1748-605X/abb2d8".

Maedeh Rahimnejad[1a], Thierry Labonté-Dupuis[2a], Nicole R. Demarquette[2] and Sophie Lerouge[1,2a*]

[1]Biomedical Engineering Institute, School of Medicine, Université de Montréal, Canada

[2]Department of Mechanical Engineering, École de technologie supérieure (ÉTS), Canada

[a]Research Centre, Centre Hospitalier de l'Université de Montréal (CRCHUM), Canada

[*]Corresponding author

E-mail: sophie.lerouge@etsmtl.ca

4.1 Abstract

For extrusion-based bioprinting, the inks must be printable and rapidly present sufficient mechanical properties to support additional layers and provide a cohesive, manipulable structure. Thermosensitive hydrogels may therefore be interesting candidates. However, the use of these materials is particularly challenging since their rheological properties evolve with time and temperature. In this work, a rheological approach to characterize the printability of chitosan-based thermosensitive inks was developed. The method consists of evaluating:1) the gelation kinetic at room temperature and at 37C; 2) shear thinning behavior to estimate the shear rate applied during printing as a function of printing parameters ; 3) the viscosity after shear removal (recovery test) to simulate behaviour after biomaterial deposition. Hydrogels containing 2 and 3%w/vol chitosan, combined with different gelling agents (Sodium-hydrogen-carbonate (SHC), Phosphate-buffer, Beta-glycerophosphate (BGP)) were tested, and compared with alginate/Gelatin bioink as controls. To correlate the rheological studies with real printing conditions, 3D-Discovery bioprinter was used to print hydrogels and the visual aspect of the printed structure was observed. Unconfined compressive tests were carried out to study the impact of applied shear rate during printing on the mechanical properties of printed structures. All pre-hydrogel solutions presented shear thinning properties. The recovery of viscosity was found to depend on the hydrogel formulation, as well as the level of shear rate and the state of gelation at the time of printing. Formulations made with SHC and phosphate buffer presented too rapid

gelation and phase separation,leading to poor printing results. One particularly promising formulation composed of SHC and BGP, when printed at a shear rate of $140s^{-1}$, before its gelation time ($t_g \leq 15min$), resulted in good printability and 3D structures with rigidity comparable with the Alginate/Gelatin bioink. The methodology introduced in this paper could be used to evaluate the printability of other time- and temperature dependent biomaterial inks in the future.

Keywords: biomaterial inks, chitosan thermosensitive hydrogel, printability, extrusion-based bioprinting, rheology

---

4.2 Introduction

Among the various challenges of extrusion-based bioprinting, one is to design biomaterial inks and bioinks that fulfill the numerous requirements. The ink must be extrudable e.g. injectable through a small needle to reach high resolution but rapidly possess sufficient mechanical properties to keep the structure intact, support additional layers and provide a cohesive, manipulable structure [260]. Moreover, for bioinks, the material and the printing process must be cell friendly [261, 262]. It should ideally also be biodegradable to be gradually replaced by extracellular matrix. All these requirements explain why the search for ideal biomaterials is still ongoing. Moreover, standard methods to characterize and optimize biomaterial inks and bioinks have yet to be developed [24, 263-265].

Among the biomaterials that could be used for bioprinting, chitosan-based hydrogels are attractive candidates due to their biocompatibility, biodegradability, low cost and thermosensitive properties. Chitosan, a natural biopolymer derived from chitin, can be dissolved in acidic solution. When combined with a weak base such as beta-glycerophosphate (BGP), it can form a solution with physiological pH that rapidly gels with increasing temperature [187, 266, 267]. However, the mechanical properties of such gel are quite poor. Our team showed that using new combinations of gelling agents (namely a mixture of sodium hydrogen carbonate (SHC) with phosphate buffer (PB) or BGP), we can strongly enhance the mechanical properties of the hydrogels, while ensuring physiological osmolality and rapid gelation at 37°C [67, 195]. These gels allow excellent cell survival and growth and were demonstrated as very interesting candidates for injectable cell-loaded scaffolds for cell therapy and tissue engineering [195, 268].

Chitosan thermosensitive properties also make them potential candidates for bioprinting, as the gel is in the form of a viscous solution at room temperature prior to its gelation through increasing temperature, which can be achieved using a warm substrate or incubator. Rapid physical crosslinking can help to keep the post-printed structure mechanically intact and prevent hydrogel dispersion, without the addition of a crosslinker or photopolymerization step; A few teams have already shown the potential of such thermosensitive hydrogels for bioprinting, alone or mixed with gelatin or hydroxyapatite [194, 218]. However, the use of these materials for bioprinting is particularly challenging since their rheological properties evolve with time and temperature. While most teams perform temperature ramps and time sweep to follow the gelation kinetics at body temperature, there has been to date no complete rheological study to characterize and optimize their printability. More generally, there is presently a lack of appropriate methods to study the printability of time- and temperature evolving materials like those.

The general aim of the present work is to propose a rheological approach to study the printability of thermosensitive hydrogels, which takes into account the time and temperature-induced gelation process. We then used this methodology to assess the potential of the chitosan thermosensitive hydrogels as biomaterial inks, in comparison with alginate/gelatin bioink which has been already demonstrated for its excellent printability [6].

In order to be used in extrusion-based deposition process a biomaterial ink must present a viscosity that allows its extrusion. It also must present shear recovery (rapid recovery of the initial viscosity once shear has stopped). An important parameter to calculate is therefore the shear rate applied during extrusion. During extrusion, the ink flows through a capillary and is subjected to a shear rate ($\dot{\gamma}_W$) given by Equation 3 [269].

Indeed, most materials are shear thinning, i.e., their viscosity decreases with increasing shear rate. Therefore, to evaluate the shear rate a bioink undergoes during bioprinting, it is first necessary to measure the viscosity as a function of shear rate [22, 74, 270]. However, carrying out rheological characterization of hydrogels can be difficult when their rheological properties are time-dependent. A simple shear rate ramp (viscosity as a function of varying shear rate) [269] is not appropriate. In those cases, since the viscosity also changes with time, the tests must be adapted in consequence.

Once a layer is printed, it needs to rapidly reach enough mechanical properties to support gravity and keep its form as well as to support other layers. In some cases, such as alginate-based bioinks, ionic crosslinking can be performed by immersion in a calcium ion rich solution after printing. Other materials can be photopolymerized layer by layer. In the case of thermosensitive hydrogels such as chitosan, rapid shear recovery is particularly important since no rapid crosslinking method can be applied between layers.

These characteristics can be evaluated using rheological tests, consisting of evaluating the biomaterial ink viscosity as a function of time once the shear rate encountered by the ink during extrusion has been applied and removed. This test is called the recovery test [74]. Performing recovery tests at different shear rates allows to estimate the maximum shear rate that should be applied during printing, i.e. at which the hydrogels return rapidly to their primary viscosity after shear removal without breakage. A potential advantage of thermosensitive hydrogels is that after printing the hydrogel continues to gel at 37°C. The recovery test must therefore be adapted to take this behaviour into account.

The hydrogel gelation kinetic is also an important parameter that determines the suitability of the hydrogel for extrusion-based bioprinting [271]. Indeed, whether gelation has been initiated at the time of printing probably has an impact on recovery after shear removal, uniformity and resolution, as well as mechanical properties. The gelation kinetics of chitosan hydrogels therefore need to be assessed at various temperatures reproducing the steps of the bioprinting process, in particular at room (storage in the cartridge and extrusion) and body temperature (substrate warming or incubator).

In this work, we show how this rheological approach can be applied to assess the printability and the time frame optimal for bioprinting thermosensitive hydrogel. In particular, we apply this approach on chitosan hydrogels of various composition, in terms of chitosan concentration and the type and concentration of gelling agents. Post-printed resolution, integrity and mechanical properties were also characterized and compared with values obtained for a previously published bioink composed of alginate and gelatin [99].

4.3 Materials and methodology

4.3.1 Materials

Shrimp shell chitosan (ChitoClear, HQG110, Mw: 155 kDa, DDA 83%) was purchased from Primex (Iceland). β-Glycerol phosphate disodium salt pentahydrate ($C_3H_7Na_2O_6P \cdot 5H_2O$, hereafter BGP), sodium

phosphate monobasic NaH_2PO_4 (SPM) and sodium phosphate dibasic Na_2HPO_4 (SPD) were purchased from Sigma-Aldrich (Oakville, ON, Canada). Sodium hydrogen carbonate $NaHCO_3$ (sodium bicarbonate, hereafter SHC) was purchased from MP Biomedicals (Solon, OH, USA). Sodium alginate salt from brown algae, Type B gelatin from bovine skin (G9391) and calcium chloride ($CaCl_2$) were purchased from Sigma-Aldrich. Other chemicals were of reagent grade, and were used without further purification.

4.4 Preparation of chitosan thermosensitive hydrogels

Chitosan solution

Chitosan powder was solubilized in hydrochloric acid (HCl) (0.09 M and 0.013M) at 3.33% w/v (for final concentration 2%) or 5%w/v chitosan (final 3%), respectively, with mechanical stirring for 2 hours. The solution was sterilized by autoclaving (20 min, 121°C) and stored at 4°C.

Gelling agent (GA) solutions

Three different GAs were used in this study, namely BGP, SHC, and PB at pH = 8. PB was prepared with a mixture of sodium phosphate dibasic and sodium phosphate monobasic at ratio of ratios of 0.047/0.540 w/w in milli-Q water. SHC was combined with either PB or BGP as previously published [67].

4.4.1 Preparation of pre-hydrogel solutions for rheological characterization

Chitosan pre-hydrogel solutions were prepared by mixing CH solution with one of the GA solutions at a volume ratio of 3:2, respectively. The two solutions were introduced in separate syringes, joined by a Luer lock connector. The content of the GA syringe was pushed into the CH syringe and the mixture was pushed from side to side for 15 repeats immediately prior to use. Pre-hydrogel solutions were then centrifuged to remove air bubbles and used immediately. Table *5* summarizes all formulations tested. Hydrogels formed with a mixture of SHC and BGP as gelling agents are identified as A, and those formed with SHC and PB as B. Hydrogels had a final chitosan concentration of 2% (w/v) or 3% (w/v). All had a physiological pH.

Table 5. Concentration of chitosan and gelling agents of the various tested hydrogels (CH: Chitosan, BGP: Beta-glycerophosphate, SHC: Sodium hydrogen carbonate, PB: Phosphate buffer at pH=8).

Hydrogel name	[GA component] (M)			Final concentration of CH% (w/v)
	SHC	BGP	PB	
A2	0.075	0.10	-	2
A3	0.113	0.15	-	3
B2	0.075	-	0.02	2
B3	0.113	-	0.03	3

4.4.2 Preparation of alginate/gelatin hydrogel (control group)

Sodium alginate and Type B gelatin powders were dissolved in milli-Q water, and stirred using a magnetic hotplate for 1 hour at 60°C and 2 hours at room temperature to achieve a homogeneous composite precursor comprised of 3 w/v% alginate and 7 w/v% gelatin as explained in detail by Kinsella's group [99]. The Alginate/Gelatin solution was then kept 2 hours at room temperature to remove air bubbles and later stored at 4°C. Before use, the solution was warmed at 22°C for 30 min [99] and centrifuged to remove air bubbles. A 1%w/v $CaCl_2$ solution for crosslinking the alginate was also prepared by dissolving $CaCl_2$ into milli-Q water.

4.4.3 Rheological tests

Rheological properties were carried out using an Anton Paar instrument (Physica MCR 301, Germany) with a cylinder geometry (CC10/T200), (1mm gap) or plate-plate geometry (PP25) of 25 mm diameter. Linear viscoelastic (LVE) range was first determined through amplitude sweep test using PP25. The following tests were then performed:

1) Time sweeps at 22 & 37°C for 1 hour were performed using the oscillatory mode in the LVE range, at a constant shear strain (1%) and constant frequency (1Hz). They allowed the study of gelation kinetic at both temperatures, as a function of gel composition, by following values of complex viscosity, the storage and loss modulus (G' and G'') and loss factor tan δ = G"/ G' as a function of time.

2) Viscosity behavior of the pre-hydrogel solutions at 22°C was assessed using rotational rheometry tests. In contrast to conventional shear thinning tests, where the viscosity change is reported with varying shear rate, here the viscosity was studied as a function of time at different shear rates (0.01, 0.1, 1, 10, 100 s^{-1}). This was done to take into account the possible variation of pre-hydrogel properties with time. To express the shear thinning behavior, the viscosity values at one particular time point were then plotted as a function of shear rate. A time point of 10 min was chosen assuming this corresponds to the time required for hydrogel preparation and printing (including mixing of chitosan solution and gelling agent, centrifugation of the solution and loading on the print head).

3) Shear recovery after different levels of shear rate (low to high-10 to 1000 s^{-1}) was evaluated using rotational rheometry. The viscosity was measured during consecutive steps which mimic the printing process: (1) Pre-printing (shear rate of 0.001 s^{-1} for 10 min at 22°C); (2) Printing (sudden increase of shear rate at 10, 100, 500 or 1000 s^{-1} for 1 min at 22°C); (3) Post printing (shear rate of 0.001 s^{-1} for 10 min at 22°C and then increasing the temperature to 37°C to take advantage of the hydrogel thermosensitivity) (Figure 19).

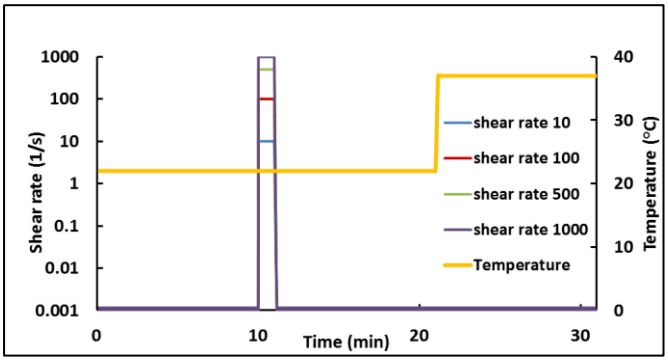

Figure 19. Schematic of the applied shear rates and temperature as a function of time during recovery tests.

4.4.4 Printing procedure

A 3D-Discovery (RegenHU) bioprinter was used to print the hydrogels via a plunger dispenser which enables to keep the dispensing rate constant during printing (volume/min) even if the hydrogel properties change with time. The cartridge was kept at room temperature, while the heated substrate temperature was

kept constant at 37° C. Different steel needles (sizes 22G/25G, length: 0.25 inch) were used to print hydrogels. Printing parameters are presented in Table 2. The flow rate of the bioink, the layer thickness (h) and the translational speed of the printing head (feed rate) (V_t) were chosen to ensure that we have proper and continuous filament formation and were kept constant throughout the study. The shear rate applied during printing was calculated according to Equation 3, using the slope of the viscosity versus shear rate graph (n-1) on a log log plot, and reported in Table 6.

4.4.5 Printing resolution, hydrogel uniformity and structural integrity

Each biomaterial ink formulation was printed using two different needle sizes (22G/25G) according to the conditions in Table 2. Images were taken from each print and analyzed using the freeware ImageJ (Fiji.sc) according to the approach studied by Gillispie et al. [272] and Webb et al. [214]. The average width of printed filaments was determined, for each printing setting, by manually selecting 6 random points. We also evaluated the quality of the angle printed (sharp (1) versus curvy (0)) and the continuity of the lines ((1) versus (0) if more than one break observed). The width of the line was also compared to the internal diameter of the needle (width/diameter). A high ratio means that the gel spreads a lot after printing, decreasing the printing resolution.

Table 6. Printing parameters used on the 3D Discovery bioprinter: needle size, n-1 slope according to viscosity vs shear rate graph and corresponding shear rate as a function of needle size according to equation 1. Constant parameters were: Flow rate = 1.25 µL/s (mm3/s); feed rate = 6 mm/s; layer thickness = 0.3 mm.

Pre-hydrogel solutions	**Needle size**		**Slope of viscosity vs shear rate (see Equation 3) (n-1)**	**Shear rate (s^{-1})**
	Gauge	**Inner diameter (mm)**		
A2	22	0.41	-0.3	203
	25	0.25		897
A3	22	0.41	-0.5	230
	25	0.25		1017
B2	22	0.41	-0.6	250
	25	0.25		1101
B3	**Not printable (lack of homogeneity and continuity)**			

To assess structural integrity, the best printable formulation was printed in 10-layer and 20-layer honeycomb structures and the theoretical height (layer thickness multiplied by number of layers) was compared to real height after 1hour incubation at 37°C (to assure solidification).

4.4.6 Post-printed mechanical properties

Unconfined compression tests were performed on 5-layer printed honeycomb structures using the MACH-1 testing device (Biomomentum, Canada). A velocity equal to 100% of the sample's height/min was used. The compressive strength and the secant Young modulus at 15% and 30% of deformation were calculated from the stress-strain curves. ImageJ software was used to calculate the real surface area of the printed structure (without the holes in the structure) for measurement of applied stress. Mechanical properties were compared with those of structures fabricated with Alginate/Gelatin bioink. Tests were performed at room temperature after 24 hours of sample gelation at 37°C.

4.4.7 Statistical analyses

All experiments were performed at least in triplicate. Results were expressed as mean ± SD. Statistical analysis was performed using GraphPad Prism 7.04 software. One-way ANOVA and Tukey's multiple comparison tests were used to compare multiple groups. $P<0.05$ was considered to be statistically significant.

4.5 Results

4.5.1 Time sweep at 22 and 37°C

Time sweeps were performed in the LVE region, first at room temperature (22°C) to estimate the stability of the pre-hydrogel solutions in the printing cartridge as a function of their composition (Figure 20a) but also at 37°C to estimate their kinetic of gelation (solidification) once on the heated substrate (Figure 20b). Both figures present the evolution of the storage (G') and loss (G'') moduli. The viscous pre-hydrogel solution is considered to become a viscoelastic gel when G'>G''. According to the approach of Winter and Chambon [273], we considered the gelation time as the time where $G' = G''$, or the loss factor $\tan\delta = G''/G' = 1$. Figure 20(c) summarizes the mean G' value after 10 min at 22°C (considered as the printing

time) and after 1 hour at 37°C (to mimic 1 hour after printing). At 22 °C (Figure 20(a)), the gelation time is less than 15 s (G'>G'' already at the first measurement) and 30 s for B2 and B3 hydrogels respectively. For A2 and A3, it takes several minutes to begin gelation (t_{gel} = 5±3.4 and 15±7.5 min respectively). B formulations also show higher values of storage modulus compared to A formulations. As expected, A3 gel (CH3%) presents higher storage moduli right after preparation than its A2 counterpart (CH2%). In contrast, B2 and B3 show similar storage modulus as a function of time.

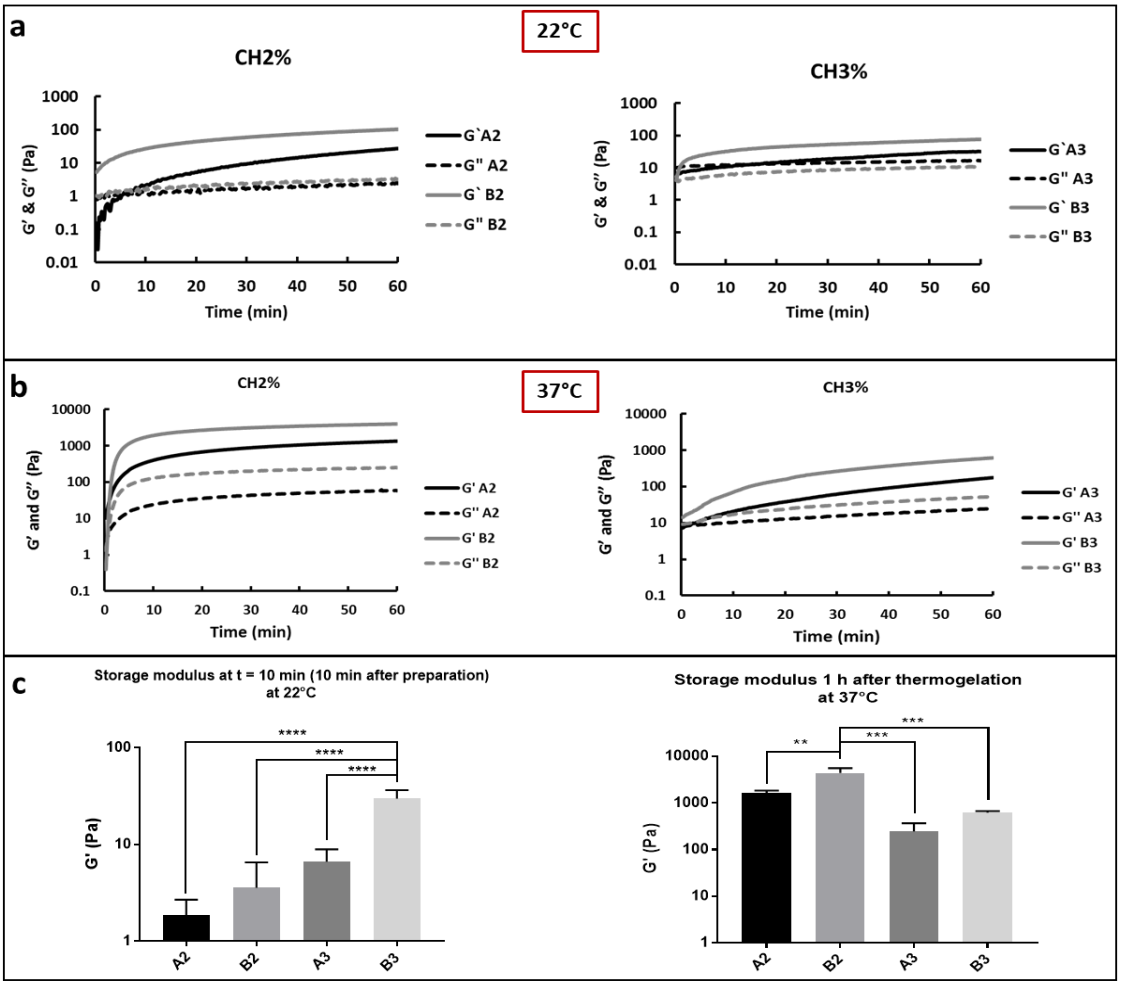

Figure 20. Gelation kinetics of A and B chitosan-based hydrogels: a) Evolution of the storage (G') and loss (G'') moduli of hydrogels as a function of time at 22°C (mean +/-SD; n≥3). b) Evolution of the storage (G') and loss (G'') moduli as a function of time at 37°C. c) G' value after 10 min at 22°C and 1h at 37°C,

respectively (mean +/-SD; n≥3); (** p<0.01, *** p<0.001, **** p<0.0001). Gels were made with SHC+BGP as gelling agents, while B gels were prepared with SHC+PB, as described in Table 5.

The evolution of the storage (G') and loss (G'') moduli at 37°C as a function of time is presented in Figure 20(b). Drastic increase of G' value during isotherms at 37°C is indicative of the gel thermosensitivity. Thermosensitivity is more evident with CH 2% formulations rather than 3%. While A2 and B2 present the lowest modulus at 22°C, they rapidly increase at 37°C, leading to the highest values after 1hour gelation, B2 being significantly higher than all others (p<0.001, Figure 20(c)). In contrast, A3 and B3 present higher initial viscosity (not shown here) and slowly gel at 37°C. Their properties after 1-hour gelation are relatively similar.

At printing time (after 10 min at 22°C), B3 formulation presents the highest storage modulus values (p<0.0001), while the difference among the three other formulations is not significant (Figure 20(c), left panel). As will be discussed later, this leads to difficult control of printing and reproducibility.

4.5.2 Shear thinning behavior

The shear thinning property of the solution is a critical property for bioprinting. Figure 21 presents the shear thinning behavior of A2 and A3 formulations. Results of B formulations and Alginate/Gelatin are shown in supporting information (Figure S 2). As explained in the materials and methods section, since the viscosity is changing as a function of time, shear thinning properties were evaluated by measuring the viscosity over time at 5 different applied shear rates (from 0.01 to 100 s^{-1}). Figure 21(a) presents the 5 viscosity curves as a function of time for sample A3. Then, the values at one particular time point (here 10 min) were plotted to form the curve of viscosity versus shear (Figure 21(b)). Results showed that both chitosan A2 and A3 pre-hydrogel solutions present shear thinning properties, characterised by a sharp decrease in viscosity value with increasing shear rate, with some differences between the gel formulations. Shear thinning was also observed for B formulations, as well as for the alginate/ gelatin (control group), although to a lesser extent (viscosity decrease from 10000 to 100 Pa.s only) (Supplemental data_Figure S 2).

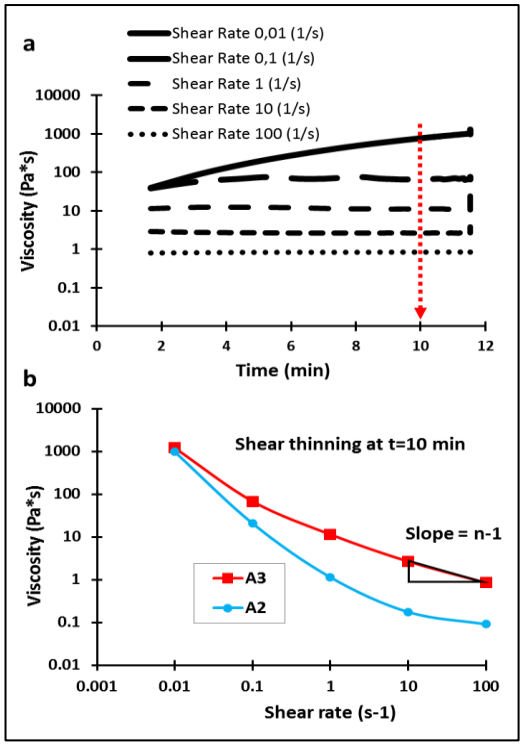

Figure 21. Shear thinning behavior of: a) viscosity of A3 formulations at various shear rates (0.01, 0.1, 1, 10 and 100 s-1) as a function of time at 22°C; b) Viscosity as a function of shear rate for both A2 and A3

formulations after 10 min at 22°C (mean; n≥3). The slope between 10 and 100 s-1 was used to evaluate the shear stress during printing using Equation 3.

Surprisingly, a variation of the viscosity as a function of time was seen only at the lowest shear rate (0.01 s^{-1}) (Figure 21(a)). Since the solutions are not completely stable at room temperature (as just shown), we were expecting the viscosity to increase with time at all shear rates. This suggests that shear rates equal or above 0.1 s^{-1} prevent the physical gelation of the chitosan bioinks and demonstrates the importance of testing conditions on rheological results.

We used the slope of the shear thinning test at shear rate between 10 and 100 s^{-1} to calculate the shear stress during printing using equation 1 as presented in the introduction and reported on Table 6.

4.5.3 Shear recovery

We concentrated on A formulations due to their slower gelation kinetics at room temperature and more homogenous fiber formation at extrusion (shown later in the manuscript). In accordance to the schematic presented in Figure 19, shear recovery tests followed the evolution of the viscosity during rest (shear rate = 0.001 s^{-1}), followed by applying shear for 1 min and let recover after shear removal at 22°C (to simulate the printing procedure), followed by temperature increase from 22 to 37°C. To study the influence of the extent of shear rate on recovery, four different applied shear rates were compared, from 10 to 1000 s^{-1}.

Figure 22(a) and (c) present the results for A2 and A3 formulations respectively. In accordance with the previous results, the viscosity increased with time at rest, followed by sudden drop during shear due to shear thinning. Viscosity recovery immediately after shear removal was only partial, especially for high shear rates, but curves show that viscosity continues to recover with time, and further increased when the temperature was increased to 37°C. For A2, the immediate recovery was much better for shear rate of 10 s-1 compared to 100 and 1000 s-1 (501 ± 127 Pa.s versus 66 ± 15 Pa.s and 2 ± 1 Pa.s respectively (see the complete data in Supplemental materials section Table S 1 and Table S 2). The difference was less drastic for A3 (10 and 100 s-1 curves are superposed, and viscosity at shear removal decreased from ~ 600 to 130 Pa.s depending on the shear rate value). Thus the viscosity values immediately after 100 s^{-1} shear removal was about 10 fold higher for A3 compared with A2 hydrogels (663 ± 95 Pa.s and 66 ±15 Pa.s, respectively).

Similar tests were performed on A3 solutions left for 20 min (instead of 10 min) at 22°C to mimic longer pre-printing times (Figure 22d). At these time points, even at 22°C, the solution has already begun to gel ($t \geq t_g$). However, no drastic impact was observed on recovery properties. Immediate recovery is slightly reduced, but viscosity then increases with time, reaching similar final values.

To confirm the importance of printing before gelation, we also performed recovery tests after 20 min gelation at 37°C. Results for A2 are presented in Figure 22(b), results for A3 in the supporting information (Figure S 3). As expected, viscosity increased more during the rest period, due to hydrogel gelation at 37°C. Following shear, only partial immediate recovery was observed, without any further increase of the viscosity with time for A2 (Figure 22(b)), some increase for A3. The difference between A2 and A3 can be explained by the fact that A3 gelation is much slower than A2 gelation, as shown in Figure 20.

As a comparison, shear recovery tests were also performed on the control bioink consisting of 3%w/v alginate with 7% w/v gelatin [99] (Figure 23). Alginate/gelatin present a different behavior compared to chitosan hydrogels, with better immediate recovery of the viscosity, but no further increase with time. As for chitosan hydrogels, the extent of recovery decreased with increasing shear rates. Interestingly, the viscosity at rest, prior to shear, was found to increase with time. This could be explained by the change of temperature of the solution (which was poured in the rheometer at 25°C since it is not liquid enough at 22°C due to the presence of gelatin). Another possible explanation is alginate-gelatin interactions after mixing the solution. In contrast, similar tests performed on pure alginate didn't show any variation of the viscosity at rest (data not shown).

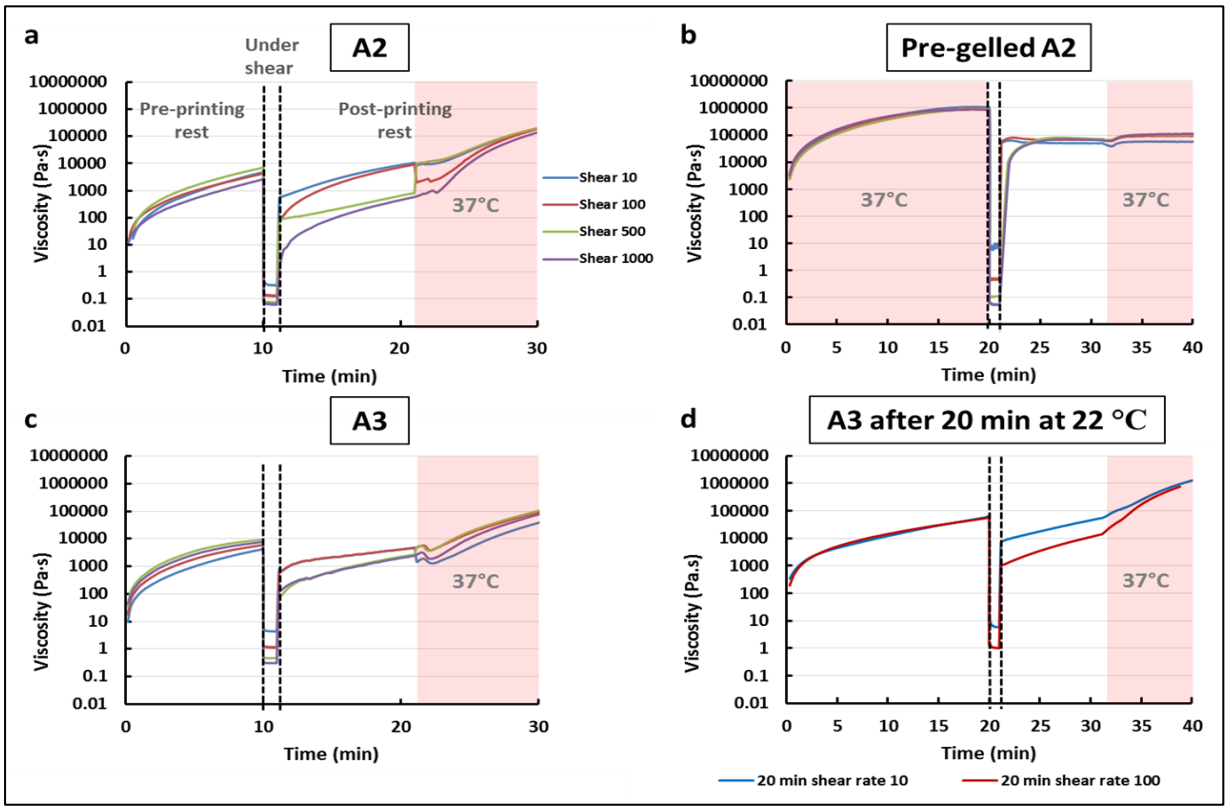

Figure 22. Shear viscosity recovery under 4 different applied shear rates (10, 100, 500, 1000 s-1). The graphs present the complete cycle, namely at-rest state (shear at 0.001 s-1, generally for 10 min), printing step (shear rate at one of the 4 different tested shear rates for 1 min), post printed rest state at 22°C and post-printed rest at 37°C (shear back at 0.001 s-1): a) A2, b) Pre-gelled A2 (shear after gelation for 20 min at 37C); c) A3, d) A3 with 20min at rest instead of 10 min. The change of the shear rate is indicated with the vertical lines; Temperature 37°C is highlighted, otherwise 22°C) (mean +/-SD; n≥3).

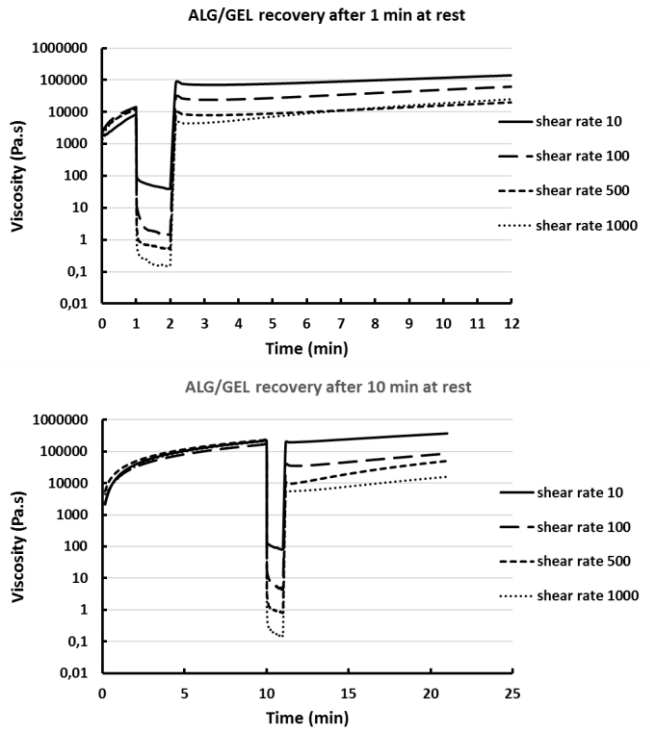

Figure 23. Shear recovery tests of Alginate/gelatin hydrogels after 1- or 10-min rest times (mimicking time in the cartridge before printing. Four different shear rates (10, 100, 500, 1000 s-1) were applied (mean; n=6).

4.5.4 3D printing of pre-hydrogel solutions

To confirm the correlation between rheological data and printability in real printing conditions, the biomaterial inks were also printed using a 3D Discovery printer as described in the experimental section and in Table 6. The size of the needle (22G needle) and the flow rate (1.25 mm^3/min) were chosen in order to keep the shear rate applied on the gel during the extrusion close to 100 s^{-1}, according to Equation 3. This value was chosen based on the results of the recovery tests, showing better recovery at such a low shear rate (Figure 22). The printing resolution was studied as a function of the feed rate (speed of needle above the substrate during deposition) and gel formulation. We analysed the width of the filaments after extrusion, the uniformity of the printed lines, their continuity and their integrity, which can be defined as the comparison of the theoretical and measured height of the printed filaments [214, 272].

B2 and B3 showed phase separation after centrifuge, even before printing (Figure S 1(a)). Printing led to a heterogeneous mix of gel and liquid regions, with non-repeatable and broken filaments. In particular, B2 led to non-uniform filaments, broken lines and curvy angles (see the example in Figure S 1(b)), which made it impossible to print multiple layer structures. Double phasing was even clearer for B3, leading to needle clogging and preventing good extrusion. Therefore, we do not present the complete data for B2 and B3 here.

Figure 24 presents data and typical images of printed lines for A2 and A3 formulations at various feed rates. Both formulations led to uniform filaments. As shown in Figure 24(a), A2 was able to print continuous lines with relatively sharp angles, but the filament width was large (1.2-1.5 mm) compared to the needle internal diameter (ratio of width/diameter = 3.5). This leads to low resolution.

A3 led to uniform, sharp angled and thinner filaments (minimum width of 0.57 mm ± 0.04 mm (ratio=1.4) at a feed rate of 11 mm/s (Figure 24b). However, at this feed rate, the lines were easily breaking, making it challenging to print multiple layer structures. Reducing the feed rate to 10 mm/s led to continuous lines with a mean width of 0.75 mm ± 0.07, making it a better option.

Printing multiple layer structures with A3 led to smooth integration between layers and cohesive structures. To observe the structural integrity of the gel, we analysed the difference between the theoretical and the real height of 5- or 10-layer structures. The average height of the layers was found to be between 0.33 and 0.27 mm, which is a variation of ± 10% from the theoretical height (0.3 mm). This shows that the structure isn't collapsing under the weight of the multiple layers.

Interestingly, structures printed at higher shear rates (higher flow rates or similar flow rate but smaller needle diameter) led to poor resolution and structural integrity, as shown in Figure 25(a). This is in agreement with recovery tests which show better recovery at low shear rates.

Filament width with A3 was quite similar to that of alginate/gelatin (0.68 ±0.06 μm) which showed very uniform fiber formation (Figure 24 (b), (c)) and ability to print in a cohesive layer-by-layer structure before post-crosslinking (Figure 25a).

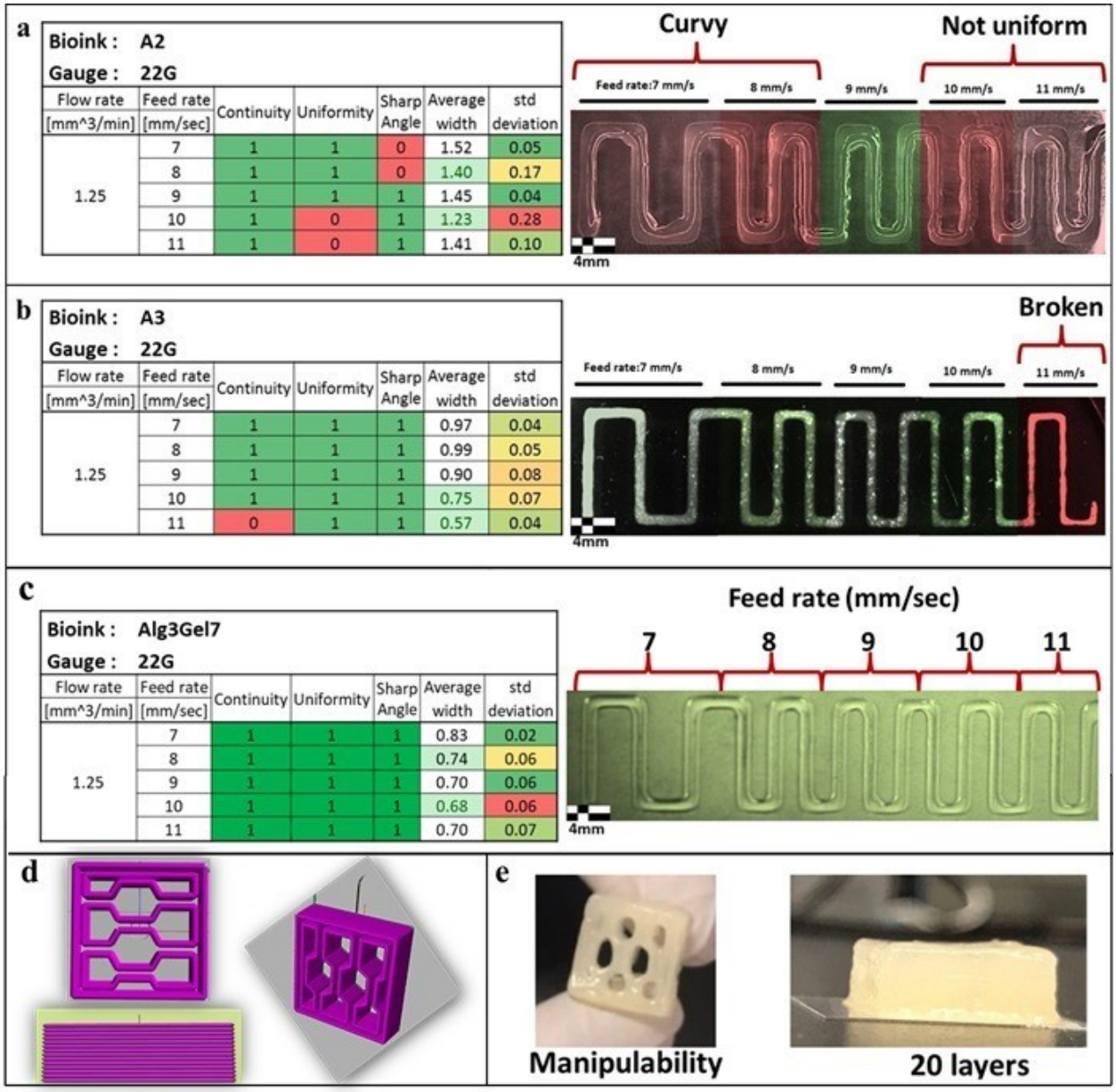

Figure 24. a) Descriptive results and images of filaments printed with a 22 G needle (0.41 mm inner diameter) with feed rates changing from 7 to 11 mm/s, for a) A2, b) A3 chitosan hydrogels and c) Alginate/gelatin filaments as comparison (mean +/-SD; n≥3).; d) 3D CAD honeycomb design model; e) picture of 10- and 20-layers printed structures made with A3 hydrogel.

4.5.5 Post printed mechanical strength

A good ink should provide tissue-mimicking rigidity and enough strength after printing. The mechanical properties of printed structures were therefore tested in compression, after 24 h gelation at 37°C (Figure 25). A3 formulation was chosen since it presented the best rheological properties in terms of adequate gelation kinetic and recovery, and printing behavior. Recovery tests suggested that A3 formulation presents better recovery when the shear rate stays at or below 100 s^{-1} (see Figure 22I). We hypothesized that the resolution and mechanical properties would thus be increased when printing the structure at low/medium shear rate (e.g. 230 s^{-1}, see Table 6) compared to high shear rate e.g. 507 s^{-1}, (generated by increasing the flow rate to 2.75 mm^3/s). Compression tests were performed on 5-layer structures since it is the best we could obtain when printing A3 at high flow rate.

Pictures, compression curves and secant Young moduli at 15 and 30% deformation are reported in Figure 25 for structures extruded at low and high shear, in comparison with structures printed with the alginate/gelatin bioink at 200 s^{-1} (flow rate of 1.25 $mm^3.s^{-1}$), soaked in $CaCl_2$ for 15 min to ensure that the structure is completely crosslinked, then incubated at 37°C for 24 hours [242].

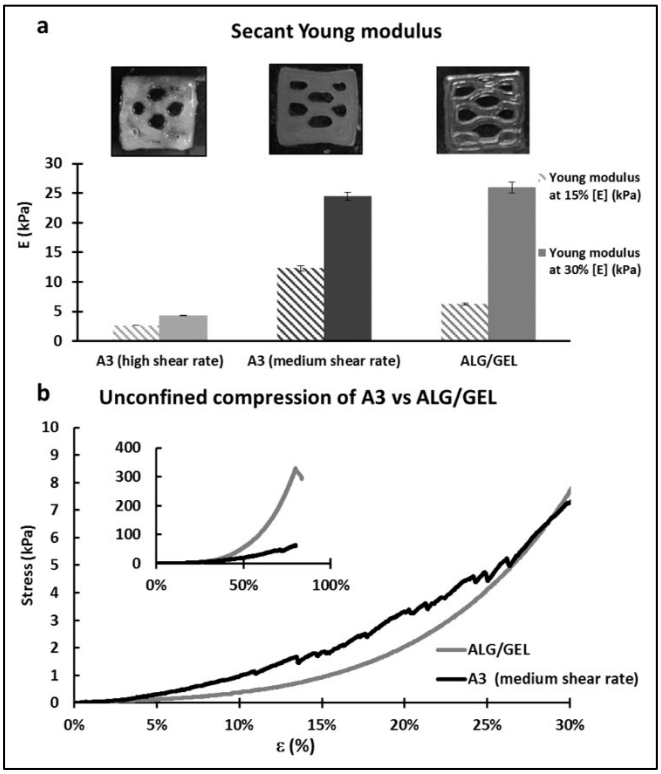

Figure 25. Behavior under unconfined compression of chitosan-based hydrogel and Alginate/Gelatin: a) secant Young modulus of A3 printed with high (507 s-1)/medium (230 s-1) shear rate and alginate/gelatin bioinks; pictures of the 5-layer honeycomb structures tested are also shown; b) stress-strain curve in unconfined compression (mean ± SD; n≥3).

When printed at a low/medium shear rate (230 s-1), the secant Young modulus of A3 chitosan structures at 15 and 30% deformation was 12.3 ± 0.5 kPa and 24.4 ± 0.7 kPa respectively. This is similar to or even more rigid than alginate/gelatin bioink (6.3± 0.2 kPa and 25.9 ± 0.9 kPa at 15% and 30% deformation respectively). Both structures presented good integrity and were easily handable, even if alginate/gelatin structures presented significantly higher resistance to rupture (329 ± 27 kPa vs 48 ± 4 kPa for A3; Figure 7b).

As expected, the mechanical properties of A3 chitosan gel printed at high shear rate (e.g. 507 s^{-1}) were lower. The secant Young modulus at 15% and 30% deformation was 2.6 ± 0.02 kPa and 4.3± 0.1 kPa,

respectively. The printed structure had a poor resolution. It was flattened and its poor structural integrity prevent it from being removed from the glass slide after printing.

4.6 Discussion

Inks for bioprinting must fulfil a number of key requirements, including printability and mechanical cohesion after printing [22]. Chitosan thermosensitive hydrogels formed with BGP, alone or combined with gelatin or hydroxyapatite have be previously shown to present interesting characteristics for bioprinting [194, 274] but they face particular challenges since they are time- and temperature-evolving materials.

While CH is normally soluble only in acidic media, the addition of a weak base such as BGP allow to form a solution with neutral pH at room temperature. The negatively charged molecules screen the chitosan positively charged ammonium groups and prevents repulsive forces between chitosan chains. When increasing temperature, heat-induced transfer of protons from CH to glycerol phosphate takes place, allowing strong interaction of CH chains, mainly through hydrophobic and hydrogen bonds [188, 197]. In the case of SHC+BGP or SC+PB, the higher mechanical properties observed could be explained by a more complete neutralization of chitosan chains due to the small size of SHC molecule and stronger interactions due to its decomposition into CO_2 [275]. While this physical gelation mainly takes place at temperature close to body temperature (due to the change of chitosan pKa), it initiates at lower temperatures. Some ionic crosslinking can also take place [197]. The lack of complete stability of the solution at room temperature is a possible limitation of these gels for bioprinting applications and must be taken into account by a rigorous rheological approach.

Yet to date, only limited rheological characterization has been performed [194, 218], which doesn't take time into account and doesn't allow to understand the benefits and limitations and optimize the printing process. In this work, we adapted rheological tests to assess and predict the printability of chitosan thermosensitive hydrogels, whose rheological properties evolve with temperature but also with time.

Gelation kinetics: We first performed time sweeps at 22°C to compare the various gel formulations in terms of stability at room temperature, i.e. how fast does the gelation start when the solution is kept in a cartridge at room temperature. This information is important since the time required to prepare the set-up and print can change the bioink properties. Crosslinking of the solution prior to extrusion could lead to needle clogging [74, 213] or to decreased shear thinning or poor recovery after shear removal.

Formulations made with a mixture of SHC+BGP (A) presented better stability at room temperature than their SHC+PB (B) counterparts, the latter presenting a gelation time of less than 30 s according to the approach of Winter and Chambon. This is in accordance with our previous data [67]. It is however important to mention that this approach (assessing gelation time by G' and G'' crossover) has limitations.

The fast gelation of SHC-PB formulations (especially B3) at room temperature can be correlated with the precipitation and phase separation observed during the centrifugation process prior to cartridge loading, as well as to the heterogeneous and non-continuous structures at printing (Figure S 1) at even room temperature. These formulations were therefore rapidly discarded.

Time sweeps at 37°C allowed us to evaluate the ability of the material to rapidly gel at 37°C. One advantage of thermosensitive hydrogels for bioprinting is the increase of their mechanical properties once incubated at 37°C, without the need of a crosslinker. Results confirmed that increasing the temperature to 37°C accelerates the gelation process in all chitosan-based bioinks, but the effect was more pronounced for CH2%w/v formulations (A2). The lower thermosensitivity of CH3% compared to CH2% hydrogel is in accordance with literature data [191, 276] and could be explained by decreased diffusion of bicarbonate molecules (SHC) and reduced movement of chitosan chains, leading to less chain interactions.

The more pronounced thermosensitivity of CH2% formulations could be an advantage for bioprinting. However, CH2% formulations also present lower viscosity before and after shear removal, which was later shown to be a more decisive property.

Shear thinning: In addition to adequate gelation time, shear-thinning behavior, characterized by viscosity decrease when the shear rate increases, is advantageous for bioprinting. This property makes it possible to reduce the pressure needed to extrude the material and therefore the potential damage to the cells encapsulated in the hydrogel via plug flow behavior [223, 277, 278]. More shear-thinning hydrogels present fewer cell damages during extrusion. Our results showed that all pre-hydrogel solutions tested were non-Newtonian, and presented shear thinning behavior (Figure 21). At a shear rate of 100 s^{-1}, the dynamic viscosity of A3 formulation was about 10^3 mPa.s, which corresponds to shear stresses of 100 Pa.

Alginate-gelatin control hydrogels also presented shear thinning properties but to a lower extent (viscosity around 10^5 mPa.s at 100 s^{-1}; Figure S 2). It suggests that applied shear stress will be 10000 Pa on cells at e.g., shear rate of 100 s^{-1}. Impact of shear stress on cell viability was studied by other researchers [223, 278].

It was reported that shear stress above 5000 Pa influences cell survival adversely in both the short- and long term [223, 278]. However, further studies are required to prove chitosan hydrogel's advantages over alginate/gelatin as bioink for cell encapsulation.

The information extracted from the shear viscosity results can assist in gaining a better understanding of a biomaterial ink or bioink's extrudability in printing. Moreover, its slope allows to evaluate the shear stress during printing as a function of flow rate and needle diameter. This approach can be applied to any extrusion-based system. However, printability cannot be concluded from these results alone [22, 279]. Shear recovery was therefore performed as a next test.

Shear recovery and printability: Since shear during printing can alter the material's properties, it is important to verify that the biomaterial ink rapidly recovers after shear, to maintain the printed structure. Therefore, shear recovery tests were performed on formulations made with SHC+BGP (A2, A3). An additional step was added to common recovery tests, i.e. temperature increase at 37°C to mimic sample heating after printing to take advantage of the gel thermosensitive properties.

Data showed that the ability to recover after shear depends on the formulation (A3 better than A2), the extent of shear rate (better recovery for shear rate of 100 s^{-1} or less), and the extent of gelification of the hydrogel prior to shear. As expected, shear recovery was very limited for the pre-gelled inks. These results show the importance of the stability of the solution at room temperature, when the solution is in the printing cartridge, and to control the time during which the solution is kept in the cartridge before printing. Change of viscosity and beginning of gelation is a limitation of chitosan thermogels compared to other bioinks. We therefore suggest controlling of the flow rate using a plunger dispenser in contrast to pressure-driven extrusion, as we did in our study, to avoid flow variability during printing. However, recovery after printing can still vary as a function of time between hydrogel mixing and printing. It is therefore important to evaluate the acceptable time frame for extrusion.

Chitosan 3% (A3) presented better recovery compared to chitosan 2% formulation (A2), especially at low and medium shear rates. This suggests that A3 filaments present a better ability to support upper layers, as it was indeed observed later during printability tests.

It is also important to note that in the case of A2, the filament width was significantly larger than for A3, the filament width/needle diameter ratio reaching up to 3.5, compared to 1.4 (Figure 24 (a) & (b)). This

indicates that the gel is taking expansion after extrusion, and could be related to the normal force that impact extruded filament during extrusion process [234].

These two reasons could explain the difficulty of bioprinting solid 3D structures with A2 hydrogels, despite their more interesting thermosensitive character.

In contrast, A3 presented high initial viscosity, good shear thinning and good recovery when printed at a low shear rate, leading to 3D structures with good integrity and a rigidity comparable to alginate/gelatin at the low deformation rate generally encountered in biological tissues (<30%). Variation between the theoretical and real height of the printed structure was less than 10%. This shows that there is no significant spreading of the printed filaments and that they support the weight of the additional layers. Moreover, the printed structure showed excellent cohesion between layers and was easy to handle. This is an important result since mechanical properties are key to ensure the fidelity of the structure during printing, but also later to ensure cohesion during maturation, handling and potential in vivo stresses. It also influence cell response [77, 277].

Recovery tests however emphasize the importance of the shear rate during printing. Indeed, recovery was poorer after high shear rates. Inability to return to the reference viscosity implies loss of chain interactions in the physical hydrogel. This was reflected by the appearance and the mechanical properties of the printed structures, which were much poorer for the 3D structure printed at a shear rate of 507 s^{-1} than at 230 s^{-1} (Figure 25(a)). Evaluating the shear stress using shear thinning tests and Equation 3, and performing recovery test at the corresponding shear stress would therefore be an important step to assess the printability or optimize the printing process of biomaterial inks.

The cytocompatibility of chitosan-based hydrogels for cell encapsulation has been already proven, by our team among others [67, 195, 218, 280, 281]. But for their use as bioinks, further work is of course needed to study the influence of gel formulation and shear rates on the survival of encapsulated cells. Further optimization could also be performed by the addition of gelatin or collagen, which have been shown to improve cell adhesion, survival and migration and could also influence [218, 280-282] and improve their printability.

Another limitation of this work is that while the substrate was heated at 37°C, temperature can be lower on top layers. Further work will be required to better assess the effect of the substrate's temperature and

possible variability of the temperature among the various layers to determine the importance of a well-controlled print bed to create homogenous structures. However, it is important to mention that we didn't observe heterogeneity in the structures created by 10 or 20 layers after 24 hour gelation in an incubator.

As expected, alginate/gelatin hydrogels presented interesting recovery properties, despite also dependant of the shear rate. Such behavior is similar than for pure alginate bioink, according to the literature data [74, 283]. In this study, alginate/gelatin was studied as considered as a stable solution since we kept the temperature constant at 22°C. We however noted that the viscosity at rest increased with time. This is probably due to the slight decrease of the temperature between the moment the material was poured in the rheometer (at 25°C) and the time it stabilizes at 22°C. Indeed, the viscosity of gelatin is strongly dependant on the temperature. It might also be due to interactions between alginate and gelatin after mixing. This emphasizes the importance of evaluating the effect of time and temperature during printability studies. Thus, the present approach could be applied to other temperature or time-evolving materials.

4.7 Conclusion

In this work, we propose a rheological approach to evaluate the printability of biomaterials inks, in particular for the case of time- and temperature-evolving materials such as chitosan thermosensitive hydrogels. The method to calculate the shear stress can be universally applied for any type of extrusion-based system. We showed that gelation kinetic, shear thinning and shear recovery tests where time and temperature is taken into account, are essential to evaluate the printability of time-evolving bioinks.

The gelation kinetics and the level of shear rate had a critical effect on shear recovery. It strongly influenced the ability to support layer-by-layer build-up, the fidelity of the printed structure and its post-printing mechanical properties.

One formulation made with sodium bicarbonate and beta-glycerophosphate as gelling agent (A3) appears a promising bioink. After 24 hours gelation at 37°C, it presents similar rigidity in compression at the low deformation (<30%, generally encountered in biological tissues) than alginate/gelatin bioink after crosslinking by calcium ions. However, its mechanical resistance is lower. Its biodegradability is a clear advantage over alginate-based bioinks which degradation is depending of many parameters and is difficult to control [284]. However, further work is needed to confirm cell viability and proliferation in these new chitosan-based bioinks.

Acknowledgement

We would like to acknowledge the Natural Science and Engineering Research Council of Canada (NSERC; RGPIN-2015-05169) and the Fonds de Recherche du Quebec – Nature et technologie (FRQNT; team project and M.R. scholarship) for funding and support of this project.

4.8 Supplemental Information

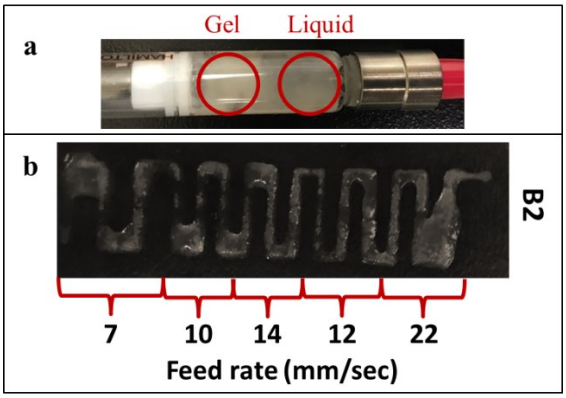

Figure S 1. (a) pha68hermos68ouion of B3 in the syringe before printing; (b) printed filaments with B2 formulation (partially gel and partially water).

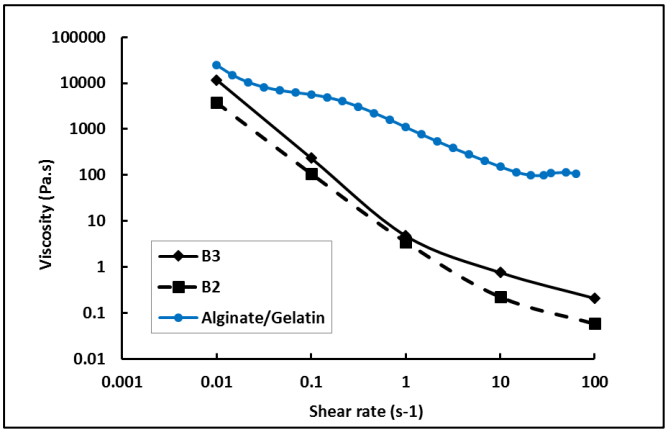

Figure S 2. Shear thinning behavior of B2, B3, and alginate/gelatin at 22°C (mean; n≥3).

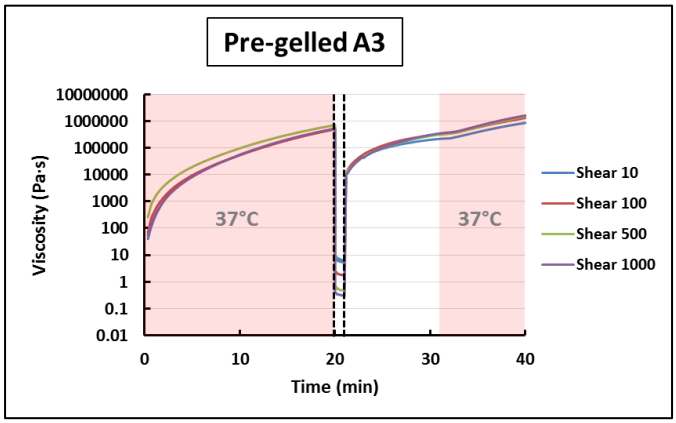

Figure S 3. Shear recovery under 4 different applied shear rates (10, 100, 500, 1000 s-1) for pre-gelled A3 (samples previously subjected to 20 min gelation at 37C). Change of the shear rate is indicated by the vertical line; part of the test done at 37°C is highlighted in red, white zone is 22ºC) (mean +/-SD ; n≥3).

Table S 1. Main shear recovery data from chitosan (mean, SD and SD%), as a function of shear rate (10, 100, 500 nd 1000 s-1).

Chitosan pre-hydrogels recovery tests					
	Formulation		**Viscosity (Pa.s)**	**± SD**	**SD%**
Shear rate 10	A2	Under shear	0,8	0,0	5%
		Instant recovery at 22°C	501,5	127,1	21%
		Post-priting 37°C	6 170,0	2 616,3	30%
	A3	Under shear	8,9	0,7	6%
		Instant recovery at 22°C	586,3	27,2	4%
		Post-priting 37°C	1 720,4	490,6	23%
Shear rate 100	A2	Under shear	0,2	0,0	11%
		Instant recovery at 22°C	65,6	15,4	19%
		Post-priting 37°C	2063,3	883,0	35%
	A3	Under shear	1,5	0,0	2%
		Instant recovery at 22°C	663,3	94,6	12%
		Post-priting 37°C	4616,7	973,0	17%
Shear rate 500	A2	Under shear	0,1	0,0	3%
		Instant recovery at 22°C	111,0	31,1	20%
		Post-priting 37°C	9610,0	1965,8	14%
	A3	Under shear	0,6	0,1	7%
		Instant recovery at 22°C	95,7	19,9	17%
		Post-priting 37°C	3100,0	678,8	15%
Shear rate 1000	A2	Under shear	0,1	0,0	5%
		Instant recovery at 22°C	1,8	0,9	40%
		Post-priting 37°C	613,7	142,1	19%
	A3	Under shear	0,4	0,1	12%
		Instant recovery at 22°C	127,4	79,4	51%
		Post-priting 37°C	2640,0	9180,5	25%

Table S 2. Main shear recovery data from alginate-gelatin (mean, SD and SD%), as a function of shear rate (10, 100, 500 nd 1000 s-1). Recovery test were performed after 1 and 10 min rest (mimicking the time in the printing cartridge).

ALG/GEL recovery tests				
Shear rate (s^{-1})		Viscosity (Pa.s)	± SD	SD (%)
	1 min rest at 22°C prior to shear			
10	Under shear	96,2	17,7	15%
	Instant recovery	83440,0	28858,7	28%
100	Under shear	11,8	2,0	15%
	Instant recovery	30875,0	5687,0	16%
500	Under shear	2,4	0,8	31%
	Instant recovery	9482,0	1935,6	18%
1000	Under shear	0,9	0,2	19%
	Instant recovery	4648,1	510,7	9%
	10 min rest at 22°C prior to shear			
10	Under shear	139,2	23,5	17%
	Instant recovery	196523,4	19517,3	10%
100	Under shear	18,3	2,5	12%
	Instant recovery	37916,2	3825,4	9%
500	Under shear	3,6	0,2	5%
	Instant recovery	10171,7	830,9	7%
1000	Under shear	1,4	0,3	21%
	Instant recovery	5631,7	1810,8	29%

4.9 Summary of paper 1 and introduction of objective 2

In the first paper, we studied whether rheological properties could predict printability of chitosan hydrogel. We propose a rheological approach to assess and optimize the printability of time-dependent hydrogels, such as thermosensitive chitosan-based hydrogels, as bioinks for bioprinting. We also demonstrated that the thermosensitive physical chitosan hydrogel made of combination of Beta-glycerophosphate (BGP) and Sodium-hydrogen-carbonate (SHC) [68], can print a structure with proper shape fidelity, and manipulability [285]. However, a high concentration of chitosan (3%w/v) was needed. We also show that the gelation kinetics and the level of shear rate had a critical effect on recovery and post-printing mechanical properties of the hydrogels. The viscosity of the solution also strongly influenced the resolution and the ability to support layer-by-layer build-up. After 24 hours gelation at 37°C, the chitosan bioink presents a compressive modulus similar to alginate/gelatin bioink after crosslinking by calcium ions. However, further work is needed to confirm cell viability and proliferation in these new chitosan-based bioinks. The methodology introduced in this paper could be used to evaluate the printability of other time-dependent bioinks in the future.

Later work, not included in paper 1, showed that cell encapsulation in CH 3% led to **a high mortality rate of encapsulated cells** due to the **high viscosity** of the cell-laden solution and the low porosity of the final hydrogel. **Decreasing chitosan concentration to 2% (w/v), a concentration previously shown adequate for cell encapsulation, resulted in a poor shape fidelity of structures formed with more than 5 layers** due to the low mechanical properties of the printed filaments immediately after printing. The printed filaments spread under the weight of the following layers.

Moreover, maintaining the substrate and environment uniformly at 37°C is an issue, leading to evaporation. Therefore, in the paper 2, we hypothesized that a **freeform reversible embedding of suspended hydrogels (FRESH) technique with a warm support bath, could support and hold bioprinted structures** and enhance chitosan therrmo-crosslinking during bioprinting and thus **increase the shape fidelity of the printed structures while keeping chitosan at a low concentration (e.g., 2% w/v) compatible with cell encapsulation**. This work has been accepted for publication in Journal of Bioprinting; DOI: 10.1016/j.bprint.2022.e00209.

Chapter–5 - FRESH Bioprinting of Biodegradable Chitosan Thermosensitive Hydrogels

Maedeh Rahimnejad[1, a], Atma Adoungotchodo[2, a], Nicole Demarquette[2], Sophie Lerouge[1, 2, a*]

[1]Biomedical Engineering Institute, School of Medicine, Université de Montréal, Canada

[2]Department of Mechanical Engineering, École de technologie supérieure (ÉTS), Canada

[a]Research Centre, Centre Hospitalier de l'Université de Montréal (CRCHUM), Canada

[*]Corresponding author

E-mail: sophie.lerouge@etsmtl.ca

5.1 Abstract

Thermosensitive chitosan (CH)-based hydrogels prepared with a mix of sodium bicarbonate and β-glycerophosphate as gelling agents rapidly pass from a liquid at room temperature to a mechanically strong solid at body temperature without any crosslinker. They show excellent potential for tissue engineering applications and could be interesting candidates for bioprinting. Unfortunately, since gelation is not instantaneous, formulations compatible with cell encapsulation (chitosan concentrations around 2% or lower) lead to very poor resolution and fidelity due to filament spreading. Here, we investigate the FRESH bioprinting approach with a warm sacrificial support bath, to overcome these limitations and enhance their bioprintability. First, a support bath, made of Pluronic including sodium chloride salt as a rheology modifier agent, was designed to meet the specific physical state requirements (solid at 37 ◦C and liquid at room temperature) and rheological properties appropriate for bioprinting. This support bath presented yield stress of over 100 Pa, a shear thinning behavior, and fast self-healing during cyclic recovery tests. Three different chitosan hydrogels (CH2%w/v, CH3%w/v, and a mixture of CH and gelatin) were tested for their ability to form filament and 3D structures, with and without a support bath. Both the resolution and mechanical properties of the printed structure were drastically enhanced using the FRESH method, with an approximate four-fold decrease of the filament diameter which is close to the needle diameter. The printed structures were easily harvested without altering their shape by cooling down the support bath, and do not swell when immersed in PBS. Live/dead assays confirmed that the viability of encapsulated mesenchymal stem cells was highest in CH2% and that the support bath-assisted bioprinting process did not adversely impact cell

viability. This study demonstrates that using a warm FRESH-like approach drastically enhances the potential for bio- printing of the thermosensitive biodegradable chitosan hydrogels and opens up a wide range of applications for 3D models and tissue engineering.

Keywords: bioink, thermosensitive chitosan-based hydrogel, support bath, FRESH bioprinting

Graphical abstract

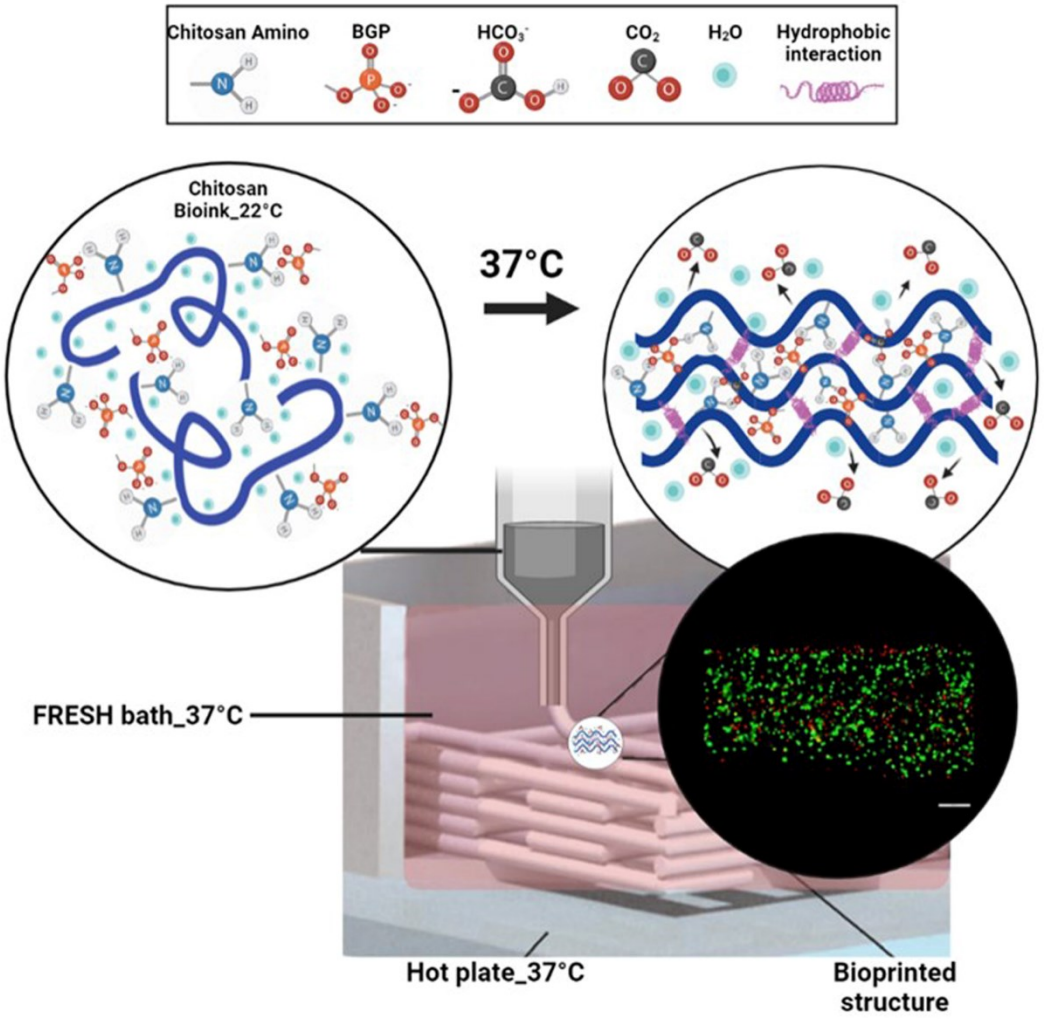

5.2 Introduction

Despite the huge recent progress in bioprinting, the quest for better biodegradable bioinks is still ongoing. Chitosan hydrogels are particularly attractive candidates due to chitosan biocompatibility and biodegradation, which can be tuned by changing the degree of deacetylation (DDA) and molecular weight [68]; a significant advantage over other biopolymers such as alginate. Chitosan thermosensitive physical hydrogels, that are liquid at room temperature, but rapidly gel at body temperature, present interesting features as bioinks [67, 68, 187]. In particular, it has been shown that when an acidic chitosan solution is mixed with a combination of Beta-glycerophosphate (BGP) and Sodium-hydrogen-carbonate (SHC), it forms a solution of physiological pH and osmolarity where cells and bioactive factors can easily be mixed. Once at 37°C, it rapidly gels into a strong porous hydrogel without the use of a chemical crosslinker [68]. Excellent survival of cells, such as mesenchymal stem cells, intervertebral disk cells, or T lymphocytes, to name just a few examples, was demonstrated and thanks to their good mechanical properties, these hydrogels have been already proposed for several cell therapy and tissue-engineering applications [268, 275].

However, the few attempts to print cell-loaded thermosensitive chitosan hydrogels [184, 218, 286], have led to disappointing results, with bioprinted structures presenting either very poor resolution and low mechanical properties, or poor cell viability. For example, Rahimnejad et al. showed that chitosan concentration around 3%w/v was necessary to result in structures with good resolution and handleability [285]. This however led to a high mortality rate of encapsulated cells due to the high viscosity of the solution in which the cells were mixed and to the low porosity of the final hydrogel. Decreasing chitosan to concentrations more suitable for cells (2% or below) resulted in poor shape-fidelity structures due to the low mechanical properties of the printed filaments (spreading under the weight of the overlying layers) as also shown by other teams [140, 141, 285]. The main reason for this is that the gelation process of chitosan hydrogel is not instantaneous. Moreover, to take advantage of the thermosensitivity of these hydrogels, it is important to maintain the environment at 37 °C. But keeping a simple warm substrate at 37 °C is quite challenging and can lead to water evaporation from the sample.

In this paper, we show how combining 2% chitosan hydrogels with the freeform reversible embedding of suspended hydrogels (FRESH) approach, modified to include a warm support bath, can overcome the

limitations observed when using other processes and allow to print pure chitosan 3D structures combining good mechanical properties, fidelity, and cell viability under gentle conditions.

The FRESH method was initially proposed by Feinberg's team in 2015 [53] to maintain the intended structure during the print process and improve print fidelity. It is now largely used in the bioprinting field, with some amazing results, such as printing a full-size model of the heart [54, 249]. This method has been applied with several biopolymers such as alginate, collagen, and fibrin, but to the best of our knowledge, it has never been applied with chitosan.

The first objective of this work was to design a support bath that presents the key features required to print chitosan hydrogels. For that the support bath should present adequate rheological properties when warmed around 37 °C, to take advantage of the thermosensitivity of these hydrogels. It must be cytocompatible, and its removal after bioprinting should not impart any mechanical or biological shock to the cells. In terms of rheological properties, three main properties are desirable. First, the support bath should behave as a rigid body when subjected to low stresses but flow as a viscous fluid when subjected to high stresses [56]. The rheological properties of such materials are generally described by the Herschel−Bulkley model [57, 58], where the shear stress τ relates to the shear rate $\dot{\gamma}$ as presented in Equation 4 [287].

For $n<1$ the material is shear-thinning, whereas for $n>1$ it is shear-thickening. If $n=1$, the model reduces to Bingham plastic fluid. It has been reported in the literature that the yield stress of the FRESH support should be equal to or higher than 100 Pa [58, 59].

Second, once the bioink is in place, the FRESH support should stop flowing and recover, to prevent the bioink to disperse. Furthermore, the recovery should be rapid to ensure no crevasses or air pockets are trailing from the moving nozzle [59]. Third, it has also been shown that the stiffness of the support bath, which can be accessed by its storage modulus G', is of paramount importance to the process. Storage moduli of FRESH support should vary between 5,000 Pa to 10,000 Pa, to provide adequate support for a low viscosity ink and yet allow its penetration [54, 58, 245, 256].

Different materials have been proposed as a FRESH support bath, such as gelatin microparticles, Carbopol microgels and nanoclays (e.g., Laponite), and Pluronic. Gelatin microparticles (slurry) is the most commonly used material [53]. However, gelatin slurry is liquid at body temperature [249], which it is not suitable for chitosan bioinks that gel at 37 °C. Carbopol microgels are anionic [250] and not recommended for use with cationic hydrogels such as chitosan [251]. Nanoclays also are not suitable for cationic

hydrogels, because possible positive charges dissolve the bath, and amine groups of chitosan can lead to the formation of small, flocculated particles, often described as "seeds" [253, 254, 288]. Another possible material for the FRESH method is Pluronic (F-127), a block copolymer, PEO-PPO-PEO, used alone or with additives [255-259]. Pluronic is generally in the gel form at 37 °C, while liquid at lower temperatures, thus enabling its gentle removal by decreasing the temperature. Moreover, its gelation temperature and modulus can be tuned by varying its concentration and by the addition of salts, such as NaCl or $CaCl_2$ [58, 257, 289]. Thus, Pluronic is a promising FRESH support bath for this chitosan thermosensitive hydrogel.

In this work, we first optimized a Pluronic-based support bath and then demonstrated how we can use this approach to very significantly increase the printability of chitosan and chitosan-gelatin hydrogels and fabricate biodegradable 3D structures with good resolution, good mechanical properties and cytocompatibility, opening for many applications in tissue engineering and 3D tissue models.

5.3 Materials and Methods

5.3.1 Materials

Shrimp shell chitosan (ChitoClear, HQG110, Mw: 155 kDa, DDA 83%) was purchased from Primex (Iceland). β-Glycerol phosphate disodium salt pentahydrate (C3H7Na2O6P·5H2O, hereafter BGP) was purchased from Sigma-Aldrich (Oakville, ON, Canada). Sodium hydrogen carbonate NaHCO3 (sodium bicarbonate, hereafter SHC) was obtained from MP Biomedicals (Solon, OH, USA). Type A gelatin from porcine skin (G1890), Pluronic F-127 (Mw=12,600 g/mol), and sodium chloride (NaCl) were purchased from Sigma-Aldrich. Other chemicals were of reagent grade and were used without further purification.

5.3.2 Chitosan and chitosan-gelatin bioinks preparation

Chitosan (CH) and chitosan-gelatin (CH-Gel) hydrogels were prepared by mixing an acidic CH or CH-Gel solution with a gelling agent solution at a volume ratio of 3:2, respectively. Chitosan (CH) powder was first solubilized in hydrochloric acid (HCl) (0.1 M) at 3.33% w/v (final concentration 2%), by way of mechanical stirring for 3 hours. For the chitosan-gelatin (CH-Gel) solution (final concentration 2% w/v for each component), gelatin powder was added to 0.1M HCl solution, heated to 37 °C for 30 min, then chitosan powder was added, and the solution was stirred for 4 hours. Chitosan solution at 5% w/v chitosan (in

0.015 M HCl; final CH 3% hydrogel) was also prepared as a control substance. The solutions were sterilized by autoclaving (20 min, 121 °C) and stored at 4 °C.

The gelling agent used in this study was a mixture of BGP and SHC, hereafter called BGP/SHC, at a final concentration in the hydrogel of 0.1 M/0.075 M and 0.15 M/0.113 M for 2% and 3% chitosan-based hydrogels, respectively, as previously published [67].

The two solutions were introduced in separate syringes, joined by a Luer lock connector. The content of the gelling agent syringe was pushed into the CH syringe, and the mixture was transferred back and forth from one syringe to another 15 times. Hydrogel solutions were then centrifuged to remove air bubbles and used immediately. Hydrogels had a final chitosan concentration of 2% (w/v) or 3% (w/v). All had a physiological pH.

5.3.3 FRESH bath preparation

Pluronic powder was solubilized under stirring in distilled water at concentrations of 17 to 23% w/v with and without 1% and 5% w/v NaCl salt for 6 hours at 4 °C. The pH and osmolality of the various solutions were measured using a Horiba LAQUAtwin pH-22 Compact and Portable pH Meter (Horiba, country), and Advanced® Micro 3300 Osmometer respectively.

5.3.4 Rheological characterization

Rheological characterization of the support bath and the bioinks were carried out using an Anton Paar instrument (Physica MCR 301, Germany) with a concentric cylinders type geometry (CC10/T200), 1 mm gap, or a cone-plate geometry (CP25) 25 mm in diameter. The linear viscoelastic (LVE) range was first determined using a plate-plate geometry (PP25) and an amplitude sweep test. The following tests were then performed, either on the support bath, the bioinks, or both:

1) Temperature sweep from 10 °C to 45 °C at a rate of 1 °C/min was first performed on various compositions of support bath, using the oscillatory mode in the LVE range, at a constant shear strain (1%) and constant frequency (1 Hz) to determine the formulations with adequate gelation temperature (temperature where the storage modulus G' was equal to the loss modulus G'').
2) Time sweeps at 37 °C were then performed to assess the stability and viscoelastic properties of the support bath. In addition, the gelation kinetics of the chitosan bioinks was studied using time sweep tests

for 10 min at 22 °C (to assess their stability at room temperature in the printing cartridge) followed by 10 min at 37 °C (to assess their gelation kinetics once printed in the support bath).

3) Amplitude sweeps with strain-controlled mode (1% to 100% strain) were performed using oscillatory rheometry at a constant frequency (1Hz) to evaluate the yield stress of the hydrogels and support bath at 22 °C and 37 °C, respectively. The yield stress was considered as the stress value where G' dropped by >10% of the deformation.
4) Shear thinning viscosity behavior of the bioinks at 22 °C was assessed using rotational rheometry tests as previously reported [285].
5) Recovery tests at 37 °C were also performed using oscillatory rheometry, to verify the self-healing properties of the support bath after printing. The storage modulus of the bath was measured during various cycles mimicking the printing process: (1) Pre-printing (rest) (2 min at 1% strain); (2) Printing (sudden increase to 100% strain for 1 min) (3) Post printing (back to 1% strain). The hydrogels' recovery behavior was also evaluated with a slightly different protocol to factor in temperature after printing and take advantage of the hydrogel's thermosensitivity: (1) Pre-printing (1% strain for 10 min at 22°C); (2) Printing (100% strain for 1 min at 22°C); (3) Post-printing (1% strain for 10 min at 37°C).

5.3.5 Printing procedure

A 3D-Discovery bioprinter (RegenHU, Villaz-St-Pierre, Switzerland) was used to print the hydrogels via a plunger dispenser, which is able to maintain a constant dispensing rate (volume/min) during printing even if the hydrogel properties change with time. The cartridge was kept at room temperature, while the heated substrate (warm glass or warm FRESH bath) temperature was kept constant at 37°C. A long stainless steel 25G needle (length: 25.4 mm; internal diameter = 0.26 mm) was used to print the hydrogels. The effect of the feed rate (3, 5, 7, 9, 11 mm/s) and flow rate (0.5, 1.0, 1.5 mm^3/s) on filament width and continuity were first studied on glass (Figure S 4 in supplemental data); then the optimal flow rate (0.5 mm^3/s) was used to print within the bath.

5.3.6 Resolution and shape fidelity

Images of printed filaments were analyzed using the freeware ImageJ (Fiji.sc), according to the approach proposed by Gillispie et al. The average width [272] and the spreading ratio (printed filament width/ needle inner diameter) [213] were determined.

The best printing parameters (flow rate 0.5 mm3/s and feed rate 9 mm/s) were then used to print hydrogels on glass and within the FRESH bath in 10-layer and 20-layer gridded structures. The FRESH bath was removed 30 min after printing by putting samples at 4 °C for 10 min. Then, the printed structures were incubated once more for 24 hours at 37 °C. Their structural resolution and fidelity were assessed visually and quantified by two parameters: 1) the height of the printed structure was compared with its theoretical value (based on the layer-to-layer distance corresponding to 80% of the needle's internal diameter); 2) the printability (Pr) based on square shape as proposed by Ouyang et al. [213] using the following equation:

$$Pr = \frac{L^2}{16A} \qquad \text{Equation 5}$$

where, L is the perimeter and A is the area of the printed squares in the gridded structure. For the ideal bioink, the Pr is close to 1, indicative of sharp angles and absence of filament spreading. The range of $0.9 < Pr < 1.1$ is considered as good printability [290].

We also verified the stability and absence of swelling of the printed structure by taking images and measuring their weight before and after immersion in PBS for 24 h.

5.3.7 Mechanical properties characterization

Unconfined compression tests were performed on 20-layer printed gridded structures using the MACH-1 testing device (Biomomentum, Canada). A velocity equal to 100% of the sample's height/min was used. The compressive strength and secant Young's modulus at 10% and 30% of deformation were calculated from the stress-strain curves. ImageJ software was used to calculate the actual surface area of the printed structure (without the holes in the structure) to determine the applied stress. Tests were performed at room temperature after 24 hours of sample incubation at 37 °C.

5.3.8 Bioprinting of stem cell loaded hydrogels

Human bone marrow mesenchymal stems cells (MSCs) (PT-2501, Lonza Inc., ON, Canada) were cultured in NutriStem XF (#cat 05-200-1A, Biological Industry, USA) supplemented with 0.6% NutriStem XF Supplement (#cat 05-201-1U, Biological Industry, USA). They were used at passage 6.

MSC were encapsulated in the hydrogels as follows: 1.2 mL of CH or CH-Gel solutions were first mixed with 0.4 mL gelling agent solution using two syringes (3 mL) connected with a Luer Lock. The obtained mixture was then mixed with 0.4 mL cell suspension ($5x10^6$ cells/mL). After mixing, the cell density was 10^6 cells/mL in a solution of 2% w/v chitosan with or without 2% w/v gelatin, 100 mM BGP and 75 mM SHC. A volume of 200 µL of the solution was placed in a 48-well plate to be used as a control and to evaluate the effect of the printing process on cell viability. The solution remaining in the syringe was centrifuged at 1000 rpm for 1 min and used to bioprint different structures. Our bioprinter is stored in a biosafety cabinet and used in routine cell culture. All surfaces within the biosafety cabinet were disinfected with 70% ethanol and irradiated with the UV lamp overnight. Structures were bioprinted on the 6-well plate filled with a 1 ml 37 °C support bath. After bioprinting, the bath was removed for a 5 min incubation at 4 °C with a cold PBS buffer. Then, MEM α media (#cat 12561056, Gibco) supplemented with 10% FBS, and 1% penicillin/streptomycin was added to the surface and left to incubate 24 h at 37 °C, 5% CO_2. As a second control to evaluate the effect of the bath on cell viability, 200 µl of the solution remaining in the cartridge after the bioprinting process was injected through the needle into an empty 48-well plate and treated similarly.

Cell viability was assessed after 24h. In short, the wells were washed twice with PBS and incubated for 45 min at 37 °C with serum-free medium supplemented with 2 µM ethidium homodimer-3 and 1 µM calcein AM (LIVE/DEAD Cell imaging kit reagents, R37601, Life Technologies, Carlsbad, USA). The samples were then washed again with PBS and immediately observed using an inverted fluorescent microscope (Leica DM IRB, Feasterville, USA). Cell viability was calculated as the ratio of live cells (green) to total number of cells (green and red). The tally was obtained using the Analyze Particles function in ImageJ (National Institute of Health, USA).

5.3.9 Statistical analyses

All experiments were performed in triplicate. Results were expressed as mean ± SD. Statistical analysis was performed using GraphPad Prism 7.04 software. One-way ANOVA and Tukey's multiple comparison tests were used to compare multiple groups. $P<0.05$ was deemed statistically significant.

5.4 Results and Discussion

5.4.1 FRESH bath optimization and characterization

As explained in the introduction, the support bath was first designed to suit the specific needs of chitosan thermosensitive hydrogels, i.e. it must be a shear thinning solid at 37 °C (to provide support during the printing and rapid gelation of the chitosan hydrogel), heal well (recovery after strain), and then liquefy at a temperature that permits the easy removal of the cells.

Temperature sweeps and time sweep at 37°C confirmed that the gelation temperature and storage modulus (G') could be fine-tuned by changing the concentration of Pluronic [291-294] and NaCl [58, 257, 295]. Main data are shown in Figure S 5. Pluronic19%+1% NaCl was chosen as a support bath for further studies since it is completely liquid at 22 °C but forms a completely gelled and stable structure at temperatures above 32 °C with a storage modulus around 5 kPa (Figure 26). This allows for a safety margin in case the temperature of the support bath slightly decreases below 37°C, due to contact with ambient air. Moreover, NaCl 1% effectively provides osmolality to the support bath to a level similar to that of the printed material (physiological level) (323 ± 17 mOsm/kg H2O (physiological level is deemed around 330 mOsm/kg)), in order to avoid osmotic exchange between the two. The support bath also had a physiological pH.

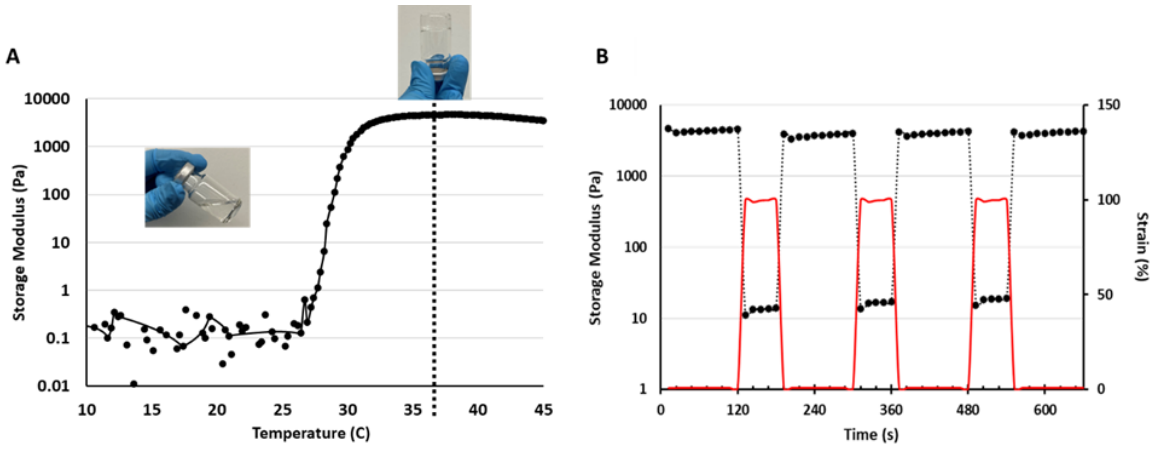

Figure 26. Rheological properties of Pluronic support bath A) Temperature ramps (10-45 °C) of Pluronic 19% (w/v) +1% (w/v) NaCl (dotted line=37°C); B) Recovery tests: Storage modulus of Pluronic 19% + 1% NaCl (black curve) during various cycles of strain at 37 °C (2 min rest at 1% strain, 1 min under shear at 100% strain, red curve) (mean; n≥3).

The support bath in the FRESH approach should also present sufficient yield stress to firmly hold the printed bioink after deposition while maintaining a shear-thinning behavior (so that it will not hinder the movement of the printing needle) and rapid recovery to a solid state after printing. Therefore, the support bath material's yield stress values, shear-thinning behavior, and self-healing were investigated. The optimized FRESH bath presents a yield stress of over 100 Pa (147 ± 3 Pa) (Figure S 6). The Herschel-Bulkley model (Equation 4) was used to fit the data and estimate the consistency index K and flow behavior index n (n=0.15; K=147; Figure S 7). The recovery properties of the FRESH bath at 37°C was demonstrated throughout cyclic deformation (1 min under shear at 100% strain followed by 2 min rest) (Figure 26B). Even after various cycles, the material showed complete recovery (storage modulus coming immediately back to its previous value). Such rapid recovery to a solid state ensures that the extruded bioink is soundly embedded [58, 218].

5.4.2 Rheological behavior of chitosan-based hydrogel bioinks

Prior to bioprinting, the rheological properties of the chitosan-based bioinks were assessed to confirm their thermosensitivity, as well as their shear thinning and recovery behavior. Figure 27 shows the evolution of the storage modulus during time sweeps, first at room temperature (22 °C) for 10 min to estimate the stability of the hydrogel solutions in the printer cartridge, and then at a temperature varying to 37 °C to assess their gelation kinetics once on the heated glass or in the warm FRESH bath.

As previously published, CH2 shows a drastic increase of G' when the temperature increases to 37 °C, indicative of the gel's thermosensitivity. This suggests that a warm FRESH bath can help ensure rapid gelation during printing. When gelatin was added to chitosan (CH-Gel), the behavior was quite similar, except for the sudden drop of the storage modulus when the temperature was increased to 37 °C, probably due to the gelatin melting. In contrast, CH3 showed a different trend, with a continuous increase of G' value as a function of time, with only a minor influence due to the temperature rise to 37 °C.

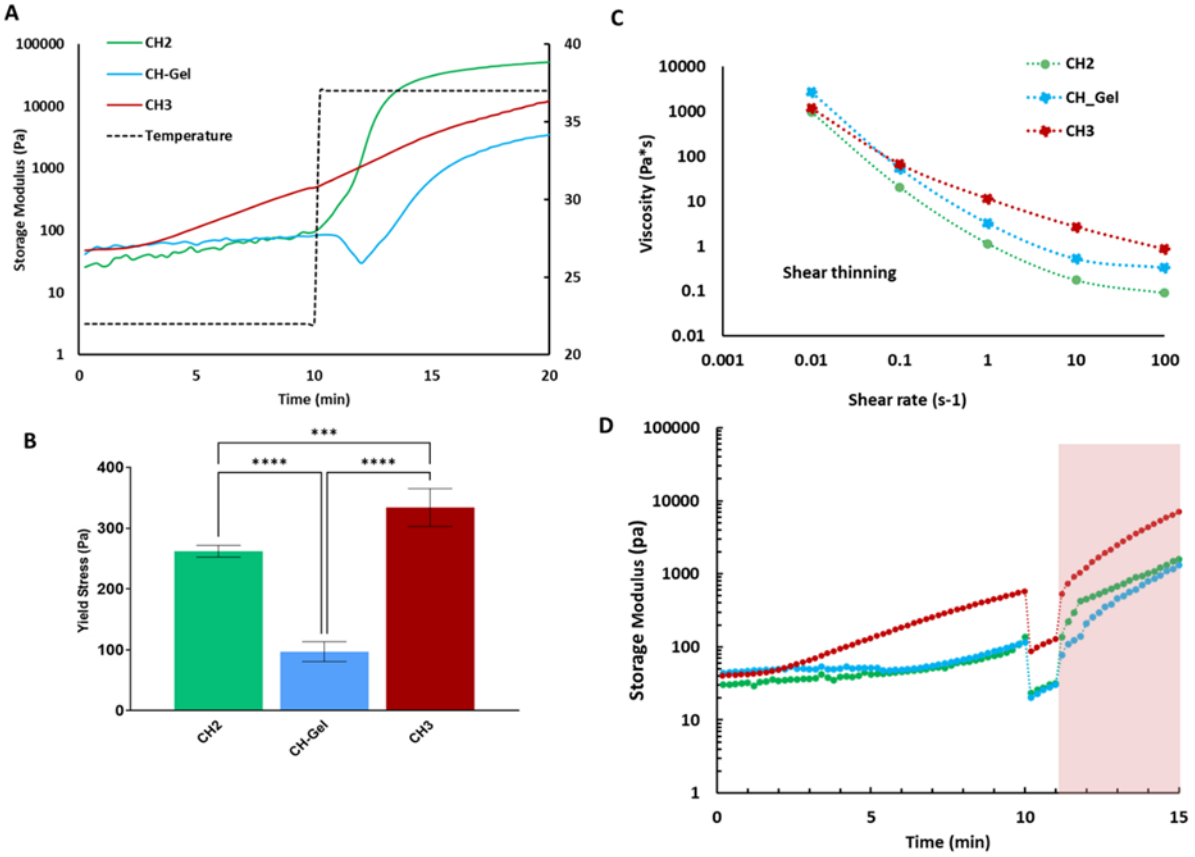

Figure 27. Rheological properties of chitosan hydrogels ; A) Evolution of the storage (G') and loss (G'') moduli of hydrogels as a function of time and following the sudden increase of the temperature from 22 to 37 °C (the dotted black line represents the temperature as a function of time).; CH2: chitosan 2% w/v hydrogel; CH3 : chitosan 3% w/v hydrogel; CH-Gel: chitosan 2% w/v gelatin hydrogel); B) Yield stress of each formulation (strain controlled, 0.01-500%) (mean +/-SD; n≥3); C) viscosity as a function of shear rate after 10 min at 22 °C (mean; n≥3); D) Recovery test, showing the evolution of the storage modulus during a complete cycle, namely at-rest state at 22 °C (1% strain for 10 min), printing step at 22 °C (100% strain for 1 min), post printed rest state at 37 °C (1% strain for 5 min) (n≥3)(the red zone shows increase of temperature from 22 °C to 37 °C).

Yield stress, shear rate sweep, and recovery tests performed to evaluate the printability of chitosan hydrogels are presented in Figure 27B-C respectively. All hydrogels present a yield stress over 100 Pa, CH-Gel exhibiting the lowest and CH3 the highest value (Figure 27B). The yield stress can be considered as a critical

stress above which the hydrogel starts to flow, showing the injectability of the material (initial force required to generate flow) [59]. Bioinks that exhibit a large yield stress will also naturally resist deformation and maintain the printed structure, a major advantage for 3D bioprinting [59].

Figure 27C shows the evolution of the storage modulus during recovery tests for each formulation. To mimic the specific recovery conditions of the warm FRESH method, the temperature was increased to 37 °C at the time of shear removal. All hydrogels showed shear thinning under applied stress. For CH2, immediate recovery is observed, with G' reaching similar and rapidly even higher values after shear removal, probably due the fact that gelation occurs at 37°C. In contrast, CH-Gel recovered only after some time, which could be explained by the melting of the gelatin in the hydrogel. CH3 shows an intermediate behaviour, a few seconds being necessary to reach back the original storage modulus after shear removal.

5.4.3 Optimization of printing parameters

The hydrogels were printed using a 3D Discovery printer with a 25G needle. Preliminary printing assays were performed on glass substrate to evaluate the influence of the flow rate (varied from 0.5 to 1.5 mm^3/s) and feed rate (speed of the printing nozzle (3-11 mm/s)) on the resolution, in terms of the thickness and continuity of the filaments (Figure S 4 in Supplemental data). The flow rate that resulted in the best resolution (0.5 mm^3/min) was then chosen to print on glass (Figure 28A-C) and within the Pluronic19%+1% NaCl FRESH bath) (Figure 28D-F).

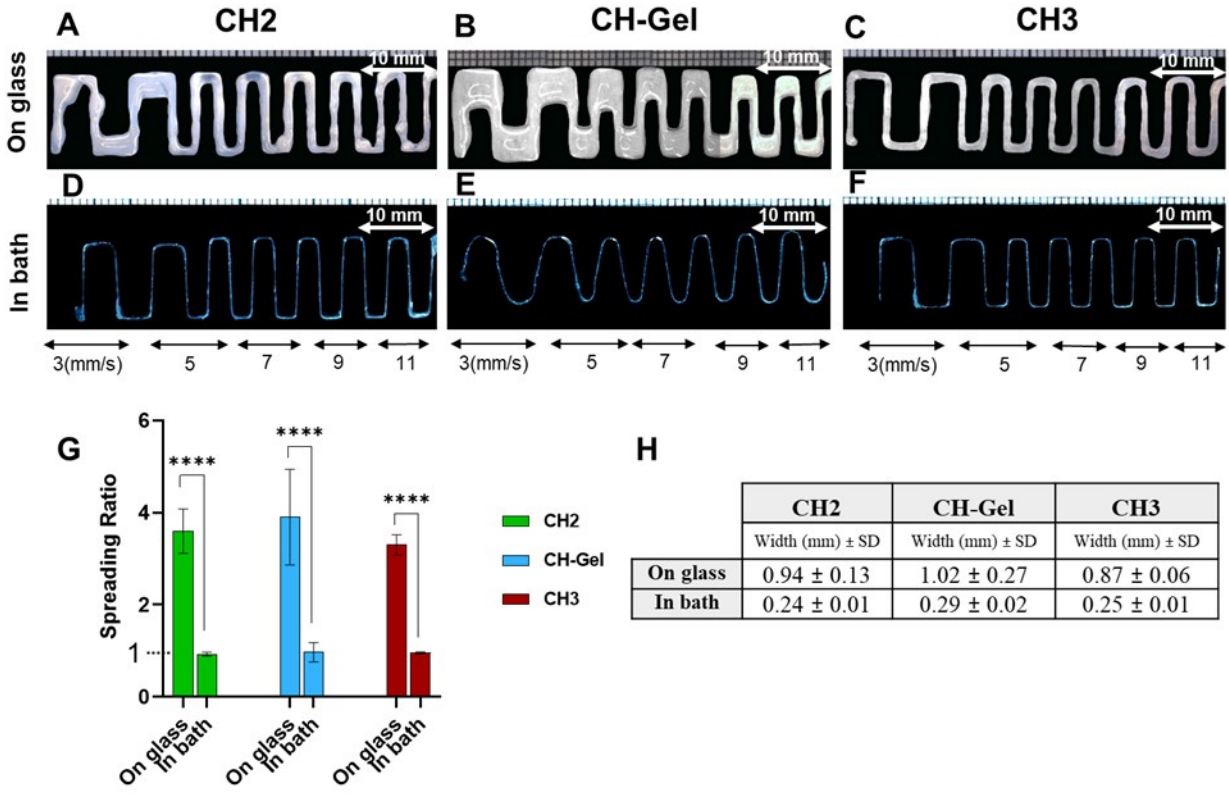

	CH2	CH-Gel	CH3
	Width (mm) ± SD	Width (mm) ± SD	Width (mm) ± SD
On glass	0.94 ± 0.13	1.02 ± 0.27	0.87 ± 0.06
In bath	0.24 ± 0.01	0.29 ± 0.02	0.25 ± 0.01

Figure 28. Illustration of how the FRESH method greatly reduces the diameter of printed filaments. Images of filaments printed with a 25G needle (0.26 mm inner diameter) with feed rates changing from 3 to 11 mm/s: A-C: on glass and D-F: within the support bath (mean +/-SD; n≥3; flow rate=0.5 mm3/s; G) Spreading ratio of the printed filaments at optimized printing condition (flow rate of 0.5 mm3/min and feed rate of 9 mm/s)(mean ± SD; n≥3; **** p<0.0001); H) Width of printed filaments (mean ± SD; n≥3).

As can be seen on Figure 28, printing within the support bath drastically enhances the resolution. The diameter of the printed filament decreased 4, 4, and 3-fold for CH2, CH-GEL, CH3 hydrogels, respectively (Figure 28H), reaching values around 0.2 to 0.3 μm, close to the needle diameter (25G=0.26 μm). Data can also be expressed as the spreading ratio (filament width on needle diameter) which was very significantly reduced with the FRESH approach (Figure 28G) (**** p<0.0001), in accordance with previous studies using the FRESH approach [296].

5.4.4 Printed structures on glass and within the FRESH bath

We then evaluated the feasibility of printing a complex multi-layer structure. The gridded structure shown in Figure 29G was printed at 10 layers, both on warm glass and within the warm FRESH bath. Figure 29 presents the resolution and handability of the printed structures after 24 h incubation at 37 °C.

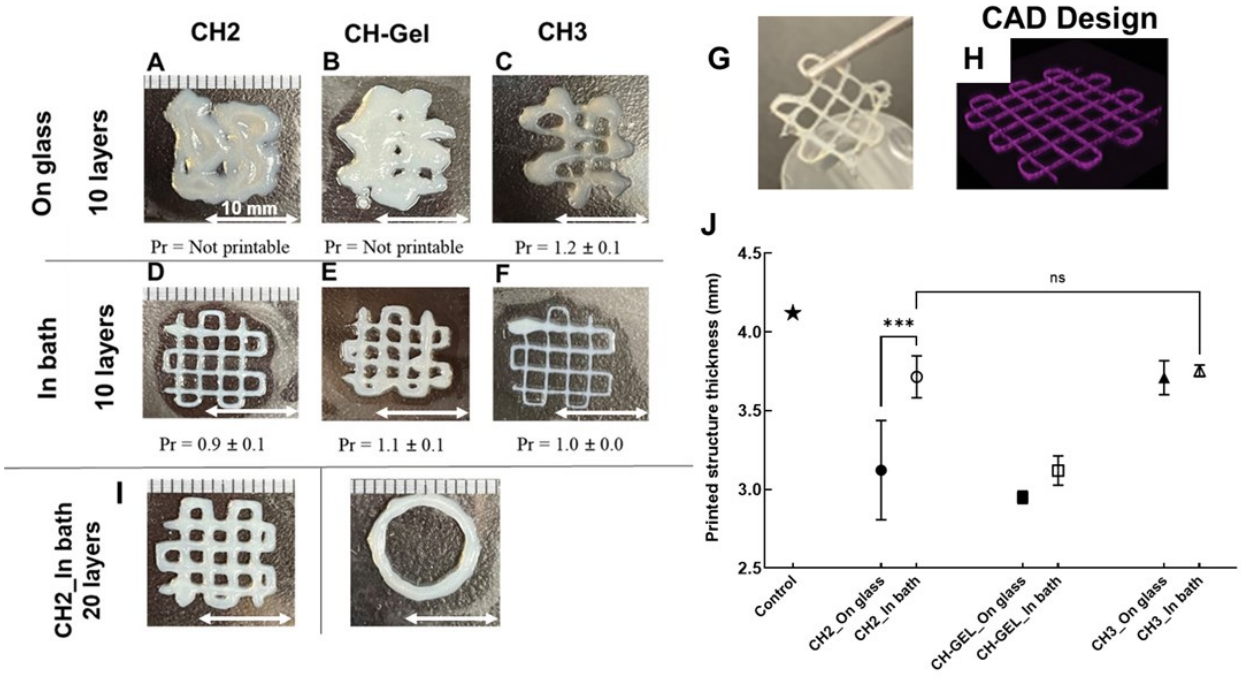

Figure 29. The FRESH method strongly enhances the resolution and feasibility of creating 3D structures with chitosan hydrogels. Pictures of gridded structures after 24 h gelation at 37 °C; A-C) printed on warm glass substrate (10-layers); D-F) printed in the Pluronic support bath (10-layers); G) Illustration of handability of CH2 10-layer printed structure; H) CAD design of the gridded structure (scale 1 cm); I) Thickness of 20-layers printed structures after 24 h gelation at 37 °C, in comparison to the theoretical height (control ★) (mean ± SD; n≥3; * p<0.5, ** p<0.01, *** p<0.001, **** p<0.0001); J) Pictures of gridded, and cylindrical CH2 structures printed in the Pluronic support bath (20-layers).

Printing more than 5 layers on warm glass resulted in a scrambled structure with bad resolution. The layers tended to collapse, especially with CH2 and CH-Gel hydrogels. These limitations are in accordance with previous work published by our team and a few others, which showed very poor resolution of the

printed structures [184, 285, 297]. Moreover, structures were very difficult to retrieve from the support. Using the FRESH bath, hydrogels were printable at least up to 20 layers, easy to remove from the substrate, and presented good cohesion, handability and relatively good correspondence to the theoretical CAD design (Figure 29D-F). CH3 showed the best printability, followed by CH2. The resolution of the CH-Gel hydrogel structure was lower, probably due to diffusion of the gelatin when increasing the temperature to 37 °C, which lead to a temporary decrease of the rheological properties as shown in Figure 27A.

All hydrogels printed in support bath showed improved printability in range of $0.9<Pr<1.1$. In addition, the thickness of the structures was increased and close to the theoretical value when printed in the bath (Figure 29J). The difference was significant for CH2 (3.7 ± 0.1 vs 3.1 ± 0.3 mm; $p<0.001$), whose values were similar to those of CH3 thanks to the support bath. These results confirm that the support bath helped to prevent the filament from spreading out during printing, as well as from collapsing under the weight of the multiple layers. In contrast, CH-Gel structures remain far from the ideal (thickness of 3.1 ± 0.1 vs 4.2 mm for the theoretical value; $p<0.0001$).

Interestingly, immersion of CH structures in PBS did not induce significant swelling and loss of resolution of CH2 printed structures (Figure S 7). This is in agreement with our previous work [68] and was confirmed by the absence of weight change as a function of time (Figure S 7 A). In contrast, when printing on glass, the weight of the structure was small and increased when immersed in PBS. This indicates that significant water loss had taken place during printing due to the dry and warm conditions. Preventing evaporation is a further advantage of the FRESH technique.

No swelling was observed with FRESH-printed CH-Gel as well but we noted that the weight of the printed structure was only 74% of its theoretical value (compared to 98% for CH). This confirms that some gelatin was lost during printing in the support bath, due to gelatin melting at 37°C. Moreover, immersion led to some deterioration of the structure (Figure S 7 B).

5.4.5 Post-printed mechanical properties

A good bioink should provide tissue-mimicking rigidity and good mechanical strength after printing. The mechanical properties of 20-layer gridded structures, printed either on glass or within the warm FRESH bath, were therefore tested in compression, after 24 h gelation at 37 °C. Figure 30A presents typical curves

up to 80% deformation. Since hydrogels present a non-linear behavior, the rigidity is expressed by the secant modulus at 30% deformation on Figure 30B.

The hydrogels printed within the bath were found to have greater rigidity than those printed on the glass. The difference was significant for all hydrogels (Figure 30B). The difference was particularly notable for CH2, which passed from 1.0 ± 0.2 kPa when printed on glass to 16.3 ± 3.1 kPa when printed in the support bath at 30% deformation. The reason for these enhanced mechanical properties is unclear. According to FTIR analysis, the increase of mechanical properties can't be related to Pluronic residues, as no trace is observed in the structure (Figure S 8). We believe this is rather due to a better cohesion between the layers, proper thermogelation, and prevention of evaporation during printing.

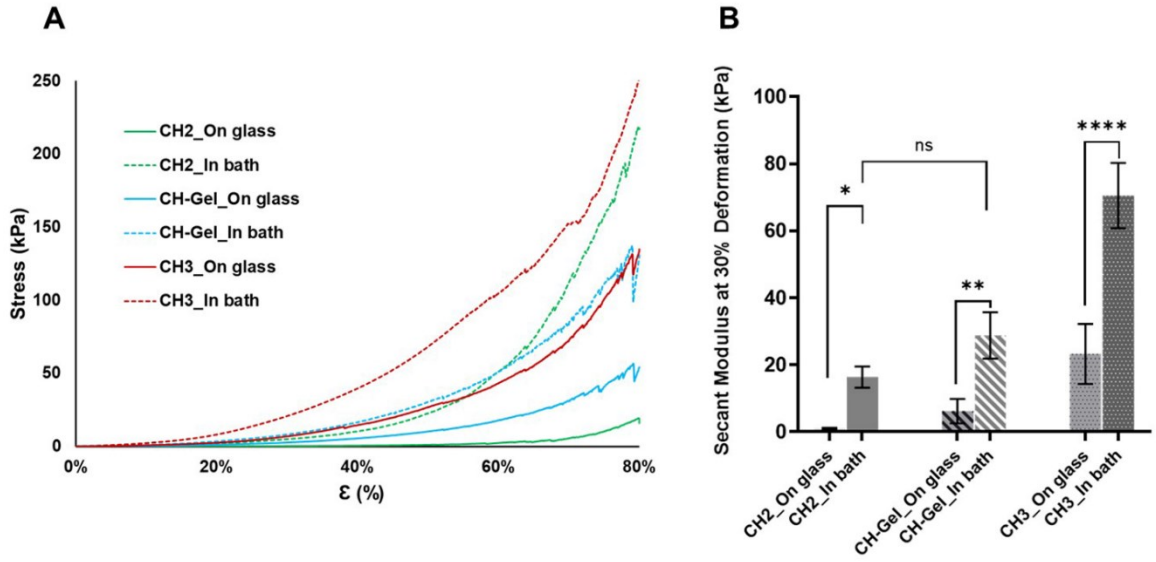

Figure 30. Mechanical properties of 20-layer structures printed on glass and within the FRESH bath: A) stress-strain curve in unconfined compression; B) secant Young's Modulus at 30% deformation (CH2: 2% w/v chitosan, CH3: 3% w/v chitosan; CH-Gel: 2% w/v chitosan-2% w/v gelatin) (mean ± SD; n≥3; * $p<0.05$, ** $p<0.01$, **** $p<0.0001$).

More importantly, these results confirm the strong mechanical properties of these chitosan hydrogels. Their secant modulus at 30% deformation reached 16 ± 3 kPa, 28 ± 7 kPa and 70 ± 10 kPa for CH2, CH-Gel and CH3 respectively (Figure 30B), and all sustained deformations up to 80% without breakage (Figure 30A). Such high values can be explained by the presence of SHC in the gelling agent solution. Indeed, it was

previously shown that CH gel made with SHC+BGP were drastically stronger that the conventional CH-BGP hydrogels [67, 188, 197]. Replacing part of the BGP with SHC is thought to lead to stronger interactions between the chitosan chains due to the SHC's decomposition into CO_2 during gelation [67] (Equation 1). SHC+BGP hydrogels also make it possible to attain rapid gelation at reduced BGP concentrations, to the benefit of cell survival (more physiological osmolality).

5.4.6 Cell viability

Preliminary assessment of the compatibility for cell encapsulation showed that CH3 resulted in high cell mortality when cells were encapsulated in this hydrogel (Figure S 9), probably because of its high density, as observed by SEM (see Figure S 10). For this reason, bioprinting was performed only with CH2 and CH-Gel hydrogels. Figure 31 presents typical live/dead images and cell viability of MSC in bioprinted hydrogels after 24 h, in comparison with hydrogels not submitted to extrusion (control 1) and submitted to the complete process except the FRESH bath and its removal (control 2).

Results show homogeneous cell distribution in the hydrogels, with good cell viability in CH bioprinted structures (76%), but significantly lower in CH-Gel (52%; $p<0.001$). In both cases the viability was lower than in the non-printed control (85% and 76% for CH and CH-Gel, respectively), possibly due to the shear stress applied during bioprinting. According to the literature, dead cells and cell damage increase as the pressure and needle length increase [223, 298, 299]. Another reason for decreased cell viability is probably the time the cells spend at temperatures <37 °C and the manipulation prior to the bioprinting process e.g., centrifugation. Short term cell viability is a key indicator for judging the processing properties of the extruded bioinks [286]. Here we used stem cells since they are more fragile than specialized cells, and long needle (25cm) with very small needle diameter (25G = 260 μm internal diameter) to maximize the risks of cell death due to shear during printing. Better cell survival can be expected if increasing needle diameter.

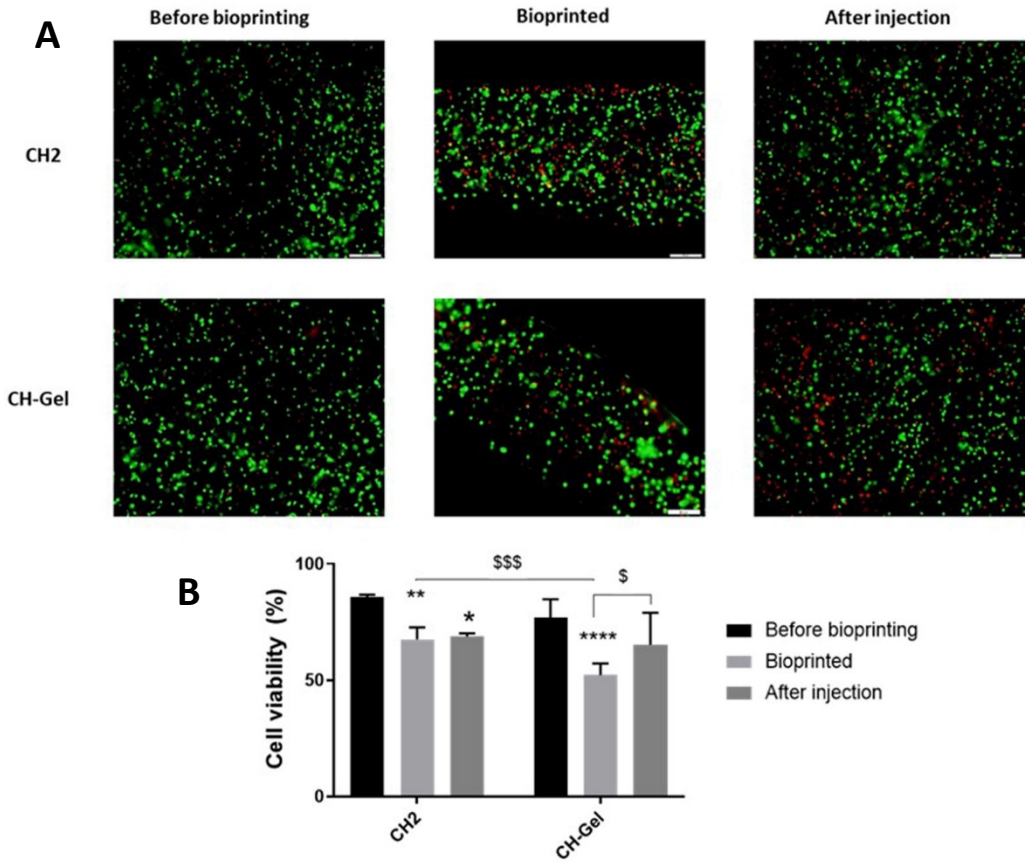

Figure 31. Viability of encapsulated MSCs loaded in CH2 and CH-Gel hydrogels, printed within the support bath A) Live-dead images (Live cells appear in green, dead cells in red); B) percentage of live cells (mean ±SD; n>4). Controls correspond to hydrogel solutions simply injected in a well before and after the bioprinting process (*p<0.05, **p<0.01, ****p<0.0001 compared to the control before bioprinting; ($ p<0.05; $$$ p<0.001, compared to CH-Gel sample) (CH2: chitosan 2% w/v; CH-Gel: chitosan 2% w/v – gelatin 2% w/v) (Live/dead assays).

The cell viability in bioprinted CH2 was similar to that of the second control, which differed only by the presence of the FRESH bath and the bath removal procedure. This suggests that the Pluronic support bath, as well as the few minutes at low temperature required to retrieve it, were not harmful to the encapsulated cells with this formulation. There was a slight difference, however, in the case of CH-Gel. The slightly lower short-term cell viability in CH-Gel compared to CH2 can be explained by the higher viscosity of the

solution during printing (as shown in Figure 27C). Ouyang et al. also observed a reduction of stem cells viability when increase gelatin concentration in a bioprinted alginate-gelatin structure [213].

Long-term cell viability and growth in both CH and CH-gel hydrogels have already been demonstrated over more than 2 weeks, with a number of cell types such as mesenchymal stem/stromal cells, T lymphocytes, intervertebral disk cells, fibroblasts and motor neuron-like NSC-34 cells [68, 275, 300-303]. Various applications can therefore be overseen with this warm FRESH bioprinting approach, thanks due to the numerous advantages of these chitosan bioinks (biocompatibility, strong mechanical properties, porosity, absence of swelling, tuneable biodegradation rate, antibacterial properties, absence of chemical modification or crosslinking etc.), the gentle physiological conditions during fabrication and the unpreceded resolution obtained compared to previous work [184, 218, 286].

This approach can be used to create complex and personalized geometries with various cell types to form 3D in vitro models to study diseases and treatments, such as the efficacy of T cell delivery system for cancer immunotherapy [268], study cell interactions or the mechanism underlying motor neuron diseases [303], to name just a few. As the viscoelastic properties of the gel can be tuned by changing the concentration of the gelling agents [68, 304], the printed constructs can be customized for specific applications or to study the impact of viscoelastic properties on stem cell behavior, under static and cyclic loading conditions, without any limitations in terms of nutrient and O2 diffusion [305]. Moreover, other components such as growth factors and bioactive agents can be easily added [194, 306] to optimize cell fate and extend their potential for tissue engineering applications.

5.5 Conclusion

In this work, we demonstrate how using the FRESH approach with a warm support bath at 37 °C, combined to a thermosensitive chitosan hydrogel with strong mechanical properties, drastically enhancesthe potential of chitosan hydrogel as bioinks for 3D bioprinting. The FRESH method provides mechanical support and assists in adequate thermo-crosslinking during printing, while preventing evaporation and easing sample removal. Printing in the support bath led to marked improvement of the resolution of the printed 3D structures for all chitosan hydrogels tested (Chitosan 2%w/v, 3% w/v and chitosan-gelatin (2-2%), but more particularly for CH2 hydrogels, without swelling after immersion in PBS. Structures had good cohesion and handability. They presented strong mechanical properties thanks to the use of a mix of sodium bicarbonate and beta-glycerophosphate as gelling agents.

CH2 presented better rheological properties, printing behavior and MSC survival than CH-gelatin hydrogel, probably because gelatin escapes from the gel into the support bath at 37 °C. Other compounds and bioactive factors could be added to optimize the hydrogel as a function of the target application. While further study is required to optimize the fabrication process, these results show how the FRESH method can overcome the main limitation of the thermosensitive chitosan-based hydrogels as bioinks. This opens the path to exciting applications for 3D in vitro models and tissue engineering applications since these biodegradable chitosan hydrogels have been already reported as excellent scaffold for many cell types and do not need any chemical modification or crosslinker.

Acknowledgements

We would like to thank the Natural Science and Engineering Research Council of Canada (NSERC; RGPIN-2015-05169) and the *Fonds de Recherche du Quebec—Nature et technologie* (FRQNT; team project and M R scholarship) for providing funding for this project. We would like to thank Thierry Labonté-Dupuis for his help with the bioprinter and S.K. Rezvaninejad for his help in producing the figures. The graphical abstract was made using www.biorender.com.

5.6 Supporting Information

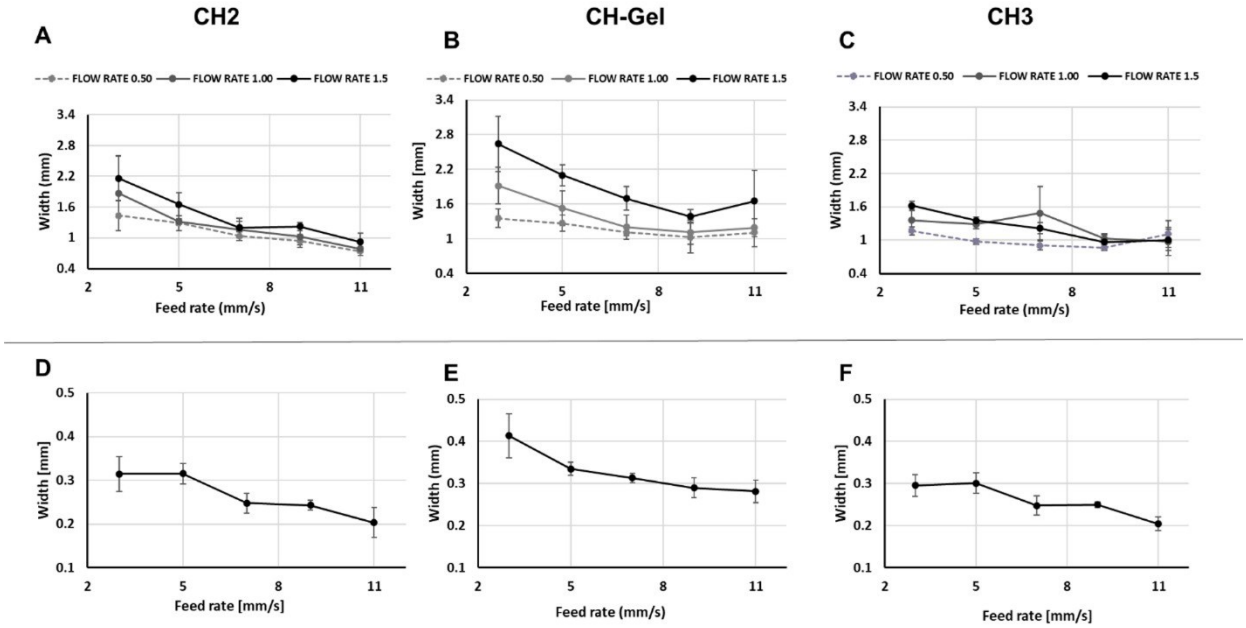

Figure S 4. Mean diameter and images of filaments printed with a 25G needle (0.26 mm inner diameter) with feed rates changing from 3 to 11 mm/s: A-C: on glass with flow rate of 0.5, 1, 1.5 mm^3/s and D-F: within the support bath with flow rate of 0.5 mm^3/s for three formulations: 2% chitosan (CH), B) 2%chitosan-2% (w/v) gelatin (CH-Gel), and C) 3% chitosan-based hydrogel (mean +/-SD; n≥3).

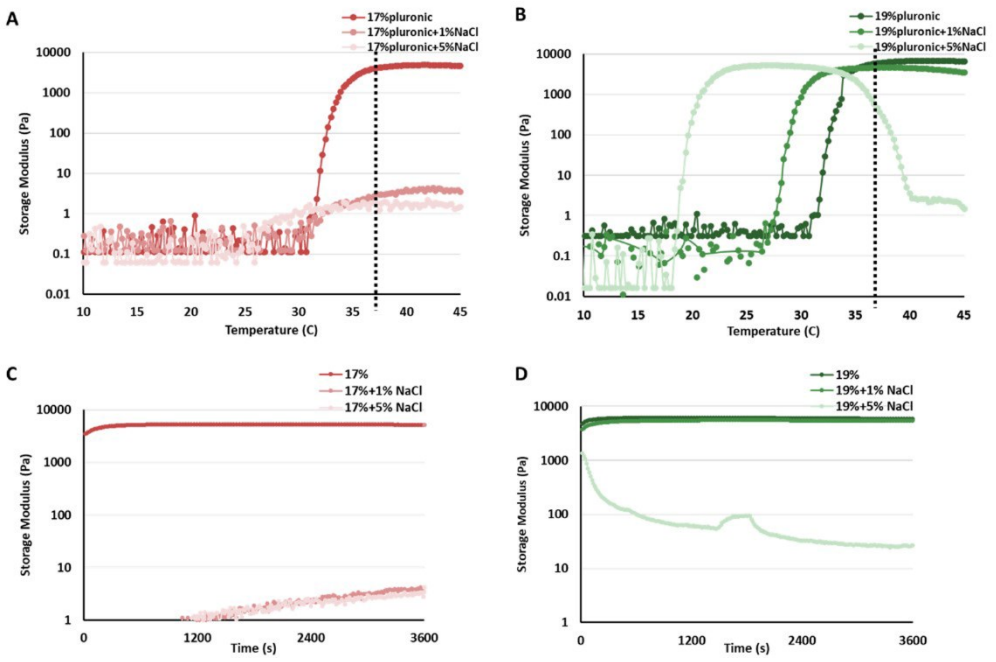

Figure S 5. Rheological properties of Pluronic support bath A-B) Effects of added NaCl on temperature ramps (10-45 °C) of Pluronic 17% and 19% (w/v) (dotted line=37°C); C-D) Time sweep of Pluronic bath at 37 °C; (mean; n≥3).

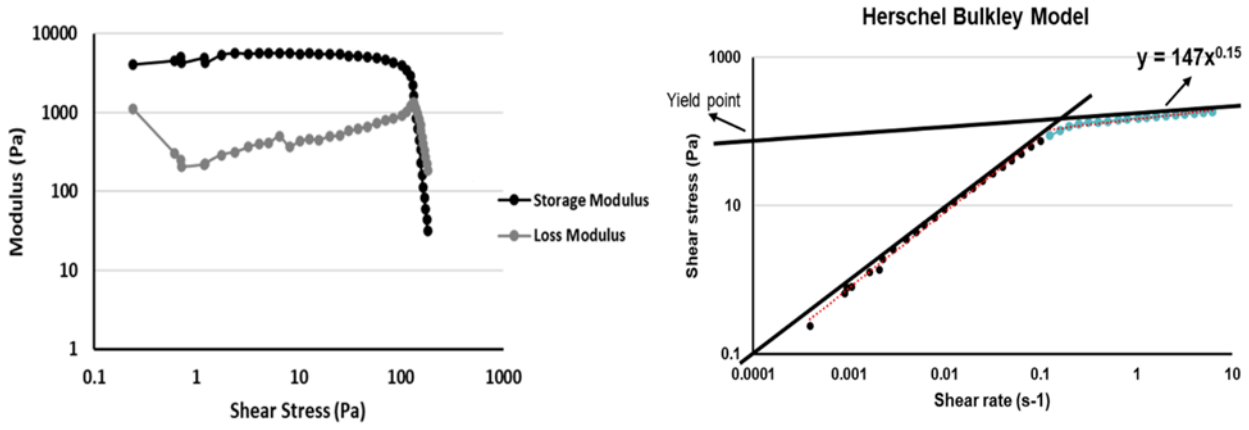

Figure S 6. Rheological properties of Pluronic + 1% NaCl FRESH support bath A) Amplitude sweep, with controlled-shear deformation (0.01%-100%) of Pluronic19% + 1% NaCl at 37 °C; (mean; n≥3); B) Herschel

Bulkley model of the Pluronic + 1% NaCl FRESH support bath (the straight line crossing the Y axis shows the yield stress).

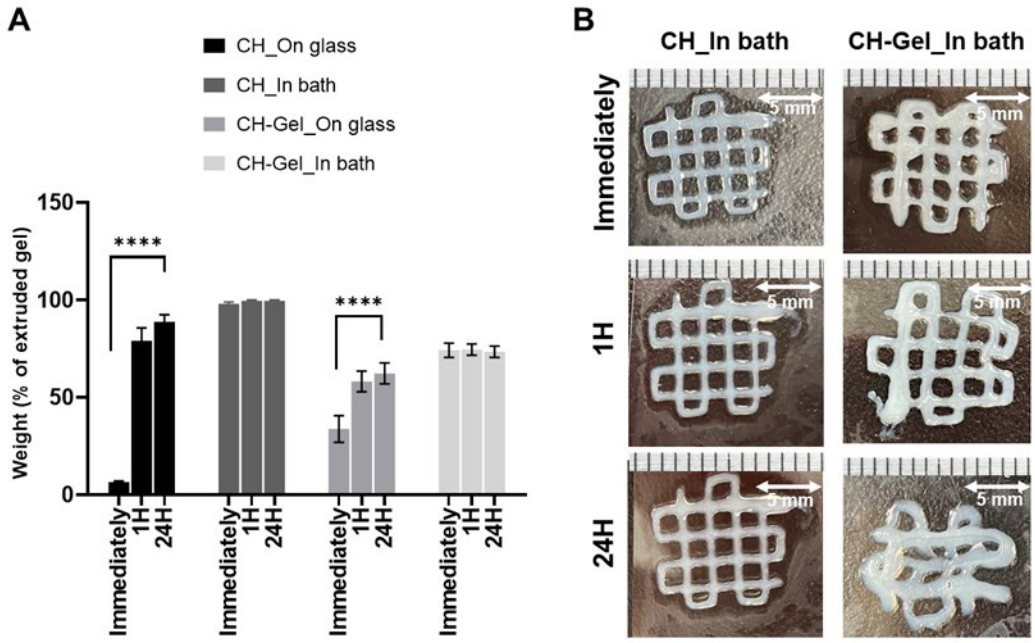

Figure S 7. FRESH-bioprinted structures do not swell once immersed in saline, in contrast to those printed on glass: A) weight of the printed structure (expressed in % of weight of the equivalent volume of extruded filament), immediately after printing, after 1 h and 24 h soaking in PBS; B) images of the corresponding structures.

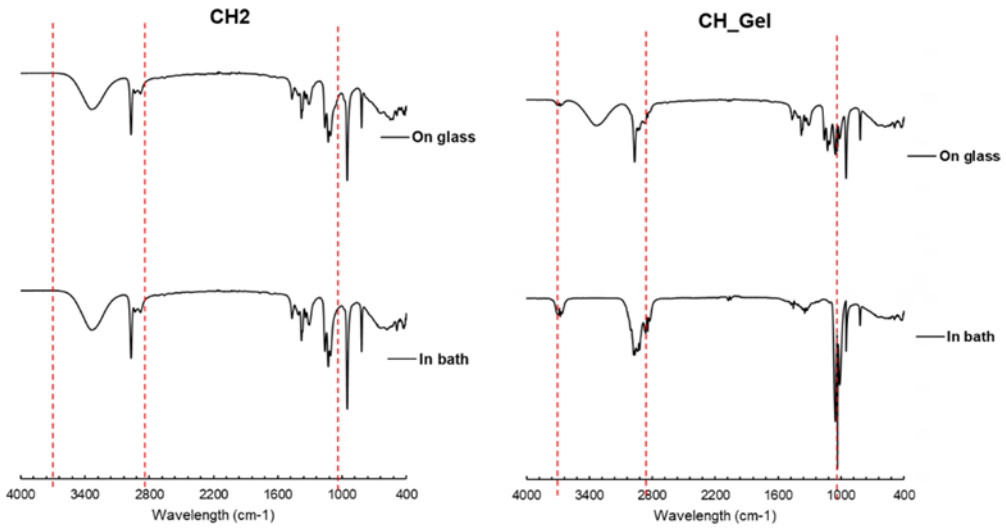

Figure S 8. FTIR analysis show absence of Pluronic in FRESH-printed CH structures. Some trace of Pluronic could however be present in CH-Gel hydrogels due to gelatin-Pluronic interactions (peaks attributed to the Pluronic are showed by dotted red lines).

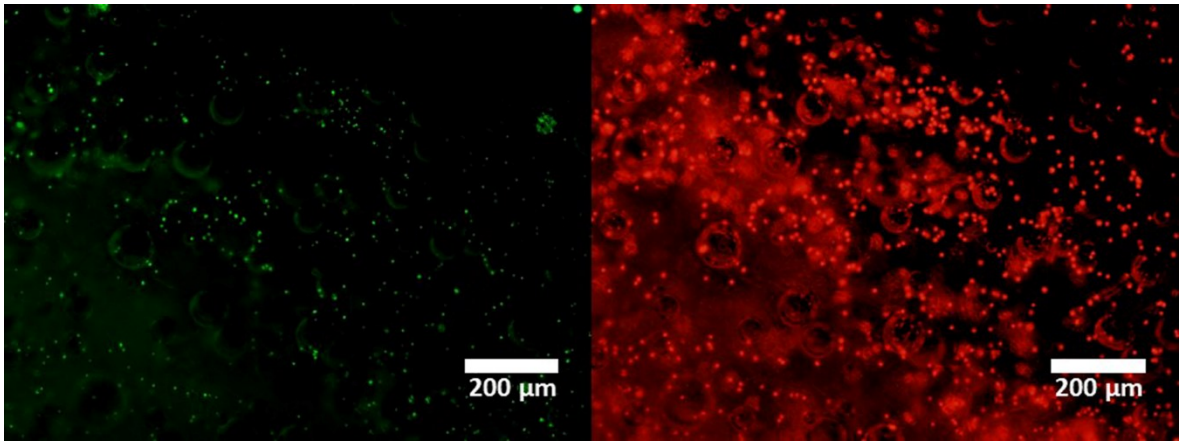

Figure S 9. Live-dead assay of L292 fibroblast cells encapsulated in 3% (w/v) chitosan-based hydrogel after 24 h (live cells were stained with Calcein (green) and dead cells were stained with EthD-1 (red)).

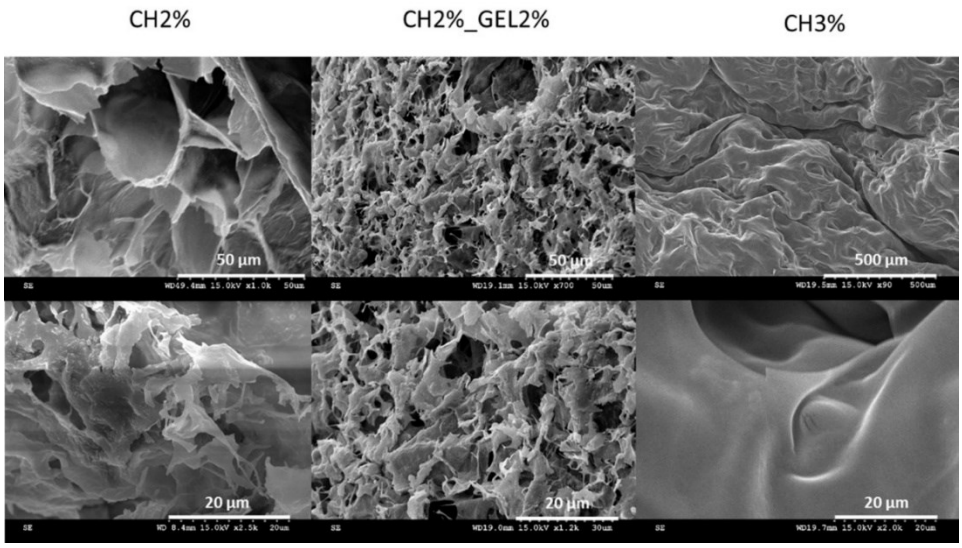

Figure S 10. SEM images of CH2%, CH-GEL and CH3% hydrogels.

5.7 Summary of paper 2 and introduction to the next objective

Paper 1 and 2, as well as previous publications of the lab, have demonstrated the potential of chitosan thermosensitive hydrogel as bioink and/or injectable scaffold for tissue engineering purposes. Chitosan has many advantages but lacks bioactivity that is necessary for mineralized tissues. To meet the general objective of this Ph.D., namely articular tissue engineering, injectable bioactive bone filler in combination with cells, could be applied in a minimally invasive manner to fulfill irregular cavities in non-load bearing sites, which do not require high mechanical strength [307-309]. Injectable chitosan-based thermosensitive hydrogels developed previously in the Lerouge lab showed drastically increased mechanical properties at body temperature and good cell cytocompatibility due to the reduced osmolality [67, 68]. This property could be interesting to fill irregular bone and mineralized tissue defects [210, 310]. However, it is not osteoconductive. Osteoconductive property can be applied in combination with inorganic ceramics e.g., **bioglass (BG)** [311, 312].

To date, **no proper gelation** was reported when the chitosan hydrogels combine with BG [210]. Additionally, preliminary trials showed that the gelation of hydrogels could not be obtained with a high loading of BG particles due to pH increase resulted from fast ion release. This impaired gelation impacts **adversely the mechanical properties** [313]. To address the limitation, **we therefore aimed** to study concentrating bioglass in small microbeads instead of their homogenous distribution in the gel could improve mechanical properties due to less interference with the gelation mechanism resulting from a slowdown rate of ions release as presented in **Chapter 6**. By reducing the rate of ion release, such a composite hydrogel could also improve the survival and growth of encapsulated cells. This work has been submitted to the Journal of Biomedical Research Part A.

Chapter 6 - Injectable Cell-laden Hybrid Bioactive Scaffold Containing Bioactive Glass Microspheres

Maedeh Rahimnejad[1, 2], Cindy Charbonneau[3], Zinan He[3], Sophie Lerouge[1, 2, 4*]

[1]Biomedical Engineering Institute, Université de Montreal

[2]Research Centre, Centre Hospitalier de l'Université de Montréal (CRCHUM)

[3]National Research Council Canada/Government of Canada, Montreal, Canada

[4]Department of Mechanical Engineering, École de technologie supérieure (ÉTS)

*Corresponding author

6.1 Abstract

The rising incidence of bone disorders has resulted in the need for minimally invasive therapies. Injectable bioactive bone filler, alone or in combination with cells, could be applied in a minimally invasive manner to fulfill irregular cavities in non-load bearing sites, which do not require high mechanical properties. Thermosensitive chitosan hydrogels that transition from a liquid to a mechanically stable solid at body temperature can provide interesting features as an in-situ injectable cytocompatible biomaterial, but it is not osteoconductive. Osteoconductive and osteointegrative properties can be obtained by combining chitosan with bioactive ceramics e.g., 45S5 Bioglass® (BG). The interest in using BG comes from the ability of the material to dissolve and release dissolution products that stimulate bone regeneration. However, BG addition in chitosan hydrogels results in pH elevation, due to rapid release of ions, which adversely affects gel formation, mechanical properties and encapsulated cell survival. To address this, we proposed to concentrate BG in small microbeads instead of their homogenous distribution in the gel. Herein, we studied the feasibility of forming BG-rich microbeads and compared the properties of such hybrid hydrogel to homogenous BG-containing hydrogel in terms of mechanical properties. BG incorporation in the form of microbeads improved the compressive modulus of hydrogels in comparison to BG powder. It also led to lower osmolality in extract medium compared to hydrogels homogeneously made with BG powder, suggesting that microbeads play a barrier role to reduce the rate of ions release, consequently resulting in proper hydrogel formation. This feature increased cell survival and metabolic activities when encapsulated within the hydrogels. The increase of calcium/phosphate on BG microbeads suggests hydroxyapatite formation. The small diameter of the microbeads could be suitable for non-invasive injections through small

needles. The feasibility of freezing and thawing of microbeads provides the possibility of long-term storage and potential for clinical applications. These data indicate that hybrid hydrogel containing BG microbeads might form a promising injectable cell-laden bioactive biomaterial for the treatment of bone defects.

Keywords: Bone defect, Chitosan-based hydrogels, Bioglass, Microbeads

Graphical Abstract:

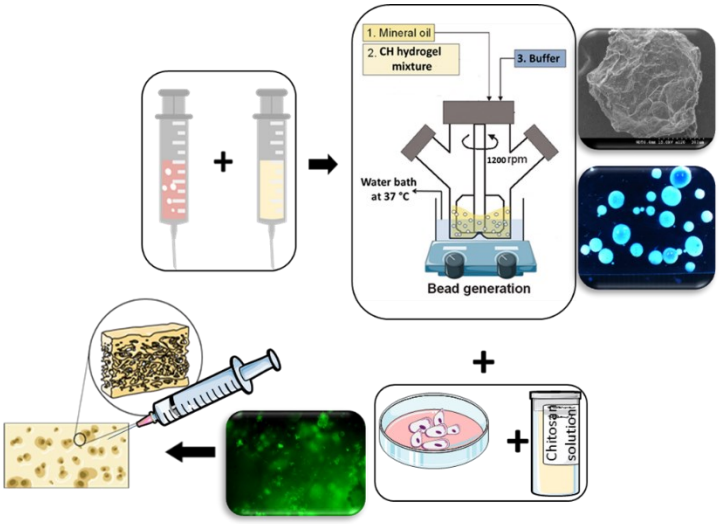

6.2 Introduction

The rising incidence of bone disorders mainly due to the aging of the population has resulted in the need for more effective treatments. Critical-size bone tissue defects (≥2-2.5 cm) cannot regenerate via normal physiological processes and usually require bone grafting interventions, which are considered invasive and complex surgical methods [314].

Several materials have been proposed for the treatment of large defects, including hydroxyapatite (HA), calcium sulfate, calcium phosphate families such as calcium phosphate, biphasic calcium phosphates (the composition of HA and β-tricalcium phosphate (β-TCP) ceramics), β-tricalcium phosphate ceramics, and bioactive glass powder or particulates in forms of foam and injectable cements [315]. Despite interesting clinical outcomes, several challenges remain, such as incomplete osteointegration and fibrosis [316], as well as poor injectability. Several studies suggest that for most large bone defects, cells and/or bioactive agents

are necessary to achieve an appropriate bone repair [180]. However, finding an appropriate injectable scaffold ensuring viability of encapsulated cells, osteointegration and some mechanical support is very challenging [180, 317].

Hydrogels are interesting candidates for cell encapsulation, since they can provide friendly suitable 3D aqueous environment for cells and mimic extracellular matrix. In situ forming hydrogels are particularly suited since they can be applied in a minimally invasive manner and fulfill irregular cavities perfectly. Among them, chitosan thermosensitive hydrogel is particularly interesting and has been widely reported for orthopedic applications [211, 318-320]. Chitosan (CH) is biocompatible, antibacterial and biodegradable. It can form thermosensitive hydrogels when made with weak bases such as beta-glycerophsophate (BGP), i.e., they are liquid and injectable at room temperature, and gel at body temperature, without significant shrinkage [321, 322]. Thermosensitive chitosan hydrogels can be interesting platforms used to fill the bone defects in non-load bearing sites, which do not require high mechanical strength. However it has been shown that the hydrogel must exhibit adequate stiffness e.g., ≥30 kPa to induce stem cell differentiation leading to osteocalcin secretion and bone-like ECM formation [323-325], and CH-BGP gels are generally very weak [307-309]. However, recent work showed that mechanical properties can be drastically enhanced using a specific mixture of two weak bases (phosphate buffer and sodium bicarbonate, hereafter called PB and SHC respectively). This also make the gel more cell friendly due to their reduced osmolality [67, 68]. They could therefore be very interesting candidates for this application. However, they do not have inherent osteoconductivity [307].

Osteoconductive and osteointegrative properties can be promoted by the addition of inorganic ceramics such as hydroxyapatite (HA) and bioactive glass [201, 206]. Bioactive glass, created by Hench in the late 60s, include a variety of silicate-based glass compositions qualified as “bioactive” for their ability to bond chemically to tissues. In particular 45S5 Bioglass® (BG) (which composition is 45 wt% SiO_2, 24.5 wt% CaO, 24.5 wt% Na_2O, and 6.0 wt% P_2O_5) is well known to form strong bonds with bone and has been already used in various FDA-approved medical devices since 1985 [311, 312]. Both HA and BG support the attachment and proliferation of bone-forming osteoblast cells. Moreover, in some cases, they can also boost the rigidity and mechanical strength of the scaffolds [326, 327]. In addition, they assist in formation of mineralized bone matrix in vitro [207, 208]. Several studies suggest BG superiority over HA because of the following reasons [328-330]: 1) The faster proliferation of osteoblasts and bone formation; 2) Better adhesion and bonding to surrounding soft tissues elements e.g., collagen without induction of fibrous

capsule in vivo; 3) Higher bioactivity due to ion release and rich silica layer; 4) Anti-microbial properties; 5) Finally bioglass' degradation products could induce the growth factors production and cell proliferation; 6) They could also trigger the gene expression of osteoblasts [204].

However, dissolution of BG is known to lead to rapid exchange of Na^+, Ca^+, H^+, and H_3O^+ that is leading to fast pH increase in static in vitro condition [331]. Based on our previous knowledge, this may prevent adequate chitosan hydrogel formation (precipitation) and strongly decrease the mechanical properties of the gel [210, 313]. It may also lead to non physiological pH with negative impact on encapsulated cells. The rapid release of ions and the fast pH increase in vitro partly explain why only very few work have been published about cells and BG particles co-encapsulation in the hydrogel and in vitro assays [211]. The presence of cells within the hydrogel is desirable because it promotes highly controlled cell-based regeneration and mineralization of bone-mineralized tissue particularly for large bone defects. In one interesting study, rat bone marrow mesenchymal stem cells' response with thermosensitive chitosan/gelatin/BGP hydrogel containing nanoBG particles was assessed in vitro and in vivo [209, 211]. High encapsulated cell viability and bone formation were achieved. However, very poor mechanical properties were reported, far from the stiffness required for cells migration and new bone growth (~10 Pa vs ≥30 kPa) [209]. Therefore, there is a need for injectable bioactive cell-laden biomaterials (hybrid biomaterial) with adequate mechanical properties to fill large irregular shaped defects in non-loading bones and mineralized tissues using minimally invasive procedures. The general objective of this work is to create BG-loaded injectable hydrogels compatible with cell encapsulation.

BG can be sintered to initiate crystallisation of this amorphous material leading to enhanced bioactivity and decreasing the rate of dissolution [332]. Two main approaches using sintered BG were studied as schematically illustrated in Figure 32. We first studied the impact of adding sintered BG powder on the physiochemical and mechanical properties of chitosan thermosensitive hydrogels. Since BG releases ions that interfere with the physical gelation process and decrease cell survival, we then created hybrid hydrogels where the BG is concentrated within small microbeads prepared by stirred emulsification. We hypothesize that concentrating BG in small microbeads, instead of their homogenous distribution in the gel, will slow down the ion release and therefore improve the gel mechanical properties as well as its compatibility with cell encapsulation.

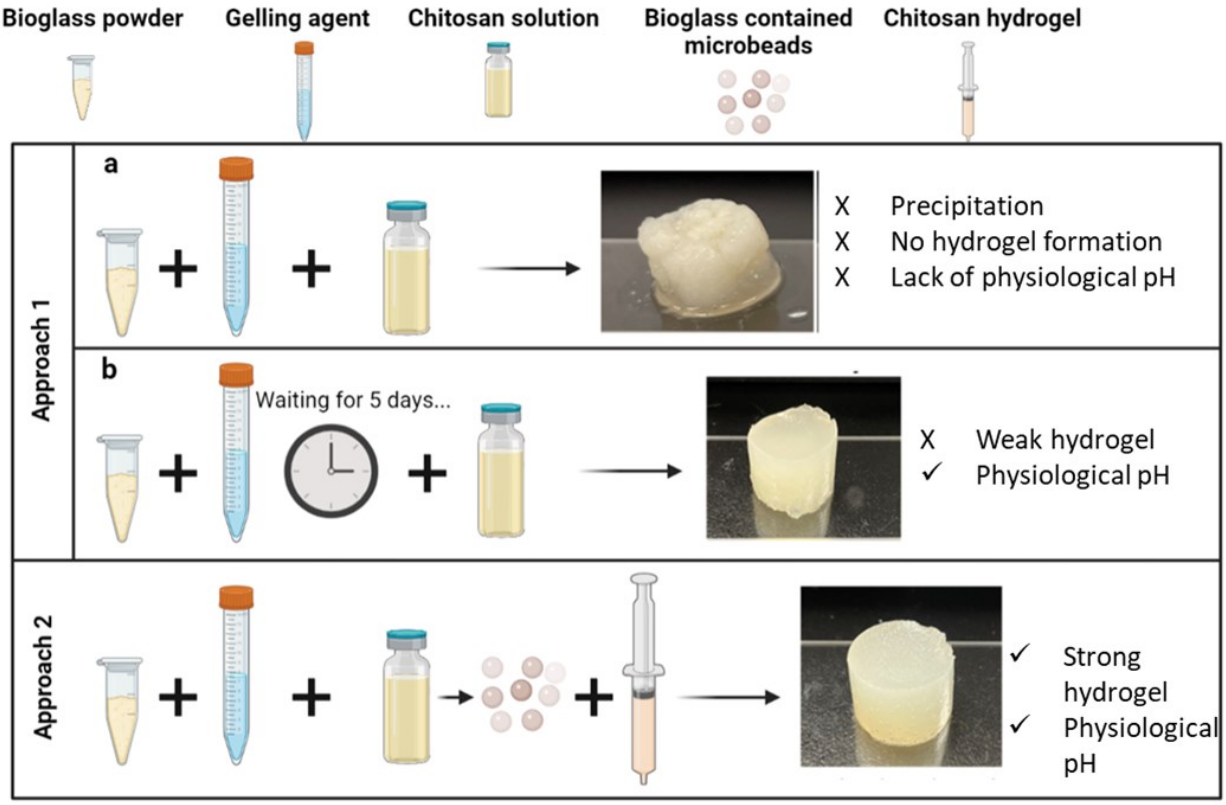

Figure 32. Schematic illustration of two main approaches studied: 1) Homogenous BG-chitosan hydrogel: and 2) Hybrid BG-chitosan hydrogel.

6.3 Materials and Methods

6.3.1 Materials

Shrimp shell chitosan (ChitoClear, HQG110, Mw: 155 kDa, DDA 83%) was purchased from Primex (Iceland). β-Glycerol phosphate disodium salt pentahydrate ($C_3H_7Na_2O_6P{\cdot}5H_2O$, hereafter BGP), sodium phosphate monobasic NaH_2PO_4, and sodium phosphate dibasic Na_2HPO_4 were purchased from Sigma-Aldrich (Oakville, ON, Canada). Sodium hydrogen carbonate $NaHCO_3$ (sodium bicarbonate, hereafter SHC) was purchased from MP Biomedicals (Solon, OH, USA). Other chemicals were of reagent grade and were used without further purification. Vitryxx® bioactive glass (BG) particles–45S5 Bioglass®, ($24.5Na_2O$-$24.5CaO$-$6P_2O_5$-$45SiO_2$ in wt.%) was purchased from SCHOTT AG company, Mainz, Germany. Before use, the particles were sintered by heat-treatment for 4 hours at 600 ºC, then ramp up to

approximately 1020 ºC for another hour. The sintered BG was ground in a mortar and pestle and then sieved to retain granules with a particle size lower than 45µm.

6.3.2 Preparation of chitosan thermosensitive macrogel with and without Bioglass

Chitosan-BG hydrogels were prepared by mixing a chitosan acidic solution with a gelling agent solution (GA) containing BG particles at a volume ratio of 3:2.

The chitosan solution was prepared as follows: chitosan powder was solubilized in hydrochloric acid (HCl) (0.1 M) at 3.33% w/v (for final concentration 2%), with mechanical stirring for 4 hours. The solution was sterilized by autoclaving (20 min, 121°C) and stored at 4°C. Two GA solutions were compared during this study: 1) a mixture of SHC+PB, as developed by ourteam, and 2) the commonly used BGP alone as a control. PB at pH 8 was prepared with a mixture of Na_2HPO_4 and NaH_2PO_4 at the ratio of 0.540/0.047 w/w in milli-Q water. SHC was then combined with PB as previously published [67]. When required, sintered BG particles were added directly to the gelling agents. The pH of these GA solutions was adjusted within the range of 8-8.5 using HCl prior to mixing with CH immediately for approach 1a and after 5 days for approach 1b.

The chitosan and gelling agent solutions were stored in separate syringes, joined by a Luer lock connector. To mix them, the content of the GA syringe was pushed into the CH syringe and the mixture was pushed from side to side for 15 repeats immediately before use, was poured into wells and left be incubate at 37°C for at least 24 hours. Hydrogels without BG particles were prepared as controls. Table 7 summarizes all formulations tested.

Table 7. Concentration of chitosan and gelling agents in the studied hydrogels (CH: Chitosan, BGP: Beta-glycerophosphate, SHC: Sodium hydrogen carbonate, PB: Phosphate buffer). BG was added to reach final concentration of 1-6% w/v for macrogels.

Hydrogel name	**[GA component] (M)**			**CH% (w/v)**	**BG % w/v**
	SHC	**BGP**	**PB**		
PB0.01 SHC0.075	0.075	-	0.01	2	0-6
BGP0.1 (control group)	-	0.1	-	2	0-6

6.3.3 Characterization of chitosan-BG hydrogels

pH and osmolarity

The pH of the chitosan solution, gelling agents with and without BG particles, and hydrogels was measured with a LAQUA twin pH-22 Compact and Portable pH Meter (Horiba, country). As an indirect mean to assess the ion release rate, the osmolarity of media incubated with hydrogels was measured with an Advanced® Micro 3300 Osmometer (company name, country). To do so, 1 mL of macrogel (hydrogel with/without BG) was poured in 12-well plate with 2 mL of media containing 10% v/v bovine serum and incubated at 37°C for different time points: 24h, 48h, and 72h. At each time point, the extract was removed, analyzed and replaced with fresh media.

Gelation kinetic

Rheological properties were studied using an Anton Paar instrument (Physica MCR 301, Germany) with a coaxial cylinder geometry (CC10/T200). Time sweeps at 22 & 37 °C for 1 hour were performed using the oscillatory mode in the linear viscoelastic (LVE) range, at a constant shear strain (1%) and constant frequency (1Hz). They allowed the study of gelation kinetics at both room and body temperatures, as a function of the gel composition, by following values of storage and loss modulus (G' and G'') as a function of time.

6.3.4 Fabrication and characterization of microbeads for hybrid hydrogels

Stirred emulsification process

To form hybrid hydrogels, CH-BG were also processed in the form of microbeads. A 50 mL spinner flask (Bellco, Vineland, NJ) containing 20 mL of light mineral oil (Fisher Chemical™) pre-warmed to 37 ºC was placed in a water bath at 37°C. Two different stirring speeds were tested (550 and 1200 rpms) to study the impact on microbeads diameter. Chitosan pre-hydrogel solution including 2, 4, 6, 8% w/v BG, prepared as previously described, was added dropwise using a 18G needle. After 15 min, the stirring speed was reduced to 200 rpm, and 10 min later, HEPES-buffered saline solution pre-warmed to 37 °C was added to the flask. After 1 min, spinning was stopped and the emulsion was centrifuged (1500 rpm, 5 min, RT) followed by oil-layer removal by suction and filtration using a 100-µm nylon cell strainer (BD Biosciences, USA). The

microbeads were washed three times with HEPES-buffered saline solution to remove any remaining oil and transferred into the desired solution with a spatula.

Microbeads size distribution and morphology

A volume of 1 mL of the beads was transferred into 4 mL HEPES-buffered saline solution and stained by adding 100 µL of 5 g/L toluidine blue O and Eosine solution for BG-laden microbeads and chitosan microbeads, respectively. Pictures were taken with a dual 12 MP camera. Image processing was performed using the CellProfiler (cellprofiler.org) [333] to determine the microbead diameter distribution and circularity (defined by the equation: 4π x area/perimeter^2).

Injectability

The injectability of BG-rich microbeads was tested through 18G needles (internal diameter: 838 µm), when in suspension in simulated body fluid (SBF) and when mixed to the chitosan-prehydrogel solution (hybrid gel with 20% v/v microbeads). The structural integrity of the beads was studied by light microscopy (OLYMPUS SZX10/Color 5 camera) before and after injection and was compared qualitatively with non-injected BG-laden microbeads.

Freezing and thawing

To show the feasibility of long-term storage of BG-rich microbeads, a volume of 1 mL of the beads was transferred into 4 mL HEPES-buffered saline solution, then stored at -20°C. After 14 days, the solutions were thawed at room temperature and studied by light microscopy to compare with original, non-frozen microbeads.

Bioactivity

Apatite formation was assessed after soaking microbeads with and without BG in SBF for 0, 1, and 7 days at room temperature. SBF solution was prepared as previously reported based on ISO/FDIS 23317 [334]. Then, the microbeads were rinsed with deionized water, recovered, frozen at -20 ºC for 48h, and lyophilized before their characterization by Fourier-transform infrared spectroscopy (FTIR, PerkinElmer, USA) and scanning electron microscopy (SEM, HITACHI S3600 secondary electron microscopy with energy dispersive X ray analysis (EDX) (INCA, Oxford instruments, UK) after sputter coating with gold.

Mechanical properties of hydrogels

Unconfined compression tests were performed on 2 ml molded hydrogels (ϕ=14 mm, height: 10 mm) after 24h incubation at 37 ºC using the MACH-1 testing device (Biomomentum, Canada). A velocity equal to 100% of the sample's height/min was used. The compressive strength and the secant Young modulus at 30% of deformation and stress at breakage were calculated from the stress-strain curves. To evaluate hybrid hydrogels (hydrogel containing BG microbeads at 20% and 50% volume ratio), microbeads were added accordingly to the 3ml syringe and then mixed using a connector with the chitosan hydrogel.

Cytocompatibility characterization

L929 mouse fibroblasts (Lonza) were encapsulated in chitosan hydrogels containing 20% v/v microbeads W and W/O BG (hybrid hydrogels) at $1x10^6$ cells/ml. A volume of 300 µl of the hydrogel was left to gel for a few minutes in 48 well plates before adding 700 µl media (DMEM +1% v/v P/S+10% v/v foetal bovine serum (FBS). Cell viability was investigated by live/dead staining after 0, 1, and 7 days using 1 µM calcein AM and 2 µM ethidium homodimer-3 in culture media without serum to stain dead cells in red and live cells in green (Life Technologies, USA). Stained cells were observed under fluorescent microscopy (Leica DM IRB) at 5x magnification. Cell metabolic activity was evaluated using the Alamar Blue assay (Resazurin Cell Viability Assay Kit, Biotium, USA, 10 % v/v) after 0, 1, and 7 days.

6.3.5 Statistical analyses

All experiments were performed at least in triplicate. Results were expressed as mean ± SD. Statistical analysis was performed using GraphPad Prism 7.04 software. One-way ANOVA and Tukey's multiple comparison tests were used to compare multiple groups. $P<0.05$ was considered to be statistically significant.

6.4 Results

6.4.1 Effect of BG addition on CH hydrogels

As expected, the addition of BG in the GA led to an immediate dose-dependent increase of the pH of the gelling agent solution, with values between 9.5 and 11 instead of 8 for the control solution (Figure S 11 A-C in supplemental data) and further increased over 10 days, reaching up to 13 for BG concentrations ≥ 3% when BGP was used as a gelling agent [335]. This pH increase can be explained by cations exchange, in

particular Na+ and H+, which subsequently leads to severing of Si-O-Si BG surface bonds and ultimately the deposition of $Ca2^{+}$ and PO_4^{3-} ions from the BG and carbonate ions from the gelling agent solution [336, 337]. The pH increase was less drastic for gels made with SHC+PB. This could be explained by the better buffering capacity of this gelling agent solution.

Since the pH is known to strongly influence the gelation of chitosan thermosensitive hydrogels [187], we tried to adjust the pH of the GA solution to 8-8.5 prior to mixing with the chitosan solution, but further immediate pH increase was observable immediately after HCl addition (due to BG further dissolution [338] (Figure S 13). The gelation kinetic of the hydrogels was therefore strongly modified (Figure 33A). While hydrogels without BG present a clear rapid increase of the storage modulus when the temperature is raised to 37°C (dotted line), this effect is strongly reduced in the presence of BG (Figure S 11). Moreover, precipitation was clearly observed visually (Figure 32, first line) and the mechanical properties of the gels were so poor that they could not be tested under compression. Moreover, the formed hydrogels presented non-physiological pH values (above 9), making same unsuitable for cell encapsulation (Figure S 12).

We therefore also tested hydrogels prepared 5 days after mixing BG in the GA solution, when the BG reaction in the GA seems to be stabilized. This allowed to reach a pH close to 8-8-5 when adding HCl, and to get hydrogels with pH close to physiological values, at least for BG1% formulations (Figure S10), In these conditions, PB-SHC gels thermosensitivity is still visible for BG1%, the storage modulus increasing rapidly when the temperature rises to 37ºC. The hydrogels presented better shapes (Figure 32, line2) and stronger mechanical properties, which could be measured by unconfined compression. Figure 33B presents the secant modulus at 30% deformation for each formulation, after 24h gelation at 37°C.

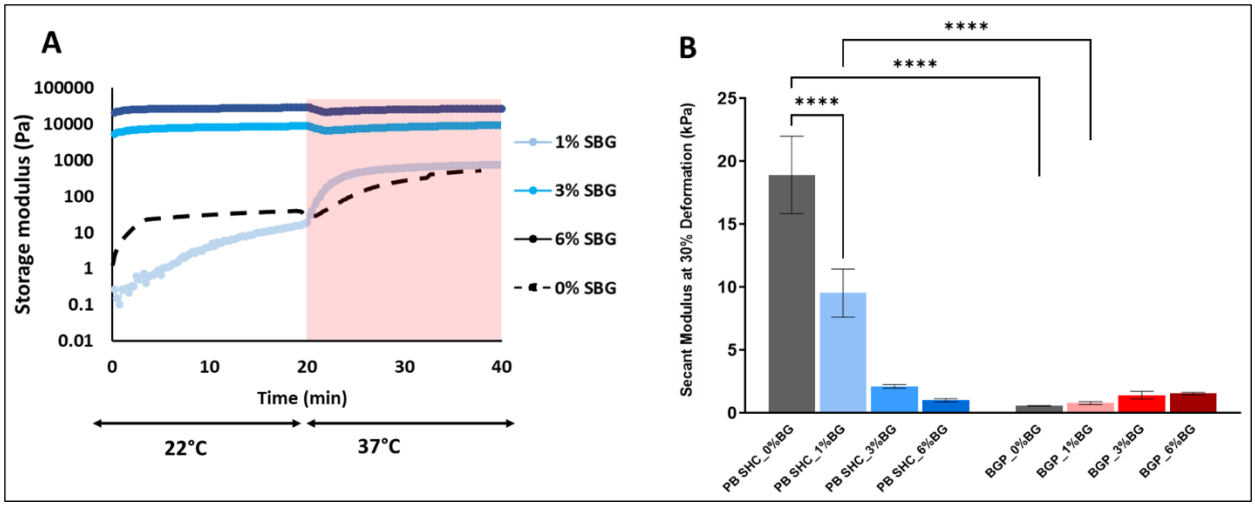

Figure 33. (A) Time sweep at 22ºC followed by 37ºC for CH/PB-SHC-BG hydrogels, when prepared 5 days after mixing BG and gelling agents (mean +/-SD; N≥3, n≥6); (B) Unconfined compression tests: secant modulus at 30% deformation; (blue zone, and red zone are for PB0.01 SHC0.075, and BGP0.1 hydrogels with 0, 1, 3 and 6% BG (mean +/-SD; N=2, n≥3); **** $p<0.0001$).

Mechanical properties are strongly influenced by the type of gelling agent. Results show that hydrogels made with PB-SHC are much more rigid (18.9 ± 3.1 kPa) than those made with BGP (0.6 ± 0.1 kPa; **** $p<0.0001$), in agreement with our previous work [67]. But BG addition strongly reduced their secant modulus in a dose-dependent manner. SHC-PB gel with 1% BG still presented interesting mechanical properties (around 8 kPa). It must be noted, however, that the BG content indicated in this figure is overestimated since part of the BG was already dissolved in the GA solution at the time of gel preparation (5 days). To evaluate partial dissolution, we measured the weight of BG particles recovered from the GA solutions at day 5. It was only around 40% of the initial weight.

Altogether, these data suggest that the addition of BG in chitosan hydrogel influences pH, thermosensitivity, mechanical properties and cytocompatibility adversely. Therefore, to further enhance the mechanical properties, increase BG concentration and possibly increase the compatibility of the PB-SHC gel for cell encapsulation, we proposed to concentrate BG in small microbeads instead of their homogenous distribution in the gel.

6.4.2 BG-rich microbeads size and morphology

Chitosan microbeads with and without BG were created using a stirred emulsification process in mineral oil. Microbead size was optimized by changing stirring speed from 550 rpm to 1200 rpm. Higher stirring rate allowed forming smaller and homogenous microbeads, in comparison to 550 rpm (data not shown). Results of 1200 rpm stirring speed are presented in Figure 34.

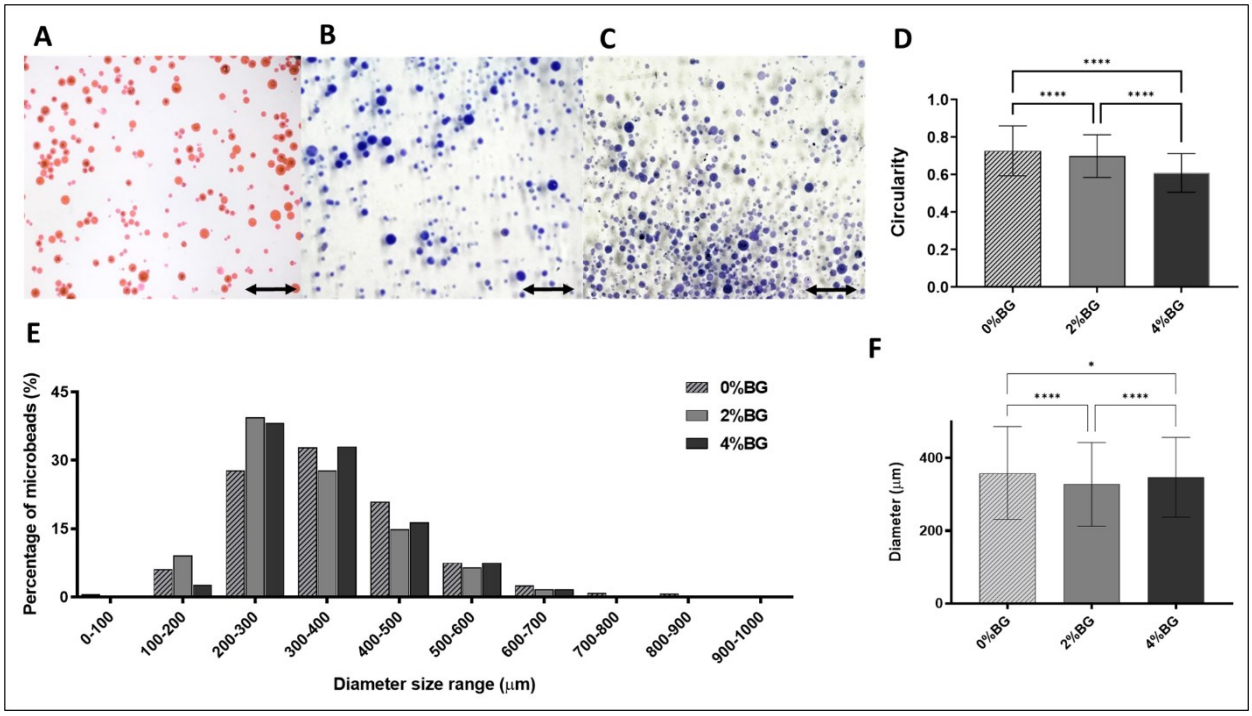

Figure 34. Beads morphology and size distribution: A-C) Light microscope images of PB-SHC microbeads containing 0, 2 and 4% (w/v) BG, respectively (Bar corresponds to 1 cm) (0%BG stained with Eosine, 2% and 4%BG stained with Toluidine blue); D) average circularity of microbeads (1=perfectly circular microbeads); E) Size distribution; and (F) mean diameter of chitosan microbeads with and without BG, quantified by the CellProfiler image analysis software (mean, N=3, n>1000), (** $p<0.01$, *** $p<0.001$, **** $p<0.0001$).

The mean diameter of the microbeads was around 340 μm, with slight differences between the 0, 2 and 4 % BG formulations (respectively 358 ± 128 μm, 327 ± 115 and 347 ± 110 μm, with 2% and 4%BG, with $p<0.0001$ and $p<0.05$, respectively). Beads with 0% and 2%BG showed a more homogeneous size

distribution, and higher circularity than the 4%BG (0.74 ± 0.13, 0.70 ± 0.11, 0.60 ± 0.11 for 0, 2 and 4%BG respectively (**** p<0.0001)). Higher BG concentrations were also tested but did not form homogenous beads (data not shown).

6.4.3 Mechanical properties of hybrid hydrogels

Hybrid hydrogels (Hyb) were created using microbeads containing 0, 2, and 4%BG embedded in a PB-SHC chitosan matrix, at microbeads/matrix volume ratios of 20/80 and 50/50% respectively. In contrast to homogenous BG gels, hybrid gels presented good gelation without precipitation (Figure 32, line 3). Their mechanical properties were compared with hydrogels of theoretical equivalent global BG content (BG content added in the GA solution), but evenly distributed in the hydrogel (from 0.4 to 2%) (Figure 35).

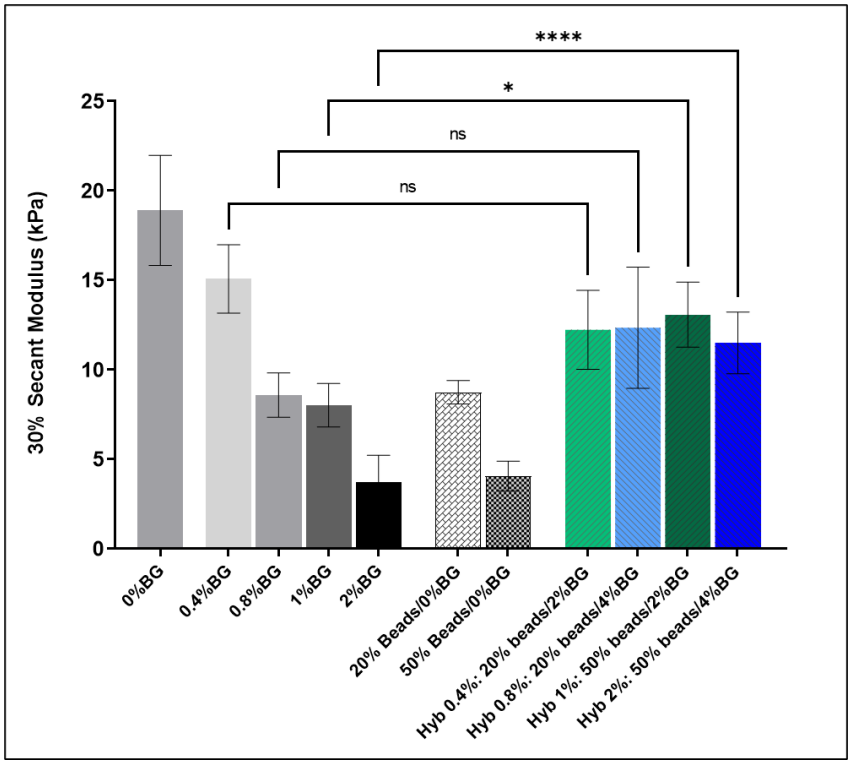

Figure 35. Unconfined compressive properties of hybrid hydrogels (Hyb), in comparison to hydrogels with similar concentration of BG but homogenously dispersed: secant modulus at 30% deformation (mean +/- SD; N=2, n=6) (** p<0.01, **** p<0.0001, ns=not significant) All hydrogels were prepared using PB0.01SHC0.075 gelling agent. For hybrid gels, since both the volumic bead content (20 or 50%) and the BG content in the beads vary, the global concentration of BG is indicated first in their name.

Concentrating BG in the microbeads instead of its uniform distribution in the hydrogel improved the secant modulus of the hydrogel. Thus, for a final composition of 2% BG, the hydrogel with homogeneously distributed BG had a modulus of 3.7 ± 1.5 kPa only, significantly lower than that for the Hyb 2% made with 4% BG microbeads in 50/50 volume ratio, which had a modulus of 11.5 ± 1.7 kPa. Similarly, for a global BG content of 1%, a hydrogel with homogeneously distributed BG had a modulus of 8.0 ± 1.2 kPa versus 13.1 ± 1.8 kPa for the hybrid gel formed with 50% volume of microbeads (* $p<0.05$). It must be noted that the differences are underestimated since the real concentration of BG in the homogenous gel is lower then indicated, as a significant part of the BG has dissolved in the GA during the 5 days prior to chitosan mixing. In contrast, in microbeads, BG concentrations indicated are real.

The enhancement of the mechanical properties is likely not due to the presence of the microbeads themselves. Indeed, in the absence of BG, hybrid hydrogels with microbeads showed lower rigidity compared to homogenous chitosan hydrogels (18.9 ± 3.1 kPa for the homogenous gel compared to 8.7 ± 0.6 for 20% v/v beads and 4.1 ± 0.8 kPa for 50% v/v beads (Figure 35). It could be rather explained by the fact that, as initially hypothesized, BG, when concentrated in the microbeads does not interact with proper gelation of the chitosan thermosensitive hydrogel embedding the microbeads.

6.4.4 Bioactivity:

The bioactivity of BG-loaded hydrogel was studied using FTIR, SEM and EDX analysis.

FTIR

To confirm whether BG addition in the gel results in apatite formation, FTIR analysis was carried out on 4%BG-loaded microbeads and 0%BG microbeads as a control, after 7 days immersion in SBF at 37ºC (Figure 36).

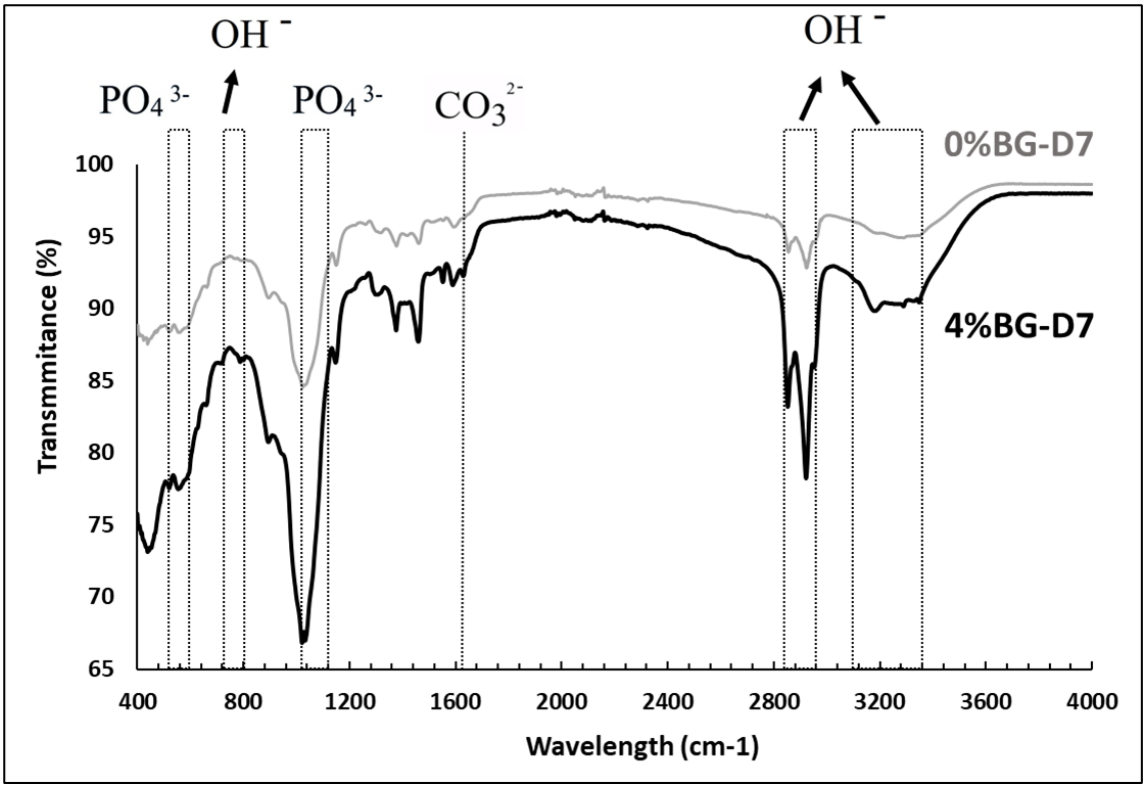

Figure 36. FTIR spectra of chitosan microbeads with and without BG after 7 days soaking in SFB (black lines correspond to BG-loaded microbeads and the grey line corresponds to the 0%BG).

The chemical groups in the FTIR spectrum of PO_4^{3-}, OH^-, CO_3^{2-}, as well as HPO_4^{2-} are characteristic of hydroxyapatite [339]. The FTIR spectrum of the BG beads (Figure 36) exhibits broadband ranging from 1200-1000 cm^{-1} associated with the asymmetric stretching of Si–O–Si groups. The peaks became sharper in BG microbeads. The vibrations increase at 1175-1170 cm^{-1} and 1100-950 cm^{-1} are related to Si-O-P stretching and P-O symmetric stretching from the PO_4^{3-}group. Additional bands related to silicate network vibrations and PO_4^{3-}group can be observed at 510-480 cm^{-1} and 760-730 cm^{-1}, which is sharper in 4%BG than 0%BG microbeads. The -OH stretching absorption could be seen in 800-700, 3000-2850, and 3300-3100 cm^{-1}. The absorption at 1644 cm^{-1} could be ascribed to the carbonyl (CO_3^{2-}) stretching, causing $CaO–P_2O_5$ crystallization. This layer is called a mixed carbonated hydroxyl apatite (HCA). These two absorptions are sharper in BG microbeads than nonBG microbeads.The main bands appearing in those spectra are summarized in Table 8.

Table 8. Main FTIR vibrational bands associated with 0% and 4%BG microbeads over 7 days soaking at SBF.

Wavelength (cm^{-1})	**Group assignment**	**Ref.**
3100-3300	-OH stretching	[339]
2850-3000	-OH stretching	[339]
1644	CO_3^{2-}stretching	[340]
1000-1200	Asymmetric stretching Si–O–Si	[209, 341]
1170-1175	stretching Si–O–P	[339]
950-1100	P-O stretching (PO43-)	[340, 341]
800-820	Stretching Si–O–Si	[209]
730-760	PO_4^{3-}group	[209]
600-610	P-O bending (PO43-)	[340]
550-560	P-O bending (amorphous)	[342]
480-510	PO_4^{3-}group & Si-O-Si bending	[342]

SEM and EDX

The morphology and composition of BG microbeads was investigated by SEM coupled to EDX analysis, to observe possible calcium phosphate deposition after soaking microbeads in SBF. Representative SEM images are shown in Figure 37. Aggregates of spherical shaped particles were observed on the surface of microbeads containing BG after day 1 and day 7.

EDX analysis showed that the relative concentration of Si and Ca (Figure 37 D-F) evolved with time, with a clear decrease in sodium and increase in Ca, and Si (Table 9). It should be mentioned that since P and Au have similar bonding energy around 2 kV, the P peak was not identified in EDX results. Although, the increase of calcium peak intensity and the peak at 2 kV with soaking time in microbeads with BG suggests the presence of calcium phosphate (apatite layer formation). In contrast, no change was observed in the control group (0%BG) after 7 days soaking in SBF, in terms of surface morphology (Figure 37 G, H) or composition (I, J). The surface was smooth, even after 7 days, with no detectable peaks for Si and Ca.

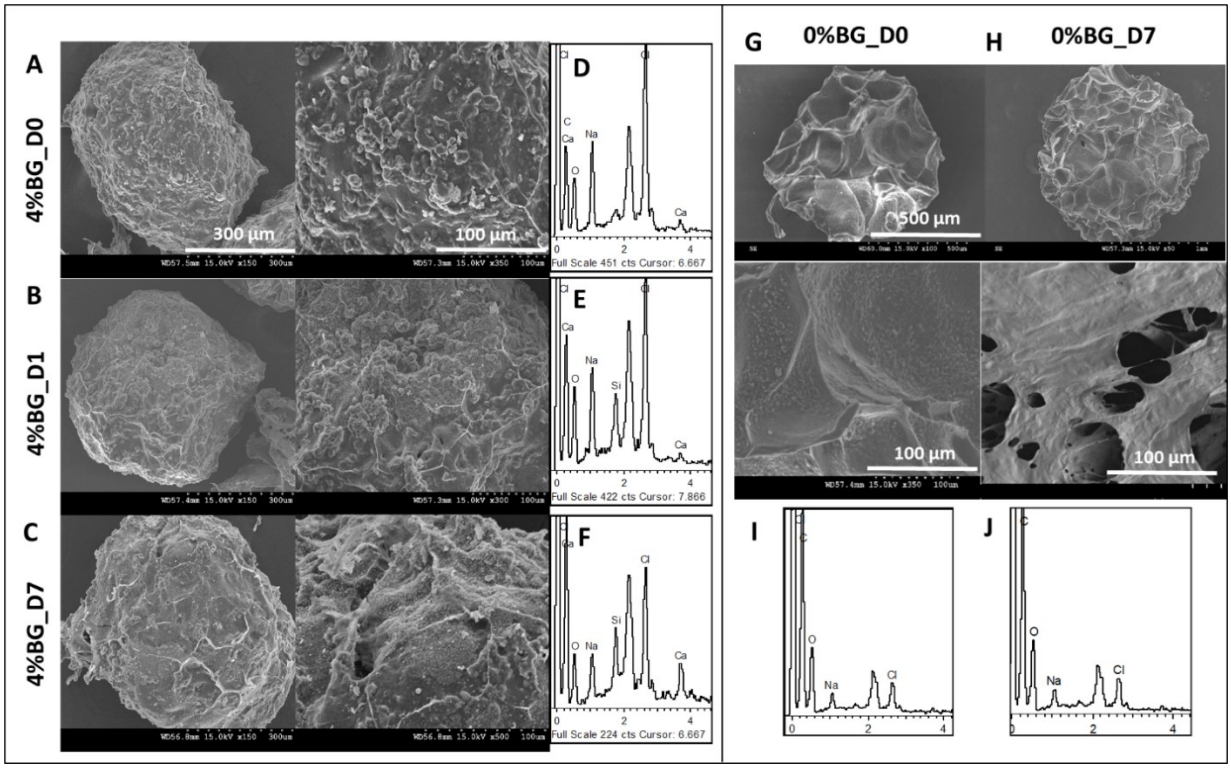

Figure 37. SEM images and EDX spectra of microbeads with and without BG after 0, 1, or 7 days soaking in simulated body fluid (SBF). A-C): SEM of 4% w/v BG at day 0, 1 and 7; D-F): corresponding EDX analysis; G, H, I, J): SEM and EDX of 0%BG control after 0 and 7 days in SFB.

Table 9. EDX analysis: elemental composition (relative atomic concentration) of chitosan microbeads containing 0, 2 and 4% BG, over 7 days soaking in SBF (NA: Not available; ND: Not detectable).

Elements (Weight %)	D0	D1	D7
2% BG			
Na	28.4	16.5	1.5
Ca	8.0	19.1	24.5
Si	0.9	6.3	10.9
O	44.7	56.0	59.2
4% BG			
Na	15.6	10.2	1.7
Ca	8.8	11.9	25.3
Si	2.7	10.0	11.9
O	22.1	47.9	59.0
0% BG			
Na	1.4	NA	1.4
Ca	ND	NA	ND
Si	ND	NA	ND
O	31.0	NA	35.0

Similar observations were made on bulk hydrogels containing BG (Figure S 15).

6.4.5 Cytocompatibility (Cell viability and Rate of ion release)

Using L929 fibroblasts as a model cell line, we evaluated whether the hybrid hydrogels could be compatible for cell encapsulation. For this purpose, the osmolality of the hydrogels extract was first measured as an indirect way to study the rate of ion release from the hydrogels over 72 hours after soaking the hydrogels in culture media (DMEM) (Figure 38 A). Then the viability (Figure 38 C) and metabolic activity (Figure 38 B) of encapsulated cells were studied over 7 days and compared to chitosan hydrogels with homogenously distributed BG prepared with GA mixed immediately with BG (1% w/v). Chitosan hydrogel without BG was studied as a positive control.

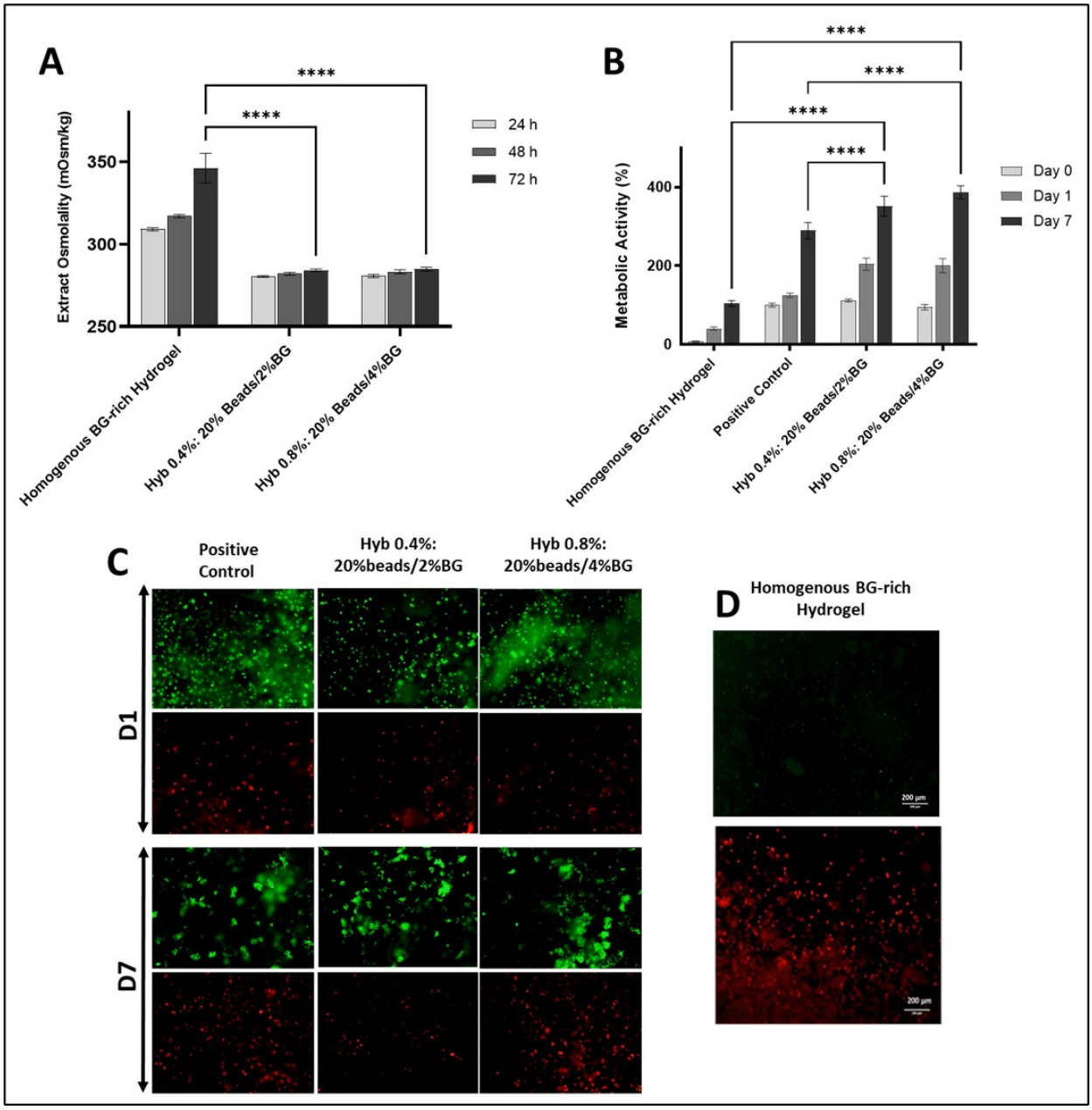

Figure 38. Viability of L929 fibroblasts encapsulated in chitosan hydrogels with either BG homogenous distribution or with BG microbeads. A) Osmolality of extracts; B) Metabolic activity (Alamar blue) and C) Viability (Live/dead) of encapsulated cells after 7 days (positive control=0%BG) (mean +/-SD; N=3, n≥6); (**** $p<0.0001$).; D) High cell mortality is already observed at day 1 in homogenous BG-rich hydrogels.

Hybrid hydrogels showed physiological osmolality (260-300 mOsm/kg), while extracts from hydrogels with homogenous BG distribution were hyperosmolar at day3 (Figure 38 A) ($p<0.0001$).
Live/dead images showed that, as expected, BG homogenous distribution in the hydrogel led to toxic effect on the encapsulated L929 cells, as demonstrated by the very high percentage of dead cells at day 1 (Figure 38 D). Viability was significantly improved for hybrid hydrogels, which reached viability similar to non-BG hydrogels. Alamar blue (Figure 38 B) results showed high metabolic activity (normalized as a function of 0%BG (positive control)), which increased between day 1 and 7, values at day 7 being even higher than the positive control (no BG) ($p<0.0001$). The negative control (homogenous BG) showed the lowest metabolic activity.

6.4.6 Injectability

To confirm injectability of the product as a bioactive bone filler, microbeads were either dispersed in SBF or in the hydrogel solution immediately after mixing the two components. They were then injected through an 18G (id=838 μm) needle [209, 343]. Figure 39 shows the microbead morphology before and after injection.

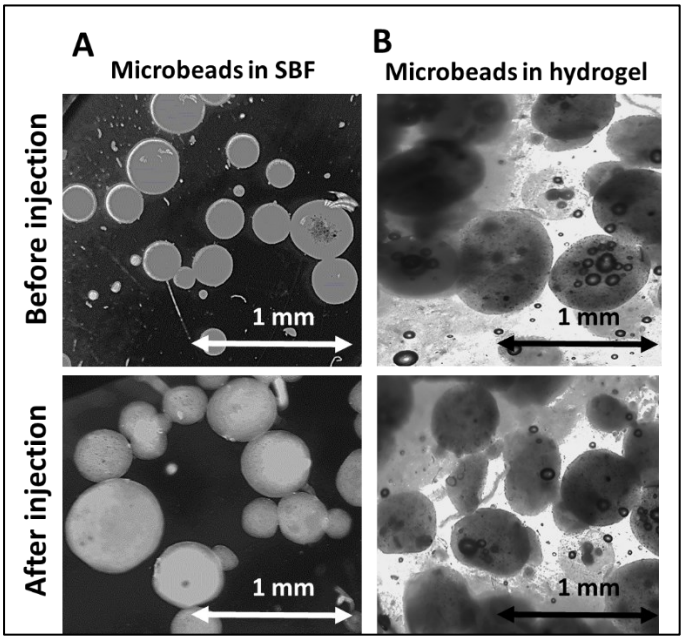

Figure 39. Light microscopy images of microbeads containing BG before and after injection through long 18G needle: A) dispersed in SBF; B) dispersed in the chitosan-based hydrogel.

A smooth injection was possible through a long 18G needle. This was expected since according to the size distribution, more than 90% of microbeads have a diameter inferior to the needle's inner diameter. Microbeads soaked in SBF maintained their morphology after injection (Figure 39 A). Microbeads encapsulated within the hydrogel were also injectable, but some bead deformation and a few breakages were observed (Figure 39 B), which can be related to shear stress during mixing and/or injection.

6.4.7 Freezing and long-term storage

Since BG rapidly react in aqueous solution to form apatite, they are difficult to store after production. Freeze-thawing the microbeads would provide opportunities of long-term storage and potential for clinical applications. Therefore, microbeads with 2% BG were studied before and after freezing at -20°C for 14 days. No change of size and morphology was observed (Figure 40).

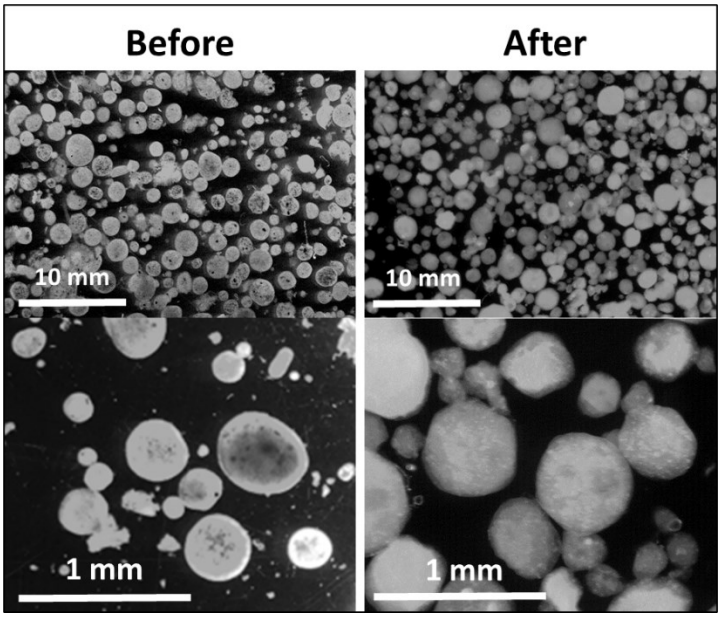

Figure 40. Light microscope image of 2% BG microbeads before and after freezing at -20°C for 14 days.

6.5 Discussion

In this study, we explored the potential of chitosan thermosensitive hydrogel containing sintered BG as a bioactive injectable hydrogel for bone tissue applications. We have previously shown that using a mixture of PB and SHC as gelling agents allows to create chitosan hydrogels with drastically enhanced mechanical properties and cytocompatibility compared to conventional chitosan–BGP hydrogels [68]. We therefore

first compared these two formulations, when adding sintered BG, in terms of pH variation, gelation kinetics, mechanical properties and cytocompatibility.

The addition of sintered BG to the gelling agent solution resulted in its strong immediate pH increase. This is in agreement with previous studies and is explained by a rapid release of Na^+ ions from bioactive glass in aqueous solutions [210, 311, 336]. When mixed with chitosan, it led to hydrogels which pH rapidly increased over the physiological range, leading to high mortality of encapsulated cells. It also strongly reduced the thermosensitive behaviour of these interesting hydrogels and led to so poor mechanical properties that compression tests could not be performed. In a previous work, the addition of 2% w/v BG to thermosensitive chitosan-based hydrogel made of BGP gelling agent has resulted in only a hydrogel with a G' of only 9 Pa after 4 min at 37 °C, compared to the nonBG loaded hydrogel (G'~6 Pa) [210]. A rapid increase of the pH above chitosan pK_a, could lead to chitosan partial precipitation instead of the progressive physical gelation normally obtained through proton transfer when increasing the temperature [67, 187]. Another explanation is that GA ions rapidly form ionic interactions with the cations released by BG, so they cannot play their important role in the physical gelation mechanism. While further work would be required to better understand this effect, we could hypothesize that the gelling agent ions (HPO_4^{2-}, $H_2PO_4^-$, HCO_3^-, CO_3^{2-}), that normally prevent precipitation by screening chitosan NH_3^+ amino groups, are directly interacting with cations from the BG until a crystallized hydroxycarbonate apatite layer is formed. Better results were obtained when mixing BG in GA 5 days before hydrogel preparation, which allows to better control the pH, but such method is impractical for clinical applications and reduces significantly the amount of BG in the hydrogel due to its partial dissolution.

These negative effects of BG addition in chitosan thermosensitive hydrogel explain why only very few works have been published on the subject. In 2018 Moreira et al. published about CH-BGP gels containing nanoBG, BG nanoparticles were added at the very end of the process, after mixing the chitosan acidic solution to the gelling agent, which avoid BG partial dissolution and interaction with the GA ions[211]. This method is however not very practical for clinical applications since it requires 3 mixing steps to create cell-loaded scaffold. More importantly the mechanical properties of the hydrogels were very poor (G' around 6-9 Pa only).

Therefore, we proposed to concentrate BG in small microbeads instead of their homogenous distribution in the gel. We hypothesized that this would reduce the number of ions in the chitosan hydrogel and thus

allowed proper gelation and enhance the mechanical properties, as well as possibly increase the compatibility of the PB-SHC gel for cell encapsulation.

BG-loaded microbeads at 2% and 4% w/w BG were formed using a simple and easily scalable emulsification process without any chemical modification or cross-linker, using a 1200 rpm stirring rate.

We loaded chitosan-based hydrogel with microbeads at a ratio of 20% and 50% v/v. Hydrogels loaded with BG microbeads (Hybrid hydrogels) were compared with BG homogeneously distributed in hydrogel. Due to the presence of the beads, rheological measurement could not be performed but visual assessment showed that the solution rapidly gelled at 37°C and compression tests showed higher rigidity of the hybrid hydrogels, although it was still lower than nonBG-loaded hydrogel. This increase is not related to the presence of microbeads since, in the absence of BG, hybrid hydrogel perform better than the conventional hydrogel. This suggests that, as expected, the BG segregated in microbeads is less interfering with physical gelation of chitosan hydrogels, probably due to slower release of ions.

Such hybrid hydrogels combine several advantages compared to chitosan hydrogels with homogenous distribution of BG: they present drastically enhanced mechanical strength; microbeads can be prepared and frozen while waiting for their addition in the gelling agent, thus preventing partial dissolution and allowing long-term storage of the product for potential clinical applications. The hybrid product is suitable for non-invasive injections through 18 G needles (smaller diameters were not tested). Cell survival was drastically better than in homogenous BG loaded hydrogels, encapsulated cells showing even higher metabolic activity at 7 days than the chitosan gel control. Such hybrid hydrogel is particularly interesting when prepared with a mixture of SHC and PB as gelling agents, since it allows to reach much higher mechanical properties than CH-BGP hydrogels.

Osteoconductivity is an important factor for bioactive scaffolds and induces osteoblasts to form new bone [180]. The FTIR results proves hydroxyapatite formation by the increase of two main wavelengths related to phosphate and carbonyl stretching [339]. The EDX results show a rapid decrease in Na^{+} ions which are known to be replaced with H_3O^{+} in the first step of apatite layer formation on the surface of BG. Alongside, Si concentration increased which supports the formation of a silica gel layer on surfaces of BG contained microbeads. Ca^{2+} and PO_3^{-4} also concentrated over 7 days indicating nucleation of hydroxycarbonate apatite as reported by Moreira et al. [209, 210]. Similarly, Oudadesse et al. presented apatite layer formation on chitosan biopolymer surface after 7 days, indicating potential of BG-chitosan bioactivity in physiological

environment [344]. Thus, our results indicate that BG-loaded microbeads are expected to form apatite in the body. However, it would be required to coat BG microbeads with palladium or another metal rather than gold to determine calcium/phosphate ratio with EDX. In addition, comprehensive osteoconductivity characterizations are needed to justify their ability to form a biological bond with the surrounding living bone.

One limitation of these hybrid hydrogels is the relatively low BG content since microbeads containing more than 4%w/v could not be formed. Another limitation is the deformation or possible breakage of microbeads when encapsulated within the hydrogel and injected which, may impact adversely the mechanical properties as well as cell survival. Though we have studied cell viability for longer time (7 days) than other researches (24h) [210]. It is also suggested to characterize the cytocompatibility with bone application cell lines e.g. osteocytes and MSCs [211, 345], since there might be the issue of the fibrous encapsulation formation and, in consequence, the risk of implant failure [346].

Chitosan is degradable in vivo, but the time scale for degradation is much slower than the solubilisation of the BG particles and the apatite formation [346]. Also, the BG particles solubilisation depend on physical form of the particles; microparticles dissolve slower than nanoparticles [347]. We expect that for long-term implantation, bone remodelling follows its own procedure while chitosan is gradually degraded.

6.6 Conclusion

Sintered bioglass was added to chitosan thermosensitive hydrogels to create cell-loaded bioactive in situ gelling hydrogels for bone applications. Despite sintering of BG particles, simple addition of BG had a drastic negative effect on physical gelation, mechanical properties, and cell survival due to rapid ion release and rapid pH elevation. In contrast, hybrid hydrogels containing BG concentrated in BG-rich microbeads, allowed to create in situ setting hydrogels with a relatively good rigidity, physiological pH and osmolarity and good cell survival. While further demonstration of osteoconductivity will be needed in the future, the hydroxyapatite formation suggested the excellent bioactivity of the hydrogels. Microbeads and hybrid hydrogels are injectable through 18 G needle. BG-rich microbeads can be frozen, providing the feasibility of long-term storage and potential for clinical application; however, further characterization is needed to validate that freezing does not alter the bioactivity or mechanical properties. These all indicate that hybrid

hydrogel containing BG microbeads might form a promising injectable cell-laden bioactive biomaterial for treatment of bone defects at non-loading sites.

Acknowledgements

We would like to acknowledge the Natural Science and Engineering Research Council of Canada (NSERC; RGPIN-2015-05169) and the Fonds de Recherche du Quebec – Nature et technologie (FRQNT; team project and M.R. scholarship) for funding and support of this project. We would like to thank Tommy Malaret for cytotoxicity characterization.

6.7 Supporting Information

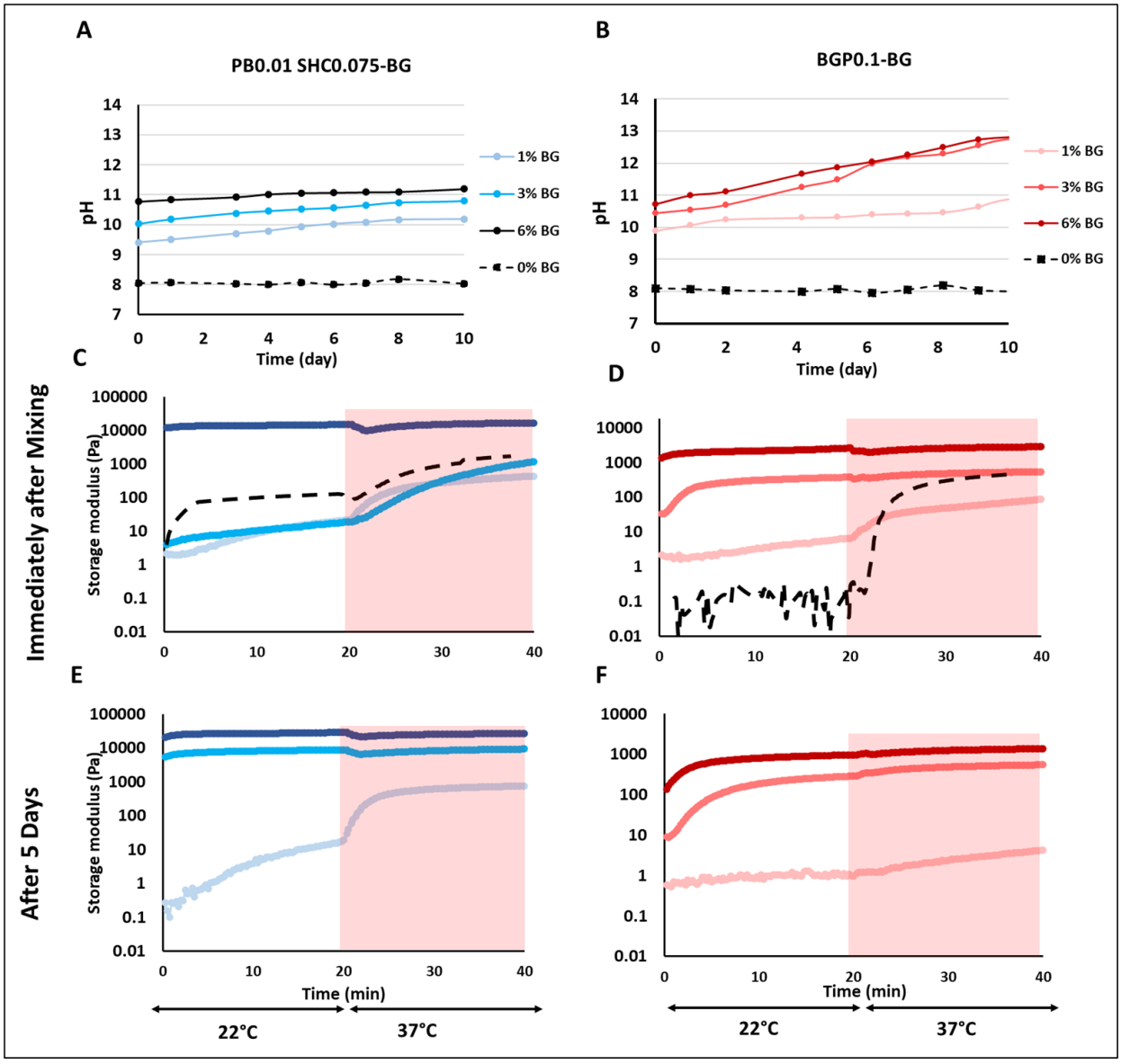

Figure S 11. Effect of BG concentration on the pH of the GA solutions and gelation kinetics of the corresponding chitosan hydrogels; A-B: pH variation of the BG-gelling agent solution over time at room temperature. C-F: Time sweep at 22ºC followed by 37ºC for CH/GA-BG hydrogels, when prepared immediately after mixing BG and gelling agents (C & D) or 5 days after mixing BG to gelling agent (E & F) (mean +/-SD; N≥3, n≥6).

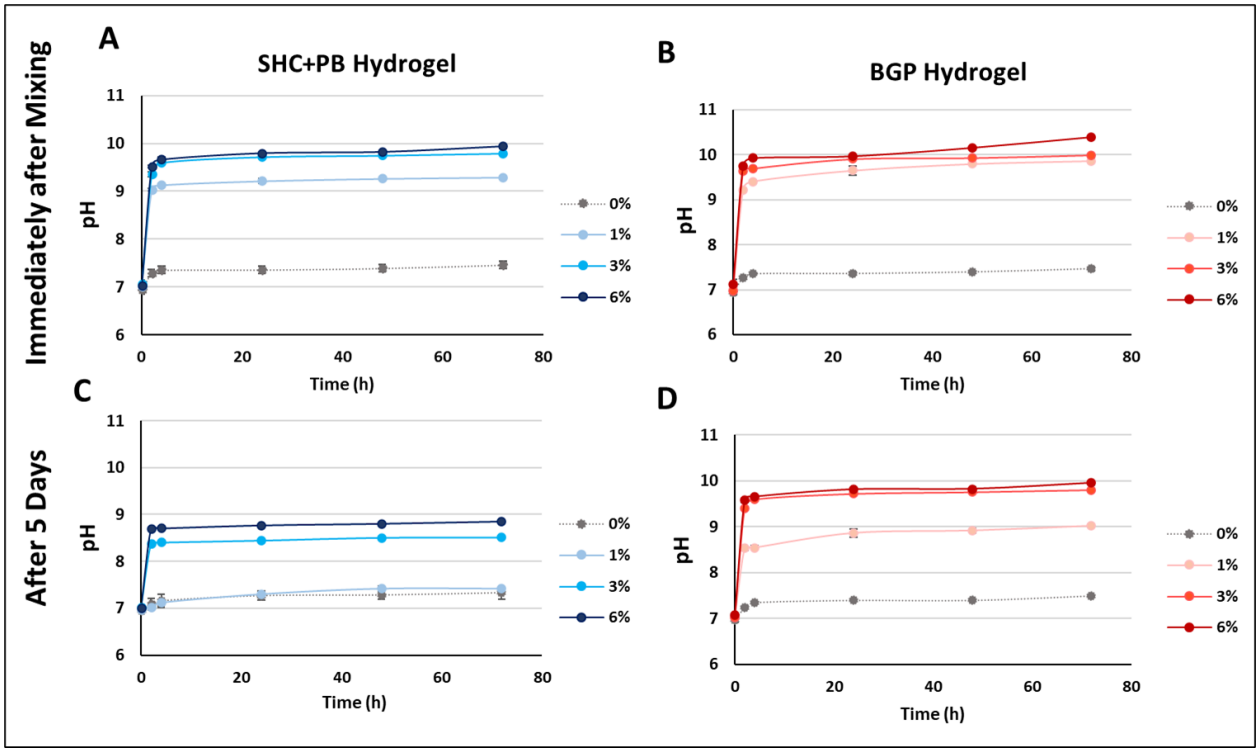

Figure S 12. Evolution of the pH of hydrogels when made of GA+BG prepared immediately or 5 days before mixing with CH (In all cases the pH of the GA solution was adjusted to 8 prior to CH mixing)

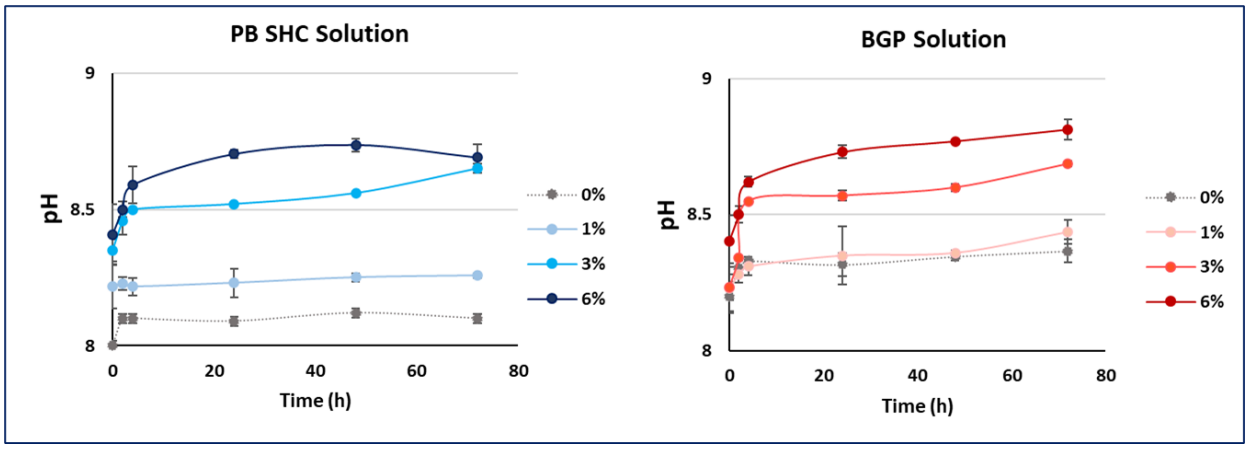

Figure S 13. The pH of GA-BG solutions after pH adjustment at 8-8.5.

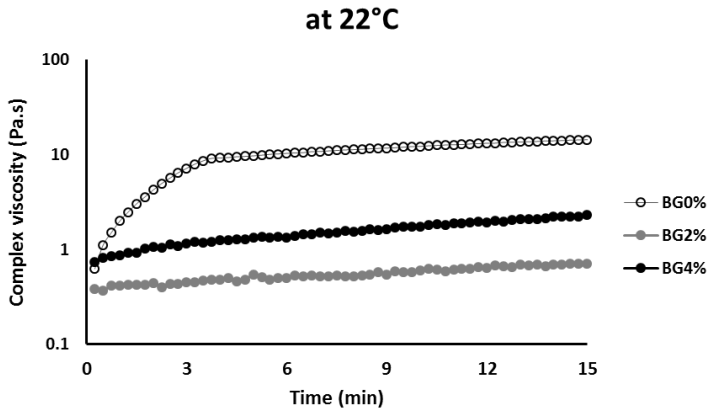

Figure S 14. Complex viscosity of 0%, 2% and 4%BG contained hydrogels at 37C

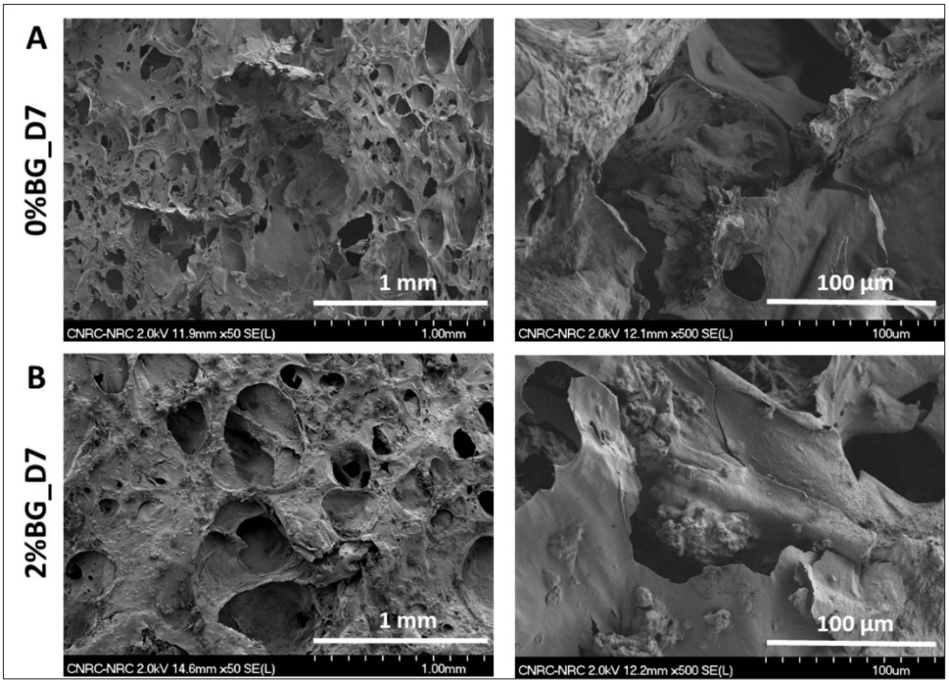

Figure S 15. SEM images of hydrogels with and without BG after 7 days soaking at SBF: A) 0%BG; B) 2%BG.

Chapter 7 – General Discussion and Conclusion

As described in the literature review, bioprinting is a very promising technology to engineer tissues, but ideal bioinks combining good resolution, mechanical properties, compatibility with cell survival and biodegradability, are still missing. Moreover, there is a need for rheological methods to predict the printability of hydrogels and better screen the possible candidates. The general objective of this Ph.D. was therefore to develop new bioinks, as well as to propose a rheological method that would help predict the printability of hydrogels.

Among the potential candidates, chitosan thermosensitive hydrogels appeared as promising materials, However, the only few studies performed to date were on CH-BGP hydrogels and were quite disappointing, since these hydrogels lead to printed structures of very poor resolution and low mechanical properties [140, 141]. Previous work from our team had shown that, when prepared with a mixture of SHC and BGP as gelling agent, chitosan hydrogels present rapid gelation, much better mechanical properties, and a more physiological pH [67, 68, 90]. This suggests that they could be better candidates for bioprinting.

In this Ph.D., we therefore, study and optimize the potential of chitosan hydrogels as bioinks. Moreover, since the rheological characteristics of these hydrogels are time-dependent, we propose a rheological approach to evaluate their printability.

7.1 Rheological approach to predict printability

As explained previously, first of all the ideal bioink requires continuity and homogeneity to show good printability without clogging. Bioink must also physically support the 3D printed structure and do not collapse by upper printed layers with particular rheological properties. Rheological analysis can provide information on the bioink's mechanical properties before, during, and after gelation and must be adjusted to the bioprinting process. In case of chitosan hydrogels, it is challenging. Gelation kinetics showed that **thermosensitive chitosan-based hydrogels are not stable at room temperature** which was in agreement with previous data [67].

The second important feature is viscosity and shear thinning properties. It is generally recognized that printable formulations must be a shear thinning and highly recoverable after shear removal in order to preserve their shape, to support their own weight, and the printed layers on top. However, the quantification

of these fundamental criteria is still ambiguous, in part because of the variety of rheological approaches employed and the absence of common protocols, and in part because of the variety of biomaterials with complicated viscoelastic characteristics currently utilized [22]. To date no comprehensive rheological protocol has been proposed. To study flow initiation of viscoelastic materials different tests including shear viscosity ramp and yield stress are introduced; however, they are all limited to the stable bioinks [74, 348] or prior to their crosslinking [349, 350]. Mostly, in extrusion-based bioprinting, the bioink is crosslinked after deposition. For example, chitosan-collagen blend was first printed, then thermocrosslinked using NaOH solution at 37°C. Shear viscosity test was used to study shear thinning viscosity [349]. Although pre-gelled chitosan-based hydrogels showed shear-thinning properties under applied shear, **the viscosity varies with time**. It is not suitable to use a simple shear rate sweep (viscosity as a function of changing shear rate) [234]. Typically for stable hydrogels like chitosan-collagen blend or alginate, viscosity is studied over the change of shear rate or stress. But for time- and temperature-dependent hydrogels, the tests must be adjusted accordingly. In this regard, we **devised firstly, new rheological studies to measure and evaluate the printability of chitosan thermosensitive hydrogels**, whose rheological characteristics change with time and temperature. To be noted that, the viscosity profile solely cannot predict the complex rheological behavior of bioinks [74].

The recovery of the materials after being subjected to shear rates similar to that during bioprinting was evaluated to characterise the window in which bioprinting can be achieved. Indeed, the recovery test is the most comprehensive and predictive test compatible with different materials, even time- and temperature-dependent hydrogels in which shear thinning behaviour, time or temperature dependency, impact of crosslinking and self-healing properties after shear removal could be studied [74]. Recovery after shear removal ranging low (10 s^{-1}) to high (1000 s^{-1}) was studied to see how chitosan hydrogel recovers after being exposed to high shear rates. No recovery could be observed either when chitosan hydrogels gelled or exposed to high shear rates. If materials do not recover to their original viscosity, permanent material damages like chain breakage may have taken place as a result of high shear rate applied during printing [74] which could be reflected in mechanical properties. However, interestingly at only low shear rates, it recovered very rapidly. Therefore, determining the optimal time frame (before complete gelation) for extrusion is critical, and this method might be extended to other temperature or time-evolving materials.

7.2 Potential of Chitosan thermogel as bioinks

In this study, various chitosan hydrogel formulations were tested for their potential as bioinks, namely CH2%, CH3% and a mix of chitosan with gelatin. As expected, viscous hydrogels result in higher resolution and shape fidelity. Thus, the most viscous **chitosan pre-gel (3% w/v) results in much better shape fidelity and narrower filament (resolution) than its 2% counterpart.** It led to 3D structures of relatively good resolution and cohesion. Unfortunately, it showed also poor cytocompatibility, with **a high mortality rate of encapsulated cells.** This can be due to the high viscosity of the cell-laden solution and/or to the high density/low porosity of the final hydrogel. In addition, viscosity has a direct relation to the applied extrusion force [223, 277, 278]. Chitosan 2% (w/v) was required shear rate range of 200-300 s^{-1}, while shear rate of 1000 s^{-1} was applied to print chitosan 3% (w/v) (4). For printing more viscous bioinks, more force is needed; therefore, the cells will experience more stress and more cell death, and damage will be caused upon the encapsulated cells during bioprinting [213, 218, 351].

In contrast, CH2% has been previously shown to be excellent injectable scaffold for cells [67]. Unfortunately, the pre-gel solution presents a low viscosity (CH2% viscosity of ~1000 Pa.s versus CH3% viscosity of ~10000 Pa.s) and spread on a substrate after printing, unable of supporting upper layers. 3D printed structures therefore lack adequate shape fidelity. Results were even less convincing for CH-Gel gels. The slow gelation of chitosan gel, as shown during rheological studies also partly explain these results.

Indeed, in contrast to alginate gels which can be ionically crosslinked within a few seconds by calcium ions, chitosan gelation is a relatively slow process that explains the difficulty of bioprinting solid 3D structures with hydrogels presents low viscosity of e.g., 1000 Pa.s, despite their more interesting thermosensitive character. Our results are in agreement with previous work with thermosensitive CH-BGP bioinks that usually show low viscosity to provide excellent cell viability, resulting in poor shape fidelity and mechanical properties [140, 141, 352]. For example, Ku et al. used PCL as support to bioprint CH-BGP hydrogels because the printed chitosan hydrogel did not have enough rigidity to support the building of multilayers [141].

Possible solutions to this problem could be to increase chitosan concentration between 2%-3% w/v. However, increasing the concentration enhances the chance of cell mortality [353]. Another team proposed the addition of nanocellulose to CH-BGP hydrogels and co-print to support CH-BGP bioink after deposition

[140], but the mechanical properties and resolution increase were not significant and still far from ideal, showing the need for support for low viscous chitosan hydrogels. To improve the printability of CH2%, we therefore proposed to take advantage of the FRESH method, pioneered by Feinberg team [53].

7.3 Chitosan bioink in FRESH bioprinting

Different FRESH support baths had been previously used, as described in Chapter 2, the most common one being gelatin slurry. But in the present case, the support bath had some unusual specifications to fit our application: the support bath must be solid at 37°C to provide support during the printing and assist in rapid gelation of the chitosan hydrogel (taking advantage of CH2% thermosensitivity compatible with cell encapsulation), with good recovery after needle movement, and then liquefy at a temperature sustainable for the cells to be easily removed. Therefore, **Pluronic was proposed and adapted to better fit the specific needs of thermosensitive hydrogels**.

Pluronic has poor mechanical strength when low concentrations are used (e.g., 7-12% w/v) and tends to dissolve in aqueous environments, which may affect printed structure shape properties while using low viscous hydrogel precursors e.g., alginate 2% [58, 259]. In this regard, we studied high concentration of 17%-20% w/v Pluronic solutions. In accordance with previous studies [58, 257, 289], we showed that the gelation temperature and storage modulus can be tuned by changing the concentration of Pluronic and salts, e.g., NaCl. Among the characterized bath formulations, one (19% (w/v) pluronic+1% (w/v) NaCl) was chosen since it forms a complete gelled structure at a temperature of about 32° C (a little bit less that 37°C as a safety margin to avoid melting of the support bath in case of poor control of the bath temperature), and being completely liquid at 22°C.

We studied the rheological properties of this support bath to make sure that it meets some specific rheological features previously identified in the literature [58]. Indeed, it must present sufficient yield stress to firmly hold the printed bioink after deposition while maintaining a shear-thinning behavior, so it would not hinder the movement of the printing needle and rapid recovery to a solid state after printing. **The Pluronic support bath showed shear thinning viscosity and recovery properties throughout cyclic deformation**, similar to gelatin slurry FRESH bath [244, 354]. Although, gelatin slurry showed much lower stiffness than Pluronic support bath (~1000 Pa vs ~5000 Pa).

The self-healing behavior of Pluronic was demonstrated and linked to the temperature-controllable dynamic micellation [58]. The hydrophilic ethylene oxide and the hydrophobic propylene oxide give Pluronic an amphiphilic structure. Amphiphilic block copolymer molecules self-assemble into micelles (a packed chain of molecules) in aqueous solution. Micelle formation is temperature dependent and affects the degradation properties of the biomaterial: below a certain characteristic temperature known as the critical micelle temperature, both the ethylene and propylene oxide blocks are hydrated, and the PPO block becomes soluble. In addition to shear thinning and recovery, Pluronic presents a yield stress over 100 Pa, which is requested for bath support according to the previous publications [59].

As previously discussed, low viscous chitosan (2% w/v) shows good thermosensitivity. This thermosensitivity demonstrates the necessity of the warm bath to provide proper thermo-crosslinking during printing. Using the FRESH bath and taking advantage of the bioink's thermosensitivity increases resolution and decreases spreading. This is in accordance with previous literature data [296], and can be related to reduced spreading, adequate placement, and prevention of evaporation. **Hydrogels were printable at least up to 20 layers using the FRESH bath, with good cohesion, handability and relatively good correspondence to the theoretical CAD design**. **This improved resolution and shape fidelity resulted in boosted compressive modulus, which is important for handability and to mimic tissue mechanical properties**. [61]. This **low concentration of chitosan hydrogel (2% w/v) showed high viability of encapsulated cells after bioprinting**.

7.4 Advantages of chitosan thermosensitive hydrogels as bioinks

Chitosan hydrogels have many advantages, as mentioned in Chapter 2. They are biocompatible and biodegradable, making them particularly interesting in comparison to other hydrogels. Their biodegradaiton rate can be tuned by changing the DDA and MW. Alginate as a most commonly used bioink alone fails to ensure better cellular adhesion and functionality in comparison with chitosan, and researches propose either binding complementary side groups e.g., peptides or mixing with other biomaterials in a certain proportion increases the composite hydrogel cellular response [355]. Also, mammals do not produce enzymes that biodegrade alginate. For bioink which is containing cells, Demirtaş et al. showed that chitosan-BGP-hydroxyapatite hydrogel is superior over alginate- hydroxyapatite hydrogel in terms of cell proliferation and differentiation [194]. Alginate hydrogels lack the stability in physiological environment due to the competition with Ca ions that can be replaced with other ions.

Chitosan physical hydrogels generally have poor rigidity and mechanical strength, which limits its use for creating hard tissues [145]. In this work, the use of SHC+BGP as gelling agents instead of BGP only allows to drastically increase mechanical properties of chitosan hydrogel through physical crosslinking at 37°C while ensuring physiological osmolality [67, 68]. These novel gelling agents, discovered by Lerouge's lab, have similar pK_a as chitosan at room temperature [188]. For example, at room temperature, chitosan's NH_3^+ is screened by SHC. Chitosan's pk_a decreases as the temperature rises, causing SHC to react with NH_3^+ and release CO_2 and completely neutralize the chitosan chains. These enhanced mechanical properties partly explain the good bioprinting results obtained in this work. However due to their slow gelation, only the FRESH bioprinting allowed to reach satisfactory results.

Using FRESH bioprinting, we could print a strong structure of a thermosensitive chitosan bioink with good shape fidelity and resolution (narrow filaments without collapsing under the weight of the next layers) without use of additional toxic crosslinkers. We demonstrated that CH2% prepared with SHC +BGP as gelling agent is a good bioink and has the potential to be used for various tissue bioprinting applications using FRESH bioprinting.

Limitations of FRESH bioprinting with chitosan thermogel

However, **we are still far from ideal** and face some limitations as listed below:

1) The possible printed 3D structures are limited: when we later tried to print other 3D structures, we observed some severe limitation of the technique. Indeed, only limited types of 3D structure could be printed in which the printed filaments are far from each other such as cylindrical structure as presented in Chapter 5. When structures including filaments closer to each other are printed, it led to filaments displacement. In contrast, other teams have used FRESH technique with other bioinks to print complex 3D structure of various geometries from compact gridded structure to human cardiac ventricle model and tri-leaflet heart valve[54, 249, 356]. The problem and what we observed could be related to the bioink limitation due to the lack of instant thermogelation of the chitosan-based hydrogels or to the FRESH bath rheological properties as explained below:
    - First the rheological properties of the support bath are slightly different than gelatin slurry and might be less appropriate. As mentioned previously in Chapter 2 and observed in Chapter 5, the Pluronic bath that we used presents a **non-Newtonian behaviour and fits Herschel Bulkley fluid behaviour**, while the most common FRESH bath, gelatin slurry fits Bingham fluid behaviour. The

difference between the two is that, once reaching the Yield point, the shear stress becomes linearly proportional to strain rate in the Bingham fluid, while it presents shear thinning properties in the Herschel Blukley model. [354, 357], We are not sure which behavior is the best for support baths and further studies are required. The yield stress required for Pluronic support bath is around 150 Pa, while gelatin slurry' yield stress is minimum ~300 Pa [53]. Maintaining the gelatin slurry at room temperature (~22°C) preserves these rheological properties [244, 354], limiting its application since cells like body temperature rather than 22°C.

- Secondly, the slow gelation of chitosan may limit feasibility of printing complex and compact 3D structures. Gelation kinetic is quick (few seconds) in case of e.g., alginate hydrogels with $CaCl_2$, but chitosan hydrogels lack instant gelation and thermo-crosslinking occurs in few minutes.

2) It is important to have a good control of the FRESH bath temperature, since preliminary work showed that the bath tended to melt from the top during the printing due to bath cooling, which occurs in contact with ambient air, despite heating at 37°C from the bottom. This is one limitation of this work. This is why we chose a bath which gelation temperature is slightly below 37°C, as a safety margin.

3) Toxic effect of the support bath:
   The bioink itself must provide an excellent biocompatibility and cell viability, but also in FRESH bioprinting, the support bath plays an important role in cell survival. The physiological condition, e.g., temperature, pH and osmolality, the bath stiffness, viscosity, porosity, and removal procedure, could highly impact cell performance [358, 359]. In chapter 5, we showed good cell survival in simple structures like gridded structure, but when we studied cell survival in bigger structures with more volume of Pluronic bath, this led to significantly more cell mortality. Since longer time was required to remove the Pluronic after bioprinting. Table 10 summarizes the various conditions tested in order to assess the effect of Pluronic support bath on cell viability within the chitosan bioinks.

Table 10. Printability window in Pluronic FRESH bath.

Bioink	Cells	Bath	Bath volume	Pre-printing centrifuge	Printing and bath removal time	Incubation time	Fridge time	Additional Info.	Results
CH2%	MSCs	19%pluronic+1% NaCl	5ml	1 min 1500 rpm	<5 min	20 min	10 min	*5 layers were printed. *30 min in contact with bath/printing a filament	100% cell dead
CH2%	MSCs	19%pluronic+1% NaCl	1ml	1 min 1500 rpm	<5 min	_	5 min	*1 layer was printed *printing filament	~80% viability D1
CH2%-Gel2%	MSCs	19%pluronic+1% NaCl	1ml	1 min 1500 rpm	<5 min	_	5 min	*1 layer was printed *printing filament	~70% viability D1
CH2%	Fibroblast L292	19%pluronic+1% NaCl	2ml	1 min 1500 rpm	10-15 min	_	20 min	*2 layers gridded structure *Wash with PBS every 5 min/printing	most cells were dead D0

As shown in the Table 10, from the first experiment (first row), it was found that **long contact time with Pluronic affect cell survival negatively**. In this regard, to remove the Pluronic quickly to decrease the cells contact with the Pluronic, the samples were cooled down to 4° immediately after bioprinting. In addition, the Pluronic bath volume was decreased from 5 ml to 1 ml to ease the removal procedure and shorten the time in contact with Pluronic. Results indicate much better survival, around 70-80%. The still significant cell mortality might be due to the stiffness or viscosity of the Pluronic (G' ~ 5000 Pa). Afghah et al. reported that the Pluronic support bath with stiffness of ~ 500-1000 Pa prepared by 7.5-12.5% w/v Pluronic showed over 80% cell viability [58]. In our case, a much higher concentration of Pluronic was used (19%) which **presents high viscosity (high stiffness) which limit access to O_2 and nutrient to the cells encapsulated in chitosan hydrogel**. The Pluronic bath showed ~ 5000 Pa storage modulus. Gelatin microparticles slurry bath storage modulus is also around 500-1000 Pa [53]. To be noted that Pluronic has been used by other teams either as a support bath or bioink, and no toxicity has been reported [58].

Recommendations:

1. Since we are not sure that the inability of printing complex 3D structure is due to lack of chitosan instant gelation or Pluronic FRESH bath rheology, we propose to compare the rheological properties of Pluronic with gelatin slurry. This would allow us to better understand the limitation of our support bath and eventually optimize it. We could also try to print our chitosan bioink within gelatin slurry, even though this would not allow taking advantage of the thermogelation of chitosan since gelatin melts at 37°C. Moreover, printing chitosan-gelatin bioinks in gelatin slurry could be challenging. In addition, variability and production of microparticles with gelatin is challenging, while Pluronic is a synthetic hydrogel and highly reproducible as shown in Chapter 4.
2. Another recommendation is addition of nanoclay e.g., Laponite to Pluronic as a rheology modifier. It would allow us to decrease the Pluronic concentration (decrease viscosity) as well as decrease the support bath stiffness.
3. To solve the lack of instant gelation and to provide the feasibility of printing complex structures, one possible recommendation is to blend chitosan hydrogels with other biopolymers like alginate, making IPN or semi-IPN bioinks.

7.5 Chitosan thermogel as embedding hydrogels

Another potential use of chitosan thermogel in bioprinting is to use it as a matrix for embedding writing. This technique involves the deposition of 3D printed structures directly within a cell-laden, self-healing matrix which mechanically supports the printed structures. The potential of CH thermogel as a self-healing matrix has been also studied in the framework of this thesis but results are still preliminary and are not presented in this thesis. In brief, sacrificial writing into functional tissue (SWIFT) is an approach that can streamline the fabrication of biomimetic artificial tissues. To demonstrate that chitosan hydrogels are suitable as embedding hydrogels, vascular templates were 3D printed directly into them using Pluronic. Once the matrix materials are fully gelled, the sacrificial materials are removed, and we show that branched, perfusable networks can be embedded within these constructs (Figure 41). The evaluation of cell viability and function within these systems are in progress.

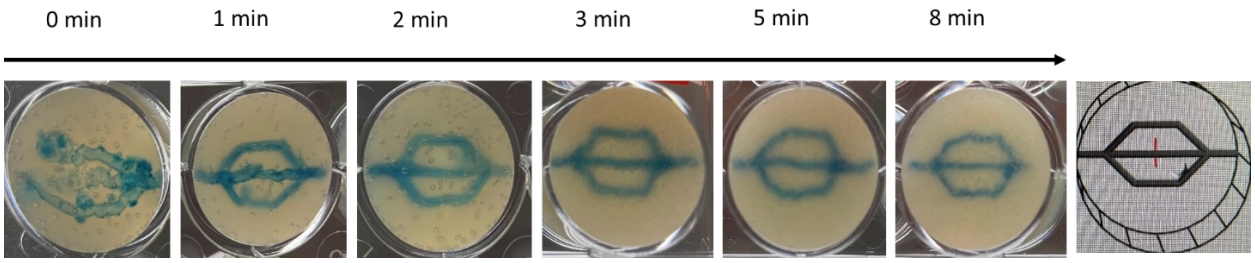

Figure 41. Illustration of printed perfusable network embedded within thermosensitive chitosan hydrogels and effect of time on the network's resolution and continuity.

Overall, this work demonstrates that **controlled gelation and gelation timeframe play a critical role for time- and temperature-dependent hydrogels, that must be taken into account**. This approach is promising in generating microstructures that mimic physiological tissues such as **vascularization within tissue-engineered constructs**.

7.6 Potential of injectable/printable chitosan thermogel for mineralized tissue engineering

As mentioned previously, our gelling agents allows creating injectable and printable chitosan hydrogels with drastically enhanced mechanical properties and cytocompatibility compared to conventional chitosan–BGP hydrogels [67, 68]. This opens the way toward many applications in tissue engineering. In particular, there is a large need for tissues such as bone and cartilage tissue regeneration, and their mineralized interface. CH hydrogels fill many of the requirement for such applications. In addition to those mentioned previously, chitosan hydrogels have been shown to induce formation of GAGs and promote the survival and growth of chondrocytes [67, 174-179]. However, chitosan hydrogels **lack inherent osteoconductivity and osteointegrativity with surrounding bone tissue**. **Osteoconductive and osteointegrative properties can be provided by the addition of bioceramics such as hydroxyapatite or bioactive glass** [198-200]. Bioactive glass was chosen here for its bioactivity, and faster osteoblast proliferation than hydroxyapatite [204]. Indeed, in combining with bioceramics e.g., bioactive glass (BG), chitosan-based scaffolds significantly enhance the osteoblasts growth [198-200].

Preliminary trials showed that the gelation of hydrogels could not be obtained with a high loading of BG particles. Dissolution of BG leads to fast ion release (an increase of pH), preventing hydrogel formation and adversely impacts the mechanical properties [210, 313]. This is in agreement with previous studies and is explained by a rapid release of Na^+ ions from BG particles in aqueous solutions [210, 311, 331, 336]. For

example, the addition of 2% w/v BG powder to thermosensitive chitosan-based hydrogel made of BGP gelling agent resulted in a hydrogel with a storage modulus (G') of only 9 Pa after 4 min at 37 °C [210]. An in-situ injectable thermosensitive chitosan-collagen-BGP hydrogel in combination with BG (0-2%w/v) was reported for bone tissue engineering with promoted bioactivity [210]. Later, by combining chitosan-gelatin-BGP with nano-BG, a thermosensitive hydrogel with enhanced elastic modulus and improved viscoelastic properties was developed but, mechanical properties are still far from ideal [209]. The hydrogel promoted proliferation of osteoblasts and angiogenesis gene expressions, resulting in bone regeneration after in vivo injection [211]. However, low BG concentration is used since higher BG concentration affects the mechanical property adversely meaning no proper gelation is taken place. Consequently, it negatively impacts the encapsulated cell survival in such basic hydrogels. The rapid release of ions and the fast pH increase in vitro explain why only very few work have been published about cell encapsulation and in vitro assays with BG particles together in one single hydrogel [211]. **For these reasons, it was not possible to create a bioglass-containing CH bioink for tissue bioprinting**. We however tried to overcome this issue to create an injectable hydrogel in which BG was concentrated in small microbeads instead of their homogenous distribution that would reduce the number of ions in the chitosan hydrogel and thus allow proper gelation, enhance the mechanical properties, and possibly increase the gel's compatibility for cell encapsulation.

Such hybrid hydrogels combine **several advantages** compared to chitosan hydrogels with homogenous distribution of BG: 1) They present drastically enhanced rigidity than homogeneous BG hydrogel. This suggests that, as expected, BG segregated in microbeads is less interfering with the physical gelation of chitosan hydrogels, probably due to the slower release of ions. 2) Microbeads can be prepared and frozen while waiting for their addition in the gelling agent, thus preventing partial dissolution and allowing long-term storage of the product for potential clinical applications. 3) The hybrid product is suitable for non-invasive injections through 18 G needles. 4) Some advantage was also observed in terms of osmolality and better cell survival compared to homogenous gel. 5) Osteoconductivity is an important factor for bioactive scaffolds and induces osteoblasts to form new bone [180]. Calcium and phosphate also concentrated over 7 days soaking in simulated body fluid, indicating nucleation of hydroxycarbonate apatite as reported by Moreira et al. [209, 210]. Similarly, Oudadesse et al. presented apatite layer formation on chitosan biopolymer surface after 7 days and good adhesion between the BG and chitosan, indicating potential of

BG-chitosan bioactivity in physiological environment [344]. Thus, our results suggest that BG-loaded microbeads are expected to form apatite in the body. However, some limitations were faced as listed below:

Limitations:

1. Hybrid hydrogels with BG microbeads showed secant modulus of ~13 kPa, which was significantly higher than hydrogels with homogenously distributed BG. Also much higher than previously reported studies [210]. But mechanical properties are still far from ideal bone and mineralized tissue [360]. Rigidity or Young modulus value is 450-650 kPa in deep zones of the articular cartilage (varied by age and sex) [361]. Rigidity or Young's modulus of bone should be range of 11-21 GPa for Cortical bone, longitudinal and 5-13 GPa for Cortical bone, transverse [362].
2. Microbeads injection was studied in two ways: 1) microbeads were injected alone; 2) microbeads were encapsulated within chitosan hydrogel and injected. There is the deformation or possible breakage of microbeads during injection when encapsulated within the hydrogel, adversely impacting mechanical properties and cell survival.
3. Another limitation of this work is type of cell line that was studied. We have studied fibroblast cell viability. We did not test our material with a cell line appropriate for bone and cartilage repair.

Recommendations and perspectives:

In the future, the following work would help better optimize and assess the potential of bioactive chitosan hydrogel

1. Still low concentration of BG was used (0-4% w/v). It would require further studies through, e.g., increasing BG concentrations.
2. Microbeads demonstrated the potential of freezing for long-term storage. But further characterization is needed to validate that freezing does not alter chemical or mechanical characterization.
3. It is suggested to characterize the biodegradation, and cytocompatibility with bone application cell lines e.g., osteocytes and MSCs.
4. In our work, in vitro studies were performed to assess osteoconductivity. Therefore, comprehensive osteoconductivity characterizations are suggested to justify their ability to form a biological bond with the surrounding living bone. For example, apatite formation should be studied in longer time than 7 days; another material for coating rather than gold (e.g., palladium) must be used in EDX to measure calcium/phosphate ratio; crystallization should be characterized using X-ray powder diffraction (XRD); biodegradation, in vitro and in vivo bone formation, and bonding to surrounding bones must be studied.
5. Although bioglass showed superiority over hydroxyapatite as discussed previously, it is not an ideal bioceramics for pH-dependent biomaterials such as chitosan-based hydrogels. Bioglass incorporation increases pH due to ion release, which influences chitosan hydrogel's mechanical properties adversely. In this regard, chitosan hydrogels can be incorporated with hydroxyapatite in order not to have ion release and consequent challenges like impaired gelation.

7.7 Conclusion

The general objective of this Ph.D. was to study and optimize the potential of thermosensitive chitosan-based hydrogels for extrusion-based bioprinting and injectable scaffold for articular tissue engineering. in addition, we proposed a new strategy to predict the printability of time- and temperature materials like thermosensitive chitosan-based hydrogels for any extrusion-based system. A comprehensive understanding of thermosensitive hydrogels rheology and their characterization methods provide an opportunity to take advantage of such promising hydrogels in bioprinting. Taking advantage of chitosan thermosensitivity, we bioprinted 20-layered structures using FRESH bioprinting technique. This work shows the potential of the thermosensitive chitosan-based hydrogels in various tissue bioprinting. The incorporation of cells into a BG-contained hydrogel recreates the in vivo environment of mineralized or bone tissue. Therefore, injectable bioactive cell-laden chitosan-based hydrogel could potentially be used as a bone filler and as a bioink to engineer mineralized tissue. The suggested strategy in this Ph.D. would open new doors toward engineering articular tissue. However, much works remains to be done for bioprinting bioactive tissues and organs which could be routinely used in the clinic.

7.8 Originality

In terms of the originality of the project, many new developments have been obtained throughout the project. We are the first to report a rheological method specifically adapted for time- and temperature-dependent materials.

In addition, we studied chitosan-based bioink in FRESH bioprinting as a new cytocompatible (gentle with encapsulated cells) and biodegradable bioink without use of any external toxic crosslinker. In fact, this work would take advantage of chitosan thermosensitivity and provide thermo-crosslinking to create a much stronger 3D bioprinted scaffold than in air printing. The strategy provided good adhesion of layers and integration to each other during bioprinting, which would open new windows toward studying promising hydrogels such as thermosensitive chitosan in bioprinting. To date, our thermosensitive chitosan hydrogel is the first pure chitosan bioink.

Our study is also the first cell-laden mineralized scaffold in which cell viability is preserved. The mineralized hydrogel studied in this Ph.D. showed potential clinical application. We hope this Ph.D. will open new horizons for personalized complex gradient implant generation.

7.9 Impact and Contribution

This project will help develop and optimize the 3D bioprinting technology in Canada. More specifically, it will help identify and optimize injectable and functional biomaterials suitable in 3D bioprinting to improve several diseases' treatment procedures. It will also enable the determination of the experimental factors that influence biomaterial's injectability, printability, cellular and biological behaviors as a 3D printed structure, either acellular with surface seeded cells or including cells encapsulated within the biomaterial. With or without cells, fabrication gradient structures could revolutionize the medical industry, in particular musculoskeletal joint prosthesis design and production, by providing an alternative to the conventional metal-polymer implant, at least for small articular tissue defects. This may provide a solution to the growing number of patients suffering from articular tissue degeneration.

References

[1] I. T. Ozbolat, "Bioprinting scale-up tissue and organ constructs for transplantation," *Trends in biotechnology,* vol. 33, no. 7, pp. 395-400, 2015.

[2] P. Lichte, H. Pape, T. Pufe, P. Kobbe, and H. Fischer, "Scaffolds for bone healing: concepts, materials and evidence," *Injury,* vol. 42, no. 6, pp. 569-573, 2011.

[3] B. Müller *et al.*, "Bio-mimetic hollow scaffolds for long bone replacement," in *Proc. of SPIE Vol*, 2009, vol. 7401, pp. 74010D-1.

[4] I. Donderwinkel, J. C. Van Hest, and N. R. Cameron, "Bio-inks for 3D bioprinting: recent advances and future prospects," *Polymer Chemistry,* vol. 8, no. 31, pp. 4451-4471, 2017.

[5] G. Filardo, E. Kon, A. Di Martino, M. Busacca, G. Altadonna, and M. Marcacci, "Treatment of knee osteochondritis dissecans with a cell-free biomimetic osteochondral scaffold: clinical and imaging evaluation at 2-year follow-up," *The American journal of sports medicine,* vol. 41, no. 8, pp. 1786-1793, 2013.

[6] H. Lee, T.-S. Jang, J. Song, H.-E. Kim, and H.-D. Jung, "The production of porous hydroxyapatite scaffolds with graded porosity by sequential freeze-casting," *Materials,* vol. 10, no. 4, p. 367, 2017.

[7] B. A. Harley, A. K. Lynn, Z. Wissner-Gross, W. Bonfield, I. V. Yannas, and L. J. Gibson, "Design of a multiphase osteochondral scaffold. II. Fabrication of a mineralized collagen–glycosaminoglycan scaffold," *Journal of biomedical materials research Part A,* vol. 92, no. 3, pp. 1066-1077, 2010.

[8] E. Kon *et al.*, "Orderly osteochondral regeneration in a sheep model using a novel nano-composite multilayered biomaterial," *Journal of orthopaedic research,* vol. 28, no. 1, pp. 116-124, 2010.

[9] S. Camarero-Espinosa, B. Rothen-Rutishauser, C. Weder, and E. J. Foster, "Directed cell growth in multi-zonal scaffolds for cartilage tissue engineering," *Biomaterials,* vol. 74, pp. 42-52, 2016.

[10] X. Miao and D. Sun, "Graded/gradient porous biomaterials," *Materials,* vol. 3, no. 1, pp. 26-47, 2009.

[11] E. Kon *et al.*, "A novel nano-composite multi-layered biomaterial for treatment of osteochondral lesions: technique note and an early stability pilot clinical trial," *Injury,* vol. 41, no. 7, pp. 693-701, 2010.

[12] W. Sun *et al.*, "The bioprinting roadmap," *Biofabrication,* vol. 12, no. 2, p. 022002, 2020.

[13] Y. Sun, Y. You, W. Jiang, B. Wang, Q. Wu, and K. Dai, "3D bioprinting dual-factor releasing and gradient-structured constructs ready to implant for anisotropic cartilage regeneration," *Science Advances,* vol. 6, no. 37, p. eaay1422, 2020.

[14] H.-B. Zhang, T.-L. Xing, R.-X. Yin, Y. Shi, S.-M. Yang, and W.-J. Zhang, "Three-dimensional bioprinting is not only about cell-laden structures," *Chinese Journal of Traumatology,* vol. 19, no. 4, pp. 187-192, 2016.

[15] C. Mandrycky, Z. Wang, K. Kim, and D.-H. Kim, "3D bioprinting for engineering complex tissues," *Biotechnology advances,* vol. 34, no. 4, pp. 422-434, 2016.

[16] L. Belk, N. Tellisi, H. Macdonald, A. Erdem, N. Ashammakhi, and I. Pountos, "Safety Considerations in 3D Bioprinting Using Mesenchymal Stromal Cells," *Frontiers in Bioengineering Biotechnology,* vol. 8, 2020.

[17] A. Atala and J. J. Yoo, *Essentials of 3D biofabrication and translation*. Academic Press, 2015.

[18] I. Matai, G. Kaur, A. Seyedsalehi, A. McClinton, and C. T. Laurencin, "Progress in 3D bioprinting technology for tissue/organ regenerative engineering," *Biomaterials,* vol. 226, p. 119536, 2020.

[19] A. Shavandi, S. Hosseini, O. V. Okoro, L. Nie, F. Eghbali Babadi, and F. Melchels, "3D bioprinting of lignocellulosic biomaterials," *Advanced Healthcare Materials,* vol. 9, no. 24, p. 2001472, 2020.
[20] S. V. Murphy and A. Atala, "3D bioprinting of tissues and organs," *Nature biotechnology,* vol. 32, no. 8, pp. 773-785, 2014.
[21] R. Abbel and E. R. Meinders, "Printing Technologies for Nanomaterials," *Nanomaterials for 2D and 3D Printing,* 2017.
[22] K. Hölzl, S. Lin, L. Tytgat, S. Van Vlierberghe, L. Gu, and A. Ovsianikov, "Bioink properties before, during and after 3D bioprinting," *Biofabrication,* vol. 8, no. 3, p. 032002, 2016.
[23] P. Kumar, S. Ebbens, and X. Zhao, "Inkjet printing of mammalian cells–Theory and applications," *Bioprinting,* p. e00157, 2021.
[24] Y.-J. Seol, H.-W. Kang, S. J. Lee, A. Atala, and J. J. Yoo, "Bioprinting technology and its applications," *European Journal of Cardio-Thoracic Surgery,* p. ezu148, 2014.
[25] J. Li, M. Chen, X. Fan, and H. Zhou, "Recent advances in bioprinting techniques: approaches, applications and future prospects," *Journal of translational medicine,* vol. 14, no. 1, p. 271, 2016.
[26] X. Li *et al.*, "Inkjet bioprinting of biomaterials," *Chemical Reviews,* vol. 120, no. 19, pp. 10793-10833, 2020.
[27] C. Dou, V. Perez, J. Qu, A. Tsin, B. Xu, and J. Li, "A State-of-the-Art Review of Laser-Assisted Bioprinting and its Future Research Trends," *ChemBioEng Reviews,* 2021.
[28] A. Patrascioiu, J. Fernández-Pradas, A. Palla-Papavlu, J. Morenza, and P. Serra, "Laser-generated liquid microjets: correlation between bubble dynamics and liquid ejection," *Microfluidics and nanofluidics,* vol. 16, no. 1-2, pp. 55-63, 2014.
[29] R. Devillard *et al.*, "Cell patterning by laser-assisted bioprinting," in *Methods in cell biology*, vol. 119: Elsevier, 2014, pp. 159-174.
[30] B. Guillotin *et al.*, "Laser assisted bioprinting of engineered tissue with high cell density and microscale organization," *Biomaterials,* vol. 31, no. 28, pp. 7250-7256, 2010.
[31] A. Ovsianikov *et al.*, "Laser printing of cells into 3D scaffolds," *Biofabrication,* vol. 2, no. 1, p. 014104, 2010.
[32] S. Catros *et al.*, "Laser-assisted bioprinting for creating on-demand patterns of human osteoprogenitor cells and nano-hydroxyapatite," *Biofabrication,* vol. 3, no. 2, p. 025001, 2011.
[33] B. Riggs *et al.*, "Matrix-assisted pulsed laser methods for biofabrication," *MRS bulletin,* vol. 36, no. 12, pp. 1043-1050, 2011.
[34] L. Koch, O. Brandt, A. Deiwick, and B. Chichkov, "Laser-assisted bioprinting at different wavelengths and pulse durations with a metal dynamic release layer: A parametric study," *International Journal of Bioprinting,* vol. 3, no. 1, 2017.
[35] R. D. Ventura, "An Overview of Laser-assisted Bioprinting (LAB) in Tissue Engineering Applications," *Medical Lasers Engineering, Basic Research, Clinical Application,* vol. 10, no. 2, pp. 76-81, 2021.
[36] C. Schmidleithner and D. M. Kalaskar, "Stereolithography," IntechOpen, 2018.
[37] F. P. Melchels, J. Feijen, and D. W. Grijpma, "A review on stereolithography and its applications in biomedical engineering," *Biomaterials,* vol. 31, no. 24, pp. 6121-6130, 2010.
[38] I. T. Ozbolat and M. Hospodiuk, "Current advances and future perspectives in extrusion-based bioprinting," *Biomaterials,* vol. 76, pp. 321-343, 2016.

[39] J. Emmermacher *et al.*, "Engineering considerations on extrusion-based bioprinting: interactions of material behavior, mechanical forces and cells in the printing needle," *Biofabrication,* vol. 12, no. 2, p. 025022, 2020.
[40] S. Kyle, Z. M. Jessop, A. Al-Sabah, and I. S. Whitaker, "'printability'of Candidate Biomaterials for Extrusion Based 3d Printing: State-of-the-art," *Advanced healthcare materials,* 2017.
[41] M. E. Hoque, Y. L. Chuan, and I. Pashby, "Extrusion based rapid prototyping technique: an advanced platform for tissue engineering scaffold fabrication," *Biopolymers,* vol. 97, no. 2, pp. 83-93, 2012.
[42] V. Mironov, R. P. Visconti, V. Kasyanov, G. Forgacs, C. J. Drake, and R. R. Markwald, "Organ printing: tissue spheroids as building blocks," *Biomaterials,* vol. 30, no. 12, pp. 2164-2174, 2009.
[43] A. N. Mehesz *et al.*, "Scalable robotic biofabrication of tissue spheroids," *Biofabrication,* vol. 3, no. 2, p. 025002, 2011.
[44] C. M. Owens, F. Marga, G. Forgacs, and C. M. Heesch, "Biofabrication and testing of a fully cellular nerve graft," *Biofabrication,* vol. 5, no. 4, p. 045007, 2013.
[45] R. Levato, J. Visser, J. A. Planell, E. Engel, J. Malda, and M. A. Mateos-Timoneda, "Biofabrication of tissue constructs by 3D bioprinting of cell-laden microcarriers," *Biofabrication,* vol. 6, no. 3, p. 035020, 2014.
[46] F. Pati *et al.*, "Printing three-dimensional tissue analogues with decellularized extracellular matrix bioink," *Nature communications,* vol. 5, p. 3935, 2014.
[47] A. B. Dababneh and I. T. Ozbolat, "Bioprinting technology: a current state-of-the-art review," *Journal of Manufacturing Science and Engineering,* vol. 136, no. 6, p. 061016, 2014.
[48] R. Suntornnond, E. Y. S. Tan, J. An, and C. K. Chua, "A mathematical model on the resolution of extrusion bioprinting for the development of new bioinks," *Materials,* vol. 9, no. 9, p. 756, 2016.
[49] H.-W. Kang, S. J. Lee, I. K. Ko, C. Kengla, J. J. Yoo, and A. Atala, "A 3D bioprinting system to produce human-scale tissue constructs with structural integrity," *Nature biotechnology,* vol. 34, no. 3, pp. 312-319, 2016.
[50] Q. Hu, B. Jiang, and H. Zhang, "Method for novel 3d bioprinting of gradient scaffold for osteochondral regeneration using a coaxial multi-nozzle and software," *Journal of Biomaterials Tissue Engineering,* vol. 9, no. 1, pp. 24-31, 2019.
[51] D. J. Shiwarski, A. R. Hudson, J. W. Tashman, and A. W. Feinberg, "Emergence of FRESH 3D printing as a platform for advanced tissue biofabrication," *APL bioengineering,* vol. 5, no. 1, p. 010904, 2021.
[52] F. Kreimendahl, C. Kniebs, A. M. Tavares Sobreiro, T. Schmitz-Rode, S. Jockenhoevel, and A. L. Thiebes, "FRESH bioprinting technology for tissue engineering–the influence of printing process and bioink composition on cell behavior and vascularization," *Journal of Applied Biomaterials Functional Materials,* vol. 19, p. 22808000211028808, 2021.
[53] T. J. Hinton *et al.*, "Three-dimensional printing of complex biological structures by freeform reversible embedding of suspended hydrogels," *Science advances,* vol. 1, no. 9, p. e1500758, 2015.
[54] A. Lee *et al.*, "3D bioprinting of collagen to rebuild components of the human heart," *Science,* vol. 365, no. 6452, pp. 482-487, 2019.
[55] A. McCormack, C. B. Highley, N. R. Leslie, and F. P. Melchels, "3D printing in suspension baths: keeping the promises of bioprinting afloat," *Trends in biotechnology,* vol. 38, no. 6, pp. 584-593, 2020.

[56] A. P. Haring *et al.*, "Process-and bio-inspired hydrogels for 3D bioprinting of soft free-standing neural and glial tissues," *Biofabrication,* vol. 11, no. 2, p. 025009, 2019.
[57] A. McCormack, C. B. Highley, N. R. Leslie, and F. P. Melchels, "3D printing in suspension baths: keeping the promises of bioprinting afloat," *Trends in biotechnology,* vol. 38, no. 6, pp. 584-593, 2020.
[58] F. Afghah, M. Altunbek, C. Dikyol, and B. Koc, "Preparation and characterization of nanoclay-hydrogel composite support-bath for bioprinting of complex structures," *Scientific reports,* vol. 10, no. 1, pp. 1-13, 2020.
[59] J. M. Townsend, E. C. Beck, S. H. Gehrke, C. J. Berkland, and M. S. Detamore, "Flow behavior prior to crosslinking: The need for precursor rheology for placement of hydrogels in medical applications and for 3D bioprinting," *Progress in polymer science,* vol. 91, pp. 126-140, 2019.
[60] T. Bhattacharjee *et al.*, "Writing in the granular gel medium," vol. 1, ed: Science Advances, 2015.
[61] J. Groll *et al.*, "A definition of bioinks and their distinction from biomaterial inks," *Biofabrication,* vol. 11, no. 1, p. 013001, 2018.
[62] J. Adhikari *et al.*, "Effects of processing parameters of 3D bioprinting on the cellular activity of bioinks," *Macromolecular Bioscience,* vol. 21, no. 1, p. 2000179, 2021.
[63] S. Ramasamy *et al.*, "Optimized construction of a full thickness human skin equivalent using 3D bioprinting and a PCL/collagen dermal scaffold," *Bioprinting,* vol. 21, p. e00123, 2021.
[64] J. Kundu, J. H. Shim, J. Jang, S. W. Kim, and D. W. Cho, "An additive manufacturing-based PCL–alginate–chondrocyte bioprinted scaffold for cartilage tissue engineering," *Journal of tissue engineering regenerative medicine,* vol. 9, no. 11, pp. 1286-1297, 2015.
[65] Y. J. Tan, K. F. Leong, J. An, K. S. Chian, X. Tan, and W. Y. Yeong, "Fabrication and in vitro analysis of tubular scaffolds by melt-drawing for esophageal tissue engineering," *Materials Letters,* vol. 159, pp. 424-427, 2015.
[66] J. P. Armstrong, M. Burke, B. M. Carter, S. A. Davis, and A. W. Perriman, "3D bioprinting using a templated porous bioink," *Advanced healthcare materials,* vol. 5, no. 14, pp. 1724-1730, 2016.
[67] E. Assaad, M. Maire, and S. Lerouge, "Injectable thermosensitive chitosan hydrogels with controlled gelation kinetics and enhanced mechanical resistance," *Carbohydrate polymers,* vol. 130, pp. 87-96, 2015.
[68] C. Ceccaldi, E. Assaad, E. Hui, M. Buccionyte, A. Adoungotchodo, and S. Lerouge, "Optimization of injectable thermosensitive scaffolds with enhanced mechanical properties for cell therapy," *Macromolecular bioscience,* vol. 17, no. 6, p. 1600435, 2017.
[69] B. Choi *et al.*, "Introduction to in situ forming hydrogels for biomedical applications," in *In-Situ Gelling Polymers*: Springer, 2015, pp. 5-35.
[70] A. L. Rutz, K. E. Hyland, A. E. Jakus, W. R. Burghardt, and R. N. Shah, "A multimaterial bioink method for 3D printing tunable, cell-compatible hydrogels," *Advanced Materials,* vol. 27, no. 9, pp. 1607-1614, 2015.
[71] X. Cui, K. Breitenkamp, M. Finn, M. Lotz, and D. D. D'Lima, "Direct human cartilage repair using three-dimensional bioprinting technology," *Tissue Engineering Part A,* vol. 18, no. 11-12, pp. 1304-1312, 2012.
[72] X. Cui, K. Breitenkamp, M. Lotz, and D. D'Lima, "Synergistic action of fibroblast growth factor-2 and transforming growth factor-beta1 enhances bioprinted human neocartilage formation," *Biotechnology and bioengineering,* vol. 109, no. 9, pp. 2357-2368, 2012.

[73] T. Q. Huang, X. Qu, J. Liu, and S. Chen, "3D printing of biomimetic microstructures for cancer cell migration," *Biomedical microdevices,* vol. 16, no. 1, pp. 127-132, 2014.
[74] N. Paxton, W. Smolan, T. Böck, F. Melchels, J. Groll, and T. Jungst, "Proposal to assess printability of bioinks for extrusion-based bioprinting and evaluation of rheological properties governing bioprintability," *Biofabrication,* vol. 9, no. 4, p. 044107, 2017.
[75] A. Ribeiro *et al.*, "Assessing bioink shape fidelity to aid material development in 3D bioprinting," *Biofabrication,* vol. 10, no. 1, p. 014102, 2017.
[76] C. B. Hutson *et al.*, "Synthesis and characterization of tunable poly (ethylene glycol): gelatin methacrylate composite hydrogels," *Tissue Engineering Part A,* vol. 17, no. 13-14, pp. 1713-1723, 2011.
[77] K. Dubbin, A. Tabet, and S. C. Heilshorn, "Quantitative criteria to benchmark new and existing bio-inks for cell compatibility," *Biofabrication,* vol. 9, no. 4, p. 044102, 2017.
[78] X. Zhou *et al.*, "Improved Human Bone Marrow Mesenchymal Stem Cell Osteogenesis in 3D Bioprinted Tissue Scaffolds with Low Intensity Pulsed Ultrasound Stimulation," *Scientific Reports,* vol. 6, 2016.
[79] J. G. Sathish *et al.*, "Challenges and approaches for the development of safer immunomodulatory biologics," *Nature Reviews Drug Discovery,* vol. 12, no. 4, p. 306, 2013.
[80] V. H. M. Mouser *et al.*, "Development of a thermosensitive HAMA-containing bio-ink for the fabrication of composite cartilage repair constructs," *Biofabrication,* vol. 9, no. 1, p. 015026, 2017.
[81] K. S. Lim, J. H. Galarraga, X. Cui, G. C. Lindberg, J. A. Burdick, and T. B. Woodfield, "Fundamentals and applications of photo-cross-linking in bioprinting," *Chemical reviews,* vol. 120, no. 19, pp. 10662-10694, 2020.
[82] D. F. Duarte Campos *et al.*, "The stiffness and structure of three-dimensional printed hydrogels direct the differentiation of mesenchymal stromal cells toward adipogenic and osteogenic lineages," *Tissue Engineering Part A,* vol. 21, no. 3-4, pp. 740-756, 2014.
[83] G. Gao, T. Yonezawa, K. Hubbell, G. Dai, and X. Cui, "Inkjet-bioprinted acrylated peptides and PEG hydrogel with human mesenchymal stem cells promote robust bone and cartilage formation with minimal printhead clogging," *Biotechnology journal,* vol. 10, no. 10, pp. 1568-1577, 2015.
[84] G. Gao, A. F. Schilling, T. Yonezawa, J. Wang, G. Dai, and X. Cui, "Bioactive nanoparticles stimulate bone tissue formation in bioprinted three-dimensional scaffold and human mesenchymal stem cells," *Biotechnology journal,* vol. 9, no. 10, pp. 1304-1311, 2014.
[85] C. C. Chang, E. D. Boland, S. K. Williams, and J. B. Hoying, "Direct-write bioprinting three-dimensional biohybrid systems for future regenerative therapies," *Journal of Biomedical Materials Research Part B: Applied Biomaterials,* vol. 98, no. 1, pp. 160-170, 2011.
[86] D. B. Kolesky, R. L. Truby, A. Gladman, T. A. Busbee, K. A. Homan, and J. A. Lewis, "3D bioprinting of vascularized, heterogeneous cell-laden tissue constructs," *Advanced materials,* vol. 26, no. 19, pp. 3124-3130, 2014.
[87] W. Wu, A. DeConinck, and J. A. Lewis, "Omnidirectional printing of 3D microvascular networks," *Advanced materials,* vol. 23, no. 24, 2011.
[88] A. Skardal and A. Atala, "Biomaterials for integration with 3-D bioprinting," *Annals of biomedical engineering,* vol. 43, no. 3, pp. 730-746, 2015.
[89] N. E. Fedorovich *et al.*, "Evaluation of photocrosslinked lutrol hydrogel for tissue printing applications," *Biomacromolecules,* vol. 10, no. 7, pp. 1689-1696, 2009.

[90] M. Müller, J. Becher, M. Schnabelrauch, and M. Zenobi-Wong, "Nanostructured Pluronic hydrogels as bioinks for 3D bioprinting," *Biofabrication,* vol. 7, no. 3, p. 035006, 2015.
[91] S. Hong *et al.*, "3D printing of highly stretchable and tough hydrogels into complex, cellularized structures," *Advanced materials,* vol. 27, no. 27, pp. 4035-4040, 2015.
[92] S. Xin, O. M. Wyman, and D. L. Alge, "Assembly of PEG microgels into porous cell-instructive 3D scaffolds via thiol-ene click chemistry," *Advanced healthcare materials,* vol. 7, no. 11, p. 1800160, 2018.
[93] J. Zhu, "Bioactive modification of poly (ethylene glycol) hydrogels for tissue engineering," *Biomaterials,* vol. 31, no. 17, pp. 4639-4656, 2010.
[94] C. M. Homenick, G. de Silveira, H. Sheardown, and A. Adronov, "Pluronics as crosslinking agents for collagen: novel amphiphilic hydrogels," *Polymer International,* vol. 60, no. 3, pp. 458-465, 2011.
[95] N. E. Fedorovich, J. R. De Wijn, A. J. Verbout, J. Alblas, and W. J. Dhert, "Three-dimensional fiber deposition of cell-laden, viable, patterned constructs for bone tissue printing," *Tissue Engineering Part A,* vol. 14, no. 1, pp. 127-133, 2008.
[96] M. Di Biase, R. E. Saunders, N. Tirelli, and B. Derby, "Inkjet printing and cell seeding thermoreversible photocurable gel structures," *Soft Matter,* vol. 7, no. 6, pp. 2639-2646, 2011.
[97] W. Jia *et al.*, "Direct 3D bioprinting of perfusable vascular constructs using a blend bioink," *Biomaterials,* vol. 106, pp. 58-68, 2016.
[98] K. Y. Lee and D. J. Mooney, "Alginate: properties and biomedical applications," *Progress in polymer science,* vol. 37, no. 1, pp. 106-126, 2012.
[99] T. Jiang *et al.*, "Directing the self-assembly of tumour spheroids by bioprinting cellular heterogeneous models within alginate/gelatin hydrogels," *Scientific Reports,* vol. 7, no. 1, p. 4575, 2017.
[100] J. Park *et al.*, "Cell-laden 3D bioprinting hydrogel matrix depending on different compositions for soft tissue engineering: Characterization and evaluation," *Materials Science and Engineering: C,* vol. 71, pp. 678-684, 2017.
[101] L. J. Pourchet *et al.*, "Human Skin 3D Bioprinting Using Scaffold-Free Approach," *Advanced healthcare materials,* vol. 6, no. 4, 2017.
[102] A. Faulkner-Jones *et al.*, "Bioprinting of human pluripotent stem cells and their directed differentiation into hepatocyte-like cells for the generation of mini-livers in 3D," *Biofabrication,* vol. 7, no. 4, p. 044102, 2015.
[103] V. L. Workman, L. B. Tezera, P. T. Elkington, and S. N. Jayasinghe, "Controlled Generation of Microspheres Incorporating Extracellular Matrix Fibrils for Three-Dimensional Cell Culture," *Advanced functional materials,* vol. 24, no. 18, pp. 2648-2657, 2014.
[104] K. Christensen, C. Xu, W. Chai, Z. Zhang, J. Fu, and Y. Huang, "Freeform inkjet printing of cellular structures with bifurcations," *Biotechnology and bioengineering,* vol. 112, no. 5, pp. 1047-1055, 2015.
[105] C. Xu, W. Chai, Y. Huang, and R. R. Markwald, "Scaffold-free inkjet printing of three-dimensional zigzag cellular tubes," *Biotechnology and bioengineering,* vol. 109, no. 12, pp. 3152-3160, 2012.
[106] J. I. Rodríguez-Dévora, B. Zhang, D. Reyna, Z.-d. Shi, and T. Xu, "High throughput miniature drug-screening platform using bioprinting technology," *Biofabrication,* vol. 4, no. 3, p. 035001, 2012.

[107] L. Gasperini, D. Maniglio, A. Motta, and C. Migliaresi, "An electrohydrodynamic bioprinter for alginate hydrogels containing living cells," *Tissue Engineering Part C: Methods,* vol. 21, no. 2, pp. 123-132, 2014.
[108] L. Gasperini, D. Maniglio, and C. Migliaresi, "Microencapsulation of cells in alginate through an electrohydrodynamic process," *Journal of Bioactive and Compatible Polymers,* vol. 28, no. 5, pp. 413-425, 2013.
[109] H. Gudapati, J. Yan, Y. Huang, and D. B. Chrisey, "Alginate gelation-induced cell death during laser-assisted cell printing," *Biofabrication,* vol. 6, no. 3, p. 035022, 2014.
[110] R. Xiong, Z. Zhang, W. Chai, Y. Huang, and D. B. Chrisey, "Freeform drop-on-demand laser printing of 3D alginate and cellular constructs," *Biofabrication,* vol. 7, no. 4, p. 045011, 2015.
[111] J. Yan, Y. Huang, and D. B. Chrisey, "Laser-assisted printing of alginate long tubes and annular constructs," *Biofabrication,* vol. 5, no. 1, p. 015002, 2012.
[112] K. Markstedt, A. Mantas, I. Tournier, H. c. Martínez Ávila, D. Hägg, and P. Gatenholm, "3D bioprinting human chondrocytes with nanocellulose–alginate bioink for cartilage tissue engineering applications," *Biomacromolecules,* vol. 16, no. 5, pp. 1489-1496, 2015.
[113] H. Li, Y. J. Tan, K. F. Leong, and L. Li, "3D bioprinting of highly thixotropic alginate/methylcellulose hydrogel with strong interface bonding," *ACS applied materials & interfaces,* 2017.
[114] X.-F. Wang, P.-J. Lu, Y. Song, Y.-C. Sun, Y.-G. Wang, and Y. Wang, "Nano hydroxyapatite particles promote osteogenesis in a three-dimensional bio-printing construct consisting of alginate/gelatin/hASCs," *RSC Advances,* vol. 6, no. 8, pp. 6832-6842, 2016.
[115] P. Shi, T. Y. S. Edgar, W. Y. Yeong, and A. Laude, "Hybrid three-dimensional (3D) bioprinting of retina equivalent for ocular research," *International Journal of Bioprinting,* vol. 3, no. 2, pp. 138-146, 2017.
[116] S. T. Bendtsen, S. P. Quinnell, and M. Wei, "Development of a novel alginate-polyvinyl alcohol-hydroxyapatite hydrogel for 3D bioprinting bone tissue engineered scaffolds," *Journal of Biomedical Materials Research Part A,* vol. 105, no. 5, pp. 1457-1468, 2017.
[117] A. Skardal, J. Zhang, L. McCoard, X. Xu, S. Oottamasathien, and G. D. Prestwich, "Photocrosslinkable hyaluronan-gelatin hydrogels for two-step bioprinting," *Tissue Engineering Part A,* vol. 16, no. 8, pp. 2675-2685, 2010.
[118] A. Skardal, J. Zhang, L. McCoard, S. Oottamasathien, and G. D. Prestwich, "Dynamically crosslinked gold nanoparticle–hyaluronan hydrogels," *Advanced Materials,* vol. 22, no. 42, pp. 4736-4740, 2010.
[119] A. Skardal, J. Zhang, and G. D. Prestwich, "Bioprinting vessel-like constructs using hyaluronan hydrogels crosslinked with tetrahedral polyethylene glycol tetracrylates," *Biomaterials,* vol. 31, no. 24, pp. 6173-6181, 2010.
[120] M. Gruene *et al.*, "Laser printing of three-dimensional multicellular arrays for studies of cell–cell and cell–environment interactions," *Tissue Engineering Part C: Methods,* vol. 17, no. 10, pp. 973-982, 2011.
[121] L. Ouyang, C. B. Highley, W. Sun, and J. A. Burdick, "A Generalizable Strategy for the 3D Bioprinting of Hydrogels from Nonviscous Photo-crosslinkable Inks," *Advanced Materials,* vol. 29, no. 8, 2017.
[122] M. T. Poldervaart *et al.*, "3D bioprinting of methacrylated hyaluronic acid (MeHA) hydrogel with intrinsic osteogenicity," *PloS one,* vol. 12, no. 6, p. e0177628, 2017.

[123] W. Zhu *et al.*, "Direct 3D bioprinting of prevascularized tissue constructs with complex microarchitecture," *Biomaterials,* vol. 124, pp. 106-115, 2017.
[124] N. Law *et al.*, "Characterisation of Hyaluronic Acid Methylcellulose Hydrogels for 3D Bioprinting," *Journal of the Mechanical Behavior of Biomedical Materials,* 2017.
[125] C. J. Ferris, K. J. Gilmore, S. Beirne, D. McCallum, and G. G. Wallace, "Bio-ink for on-demand printing of living cells," *Biomaterials Science,* vol. 1, no. 2, pp. 224-230, 2013.
[126] R. Lozano *et al.*, "3D printing of layered brain-like structures using peptide modified gellan gum substrates," *Biomaterials,* vol. 67, pp. 264-273, 2015.
[127] F. P. Melchels, W. J. Dhert, D. W. Hutmacher, and J. Malda, "Development and characterisation of a new bioink for additive tissue manufacturing," *Journal of Materials Chemistry B,* vol. 2, no. 16, pp. 2282-2289, 2014.
[128] S. Moon *et al.*, "Layer by layer three-dimensional tissue epitaxy by cell-laden hydrogel droplets," *Tissue Engineering Part C: Methods,* vol. 16, no. 1, pp. 157-166, 2009.
[129] M. Yanez, J. Rincon, A. Dones, C. De Maria, R. Gonzales, and T. Boland, "In vivo assessment of printed microvasculature in a bilayer skin graft to treat full-thickness wounds," *Tissue Engineering Part A,* vol. 21, no. 1-2, pp. 224-233, 2014.
[130] A. Skardal *et al.*, "Bioprinted Amniotic Fluid-Derived Stem Cells Accelerate Healing of Large Skin Wounds," *Stem cells translational medicine,* vol. 1, no. 11, pp. 792-802, 2012.
[131] S. Rhee, J. L. Puetzer, B. N. Mason, C. A. Reinhart-King, and L. J. Bonassar, "3D bioprinting of spatially heterogeneous collagen constructs for cartilage tissue engineering," *ACS Biomaterials Science & Engineering,* vol. 2, no. 10, pp. 1800-1805, 2016.
[132] K. C. Hribar, K. Meggs, J. Liu, W. Zhu, X. Qu, and S. Chen, "Three-dimensional direct cell patterning in collagen hydrogels with near-infrared femtosecond laser," *Scientific reports,* vol. 5, 2015.
[133] J. Y. Park *et al.*, "A comparative study on collagen type I and hyaluronic acid dependent cell behavior for osteochondral tissue bioprinting," *Biofabrication,* vol. 6, no. 3, p. 035004, 2014.
[134] X. Ren, F. Wang, C. Chen, X. Gong, L. Yin, and L. Yang, "Engineering zonal cartilage through bioprinting collagen type II hydrogel constructs with biomimetic chondrocyte density gradient," *BMC Musculoskeletal Disorders,* vol. 17, no. 1, p. 301, 2016.
[135] E. A. Roth, T. Xu, M. Das, C. Gregory, J. J. Hickman, and T. Boland, "Inkjet printing for high-throughput cell patterning," *Biomaterials,* vol. 25, no. 17, pp. 3707-3715, 2004.
[136] W. L. Ng, W. Y. Yeong, and M. W. Naing, "Development of Polyelectrolyte Chitosan-gelatin Hydrogels for Skin Bioprinting," *Procedia CIRP,* vol. 49, pp. 105-112, 2016.
[137] W. L. Ng, W. Y. Yeong, and M. W. Naing, "Potential of bioprinted films for skin tissue engineering," presented at the Proc. of the Intl. Conf. on Progress in Additive Manufacturing, 2014.
[138] J. Huang *et al.*, "BMSCs-laden gelatin/sodium alginate/carboxymethyl chitosan hydrogel for 3D bioprinting," *RSC Advances,* vol. 6, no. 110, pp. 108423-108430, 2016.
[139] W. E. Müller *et al.*, "A new printable and durable N, O-carboxymethyl chitosan–Ca 2+–polyphosphate complex with morphogenetic activity," *Journal of Materials Chemistry B,* vol. 3, no. 8, pp. 1722-1730, 2015.
[140] P. Maturavongsadit, L. K. Narayanan, P. Chansoria, R. Shirwaiker, and S. R. Benhabbour, "Cell-Laden Nanocellulose/Chitosan-Based Bioinks for 3D Bioprinting and Enhanced Osteogenic Cell Differentiation," *ACS Applied Bio Materials,* vol. 4, no. 3, pp. 2342-2353, 2021.

[141] J. Ku *et al.*, "Cell-laden thermosensitive chitosan hydrogel bioinks for 3D bioprinting applications," *Applied Sciences,* vol. 10, no. 7, p. 2455, 2020.
[142] S.-H. Park, C. S. Jung, and B.-H. Min, "Advances in three-dimensional bioprinting for hard tissue engineering," *Tissue Engineering and Regenerative Medicine,* vol. 13, no. 6, pp. 622-635, 2016.
[143] R. F. Pereira, C. C. Barrias, P. L. Granja, and P. J. Bartolo, "Advanced biofabrication strategies for skin regeneration and repair," *Nanomedicine,* vol. 8, no. 4, pp. 603-621, 2013.
[144] V. B. Morris, S. Nimbalkar, M. Younesi, P. McClellan, and O. Akkus, "Mechanical properties, cytocompatibility and manufacturability of chitosan: PEGDA hybrid-gel scaffolds by stereolithography," *Annals of biomedical engineering,* vol. 45, no. 1, pp. 286-296, 2017.
[145] Y. He *et al.*, "Characterization and application of carboxymethyl chitosan-based bioink in cartilage tissue engineering," *Journal of Nanomaterials,* vol. 2020, 2020.
[146] N. R. Schiele, D. B. Chrisey, and D. T. Corr, "Gelatin-based laser direct-write technique for the precise spatial patterning of cells," *Tissue Engineering Part C: Methods,* vol. 17, no. 3, pp. 289-298, 2010.
[147] N. A. Raof, N. R. Schiele, Y. Xie, D. B. Chrisey, and D. T. Corr, "The maintenance of pluripotency following laser direct-write of mouse embryonic stem cells," *Biomaterials,* vol. 32, no. 7, pp. 1802-1808, 2011.
[148] W. Xu *et al.*, "Rapid prototyping three-dimensional cell/gelatin/fibrinogen constructs for medical regeneration," *Journal of bioactive and compatible polymers,* vol. 22, no. 4, pp. 363-377, 2007.
[149] T. Boland *et al.*, "Drop-on-demand printing of cells and materials for designer tissue constructs," *Materials Science and Engineering: C,* vol. 27, no. 3, pp. 372-376, 2007.
[150] W. Schuurman *et al.*, "Gelatin-methacrylamide hydrogels as potential biomaterials for fabrication of tissue-engineered cartilage constructs," *Macromolecular bioscience,* vol. 13, no. 5, pp. 551-561, 2013.
[151] V. H. Mouser, F. P. Melchels, J. Visser, W. J. Dhert, D. Gawlitta, and J. Malda, "Yield stress determines bioprintability of hydrogels based on gelatin-methacryloyl and gellan gum for cartilage bioprinting," *Biofabrication,* vol. 8, no. 3, p. 035003, 2016.
[152] C. Colosi *et al.*, "Microfluidic Bioprinting of Heterogeneous 3D Tissue Constructs Using Low-Viscosity Bioink," *Advanced Materials,* vol. 28, no. 4, pp. 677-684, 2016.
[153] L. E. Bertassoni *et al.*, "Direct-write bioprinting of cell-laden methacrylated gelatin hydrogels," *Biofabrication,* vol. 6, no. 2, p. 024105, 2014.
[154] D. B. Kolesky, K. A. Homan, M. A. Skylar-Scott, and J. A. Lewis, "Three-dimensional bioprinting of thick vascularized tissues," *Proceedings of the National Academy of Sciences,* vol. 113, no. 12, pp. 3179-3184, 2016.
[155] S. A. Irvine *et al.*, "Printing cell-laden gelatin constructs by free-form fabrication and enzymatic protein crosslinking," *Biomedical microdevices,* vol. 17, no. 1, p. 16, 2015.
[156] J. Huang *et al.*, "3D printed gelatin/hydroxyapatite scaffolds for stem cell chondrogenic differentiation and articular cartilage repair," *Biomaterials Science,* vol. 9, no. 7, pp. 2620-2630, 2021.
[157] L. Koch *et al.*, "Laser printing of skin cells and human stem cells," *Tissue Engineering Part C: Methods,* vol. 16, no. 5, pp. 847-854, 2009.

[158] A. Blaeser *et al.*, "Biofabrication under fluorocarbon: a novel freeform fabrication technique to generate high aspect ratio tissue-engineered constructs," *BioResearch open access,* vol. 2, no. 5, pp. 374-384, 2013.
[159] Y. Fang *et al.*, "Rapid generation of multiplexed cell cocultures using acoustic droplet ejection followed by aqueous two-phase exclusion patterning," *Tissue Engineering Part C: Methods,* vol. 18, no. 9, pp. 647-657, 2012.
[160] L. Pescosolido *et al.*, "Hyaluronic acid and dextran-based semi-IPN hydrogels as biomaterials for bioprinting," *Biomacromolecules,* vol. 12, no. 5, pp. 1831-1838, 2011.
[161] V. K. Lee, A. M. Lanzi, H. Ngo, S.-S. Yoo, P. A. Vincent, and G. Dai, "Generation of multi-scale vascular network system within 3D hydrogel using 3D bio-printing technology," *Cellular and molecular bioengineering,* vol. 7, no. 3, pp. 460-472, 2014.
[162] J. Snyder *et al.*, "Bioprinting cell-laden matrigel for radioprotection study of liver by pro-drug conversion in a dual-tissue microfluidic chip," *Biofabrication,* vol. 3, no. 3, p. 034112, 2011.
[163] N. E. Fedorovich, H. M. Wijnberg, W. J. Dhert, and J. Alblas, "Distinct tissue formation by heterogeneous printing of osteo-and endothelial progenitor cells," *Tissue Engineering Part A,* vol. 17, no. 15-16, pp. 2113-2121, 2011.
[164] M. T. Poldervaart *et al.*, "Prolonged presence of VEGF promotes vascularization in 3D bioprinted scaffolds with defined architecture," *Journal of controlled release,* vol. 184, pp. 58-66, 2014.
[165] N. R. Schiele *et al.*, "Laser direct writing of combinatorial libraries of idealized cellular constructs: biomedical applications," *Applied Surface Science,* vol. 255, no. 10, pp. 5444-5447, 2009.
[166] L. Ouyang, C. B. Highley, C. B. Rodell, W. Sun, and J. A. Burdick, "3D printing of shear-thinning hyaluronic acid hydrogels with secondary cross-linking," *ACS Biomaterials Science & Engineering,* vol. 2, no. 10, pp. 1743-1751, 2016.
[167] B. Duan, E. Kapetanovic, L. A. Hockaday, and J. T. Butcher, "Three-dimensional printed trileaflet valve conduits using biological hydrogels and human valve interstitial cells," *Acta biomaterialia,* vol. 10, no. 5, pp. 1836-1846, 2014.
[168] A. Bayrak *et al.*, "Human immune responses to porcine xenogeneic matrices and their extracellular matrix constituents in vitro," *Biomaterials,* vol. 31, no. 14, pp. 3793-3803, 2010.
[169] S. Yeleswarapu, S. Chameettachal, A. K. Bera, and F. Pati, "Tissue-specific bioink from xenogeneic sources for 3D bioprinting of tissue constructs," *Xenotransplantation Comprehensive Study,* 2019.
[170] S. V. Murphy, A. Skardal, and A. Atala, "Evaluation of hydrogels for bio-printing applications," *Journal of Biomedical Materials Research Part A,* vol. 101, no. 1, pp. 272-284, 2013.
[171] H. Ong and K. K. Kolli, "Assessing Perfusion Using 3D Bioprinting," in *3D Printing Applications in Cardiovascular Medicine*: Elsevier, 2018, pp. 211-226.
[172] F. P. Melchels, M. A. Domingos, T. J. Klein, J. Malda, P. J. Bartolo, and D. W. Hutmacher, "Additive manufacturing of tissues and organs," *Progress in Polymer Science,* vol. 37, no. 8, pp. 1079-1104, 2012.
[173] Y. Loo, A. Lakshmanan, M. Ni, L. L. Toh, S. Wang, and C. A. Hauser, "Peptide bioink: self-assembling nanofibrous scaffolds for three-dimensional organotypic cultures," *Nano letters,* vol. 15, no. 10, pp. 6919-6925, 2015.
[174] H. R. Avilez, D. C. Casadiego, A. V. Avila, O. P. Perez, and J. Almodovar, "Production of chitosan coatings on metal and ceramic biomaterials," in *Chitosan Based Biomaterials Volume 1*: Elsevier, 2017, pp. 255-293.

[175] J. Berretta, J. Bumgardner, and J. Jennings, "Lyophilized chitosan sponges," in *Chitosan Based Biomaterials Volume 1*: Elsevier, 2017, pp. 239-253.
[176] J. Radhakrishnan, A. Subramanian, U. M. Krishnan, and S. Sethuraman, "Injectable and 3D bioprinted polysaccharide hydrogels: from cartilage to osteochondral tissue engineering," *Biomacromolecules,* vol. 18, no. 1, pp. 1-26, 2017.
[177] H. Park, B. Choi, J. Hu, and M. Lee, "Injectable chitosan hyaluronic acid hydrogels for cartilage tissue engineering," *Acta biomaterialia,* vol. 9, no. 1, pp. 4779-4786, 2013.
[178] B. Choi *et al.*, "Covalently conjugated transforming growth factor-β1 in modular chitosan hydrogels for the effective treatment of articular cartilage defects," *Biomaterials science,* vol. 3, no. 5, pp. 742-752, 2015.
[179] Y. Zhu, Y. Wan, J. Zhang, D. Yin, and W. Cheng, "Manufacture of layered collagen/chitosan-polycaprolactone scaffolds with biomimetic microarchitecture," *Colloids and Surfaces B: Biointerfaces,* vol. 113, pp. 352-360, 2014.
[180] J. Yang, Y. S. Zhang, K. Yue, and A. Khademhosseini, "Cell-laden hydrogels for osteochondral and cartilage tissue engineering," *Acta biomaterialia,* vol. 57, pp. 1-25, 2017.
[181] J. Radhakrishnan, A. Subramanian, U. M. Krishnan, and S. Sethuraman, "Injectable and 3D bioprinted polysaccharide hydrogels: from cartilage to osteochondral tissue engineering," *Biomacromolecules,* vol. 18, no. 1, pp. 1-26, 2016.
[182] C. Arakawa, R. Ng, S. Tan, S. Kim, B. Wu, and M. Lee, "Photopolymerizable chitosan–collagen hydrogels for bone tissue engineering," *Journal of tissue engineering and regenerative medicine,* vol. 11, no. 1, pp. 164-174, 2017.
[183] R. A. Muzzarelli, M. El Mehtedi, C. Bottegoni, A. Aquili, and A. Gigante, "Genipin-crosslinked chitosan gels and scaffolds for tissue engineering and regeneration of cartilage and bone," *Marine drugs,* vol. 13, no. 12, pp. 7314-7338, 2015.
[184] W. L. Ng, W. Y. Yeong, and M. W. Naing, "Polyelectrolyte gelatin-chitosan hydrogel optimized for 3D bioprinting in skin tissue engineering," *International Journal of Bioprinting,* vol. 2, no. 1, 2016.
[185] R. Riva, H. Ragelle, A. des Rieux, N. Duhem, C. Jérôme, and V. Préat, "Chitosan and chitosan derivatives in drug delivery and tissue engineering," in *Chitosan for biomaterials II*: Springer, 2011, pp. 19-44.
[186] A. Chenite *et al.*, "Novel injectable neutral solutions of chitosan form biodegradable gels in situ," *Biomaterials,* vol. 21, no. 21, pp. 2155-2161, 2000.
[187] A. Chenite, M. Buschmann, D. Wang, C. Chaput, and N. Kandani, "Rheological characterisation of thermogelling chitosan/glycerol-phosphate solutions," *Carbohydrate polymers,* vol. 46, no. 1, pp. 39-47, 2001.
[188] M. Lavertu, D. Filion, and M. D. Buschmann, "Heat-induced transfer of protons from chitosan to glycerol phosphate produces chitosan precipitation and gelation," *Biomacromolecules,* vol. 9, no. 2, pp. 640-650, 2008.
[189] T. Irimia *et al.*, "Chitosan-based in situ gels for ocular delivery of therapeutics: A state-of-the-art review," *Marine drugs,* vol. 16, no. 10, p. 373, 2018.
[190] S. Saravanan, S. Vimalraj, P. Thanikaivelan, S. Banudevi, and G. Manivasagam, "A review on injectable chitosan/beta glycerophosphate hydrogels for bone tissue regeneration," *International journal of biological macromolecules,* vol. 121, pp. 38-54, 2019.

[191] H. Y. Zhou, L. J. Jiang, P. P. Cao, J. B. Li, and X. G. Chen, "Glycerophosphate-based chitosan thermosensitive hydrogels and their biomedical applications," *Carbohydrate polymers,* vol. 117, pp. 524-536, 2015.
[192] L. Wang and J. P. Stegemann, "Thermogelling chitosan and collagen composite hydrogels initiated with β-glycerophosphate for bone tissue engineering," *Biomaterials,* vol. 31, no. 14, pp. 3976-3985, 2010.
[193] Z. Huang, R. Yue, H. Chan, and C. Choy, "Effect of processing on the positive temperature coefficient of resistivity in lead metaplumbate/polyethylene composites," *Polymer composites,* vol. 19, no. 6, pp. 781-786, 1998.
[194] T. T. Demirtaş, G. Irmak, and M. Gümüşderelioğlu, "A bioprintable form of chitosan hydrogel for bone tissue engineering," *Biofabrication,* vol. 9, no. 3, p. 035003, 2017.
[195] C. Ceccaldi, E. Assaad, E. Hui, M. Buccionyte, A. Adoungotchodo, and S. Lerouge, "Optimization of injectable thermosensitive scaffolds with enhanced mechanical properties for cell therapy," *Macromolecular bioscience,* vol. 17, no. 6, 2017.
[196] L. Liu, X. Tang, Y. Wang, and S. Guo, "Smart gelation of chitosan solution in the presence of NaHCO3 for injectable drug delivery system," *International journal of pharmaceutics,* vol. 414, no. 1-2, pp. 6-15, 2011.
[197] J. Cho, M.-C. Heuzey, A. Bégin, and P. J. Carreau, "Physical gelation of chitosan in the presence of β-glycerophosphate: the effect of temperature," *Biomacromolecules,* vol. 6, no. 6, pp. 3267-3275, 2005.
[198] W. Thein-Han and R. Misra, "Biomimetic chitosan–nanohydroxyapatite composite scaffolds for bone tissue engineering," *Acta biomaterialia,* vol. 5, no. 4, pp. 1182-1197, 2009.
[199] S. H. Teng, E. J. Lee, B. H. Yoon, D. S. Shin, H. E. Kim, and J. S. Oh, "Chitosan/nanohydroxyapatite composite membranes via dynamic filtration for guided bone regeneration," *Journal of Biomedical Materials Research Part A,* vol. 88, no. 3, pp. 569-580, 2009.
[200] C. Xianmiao, L. Yubao, Z. Yi, Z. Li, L. Jidong, and W. Huanan, "Properties and in vitro biological evaluation of nano-hydroxyapatite/chitosan membranes for bone guided regeneration," *Materials Science and Engineering: C,* vol. 29, no. 1, pp. 29-35, 2009.
[201] M. Rahimnejad, R. Raziyehsadat, R. Rezvaninejad, and R. França, "Biomaterials in bone and mineralized tissue engineering using 3D printing and bioprinting technologies," *Biomedical Physics Engineering Express,* 2021.
[202] L. L. Hench, "Biomaterials: a forecast for the future," *Biomaterials,* vol. 19, no. 16, pp. 1419-1423, 1998.
[203] L. L. Hench, "The story of Bioglass®," *Journal of Materials Science: Materials in Medicine,* vol. 17, no. 11, pp. 967-978, 2006.
[204] K. Rezwan, Q. Chen, J. J. Blaker, and A. R. Boccaccini, "Biodegradable and bioactive porous polymer/inorganic composite scaffolds for bone tissue engineering," *Biomaterials,* vol. 27, no. 18, pp. 3413-3431, 2006.
[205] A. Ressler, J. Ródenas-Rochina, M. Ivanković, H. Ivanković, A. Rogina, and G. G. Ferrer, "Injectable chitosan-hydroxyapatite hydrogels promote the osteogenic differentiation of mesenchymal stem cells," *Carbohydrate polymers,* vol. 197, pp. 469-477, 2018.
[206] T. Albrektsson and C. Johansson, "Osteoinduction, osteoconduction and osseointegration," *European spine journal,* vol. 10, no. 2, pp. S96-S101, 2001.

[207] Y.-J. Seol *et al.*, "Chitosan sponges as tissue engineering scaffolds for bone formation," *Biotechnology letters,* vol. 26, no. 13, pp. 1037-1041, 2004.
[208] J. Mota *et al.*, "Chitosan/bioactive glass nanoparticle composite membranes for periodontal regeneration," *Acta biomaterialia,* vol. 8, no. 11, pp. 4173-4180, 2012.
[209] C. D. Moreira, S. M. Carvalho, R. G. Sousa, H. S. Mansur, M. M. J. M. C. Pereira, and Physics, "Nanostructured chitosan/gelatin/bioactive glass in situ forming hydrogel composites as a potential injectable matrix for bone tissue engineering," *Materials Chemistry Physics,* vol. 218, pp. 304-316, 2018.
[210] C. D. Moreira, S. M. Carvalho, H. S. Mansur, M. M. J. M. S. Pereira, and E. C, "Thermogelling chitosan–collagen–bioactive glass nanoparticle hybrids as potential injectable systems for tissue engineering," *Materials Science Engineering: C,* vol. 58, pp. 1207-1216, 2016.
[211] C. D. Moreira *et al.*, "Injectable chitosan/gelatin/bioactive glass nanocomposite hydrogels for potential bone regeneration: In vitro and in vivo analyses," *International journal of biological macromolecules,* vol. 132, pp. 811-821, 2019.
[212] S. Naghieh and D. Chen, "Printability–a key issue in extrusion-based bioprinting," *Journal of Pharmaceutical Analysis,* 2021.
[213] L. Ouyang, R. Yao, Y. Zhao, and W. Sun, "Effect of bioink properties on printability and cell viability for 3D bioplotting of embryonic stem cells," *Biofabrication,* vol. 8, no. 3, p. 035020, 2016.
[214] B. Webb and B. J. Doyle, "Parameter optimization for 3D bioprinting of hydrogels," *Bioprinting,* vol. 8, pp. 8-12, 2017.
[215] M. Di Giuseppe *et al.*, "Mechanical behaviour of alginate-gelatin hydrogels for 3D bioprinting," *Journal of the mechanical behavior of biomedical materials,* vol. 79, pp. 150-157, 2018.
[216] A. C. Daly, S. E. Critchley, E. M. Rencsok, and D. J. Kelly, "A comparison of different bioinks for 3D bioprinting of fibrocartilage and hyaline cartilage," *Biofabrication,* vol. 8, no. 4, p. 045002, 2016.
[217] K. Kang, L. Hockaday, and J. Butcher, "Quantitative optimization of solid freeform deposition of aqueous hydrogels," *Biofabrication,* vol. 5, no. 3, p. 035001, 2013.
[218] K. D. Roehm and S. V. Madihally, "Bioprinted chitosan-gelatin thermosensitive hydrogels using an inexpensive 3D printer," *Biofabrication,* vol. 10, no. 1, p. 015002, 2017.
[219] J. Göhl, K. Markstedt, A. Mark, K. Håkansson, P. Gatenholm, and F. Edelvik, "Simulations of 3D bioprinting: predicting bioprintability of nanofibrillar inks," *Biofabrication,* vol. 10, no. 3, p. 034105, 2018.
[220] G. Ahn *et al.*, "Precise stacking of decellularized extracellular matrix based 3D cell-laden constructs by a 3D cell printing system equipped with heating modules," *Scientific reports,* vol. 7, no. 1, pp. 1-11, 2017.
[221] M. Hospodiuk, M. Dey, D. Sosnoski, and I. T. Ozbolat, "The bioink: A comprehensive review on bioprintable materials," *Biotechnology advances,* vol. 35, no. 2, pp. 217-239, 2017.
[222] J. Malda *et al.*, "25th anniversary article: engineering hydrogels for biofabrication," *Advanced materials,* vol. 25, no. 36, pp. 5011-5028, 2013.
[223] A. Blaeser, D. F. Duarte Campos, U. Puster, W. Richtering, M. M. Stevens, and H. Fischer, "Controlling shear stress in 3D bioprinting is a key factor to balance printing resolution and stem cell integrity," *Advanced healthcare materials,* vol. 5, no. 3, pp. 326-333, 2016.
[224] A. Y. Malkin and A. I. Isayev, *Rheology: concepts, methods, and applications*. Elsevier, 2017.

[225] H. Suo, J. Zhang, M. Xu, and L. Wang, "Low-temperature 3D printing of collagen and chitosan composite for tissue engineering," *Materials Science Engineering: C,* vol. 123, p. 111963, 2021.
[226] T. Hu *et al.*, "3D-printable supramolecular hydrogels with shear-thinning property: fabricating strength tunable bioink via dual crosslinking," *Bioactive materials,* vol. 5, no. 4, pp. 808-818, 2020.
[227] F. P. Melchels *et al.*, "Hydrogel-based reinforcement of 3D bioprinted constructs," *Biofabrication,* vol. 8, no. 3, p. 035004, 2016.
[228] C. Khatiwala, R. LAW, B. SHEPHERD, S. DORFMAN, and M. CSETE, "3D cell bioprinting for regenerative medicine research and therapies," *Gene Therapy and Regulation,* vol. 7, no. 01, p. 1230004, 2012.
[229] M. Chopin-Doroteo, E. A. Mandujano-Tinoco, and E. Krötzsch, "Tailoring of the rheological properties of bioinks to improve bioprinting and bioassembly for tissue replacement," *Biochimica et Biophysica Acta (BBA)-General Subjects,* p. 129782, 2020.
[230] R. Chang, J. Nam, and W. Sun, "Effects of dispensing pressure and nozzle diameter on cell survival from solid freeform fabrication–based direct cell writing," *Tissue Engineering Part A,* vol. 14, no. 1, pp. 41-48, 2008.
[231] K. Nair *et al.*, "Characterization of cell viability during bioprinting processes," *Biotechnology Journal: Healthcare Nutrition Technology,* vol. 4, no. 8, pp. 1168-1177, 2009.
[232] R. Busch *et al.*, "Regulation of the endothelial apelin/APJ system by hemodynamic fluid flow," *Cellular signalling,* vol. 27, no. 7, pp. 1286-1296, 2015.
[233] S. Connolly, K. McGourty, and D. Newport, "The in vitro inertial positions and viability of cells in suspension under different in vivo flow conditions," *Scientific reports,* vol. 10, no. 1, pp. 1-13, 2020.
[234] J. M. Dealy and K. F. Wissbrun, *Melt rheology and its role in plastics processing: theory and applications*. Springer Science & Business Media, 2012.
[235] A. Z. Nelson, K. S. Schweizer, B. M. Rauzan, R. G. Nuzzo, J. Vermant, and R. H. Ewoldt, "Designing and transforming yield-stress fluids," *Current Opinion in Solid State Materials Science,* vol. 23, no. 5, p. 100758, 2019.
[236] Z. Zhang *et al.*, "Evaluation of bioink printability for bioprinting applications," *Applied Physics Reviews,* vol. 5, no. 4, p. 041304, 2018.
[237] A. K. Grosskopf, R. L. Truby, H. Kim, A. Perazzo, J. A. Lewis, and H. A. Stone, "Viscoplastic matrix materials for embedded 3D printing," *ACS applied materials interfaces,* vol. 10, no. 27, pp. 23353-23361, 2018.
[238] M. E. Cooke and D. H. Rosenzweig, "The rheology of direct and suspended extrusion bioprinting," *APL bioengineering,* vol. 5, no. 1, p. 011502, 2021.
[239] P. Datta, A. Barui, Y. Wu, V. Ozbolat, K. K. Moncal, and I. T. Ozbolat, "Essential steps in bioprinting: From pre-to post-bioprinting," *Biotechnology advances,* vol. 36, no. 5, pp. 1481-1504, 2018.
[240] M. Chopin-Doroteo, E. A. Mandujano-Tinoco, and E. Krötzsch, "Tailoring of the rheological properties of bioinks to improve bioprinting and bioassembly for tissue replacement," *Biochimica et Biophysica Acta -General Subjects,* vol. 1865, no. 2, p. 129782, 2021.
[241] A. Schwab, R. Levato, M. D'Este, S. Piluso, D. Eglin, and J. Malda, "Printability and shape fidelity of bioinks in 3D bioprinting," *Chemical reviews,* vol. 120, no. 19, pp. 11028-11055, 2020.
[242] J. H. Chung *et al.*, "Bio-ink properties and printability for extrusion printing living cells," *Biomaterials Science,* vol. 1, no. 7, pp. 763-773, 2013.

[243] A. Z. Nelson, B. Kundukad, W. K. Wong, S. A. Khan, and P. S. Doyle, "Embedded droplet printing in yield-stress fluids," *Proceedings of the National Academy of Sciences,* vol. 117, no. 11, pp. 5671-5679, 2020.

[244] J. J. Senior, M. E. Cooke, L. M. Grover, and A. M. Smith, "Fabrication of complex hydrogel structures using suspended layer additive manufacturing (SLAM)," *Advanced Functional Materials,* vol. 29, no. 49, p. 1904845, 2019.

[245] A. M. Compaan, K. Song, and Y. Huang, "Gellan fluid gel as a versatile support bath material for fluid extrusion bioprinting," *ACS applied materials & interfaces,* vol. 11, no. 6, pp. 5714-5726, 2019.

[246] C. S. O'Bryan *et al.*, "Self-assembled micro-organogels for 3D printing silicone structures," *Science advances MRS bulletin,* vol. 3, no. 5, p. e1602800, 2017.

[247] Y. Jin, W. Chai, and Y. Huang, "Printability study of hydrogel solution extrusion in nanoclay yield-stress bath during printing-then-gelation biofabrication," *Materials Science Engineering: C,* vol. 80, pp. 313-325, 2017.

[248] C. S. O'Bryan *et al.*, "Three-dimensional printing with sacrificial materials for soft matter manufacturing," *MRS bulletin,* vol. 42, no. 8, pp. 571-577, 2017.

[249] E. Mirdamadi, J. W. Tashman, D. J. Shiwarski, R. N. Palchesko, and A. W. Feinberg, "FRESH 3D bioprinting a full-size model of the human heart," *ACS Biomaterials Science Engineering,* vol. 6, no. 11, pp. 6453-6459, 2020.

[250] L. Ning *et al.*, "Embedded 3D Bioprinting of Gelatin Methacryloyl-Based Constructs with Highly Tunable Structural Fidelity," *ACS Applied Materials & Interfaces,* vol. 12, no. 40, pp. 44563-44577, 2020.

[251] T. J. Hinton, A. Hudson, K. Pusch, A. Lee, and A. W. Feinberg, "3D printing PDMS elastomer in a hydrophilic support bath via freeform reversible embedding," *ACS biomaterials science & engineering,* vol. 2, no. 10, pp. 1781-1786, 2016.

[252] Y. Jin, A. Compaan, W. Chai, and Y. Huang, "Functional nanoclay suspension for printing-then-solidification of liquid materials," *ACS Applied Materials Interfaces,* vol. 9, no. 23, pp. 20057-20066, 2017.

[253] H. Ding and R. C. Chang, "Printability study of bioprinted tubular structures using liquid hydrogel precursors in a support bath," *Applied Sciences,* vol. 8, no. 3, p. 403, 2018.

[254] S. Jatav and Y. M. Joshi, "Phase behavior of aqueous suspension of laponite: New insights with microscopic evidence," *Langmuir,* vol. 33, no. 9, pp. 2370-2377, 2017.

[255] A. Ferdows, A. Mine, D. Caner, and K. Bahattin, "Preparation and characterization of nanoclay-hydrogel composite support-bath for bioprinting of complex structures," *Scientific Reports,* vol. 10, no. 1, 2020.

[256] A. Basu, A. Saha, C. Goodman, R. T. Shafranek, and A. Nelson, "Catalytically initiated gel-in-gel printing of composite hydrogels," *ACS applied materials & interfaces,* vol. 9, no. 46, pp. 40898-40904, 2017.

[257] M. Rocca, A. Fragasso, W. Liu, M. A. Heinrich, and Y. S. Zhang, "Embedded multimaterial extrusion bioprinting," *SLAS TECHNOLOGY: Translating Life Sciences Innovation,* vol. 23, no. 2, pp. 154-163, 2018.

[258] S. M. Hull *et al.*, "3D Bioprinting using UNIversal Orthogonal Network (UNION) Bioinks," *Advanced Functional Materials,* p. 2007983, 2020.

[259] R. Bayaniahangar, S. B. Ahangar, Z. Zhang, B. P. Lee, and J. M. Pearce, "3-D printed soft magnetic helical coil actuators of iron oxide embedded polydimethylsiloxane," *Sensors and Actuators B: Chemical,* vol. 326, p. 128781, 2021.
[260] J. Groll *et al.*, "A definition of bioinks and their distinction from biomaterial inks," *Biofabrication,* vol. 11, no. 1, p. 013001, 2018.
[261] T. D. Jones, "Extrusion Based Bioprinting: An In Vitro Model for Dental Pulp Tissue Engineering," 2018.
[262] L. Hsu and X. Jiang, "'Living'Inks for 3D Bioprinting," *Trends in biotechnology,* 2019.
[263] A. Panwar and L. P. Tan, "Current status of bioinks for micro-extrusion-based 3D bioprinting," *Molecules,* vol. 21, no. 6, p. 685, 2016.
[264] D. Chimene, K. K. Lennox, R. R. Kaunas, and A. K. Gaharwar, "Advanced bioinks for 3D printing: a materials science perspective," *Annals of biomedical engineering,* vol. 44, no. 6, pp. 2090-2102, 2016.
[265] T. Gao *et al.*, "Optimization of gelatin–alginate composite bioink printability using rheological parameters: A systematic approach," *Biofabrication,* vol. 10, no. 3, p. 034106, 2018.
[266] M. Yao, Y. Chen, J. Zhang, F. Gao, S. Ma, and F. Guan, "Chitosan-based thermosensitive composite hydrogel enhances the therapeutic efficacy of human umbilical cord MSC in TBI rat model," *Materials Today Chemistry,* vol. 14, p. 100192, 2019.
[267] H. Xu *et al.*, "Enhanced cutaneous wound healing by functional injectable thermo-sensitive chitosan-based hydrogel encapsulated human umbilical cord-mesenchymal stem cells," *International journal of biological macromolecules,* vol. 137, pp. 433-441, 2019.
[268] A. Monette, C. Ceccaldi, E. Assaad, S. Lerouge, and R. Lapointe, "Chitosan thermogels for local expansion and delivery of tumor-specific T lymphocytes towards enhanced cancer immunotherapies," *Biomaterials,* vol. 75, pp. 237-249, 2016.
[269] J. Dealy and K. Wissbrun, "Melt rheology and its role in plastics processing: Theory and applications," ed: New York, Van Nostrand Reinhold, 1990.
[270] M. Kesti, P. Fisch, M. Pensalfini, E. Mazza, and M. Zenobi-Wong, "Guidelines for standardization of bioprinting: a systematic study of process parameters and their effect on bioprinted structures," *BioNanoMaterials,* vol. 17, no. 3-4, pp. 193-204, 2016.
[271] M. Guvendiren, H. D. Lu, and J. A. Burdick, "Shear-thinning hydrogels for biomedical applications," *Soft matter,* vol. 8, no. 2, pp. 260-272, 2012.
[272] G. Gillispie *et al.*, "Assessment methodologies for extrusion-based bioink printability," *Biofabrication,* vol. 12, no. 2, p. 022003, 2020.
[273] H. H. Winter and F. Chambon, "Analysis of linear viscoelasticity of a crosslinking polymer at the gel point," *Journal of rheology,* vol. 30, no. 2, pp. 367-382, 1986.
[274] C. Tonda-Turo *et al.*, "Photocurable chitosan as bioink for cellularized therapies towards personalized scaffold architecture," *Bioprinting,* vol. 18, p. e00082, 2020.
[275] Y. Alinejad, A. Adoungotchodo, E. Hui, F. Zehtabi, and S. Lerouge, "An injectable chitosan/chondroitin sulfate hydrogel with tunable mechanical properties for cell therapy/tissue engineering," *International journal of biological macromolecules,* vol. 113, pp. 132-141, 2018.
[276] J. Cho, M.-C. Heuzey, A. Bégin, and P. J. Carreau, "Chitosan and glycerophosphate concentration dependence of solution behaviour and gel point using small amplitude oscillatory rheometry," *Food Hydrocolloids,* vol. 20, no. 6, pp. 936-945, 2006.

[277] B. A. Aguado, W. Mulyasasmita, J. Su, K. J. Lampe, and S. C. Heilshorn, "Improving viability of stem cells during syringe needle flow through the design of hydrogel cell carriers," *Tissue Engineering Part A,* vol. 18, no. 7-8, pp. 806-815, 2011.
[278] A. A. Foster, L. M. Marquardt, and S. C. Heilshorn, "The diverse roles of hydrogel mechanics in injectable stem cell transplantation," *Current opinion in chemical engineering,* vol. 15, pp. 15-23, 2017.
[279] S. V. Murphy and A. Atala, "3D bioprinting of tissues and organs," *Nature biotechnology,* vol. 32, no. 8, p. 773, 2014.
[280] N.-C. Cheng, W.-J. Lin, T.-Y. Ling, and T.-H. Young, "Sustained release of adipose-derived stem cells by thermosensitive chitosan/gelatin hydrogel for therapeutic angiogenesis," *Acta biomaterialia,* vol. 51, pp. 258-267, 2017.
[281] Q. Tang *et al.*, "Thermosensitive chitosan-based hydrogels releasing stromal cell derived factor-1 alpha recruit MSC for corneal epithelium regeneration," *Acta biomaterialia,* vol. 61, pp. 101-113, 2017.
[282] Q. Dang *et al.*, "Fabrication and evaluation of thermosensitive chitosan/collagen/α, β-glycerophosphate hydrogels for tissue regeneration," *Carbohydrate polymers,* vol. 167, pp. 145-157, 2017.
[283] H. Li, S. Liu, and L. Lin, "Rheological study on 3D printability of alginate hydrogel and effect of graphene oxide," *Int J Bioprinting,* vol. 2, no. 2, pp. 54-66, 2016.
[284] A. Asti and L. Gioglio, "Natural and synthetic biodegradable polymers: different scaffolds for cell expansion and tissue formation," *The International journal of artificial organs,* vol. 37, no. 3, pp. 187-205, 2014.
[285] M. Rahimnejad, T. Labonté-Dupuis, N. R. Demarquette, and S. Lerouge, "A rheological approach to assess the printability of thermosensitive chitosan-based biomaterial inks," *Biomedical Materials,* vol. 16, no. 1, p. 015003, 2020.
[286] M. Taghizadeh *et al.*, "Chitosan-based inks for 3D printing and bioprinting," *Green Chemistry,* vol. 24, no. 1, pp. 62-101, 2022.
[287] E. Mitsoulis, S. Abdali, and N. Markatos, "Flow simulation of herschel-bulkley fluids through extrusion dies," *The Canadian Journal of Chemical Engineering,* vol. 71, no. 1, pp. 147-160, 1993.
[288] Y. Jin, A. Compaan, W. Chai, and Y. Huang, "Functional nanoclay suspension for printing-then-solidification of liquid materials," *ACS applied materials & interfaces,* vol. 9, no. 23, pp. 20057-20066, 2017.
[289] J. Jiang *et al.*, "The effect of physiologically relevant additives on the rheological properties of concentrated Pluronic copolymer gels," *Polymer,* vol. 49, no. 16, pp. 3561-3567, 2008.
[290] J. J. Y. Tan, C. P. Lee, and M. Hashimoto, "Preheating of gelatin improves its printability with transglutaminase in direct ink writing 3D printing," *International Journal of Bioprinting,* vol. 6, no. 4, 2020.
[291] M. Cidade, D. Ramos, J. Santos, H. Carrelo, N. Calero, and J. Borges, "Injectable hydrogels based on pluronic/water systems filled with alginate microparticles for biomedical applications," *Materials,* vol. 12, no. 7, p. 1083, 2019.
[292] H. Geng, H. Song, J. Qi, and D. Cui, "Sustained release of VEGF from PLGA nanoparticles embedded thermo-sensitive hydrogel in full-thickness porcine bladder acellular matrix," *Nanoscale research letters,* vol. 6, no. 1, pp. 1-8, 2011.

[293] B. Shriky *et al.*, "Pluronic F127 thermosensitive injectable smart hydrogels for controlled drug delivery system development," *Journal of colloid interface science,* vol. 565, pp. 119-130, 2020.
[294] C. C. Hopkins and J. R. de Bruyn, "Gelation and long-time relaxation of aqueous solutions of Pluronic F127," *Journal of Rheology,* vol. 63, no. 1, pp. 191-201, 2019.
[295] J. Jiang *et al.*, "The effect of physiologically relevant additives on the rheological properties of concentrated Pluronic copolymer gels," *Polymer*

vol. 49, no. 16, pp. 3561-3567, 2008.
[296] D. C. Corbett, E. Olszewski, and K. Stevens, "A FRESH take on resolution in 3D bioprinting," *Trends in biotechnology,* vol. 37, no. 11, pp. 1153-1155, 2019.
[297] J. Ku *et al.*, "Cell-laden thermosensitive chitosan hydrogel bioinks for 3D bioprinting applications," vol. 10, no. 7, p. 2455, 2020.
[298] S. Han, C. M. Kim, S. Jin, and T. Y. Kim, "Study of the process-induced cell damage in forced extrusion bioprinting," *Biofabrication,* vol. 13, no. 3, p. 035048, 2021.
[299] S. Boularaoui, G. Al Hussein, K. A. Khan, N. Christoforou, and C. Stefanini, "An overview of extrusion-based bioprinting with a focus on induced shear stress and its effect on cell viability," *Bioprinting,* p. e00093, 2020.
[300] A. Adoungotchodo, L. Epure, F. Mwale, and S. Lerouge, "Chitosan-based hydrogels supplemented with gelatine and Link N enhance extracellular matrix deposition by encapsulated cells in a degenerative intervertebral disc environment," *European cells materials,* vol. 40, pp. 471-484, 2021.
[301] F. K. Touani *et al.*, "Pharmacological preconditioning improves the viability and proangiogenic paracrine function of hydrogel-encapsulated mesenchymal stromal cells," *Stem cells international,* vol. 2021, 2021.
[302] G. Morello, A. Polini, F. Scalera, R. Rizzo, G. Gigli, and F. J. P. Gervaso, "Preparation and Characterization of Salt-Mediated Injectable Thermosensitive Chitosan/Pectin Hydrogels for Cell Embedding and Culturing," vol. 13, no. 16, p. 2674, 2021.
[303] A. Stanzione *et al.*, "Thermosensitive chitosan-based hydrogels supporting motor neuron-like NSC-34 cell differentiation," *Biomaterials Science,* vol. 9, no. 22, pp. 7492-7503, 2021.
[304] E. Assaad, M. Maire, and S. Lerouge, "Injectable thermosensitive chitosan hydrogels with controlled gelation kinetics and enhanced mechanical resistance," *Carbohydrate polymers,* vol. 130, pp. 87-96, 2015.
[305] A. L. Rutz, P. L. Lewis, and R. N. Shah, "Toward next-generation bioinks: tuning material properties pre-and post-printing to optimize cell viability," *MRS Bulletin,* vol. 42, no. 8, pp. 563-570, 2017.
[306] P. Maturavongsadit, L. K. Narayanan, P. Chansoria, R. Shirwaiker, and S. R. J. A. A. B. M. Benhabbour, "Cell-Laden Nanocellulose/Chitosan-Based Bioinks for 3D Bioprinting and Enhanced Osteogenic Cell Differentiation," vol. 4, no. 3, pp. 2342-2353, 2021.
[307] S. K. L. Levengood and M. J. J. o. M. C. B. Zhang, "Chitosan-based scaffolds for bone tissue engineering," *Journal of Materials Chemistry B,* vol. 2, no. 21, pp. 3161-3184, 2014.
[308] R. LogithKumar, A. KeshavNarayan, S. Dhivya, A. Chawla, S. Saravanan, and N. J. C. p. Selvamurugan, "A review of chitosan and its derivatives in bone tissue engineering," *Carbohydrate polymers,* vol. 151, pp. 172-188, 2016.

[309] S. Saravanan, R. Leena, and N. J. I. j. o. b. m. Selvamurugan, "Chitosan based biocomposite scaffolds for bone tissue engineering," *International journal of biological macromolecules,* vol. 93, pp. 1354-1365, 2016.
[310] D.-A. Kim, J.-H. Lee, S.-K. Jun, H.-W. Kim, M. Eltohamy, and H.-H. Lee, "Sol–gel-derived bioactive glass nanoparticle-incorporated glass ionomer cement with or without chitosan for enhanced mechanical and biomineralization properties," *Dental Materials,* vol. 33, no. 7, pp. 805-817, 2017.
[311] L. L. J. B. Hench, "Biomaterials: a forecast for the future," vol. 19, no. 16, pp. 1419-1423, 1998.
[312] L. L. J. J. o. M. S. M. i. M. Hench, "The story of Bioglass®," vol. 17, no. 11, pp. 967-978, 2006.
[313] S. Jebahi *et al.*, "Effect of pH and ionic exchange on the reactivity of bioglass/chitosan composites used as a bone graft substitute," *Int. J. Chem. Mol. Nucl. Mater. Metall. Eng,* vol. 7, pp. 159-164, 2013.
[314] P. Baldwin, D. J. Li, D. A. Auston, H. S. Mir, R. S. Yoon, and K. J. J. J. o. o. t. Koval, "Autograft, allograft, and bone graft substitutes: clinical evidence and indications for use in the setting of orthopaedic trauma surgery," *Journal of orthopaedic trauma,* vol. 33, no. 4, pp. 203-213, 2019.
[315] G. Fernandez de Grado *et al.*, "Bone substitutes: a review of their characteristics, clinical use, and perspectives for large bone defects management," vol. 9, p. 2041731418776819, 2018.
[316] T. Winkler, F. Sass, G. Duda, K. J. B. Schmidt-Bleek, and j. research, "A review of biomaterials in bone defect healing, remaining shortcomings and future opportunities for bone tissue engineering: The unsolved challenge," vol. 7, no. 3, pp. 232-243, 2018.
[317] I. El-Sherbiny and M. Yacoub, "Hydrogel scaffolds for tissue engineering: progress and challenges. 2013: 38," *Global Cardiology Science and Practice,* no. 3, 2013.
[318] M. Liu *et al.*, "Injectable hydrogels for cartilage and bone tissue engineering," *Bone research,* vol. 5, no. 1, pp. 1-20, 2017.
[319] S. H. Park *et al.*, "BMP2-modified injectable hydrogel for osteogenic differentiation of human periodontal ligament stem cells," *Scientific reports,* vol. 7, no. 1, pp. 1-15, 2017.
[320] K. Lavanya, S. V. Chandran, K. Balagangadharan, N. J. M. S. Selvamurugan, and E. C, "Temperature- and pH-responsive chitosan-based injectable hydrogels for bone tissue engineering," *Materials Science,* p. 110862, 2020.
[321] G. Ma *et al.*, "Injectable hydrogels based on chitosan derivative/polyethylene glycol dimethacrylate/N, N-dimethylacrylamide as bone tissue engineering matrix," *Carbohydrate Polymers,* vol. 79, no. 3, pp. 620-627, 2010.
[322] K. Ding, Y. L. Zhang, Z. Yang, and J. Z. Xu, "A promising injectable scaffold: The biocompatibility and effect on osteogenic differentiation of mesenchymal stem cells," *Biotechnology and bioprocess engineering,* vol. 18, no. 1, pp. 155-163, 2013.
[323] A. J. Engler, S. Sen, H. L. Sweeney, and D. E. J. C. Discher, "Matrix elasticity directs stem cell lineage specification," *Cell,* vol. 126, no. 4, pp. 677-689, 2006.
[324] H. Sun, F. Zhu, Q. Hu, and P. H. J. B. Krebsbach, "Controlling stem cell-mediated bone regeneration through tailored mechanical properties of collagen scaffolds," *Biomaterials,* vol. 35, no. 4, pp. 1176-1184, 2014.
[325] J. K. Leach, J. J. A. b. s. Whitehead, and engineering, "Materials-directed differentiation of mesenchymal stem cells for tissue engineering and regeneration," *ACS biomaterials science,* vol. 4, no. 4, pp. 1115-1127, 2017.

[326] Y. Han, Q. Zeng, H. Li, and J. J. A. b. Chang, "The calcium silicate/alginate composite: preparation and evaluation of its behavior as bioactive injectable hydrogels," *Acta biomaterialia,* vol. 9, no. 11, pp. 9107-9117, 2013.
[327] G. C. Ingavle *et al.*, "Injectable mineralized microsphere-loaded composite hydrogels for bone repair in a sheep bone defect model," *Biomaterials,* vol. 197, pp. 119-128, 2019.
[328] S. Nosouhian, M. Razavi, N. Jafari-Pozve, and M. Rismanchian, "Comparative evaluation of hydroxyapatite and nano-bioglass in two forms of conventional micro-and nano-particles in repairing bone defects (an animal study)," *Indian Journal of Dental Research,* vol. 26, no. 4, p. 366, 2015.
[329] S. Mistry, D. Kundu, S. Datta, and D. Basu, "Effects of bioactive glass, hydroxyapatite and bioactive glass–hydroxyapatite composite graft particles in the treatment of infrabony defects," *Journal of Indian Society of Periodontology,* vol. 16, no. 2, p. 241, 2012.
[330] F. Baino, G. Novajra, C. J. F. i. b. Vitale-Brovarone, and biotechnology, "Bioceramics and scaffolds: a winning combination for tissue engineering," *Frontiers in Bioengineering and Biotechnology,* vol. 3, p. 202, 2015.
[331] F. E. Ciraldo, E. Boccardi, V. Melli, F. Westhauser, and A. R. J. A. b. Boccaccini, "Tackling bioactive glass excessive in vitro bioreactivity: Preconditioning approaches for cell culture tests," *Acta biomaterialia,* vol. 75, pp. 3-10, 2018.
[332] E. A. Aguilar-Reyes, C. A. León-Patiño, B. Jacinto-Diaz, and L. P. J. J. o. t. A. C. S. Lefebvre, "Structural characterization and mechanical evaluation of bioactive glass 45S5 foams obtained by a powder technology approach," vol. 95, no. 12, pp. 3776-3780, 2012.
[333] A. E. Carpenter *et al.*, "CellProfiler: image analysis software for identifying and quantifying cell phenotypes," *Genome biology,* vol. 7, no. 10, p. R100, 2006.
[334] A. L. Macon *et al.*, "A unified in vitro evaluation for apatite-forming ability of bioactive glasses and their variants," *Journal of Materials Science: Materials in Medicine,* vol. 26, no. 2, p. 115, 2015.
[335] T. T. Tauböck, M. Zehnder, T. Schweizer, W. J. Stark, T. Attin, and D. Mohn, "Functionalizing a dentin bonding resin to become bioactive," *Dental Materials,* vol. 30, no. 8, pp. 868-875, 2014.
[336] M. Cerruti, D. Greenspan, and K. J. B. Powers, "Effect of pH and ionic strength on the reactivity of Bioglass® 45S5," vol. 26, no. 14, pp. 1665-1674, 2005.
[337] P. F. Menci, A. Mari, C. Charbonneau, L.-P. Lefebvre, and L. J. M. De Nardo, "Aging of Bioactive Glass-Based Foams: Effects on Structure, Properties, and Bioactivity," vol. 12, no. 9, p. 1485, 2019.
[338] M. Cerruti, D. Greenspan, and K. Powers, "Effect of pH and ionic strength on the reactivity of Bioglass® 45S5," *Biomaterials,* vol. 26, no. 14, pp. 1665-1674, 2005.
[339] A. A. Shaltout, M. A. Allam, and M. A. Moharram, "FTIR spectroscopic, thermal and XRD characterization of hydroxyapatite from new natural sources," *Spectrochimica Acta Part A: Molecular Biomolecular Spectroscopy,* vol. 83, no. 1, pp. 56-60, 2011.
[340] A. Lucas-Girot, F. Z. Mezahi, M. Mami, H. Oudadesse, A. Harabi, and M. J. J. o. N.-C. S. Le Floch, "Sol–gel synthesis of a new composition of bioactive glass in the quaternary system SiO2–CaO–Na2O–P2O5: comparison with melting method," *Journal of Non-Crystalline Solids,* vol. 357, no. 18, pp. 3322-3327, 2011.
[341] A. A. R. De Oliveira, D. A. De Souza, L. L. S. Dias, S. M. De Carvalho, H. S. Mansur, and M. J. B. M. de Magalhaes Pereira, "Synthesis, characterization and cytocompatibility of spherical bioactive

glass nanoparticles for potential hard tissue engineering applications," *Biomedical Materials,* vol. 8, no. 2, p. 025011, 2013.
[342] J. R. Jones, L. M. Ehrenfried, and L. L. J. B. Hench, "Optimising bioactive glass scaffolds for bone tissue engineering," *Biomaterials,* vol. 27, no. 7, pp. 964-973, 2006.
[343] F. S. Abdel-Salam *et al.*, "In-situ forming chitosan implant-loaded with raloxifene hydrochloride and bioactive glass nanoparticles for treatment of bone injuries: Formulation and biological evaluation in animal model," *International Journal of Pharmaceutics,* p. 119213, 2020.
[344] H. Oudadesse *et al.*, "Development of hybrid scaffold: Bioactive glass nanoparticles/chitosan for tissue engineering applications," vol. 109, no. 5, pp. 590-599, 2021.
[345] J. Wu *et al.*, "Thermally triggered injectable chitosan/silk fibroin/bioactive glass nanoparticle hydrogels for in-situ bone formation in rat calvarial bone defects," vol. 91, pp. 60-71, 2019.
[346] D. S. Couto, Z. Hong, and J. F. Mano, "Development of bioactive and biodegradable chitosan-based injectable systems containing bioactive glass nanoparticles," *Acta Biomaterialia,* vol. 5, no. 1, pp. 115-123, 2009.
[347] M. G. Cerruti, D. Greenspan, and K. J. B. Powers, "An analytical model for the dissolution of different particle size samples of Bioglass® in TRIS-buffered solution," vol. 26, no. 24, pp. 4903-4911, 2005.
[348] E. A. Kiyotake, A. W. Douglas, E. E. Thomas, S. L. Nimmo, and M. S. Detamore, "Development and quantitative characterization of the precursor rheology of hyaluronic acid hydrogels for bioprinting," *Acta biomaterialia,* vol. 95, pp. 176-187, 2019.
[349] A. C. Heidenreich, M. Pérez-Recalde, A. G. Wusener, and É. B. Hermida, "Collagen and chitosan blends for 3D bioprinting: A rheological and printability approach," *Polymer Testing,* vol. 82, p. 106297, 2020.
[350] N. Diamantides *et al.*, "Correlating rheological properties and printability of collagen bioinks: the effects of riboflavin photocrosslinking and pH," *Biofabrication,* vol. 9, no. 3, p. 034102, 2017.
[351] L. Ning, N. Betancourt, D. J. Schreyer, and X. Chen, "Characterization of cell damage and proliferative ability during and after bioprinting," *ACS Biomaterials Science Engineering,* vol. 4, no. 11, pp. 3906-3918, 2018.
[352] J. Adhikari, M. S. Perwez, A. Das, and P. Saha, "Development of hydroxyapatite reinforced alginate–chitosan based printable biomaterial-ink," *Nano-Structures Nano-Objects,* vol. 25, p. 100630, 2021.
[353] Q. Wu, M. Maire, S. Lerouge, D. Therriault, and M. C. Heuzey, "3D printing of microstructured and stretchable chitosan hydrogel for guided cell growth," *Advanced Biosystems,* vol. 1, no. 6, p. 1700058, 2017.
[354] A. R. Spencer *et al.*, "Bioprinting of a cell-laden conductive hydrogel composite," *ACS applied materials interfaces,* vol. 11, no. 34, pp. 30518-30533, 2019.
[355] F. You, X. Wu, and X. Chen, "3D printing of porous alginate/gelatin hydrogel scaffolds and their mechanical property characterization," *International Journal of Polymeric Materials Polymeric Biomaterials,* vol. 66, no. 6, pp. 299-306, 2017.
[356] J. Lewicki, J. Bergman, C. Kerins, and O. J. B. Hermanson, "Optimization of 3D bioprinting of human neuroblastoma cells using sodium alginate hydrogel," vol. 16, p. e00053, 2019.

[357] E. Mirdamadi, N. Muselimyan, P. Koti, H. Asfour, and N. Sarvazyan, "Agarose slurry as a support medium for bioprinting and culturing freestanding cell-laden hydrogel constructs," *3D printing additive manufacturing,* vol. 6, no. 3, pp. 158-164, 2019.

[358] S. Ding, L. Feng, J. Wu, F. Zhu, Z. e. Tan, and R. Yao, "Bioprinting of stem cells: Interplay of bioprinting process, bioinks, and stem cell properties," *ACS Biomaterials Science Engineering,* vol. 4, no. 9, pp. 3108-3124, 2018.

[359] T. Vieira de Souza, S. M. Malmonge, and A. R. Santos Jr, "Development of a chitosan and hyaluronic acid hydrogel with potential for bioprinting utilization: A preliminary study," *Journal of Biomaterials Applications,* p. 08853282211024164, 2021.

[360] P. Mente and J. Lewis, "Elastic modulus of calcified cartilage is an order of magnitude less than that of subchondral bone," *Journal of Orthopaedic Research,* vol. 12, no. 5, pp. 637-647, 1994.

[361] J. M. Mansour, "Biomechanics of cartilage," *Kinesiology: the mechanics pathomechanics of human movement,* vol. 2, pp. 66-79, 2003.

[362] L. Polo-Corrales, M. Latorre-Esteves, and J. E. Ramirez-Vick, "Scaffold design for bone regeneration," *Journal of nanoscience nanotechnology,* vol. 14, no. 1, pp. 15-56, 2014.